

Karoo Aquifers

Their Geology, Geometry and Physical Properties

J.F. Botha, J.P. Verwey, I. van der Voort, J.J.P. Vivier, J. Buys,
W.P. Colliston and J.C. Loock

Report to the Water Research Commission
by the
Institute for Groundwater Studies
University of the Free State

WRC Report No: 487/1/98



Disclaimer

This report emanates from a project financed by the Water Research Commission (WRC) and is approved for publication. Approval does not signify that the contents necessarily reflect the views and policies of the WRC or members of the project steering committee, nor does mention of trade names or commercial products constitute endorsement or recommendation for use.

Vrywaring

Hierdie verslag spruit voort uit 'n navorsingsprojek wat deur die Waternavorsingskommissie (WVK) gefinansier is en goedgekeur is vir publikasie. Goedkeuring beteken nie noodwendig dat die inhoud die siening en beleid van die WVK of lede van die projek-loodskomitee weerspieël nie of dat melding van handelsname of ware deur die WVK vir gebruik goedgekeur of aanbeveel word nie.

ACKNOWLEDGEMENTS

The research in this report emanated from a project funded by the Water Research Commission entitled:

‘The Analysis and Interpretation of Aquifer Tests in Secondary Aquifers’

The Steering Committee responsible for the project consisted of the following persons:

Mr A.G. Reynders	Water Research Commission (Chairman)	
Mr H.M. du Plessis	Water Research Commission	
Mr M.E. Mosia	Water Research Commission (Secretary)	
Mr N.J.B. Anderson	Atomic Energy Commission	
Mr E. Braune	Department of Water Affairs and Forestry	
Mr A. du Plessis	Council for Geoscience	
Mr R. Meyer	Environmentek, CSIR	
Mr J. Weaver	Environmentek, CSIR	
Prof J.G.C. Small	University of the Free State	
Prof J.F. Botha	University of the Free State	} Research Team
Dr J Buys	University of the Free State	
Dr W.P. Colliston	University of the Free State	
Mr J. Looek	University of the Free State	
Mr J.P. Verwey	University of the Free State	

The financing of the project by the Water Research Commission and the contributions of members of the Steering Committee are hereby gratefully acknowledged.

The authors would also like to take this opportunity to express their sincere thanks to the following institutions and people, without whose help the investigation could not have been carried out:

The University of the Orange Free State for the facilities provided in conducting this research.

The Department of Water Affairs and Forestry for the drilling of the core-boreholes.

The Institute for Groundwater Studies, in particular the Director, Prof F.D.I. Hodgson, and Prof G.J. van Tonder for their assistance and encouragement during the investigation and Mrs M. Botha and C. Bitzer for their contributions in the editing of this report.

PREFACE

The common view in South Africa is that Karoo aquifers do not contain large quantities of groundwater. However, large volumes of groundwater are pumped from mines and the basements of buildings daily, in areas underlain by the Karoo sediments, which is not what one would expect from aquifers with a limited yield. An attempt is made in this report to explain this apparent discrepancy. However, the objective could only be achieved by reinterpreting some characteristics of the Karoo landscape, particularly the presence of dolerite dykes. The present interpretation is somewhat controversial, but it allowed the authors to explain the physical behaviour and properties of the aquifers concisely and consistently. The authors would therefore appreciate any contribution that could explain the behaviour of the aquifers as concisely and consistently, since these intrusions seem to have been the main mechanism responsible for the present properties of the aquifers.

EXECUTIVE SUMMARY

1 GENERAL

Water, particularly fresh or potable water, is indispensable for all man's activities on earth. Approximately 75% of the total volume of fresh water on earth is frozen in glaciers, while rivers and lakes hold approximately 0,33%. The remaining 24,67% occurs as groundwater. Since the water in glaciers is not available for general consumption, groundwater forms the largest source of fresh water available to man.

The situation in South Africa, however, is complicated because of the nature of the aquifers, which occur mainly in hard-rock formations. Groundwater is consequently usually regarded as an unreliable source of water. The result is that groundwater contributed only 10% to the national water budget in 1986. The surface water resources, however, have now almost been exploited to their limits. South Africa, therefore, will have to make more use of its groundwater resources in the future, and will then also have to meet the demand of the growing population very efficiently. This is especially true in the semi-arid and arid central and western regions, which covers approximately 66% of the country, where there are no major rivers or other surface sources. The majority of the inhabitants in these areas therefore depend on groundwater for their water supply. A large part of these regions, and approximately 50% of the country as a whole, are underlain by the so-called *Karoo Supergroup* of geological formations. The potential thus exists that aquifers in the Karoo Supergroup can make a significant contribution to the water budget of the country. Unfortunately, Karoo aquifers are very complex and unpredictable in their behaviour. The general view is thus that Karoo aquifers are not reliable sources of water, although there are boreholes which have provided the residents of farms and towns with water on a sustained basis for many years.

A major characteristic of the Karoo Supergroup, which consists mainly of sandstones, mudstones, shales and siltstones, is its low permeability. The majority of boreholes drilled in the Karoo sediments therefore have very low yields ($< 3,6 \text{ m}^3 \text{ h}^{-1}$). Indeed, the common view is that Karoo aquifers do not contain large quantities of groundwater, hence the name Karoo, which is the Hottentot word for dry. However, large volumes of groundwater are pumped from mines and basements of buildings daily, in areas underlain by the Karoo sediments, which is not what one would expect from aquifers with a limited yield. A number of studies were therefore undertaken in the past to try to use these aquifers more efficiently.

2 BACKGROUND TO THE STUDY

The main objective in one of the previous studies (Kirchner *et al.*, 1991) was to determine the recharge potential of the aquifers. To achieve this, Kirchner and his co-workers had to know the storage capacity of the aquifers. Two approaches were used for this purpose. The first was to determine the storativity of the aquifers through hydraulic tests, and the second was to study the water balance of the aquifers. Since the Karoo Supergroup consists of sedimentary rocks, they assumed that their hydraulic tests could be analysed with the classical Theis equation. However, this yielded storativity values $\sim 10^{-6}$, three orders of magnitude smaller than that obtained from the water balance studies. Since the result of the water balance studies agreed more with the historical operation of the aquifers, Kirchner and his co-workers assumed that the result from the hydraulic tests was wrong, and neglected it.

Although there exist other methods with which the hydraulic parameters of an aquifer can be determined, the hydraulic (or pumping) test still remains the much-preferred method. One reason for this popularity is that there exist a large number of methods, often referred to as *type curves*, for the analysis of the data, some of which have even been automated. However, the application of these methods is not as straightforward as textbooks would like one to believe. This applies particularly in cases where the behaviour of the aquifer may deviate from the basic assumptions made in the derivation of the methods. There was thus a strong possibility that the methods Kirchner *et al.* (1991) used to analyse their hydraulic tests, misrepresented the aquifers' properties and physical behaviour. It was thus quite natural to doubt the results of the hydraulic tests and the method used in the analysis. Unfortunately, too little information was available on the

nature of Karoo aquifers at that stage to try to determine precisely what the problem was. The Water Research Commission was therefore approached with the request to fund a more detailed investigation of these and other hard-rock aquifers in South Africa.

3 OBJECTIVES OF THE STUDY

The objectives of the present study, as set out in the original contract with the Water Research Commission, were as follows:

- (a) An investigation of the nature and behaviour of secondary aquifers, with special reference to the applicability and reliability of existing conceptual models for the description and analysis of hydraulic tests, conducted in these aquifers.
- (b) The development of improved and/or new techniques for use with the implementation and analysis of hydraulic tests in secondary aquifers.
- (c) Implementation of the improved and/or new techniques, developed in (b), into a user-friendly computer package for the analysis of hydraulic tests in secondary aquifers.

The original idea was to cover all the major secondary aquifers that occur in South Africa—Karoo, dolomitic, igneous and metamorphic—in the project. Since Karoo aquifers were the most accessible to the project team, it was natural to start the investigations with these aquifers. However, it soon became clear that the behaviour of these aquifers does not conform to the behaviour of conventional aquifers, as described in the literature. This presented the project team with a difficult decision—abandon Karoo aquifers and continue with the other aquifers, or concentrate exclusively on Karoo aquifers and try to understand their behaviour. Since Karoo aquifers are the most extensive type of aquifer present in South Africa, the latter alternative was put to the Steering Committee of the project, who accepted it. The discussion in this report is therefore limited to Karoo aquifers, to which the research effort was restricted.

A Technical Committee, appointed by the Steering Committee, decided during a field visit in March 1994 that the project could benefit from a more detailed analysis of the structural and geological aspect of Karoo formations. They therefore requested that Dr. W.P. Colliston and Mr. J.C. Loock of the Department of Geology, at the University of the Orange Free State, should become active co-workers on the project, and that the duration of the project be extended by one year. The objectives of this extension set out in the revised, final contract with the Water Research Commission were as follows:

- (a) To provide an integrated geological working model for the sandstone/shale aquifer(s), at the Campus Test Site of the Institute for Groundwater Studies. This model may be used to supplement and test the current and future numerical models for fractured aquifers as, for example, those determined by the Institute for Groundwater Studies at the UOFS.
- (b) To investigate the association of structural geological planar structures (e.g. joints, fractures and faults) and sedimentology (palaeoflow direction, grain framework and microstructure) with potential groundwater reservoirs in the competent rocks of the Karoo Supergroup.
- (c) To represent the aquifers' geometry by means of fractals.
- (d) To develop hydraulic tests that will also reflect the geometry of the aquifer and not only its relational parameters, as is the case with existing methods.

The attainment of the latter objectives was, unfortunately, hampered by two unexpected developments. The first was a considerable delay in the approval for the continuation of the project, and the second the resignation of Mr. J.P. Verwey, the key researcher, responsible for the field investigations. The result was that the field work had to be restricted to the Campus Test Site, and that none of the more esoteric aquifer tests, envisaged in the motivation for the continuation of the project, could be performed. The attempt to represent the aquifers' geometry by means of fractals also had to be abandoned. However, this loss was somewhat offset by the information gained during the co-operation with the Consulting Engineers, Cahi De Vries, in the development of a new well-field for the Municipality of Philippolis, and later also for the Municipality of Rouxville.

4 METHODOLOGY USED IN THE INVESTIGATIONS

4.1 The Nature and Description of Groundwater Motion

Groundwater does not exist in a vacuum, but in the interstices that occur naturally in all geological formations on earth. There are thus essentially three research fields that need to be considered in a scientific study of groundwater phenomena.

- (a) The environment, i.e. the geological formations and structures in which groundwater flow occurs.
- (b) A study of interactions between the water and the geological formations.
- (c) The formal description of the interactions and how they control the behaviour of an aquifer.

The first step in the study of any aquifer should therefore be to understand the geology of the area in which it occurs. Although the behaviour of the aquifer will mainly be determined by the current state of the geology, this state is the result of an evolutionary process that took place over many years, even millions of years, as is the case with Karoo aquifers. It was thus thought worthwhile not to concentrate on the present state of the Karoo Supergroup alone, but also to look at its historical evolution, as this may explain some current features of the Supergroup that would be difficult to explain otherwise.

The interactions between the water and the geological formations will obviously be controlled by the laws of physics and chemistry. These laws are embedded in physical theories and described in the conventional language of physics—mathematics. Any discussion of groundwater motion must consequently refer to elements from these three subjects at one time or another.

A theory is in essence an abstract and general description of a natural phenomenon, or a group of such phenomena. To apply it to a particular object of study, such as a specific aquifer, requires that one must develop a so-called *conceptual model* for the object. A conceptual model is nothing more than a mental interpretation of the object, and can be expressed in any convenient form. However, the easiest method to relate the model to the underlying theory, is to also couch it in the mathematical language of physics. This *mathematical model* can assume one of two forms—an *analytical model*, where one is able to express the model in terms of elementary mathematical functions, or a *numerical model*, where the model can only be expressed as numbers. The type curves, used in the analysis of hydraulic tests, are prime examples of analytical models, while a computer model for an aquifer is a numerical model.

4.2 Geological Studies

The geology and behaviour of the aquifers were studied at five experimental sites, developed specifically for this project, and during the development of water supply schemes for the Municipalities of Philippolis and Rouxville. The first experimental site, henceforth referred to as the Campus Test Site, is situated on the Campus of the University of the Orange Free State in Bloemfontein, and the other four at Dewetsdorp, 77 km east of Bloemfontein.

The original purpose of the experimental sites was to acquire data on the behaviour of the aquifers by analysing the results of accurately controlled hydraulic tests with existing analytical models. A series of percussion boreholes was therefore drilled on each site. However, a new approach had to be adopted when the results of the initial hydraulic tests made it clear that the existing analytical models were inadequate for the analysis of hydraulic test data from Karoo aquifers.

Five percussion boreholes, scattered across the Campus Test Site, existed at the beginning of the project in 1992. These boreholes were drilled by the Department of Geohydrology, at the University of the Orange Free State, to whom the site belongs. The first step was thus to drill an additional 11 percussion boreholes on the site. The first 10 of these boreholes were drilled with funds from the Water Research Commission, while the other one was drilled by the Department of Geohydrology. Six of these boreholes were drilled specifically with the view to perform cross-borehole packer tests, since the work at Atlantis (Botha *et al.*, 1990), suggested that it is an ideal method to use in the investigation of hard-rock aquifers. The other five boreholes were drilled mainly to try to clarify anomalies, observed in the water levels of the newly drilled six and the existing five boreholes on the site. However, it turned out that these 16 boreholes were not enough to clarify all anomalies. An additional 15 boreholes has since been drilled on the site. Seven of the additional boreholes are core-boreholes, drilled by the Department of Water Affairs and Forestry, and the other eight percussion boreholes, drilled by the Department of Geohydrology. The Department of Geohydrology also installed piezometers in three of the percussion boreholes on the Campus Test Site.

There are 19 percussion boreholes on the test sites at Dewetsdorp. Eleven of these were drilled as part of this project, while seven were drilled by the Department of Water Affairs and Forestry as part of the project of Kirchner *et al.* (1991). The other borehole, for which no information is available, has been used by the Municipality of Dewetsdorp for production purposes for years. The Department of Water Affairs and Forestry also drilled two core-boreholes on two of the sites.

The cores from the first core-boreholes indicated that the geometry of Karoo aquifers differs completely from that used in deriving models for aquifers, and even from the customary interpretation of Karoo formations. Two steps were therefore taken to try to explain the observed geometry of the aquifers. The first was to review the genesis of the Karoo formations and the second to try to confirm the results of the review with

field observations. The information on the geology of the central Free State that existed at the time was, unfortunately, too limited for this purpose. The objective could thus only be achieved by studying the geology of the area in greater detail. Since the resources available for this purpose were limited, the investigation had to be limited to the area around Bloemfontein, and to the following three objectives.

- (a) Provide a regional perspective for the clastic aquifers at the Campus Test Site.
- (b) Study the stratigraphy, sedimentology and structure through a multi-disciplinary approach.
- (c) Determine the aquifer potential of rocks in the Karoo Supergroup in this area.

4.3 Interactions between the Water and Geological Formations

The interactions between the water and geological formations were studied by performing a series of hydraulic tests on the boreholes at the various test sites. Tests used for this purpose included: constant rate tests, slug tests, step drawdown tests, cross-packer borehole and conventional packer tests. The constant rate and slug tests were performed on selected boreholes at all the experimental sites, the latter mainly for exploratory purposes, and the step drawdown tests only at Philippolis. The conventional packer and cross-packer borehole tests were, however, restricted to boreholes on the Campus Test Site. The behaviour of the water levels in most of these tests was monitored electronically with pressure transducers.

The sites investigated during the project are all limited to the Central and Southern Free State. An attempt was therefore made to extend the study of the interactions between the water and geological formations to other parts of the Karoo Supergroup. This was achieved by extending the analyses of the constant rate tests to tests performed in other parts of the Supergroup. These include tests Alan Woodford from the Department of Water Affairs and Forestry's office in Cape Town performed on boreholes at Calvinia, a consultant's constant rate test at Kokstad, and the constant rate tests of Kirchner *et al.* (1991).

4.4 Description of the Interactions

As mentioned above, the difficulties experienced by Kirchner *et al.* (1991) in interpreting their results of constant rate tests, with conventional type curves, was the primary reason for the motivation of this project. The first step in the project was thus to use more sophisticated, but lesser-known, methods for this purpose. However, it soon became clear that these methods are not suitable either. The next step was therefore to study the behaviour of the aquifers in more detail, through more refined hydraulic tests, field investigations and the structural analysis of the aquifers. These studies showed that Karoo formations are best described as multi-porous, sparsely fractured media, and that their behaviour can only be described by a full three-dimensional mathematical model. The three-dimensional numerical model, developed by Verwey and Botha (1992) for the groundwater flow equation, was therefore adapted to Karoo aquifers and used throughout the study, with excellent results.

5 DISCUSSION

The most important conclusion derived from the present study is that *the behaviour of a stressed Karoo aquifer is determined by its very complex geometry*, that results from the presence of bedding-parallel fractures and the multi-porosity of the rock matrix. Any neglect of this property in the management and operation of these aquifers can ruin an aquifer completely. Indeed, all indications are that the inability of previous investigators to take the internal geometry of Karoo aquifers into account, must be regarded as the main reason for the difficulties experienced with these aquifers, and why people distrust them.

Although the concept that the behaviour of an aquifer is largely determined by its geometry is well-known, this dependence is usually neglected in groundwater investigations. One reason for this is that the methods commonly applied in these investigations are all based on porous formations, whose geometry is so simple that it is often neglected (Black, 1993). However, as Black points out, this geometry is of vital importance in the analysis and interpretation of hydraulic tests in any secondary aquifer—a view shared by Prof. Ghislain de Marsily (Personal Communication). The neglect of this geometry in previous investigations of Karoo aquifers is probably the main reason for the difficulties experienced with these aquifers, and why people distrust them.

The apertures of the bedding-parallel fractures in Karoo aquifers are not very large (see Figure 1), although a fracture can have a considerable areal extent. The fracture can, therefore, only store a limited volume of water. *The major storage units of water in Karoo aquifers must therefore be the formations themselves, while bedding-parallel fractures provide the main conduits of water to boreholes.*



Figure 1 Photograph of the water-yielding fracture in a core sample from the Campus Test Site.

The first indication of the important role that bedding-parallel fractures play in the ability of Karoo boreholes to yield water came from an analysis of the cores from the core-boreholes drilled on the Campus Test Site and Dewetsdorp. These cores showed that the water-yielding fractures in the boreholes on these sites are parallel to the bedding planes of the Karoo formations, and therefore mainly horizontally orientated. This conclusion was further confirmed by observations made during the drilling of boreholes at Philippolis and Rouxville. The study of the regional fracture development in the sediments, in and around Bloemfontein, also supports this conclusion and, moreover, showed that subvertical fractures only provide conduits for surface water. The best place to site boreholes in Karoo aquifers is therefore in those areas where bedding-parallel fractures are present.

The bedding-parallel fractures in the Karoo formations have a low frequency and weak connectivity. However, a borehole that does not intersect such a water-yielding fracture, does not have a high yield. Although this fact is well-known to groundwater practitioners, they usually pay very little attention to the nature of fracture, or how it influences the movement of water in these aquifers. One reason for this lack of interest is the assumption that the water-yielding fractures in Karoo aquifers are vertically or subvertically orientated, and do not influence the flow pattern. This assumption seems to have been quite common amongst geologists, judging from their reaction when the first cores showed the fractures to be horizontally orientated. Thus it seems natural to ask: why do bedding-parallel fractures exist in the Karoo formations?

A major feature of the Karoo landscape in the southern Free State and adjacent areas is the presence of circular doleritic dykes. A review of the historical evolution of the Karoo Supergroup of geological formations, suggested that these dykes were formed by the intrusion of magma, in the form of laccoliths. This interpretation may be controversial, but has an advantage over conventional interpretations in that it provides a natural explanation for the existence of the structures, without invoking some rather esoteric mechanisms. Another advantage of the interpretation is that the theory behind the intrusions suggests that the intrusions would have bent and weakened the overlying Karoo strata, thereby creating the necessary conditions for bedding-parallel fractures to form. Bedding-parallel fractures could thus have formed, either during the intrusions themselves, or during the uplift that accompanied the weathering of the overlying layers. Bedding-parallel fractures may therefore be present in areas that seemingly are not directly connected to dolerite dykes. This may explain why 63% of the 1 245 boreholes that Burger *et al.* (1981) surveyed in the districts of Bethulie, Springfontein and Trompsburg are not situated near dolerite dykes. The water-yielding, bedding-parallel fracture on the Campus Test Site, which is certainly not associated with any dolerite dyke, may also owe its existence to such a laccolithic intrusion. For, as shown by the geological model of Bloemfontein and its immediate surroundings, developed as part of this project, the city is situated on a dome-shaped structure, typical of laccolithic intrusions.

There are a number of very important consequences, particularly for the management of Karoo aquifers, that can be derived from the present project. The first, and perhaps most important one, is that the behaviour of boreholes in Karoo aquifers should differ from aquifers in which the flow is horizontal. This conclusion has been confirmed by a number of hydraulic tests, performed at the Campus Test Site, Philippolis and Rouxville. What typically happened in these tests is that the water level in the pumped borehole at first drops continuously, until it reaches a depth of approximately 2 m above a water-yielding fracture. Here, the water level stabilizes, for as long as the fracture can sustain the yield. This phenomenon repeats itself for every water-yielding fracture that the borehole intersects, only to drop to the pump intake, if the test is performed long enough. The water level, nevertheless, recovers almost instantaneously to the depth of the fracture, and then gradually when the pump is switched off or the discharge rate is decreased. At no stage, however, did the water levels in nearby observation boreholes, *even those that intersect the same water-yielding fracture*, drop below the fracture in any of the tests.

It was very difficult to explain the '*fracture-controlled*' behaviour of boreholes in a Karoo aquifer from the field observations alone. One possibility that did emerge though, is that the behaviour is caused by the fact that water has to flow from the Karoo formations to the bedding-parallel fractures before it reaches the borehole. The major flow direction in a stressed Karoo aquifer therefore seems to be vertical and not horizontal, as is commonly assumed in groundwater flow models. This means that it will be difficult, if not impossible, to study the behaviour of these aquifers without the use of a three-dimensional flow model.

Three-dimensional mathematical models of groundwater flow are not very popular in geohydrological circles, mainly for two reasons. The first is that such models require considerably more field data and sophisticated computer resources than an equivalent two-dimensional model. The second is that very little attention is usually paid to the geometry and structure of an aquifer in field investigations; factors that are of prime importance in the development of three-dimensional flow models. Fortunately there were sufficient observational data available to develop such a model for the Campus Test Site. The three-dimensional computer program, SAT3, developed in a previous contract with the Water Research Commission (Verwey and Botha, 1992), was therefore adapted and used to develop a numerical model for the Campus Test Site. This model showed that the piezometric head declines constantly throughout the fracture, during the time a borehole is pumped. The piezometric cone in the fracture thus does not widen with time, as is conventionally assumed, but always keeps the same shape, as the piezometric heads decrease. The piezometric gradient, and thus the discharge rate, from the fracture to the borehole must therefore remain constant during the time a borehole is pumped. *There thus exists a limit to the rate at which a borehole in a Karoo aquifer can be pumped*—a conclusion supported by the observation that the phenomenon is only observed if the discharge rate of a borehole is above a certain value. This limiting rate does not depend on the conventional hydraulic parameters, transmissivity and storativity, but the hydraulic conductivities and specific storativities of both the fracture and rock matrix, and the *areal extent of the fracture*. *It is thus imperative that the geometry of a Karoo aquifer must be known, before the aquifer is developed for the supply of water to larger communities.*

The geometry of Karoo aquifers, outlined above, differs completely from that of the media usually considered in the literature on aquifer hydraulics, particularly in horizontal flow models. The hydraulic parameters, transmissivity and storativity, derived from conventional two-dimensional horizontal flow models, are therefore meaningless for Karoo aquifers. No wonder that previous investigators experienced difficulties in interpreting their hydraulic test data. The only way to study the behaviour of a Karoo aquifer is through a three-dimensional conceptual model. *The common practice of analysing hydraulic test data from these aquifers with horizontal flow models should therefore be discouraged.*

There is, unfortunately, not sufficient information or appropriate computer equipment available in South Africa to run a three-dimensional groundwater model on a routine basis. Although steps should be taken to correct the situation if Karoo aquifers are to play a significant role in the future water budget of the country, it is unrealistic to expect that this will be achieved in the short term. A new two-dimensional vertical flow model for the analysis of hydraulic test data was therefore developed towards the end of the project, when it became clear that the flow in Karoo aquifers is mainly vertical. The model is therefore still not fully developed, but case studies have shown that it at least yields more realistic hydraulic parameters than horizontal two-dimensional flow models. *However, this two-dimensional representation will not be suitable for a management model of these aquifers*

Another interesting result that followed from the three-dimensional model of the Campus Test Site is that the water level in an open borehole represents an average of the piezometric levels in the fracture and the aquifer, weighted in favour of the piezometric level in the fracture. It is thus difficult to decide precisely how to interpret the water levels in open boreholes. Future observations of Karoo aquifers should therefore preferably be conducted with piezometers. This may add to the cost in developing these aquifers, but one will

then be able to interpret the results meaningfully, and at the same time to collect the data required by a three-dimensional model.

The limited capacity of a water-yielding fracture implies that it can easily be dewatered, with a number of undesirable consequences, of which the first and most obvious one is a reduction in the borehole's yield. However, there are other and more serious consequences that may take a long time to become noticeable. For example, the three-dimensional model of the Campus Test Site has shown that the flow velocities in the fracture are very high. The borehole and pump may then become clogged with mud particles set loose by the high flow velocities. A fully, or even partially, dewatered fracture may of course also deform, and even collapse.

Deformation in an aquifer or borehole is usually neglected in the management and operation of boreholes. However, there are strong indications that deformations of water-yielding fractures in Karoo aquifers are more common than usually thought. The complaint '*my borehole has dried up*', often heard from people who depend on Karoo aquifers for their water supply, may indeed be the result of a collapsed fracture. This interpretation is supported by the observation that it is often possible to drill a new, successful borehole within a short distance from the one that 'dried up'. Another, less spectacular, but probably related phenomenon, is a borehole whose yield decreases with time. The phenomenon has never been discussed in the literature to the knowledge of the authors, but discussions with farmers indicated that it is quite common in Karoo boreholes, especially those older than 10 years. Hydraulic tests performed during the project also indicated that the deformation of a borehole in a Karoo aquifer may affect its yield adversely. Unfortunately, none of these observations could provide an estimate of the magnitude of such a deformation. This only became apparent when the high-yielding Borehole UO5 on the Campus Test Site was imaged with an acoustic televiewer in June 1996. The image, reproduced in Figure 2, becomes more remarkable if one compares it with the calliper traces of two previous geological surveys of the same borehole, also reproduced in Figure 2.

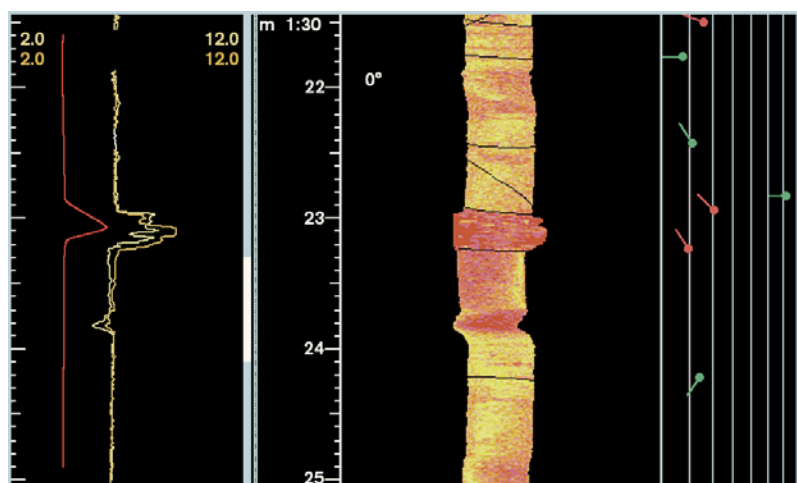


Figure 2 Calliper (left) and acoustic scanner (centre) images of Borehole UO5 on the Campus Test Site. The tadpoles on the right show the orientation of the various fractures (the thin black lines on the scanner image).

The water-bearing fracture is situated within the fracture zone, at 23,0 – 23,3 m in Borehole UO5, at a depth of 23,116 m. The zone is also clearly visible in two previous geophysical surveys of the borehole; the first one carried out on 1992-06-04 and the second on 1993-12-01. However, neither the subvertical fracture (between 22,5 and 23,0 m) nor the highly warped zone (at 23,8 m) appears on the scans of these surveys. These features, therefore, must have developed between the survey of 1993-12-01 and 1996-06-02; the date when the acoustic scanner image was taken.

It is difficult to explain the deformations in Borehole UO5 at the moment. One possibility is that they formed through the reactivation of existing planes of weakness, caused by the extensive hydraulic tests performed on the borehole. Nevertheless, they do show that deformations, be it only of boreholes, may be more common in Karoo aquifers than previously thought.

In conclusion it can be said that there is little doubt that the behaviour of boreholes in Karoo aquifers is completely determined by the presence of bedding-parallel fractures, which are mainly horizontally orientated. This does not mean that there are no vertical or subvertical fractures in these aquifers, or that they play

an insignificant role, but only that they do not influence the behaviour of boreholes significantly. Indeed, there are indications that vertical and subvertical fractures play a significant role in recharging the aquifers. For, as shown by the contour map in Figure 4.39 of Kirchner *et al.* (1991), Karoo aquifers are not recharged locally, but only in the surrounding hill tops, which usually contain large numbers of vertical fractures.

6 RECOMMENDATIONS

The most important conclusion of the present study is that Karoo aquifers may contain significant quantities of water, but that their complex geometry makes it difficult to withdraw the water reliably. There is thus no reason, in principle, why Karoo aquifers cannot make a significant contribution to the water budget of the country. The only prerequisite is that *they are managed properly*, and according to their basic physical properties, although this is probably more easily said than done. This conclusion, admittedly, differs considerably from the conventional interpretation of the aquifers. However, it is the only conclusion the project team is aware of that allows one to interpret the observed behaviour of the aquifers concisely and consistently.

The present interpretation of Karoo aquifers emerged from a study of the history of the aquifers, and the interpretation of a limited number of hydraulic tests with a three-dimensional numerical model. Nevertheless, it did show that one will have to take the three-dimensional nature of the aquifers into account, in managing the aquifers. However, this should not be so much of a problem, provided that the following prerequisites are met.

It is well-known that any management model is useless, unless supported by sound and accurate measurements. Unfortunately, previous studies of Karoo aquifers were usually based on the assumption that flow in these aquifers is horizontal. Little attention was therefore paid to the three-dimensionality of these aquifers. Future studies should therefore try to correct this imbalance in the observational data.

The success in implementing the recommended approach will ultimately depend on the solution of two related problems—what observational techniques to use, and how to gather, store and manipulate the observational data. The observational equipment available today, such as packers, are expensive and their applicability often limited. Special attention should thus be given to develop less expensive, and more appropriate observational equipment. The present attempt at the Institute for Groundwater Studies to develop more suitable and less expensive packers should thus be encouraged. Attention should also be given to incorporate more innovative techniques, such as *in situ* flow measurements, into the observations. Nevertheless, there are some steps that can be taken immediately, without increasing the cost of the study exorbitantly. These include:

- (a) Detailed geological logs must be kept of *all* new boreholes drilled in Karoo aquifers, *with special emphasis on the depths of water strikes*.
- (b) At least one observation borehole should be drilled, for every production borehole, *and equipped with piezometers*.
- (c) Every production borehole should be equipped with a flow meter.
- (d) The discharge rates of production boreholes and piezometric levels in the observation boreholes should be measured routinely and stored in a suitable database.

Experience at Philippolis has shown that the local population are quite prepared to gather the necessary information, accurately and reliably, if they are trained sufficiently and given the reason for collecting the data. No severe difficulties are thus foreseen with the gathering of the data. The storage and manipulation of the observational data are another matter, however. As anyone with experience in three-dimensional modelling knows, such models are quite complex, cannot be duplicated at will, require special computer resources and highly trained personnel. It may thus be worthwhile for the Department of Water Affairs and Forestry to establish a special unit that controls Karoo aquifers, and directs their management, operation and future investigations.

The single most important prerequisite to satisfy the program outlined above, is also perhaps the most difficult to achieve; that is, to change the attitude of groundwater practitioners. Considerable progress has been made in the physics and chemistry of groundwater flow, yet these new principles are often shrugged off with the remark: ‘... *it cannot easily be used by practitioners*’, or the present methods are quite adequate, so why bother with new methods? As Sir Winston Churchill once said: ‘*Men occasionally stumble over the truth, but most pick themselves up and hurry off as if nothing ever happened.*’ It is therefore important to remember that *Nature behaves in its own subtle ways, and not as prescribed by man*. The possibility thus always exists that factors discarded today in managing Karoo aquifers, may have devastating effects on the future behaviour of the aquifer. Since the Karoo aquifers have not been used extensively until recently, and groundwater moves very slowly, there may still be a chance to avoid such a disaster, *but only if appropriate*

observational and managerial techniques are implemented now. This will not only ensure that future generations will still be able to withdraw water from the aquifers, but can also lead to a considerable reduction in development costs, if recent experiences in the oil industry (Clementz, 1997) can be used as a measure.

All known physical properties of Karoo aquifers were included in the computer program used to establish the three-dimensional model for the Campus Test Site. However, as pointed out in Chapter 2, it is almost impossible to achieve this objective in an initial study. The present version of the computer program is no exception to this rule. For example, the model does not take the deformation of the fracture or the aquifer into account. The simulated flow velocities near the fracture in a pumped borehole are also very high. A future version of the model, therefore, may have to be based on the more general Navier-Stokes equation, rather than on the conventional groundwater flow equation. However, there does not exist sufficient observational data to justify such a drastic revision of the model at the moment. It is therefore recommended that particular attention be given to: (a) the behaviour of the *in situ* flow field, and (b) the deformation of the water-yielding fractures, and aquifers as well, in future investigations of Karoo aquifers.

The most controversial aspects in using Karoo aquifers for water-supply purposes are probably to site suitable production boreholes and to determine the depth where the water will be struck. These problems were not addressed specifically in this study, but were especially noticeable in the investigations at Rouxville. Here, water was struck only at depths greater than 90 m, in contrast to the depths of 20–30 m, at Campus Test Site, Dewetsdorp and Philippolis. None of the available geophysical techniques is able to detect at what depths water will be struck, or delineate the bedding-parallel fractures in Karoo aquifers. It is therefore recommended that attention should be given to more innovative geophysical techniques that may solve these problems.

A particularly interesting method that promises to solve both problems at once is the nuclear magnetic resonance method (Schirov *et al.*, 1991). This method is based on properties of the hydrogen nucleus itself. It should thus not be influenced by clay, or other electrically conductive layers that appear frequently in Karoo formations and influence electromagnetic techniques adversely.

Another technique that seems equally promising is a seismic method which uses the drill bit as the seismic source (Rector and Marion, 1991). This method is able to provide real time data on the structure of the aquifer and the horizons below the drill bit. However, it may be necessary to analyse the data with more sophisticated techniques than is commonly used in seismic work, including the paper of Rector and Marion (1991), if the method is to be applied successfully.

Irrigation farmers are perhaps the people that benefit most from Karoo aquifers at the moment. However, the water canon and sprinkler systems they use are inefficient and a waste of water. An attempt should therefore be made to encourage them to use more efficient irrigation methods, such as drip- and micro-irrigation systems. Experience in Israel has shown that these systems conserve considerable quantities of water and increase the crop production at the same time. Moreover, the systems do not require high-yielding boreholes, and are therefore ideal for Karoo aquifers. An irrigation farmer who installs one of these systems, therefore, will not only increase the productivity of his farm, but will also contribute to the conservation of perhaps the most precious natural resource in South Africa: water.

Boreholes are, undoubtedly, the most cost-effective method to withdraw water from an aquifer. However, the dependence of a borehole's yield on the presence and properties of a fracture raises the question whether boreholes are the best method with which to withdraw water from Karoo aquifers. Although some of the adverse effects can be limited by pumping and spacing the boreholes judiciously, it may still be advantageous to introduce other production methods, such as the ganats of the ancient Persians, in future studies of these aquifers.

7 SUMMARY AND CONCLUSIONS

The prime objective of the project was to try to understand the physical behaviour of secondary aquifers in South Africa better, and to use this information to develop improved and/or new techniques for the implementation and analysis of hydraulic tests in secondary aquifers. However, it became clear in the initial study that the Karoo aquifers require special attention. The project thereafter concentrated exclusively on these aquifers, with the permission of the Steering Committee.

As discussed in the main report, considerable progress has been made in this regard. This applies in particular to the attempt made to understand the physical nature of the aquifers better. These aquifers occur in highly stratified and alternating layers of mudstones, sandstones and siltstones, sparsely intersected by very few horizontal bedding-parallel fractures, which act as the main conduits of water for boreholes. The geometry of the aquifers therefore differs completely from that of the media, conventionally used in the

description of aquifers. Nevertheless, the study has shown that the aquifers should be able to supply in all reasonable demands for water, provided that they are managed properly, and in accordance with the principles underlying their physical behaviour.

Two computer programs, the one based on the full three-dimensional representation of the aquifers and the other a simplified two-dimensional representation, were developed during the project. These programs will not only enable future researchers to interpret the results of hydraulic tests in these aquifers more consistently, but also to manage Karoo aquifers more consistently. The three-dimensional program can also be used to elucidate the behaviour of the aquifers in those cases where there is a lack of observational data. Interested researchers and practitioners can obtain copies of both programs from the Institute for Groundwater Studies. The three-dimensional program is still in research form, but there is a user-friendly Windows 95 version of the two-dimensional program.

The only original objectives of the project that could not be fulfilled were to represent the geometry of the aquifers with fractals and the development of hydraulic tests that reflect the geometry of the aquifer and not only its hydraulic parameters.

8 REFERENCES

- Black, J. H. (1993) Hydrogeology of fractured rocks—a question of uncertainty about geometry. In: Proceedings of the *Hydrogeology of Hard Rocks. Memoires of the XXIVth Congress of the IAH*. S. Banks and D. Banks (eds.) Ås (Oslo), Norway. Vol 2, 783–796. International Association of Hydrogeologists.
- Botha, J. F., Buys, J., Verwey, J. P., Tredoux, G., Moodie, J. W. and Hodgkiss, M. (1990) *Modelling Groundwater Contamination in the Atlantis Aquifer*. WRC Report No 175/1/90. Water Research Commission, P.O. Box 824, Pretoria 0001.
- Burger, C. A. J., Hodgson, F. D. I. and Van der Linde, P. J. (1981) *Hidrouliese Eienskappe van Akwifere in die Suid-Vrystaat*. Bulletin 7. Instituut vir Grondwaterstudies, Universiteit van die Oranje-Vrystaat, Posbus 339, Bloemfontein.
- Clementz, D. M. (1997) Company R&D: Does it add value to the bottom line? *Journal of Petroleum Technology*. **49** (2), 144–148.
- Kirchner, J. O. G., Van Tonder, G. J. and Lukas, E. (1991) *Exploitation Potential of Karoo Aquifers*. WRC Report No 170/1/91. Water Research Commission, P.O. Box 824, Pretoria 0001.
- Rector, J. W. and Marion, B. P. (1991) The use of drill-bit energy as a downhole seismic source. *Geophysics*. **56** (5), 328–634.
- Schirov, M., Legchenko, A. and Creer, G. (1991) A new direct non-invasive groundwater detection technology for Australia. *Exploration Geophysics*. **22**, 333–338.
- Verwey, J. P. and Botha, J. F. (1992) *A Comparative Study of Two- and Three-dimensional Groundwater Models*. WRC Report No 271/1/92. Water Research Commission, P.O. Box 824, Pretoria 0001.

CONTENTS

Acknowledgements	i
Preface	ii
Executive Summary	iii
Contents	xiii
List of Figures	xix
List of Tables	xxv
List of Symbols	xxvii

Chapter 1

Introduction

1.1 General	1
1.2 Background of the Study	1
1.3 Objectives of the study	3
1.4 Methodology used in the Investigations	4
4.1 The Nature of Groundwater Motion	4
4.2 Experimental Sites	4
1.5 Structure of the Report	5

Chapter 2

The Physical Behaviour of an Aquifer

2.1 Introduction	7
2.2 Determination of an Aquifer's Void Geometry	7
2.1 Geological Methods	7
2.2 Geophysical Methods	8
2.3 Groundwater Models	8
3.1 Definition of the Term Model	8
3.2 Hydraulic Tests	9
2.4 Conclusion	11

Chapter 3

The Karoo Supergroup

3.1 General	13
3.2 The Cape Fold Belt	15
3.3 The Dwyka Formation	15
3.1 Deposition	15
3.2 Hydrological Properties of the Dwyka Formation	15
3.4 The Eccra Group	16

4.1	Deposition	16
4.2	Hydrological Properties of the Eccu Group	17
3.5	The Beaufort Group	18
5.1	General	18
5.2	Deposition	18
5.3	Hydrological Properties of The Beaufort Group	18
3.6	The Stormberg Group	20
6.1	The Stormberg Basin	20
6.2	The Molteno Formation	20
6.3	The Elliot Formation	20
6.4	The Clarens Formation	20
6.5	Hydrological Properties of The Stormberg Group	21
3.7	Transformations of the Original Sediments	21
7.1	Lithification, Compaction and Cementation	21
7.2	Isostatic Uplift and Development of Fractures	22
3.8	Recent Formations	22
3.9	Conclusions	22

Chapter 4

Magmatic Intrusions

4.1	Introduction	25
4.2	The Drakensberg Lavas	25
2.1	General	25
2.2	Ring Dykes	26
2.3	Dolerite Sills	27
4.3	Linear Dolerite Dykes	27
4.4	Kimberlites	29
4.5	The Geohydrology of Dolerite Intrusions	30
5.1	General	30
5.2	Mechanical Deformation of Karoo Rocks	30
5.3	Weathering of Dolerite Dykes	32
4.6	Discussion	34

Chapter 5

Geology of the Campus and Dewetsdorp Test Sites

5.1	Introduction	37
5.2	Geology of the Bloemfontein Area	37
2.1	Previous Studies and Sources of Information	37
2.2	Regional Survey	38
5.3	Geomorphology of The Central Free State	38
3.1	General	38
3.2	Beaufort Stratigraphy	39
5.4	Regional Structural Geology	45
4.1	Structural-Stratigraphic Mapping	45
4.2	The Rock Mass Structure	46
5.5	The Campus Test Site	48
5.1	General	48
5.2	Mapping and Macroscopic Bedding Orientation	50
5.3	Stratigraphy and Sedimentology	50
5.4	Rock Mass Structure	57
5.5	Geometry of the Aquifer	63
5.6	The Dewetsdorp Test Sites	67
6.1	Introduction	67
6.2	Geology	67
6.3	Geohydrology of the Experimental Sites	69

5.7	Discussion	71
-----	------------------	----

Chapter 6

The Physical Behaviour of Karoo Aquifers

6.1	Introduction	75
6.2	The Nature of Flow in Karoo Aquifers	75
2.1	General	75
2.2	Matrix Flow	75
2.3	Fracture Flow	76
6.3	Hydraulic Tests	77
3.1	General	77
3.2	Multiple Constant Rate Tests	77
3.3	Cross-borehole Packer Tests	81
3.4	Double-packer Tests	82
3.5	Other Constant Rate Tests	84
6.4	Fractured-controlled Behaviour of Karoo Boreholes	87
4.1	Fracture Hydraulics	87
4.2	Fracture Mechanics	89
6.5	Dolerite Dykes	90
6.6	Hydrochemical Action	90
6.7	Analytical Models for Karoo Aquifers	91
6.8	Discussion	92

Chapter 7

A Numerical Model for the Campus Test Site

7.1	Introduction	95
7.2	Geometry of the Aquifer	95
2.1	Spatial Geometry	95
2.2	The Void Geometry	96
7.3	The Mathematical Model	96
3.1	The Saturated Flow Equation	96
3.2	Initial Condition	98
3.3	Boundary Conditions	98
3.4	Hydraulic Parameters	98
7.4	The Numerical Model	99
4.1	Discretization of the Flow Equation	99
4.2	Representation of a Borehole	99
7.5	Discussion	101

Chapter 8

Implementation of the Numerical Model

8.1	Introduction	103
8.2	Program KARO	103
2.1	General	103
2.2	Discontinuous Hydraulic Parameters	104
8.3	Pre- and Post-Processors	104
8.4	Comparison of Program KARO with Analytical Models	105
4.1	General	105
4.2	The Dirichlet Surface Source Approximation	105
4.3	The Dirichlet Line Source Approximation	107
4.4	Convergence of the Dirichlet Surface Source Approximation in Time	109
4.5	Convergence of the Dirichlet Line Source Approximation in Time	109
4.6	Convergence of the Dirichlet Surface Source Approximation in Space	109
4.7	Convergence of the Dirichlet Line Source Approximation in Space	111

4.8	Discussion	113
8.5	Numerical Model for a Simplified Karoo Aquifer	113
5.1	Description of the Aquifer	113
5.2	Results and Discussion	117

Chapter 9

Modelling the Campus Test Site

9.1	Introduction	119
9.2	Calibration and Verification of the Model	119
2.1	The Finite Element Grid	119
2.2	Calibration of the Model	119
2.3	Verification of the Model	121
9.3	Simulation of Hydraulic Tests	122
3.1	The Constant Rate Test on Borehole UP16	122
3.2	Simulation of a Short-term Constant Rate Test on Borehole UP15	124
3.3	Simulation of a Recovery Test on Borehole UP16	127
3.4	Linear Flow	128
9.4	Conclusions	128

Chapter 10

Analysis of Hydraulic Test Data from Karoo Aquifers

10.1	Introduction	133
10.2	The Numerical Vertical Flow Model	133
2.1	General	133
2.2	Numerical Experiments	134
10.3	Inverse Modelling of Hydraulic Tests	135
3.1	General	135
3.2	Computer Implementation of RPTsolv	138
3.3	Thickness of the Aquifer	139
3.4	Aquifer Boundary	140
3.5	Boundary Conditions on the Outside Boundary	141
10.4	Examples of Hydraulic Tests Analysed with program RPTSOLV	142
4.1	Constant Rate Tests at the Campus Test Site and Philippolis	142
4.2	Step Drawdown Test at Philippolis	143
4.3	Dependence of Storativity on Distance	144
10.5	Discussion	145

Chapter 11

Summary and Recommendations

11.1	General	149
11.2	Summary of the Results	149
11.3	Recommendations	152

Appendix A

The Intrusion of Laccoliths

A.1	Introduction	155
A.2	Gilbert's Theory for the Intrusion of a Laccolith	155
A.3	Bending of the Overburden	156
3.1	Uniform Driving Pressure	156
3.2	Linear Driving Pressure	158
3.3	Distribution of Shearing Stresses in the Overburden	160
A.4	Deformation of the Displaced Overburden	160
4.1	Viscosity of the Magma	160

4.2	Stretching of the Overburden	161
A.5	A Multi-layered Overburden	163

Appendix B

Description of Equipment used in the Hydraulic Tests

B.1	General	165
B.2	The Pumping System	165
B.3	Pressure transducers	165

Appendix C

Mathematical Reduction of Dimensions

C.1	Introduction	167
C.2	Mathematical Preliminaries	167
2.1	Transformation of the Elementary Volume Element	167
2.2	Cylindrical Co-ordinates	169
2.3	Leibnitz' Rule for a Vector-valued Function	169
C.3	Reducing the Dimensions of the Groundwater Flow Equation	171
	References	175
	Index	181

LIST OF FIGURES

Chapter 1

Introduction

Figure 1–1	Geological map of South Africa with the main Karoo basin.	2
Figure 1–2	Example of the fit between water levels, in a two-layer confined aquifer and the Neuman type curve for a phreatic aquifer, taken from Botha and Verwey (1992).	3

Chapter 3

The Karoo Supergroup

Figure 3–1	The Karoo Supergroup. [Adapted from Tankard et al. (1982).]	13
Figure 3–2	Schematic cross-section through the Karoo Basin. [After Rowsell and De Swardt (1976).] ..	14
Figure 3–3	Diagrammatic sketch of the Eccra Group's deposition. [Adapted from Reineck and Singh (1973).]	16
Figure 3–4	Contour map of the porosities and bulk densities of the Eccra shales in South Africa. [Redrawn from the map in Rowsell and De Swardt (1976).]	17
Figure 3–5	Models of (a) a braided river environment, and (b) a meandering river environment. [Redrawn from Scholle and Spearing (1982).]	19

Chapter 4

Magmatic Intrusions

Figure 4–1	Vertical cross-section through the laccolithic body at Insizwa. [Redrawn from Truswell (1970).]	26
Figure 4–2	Examples of linear dolerite dykes that cuts ring dykes and sills near Philippolis. [After Burger <i>et al.</i> (1981).]	28
Figure 4–3	Hypothetical shape of an intruding dyke, adapted from Maaløe (1985). The magma has reached Stage 1, where it caused the overburden to fracture to Stage 2, into which it will intrude in a fraction of a second.	28
Figure 4–4	Possible shape of a dyke, extending from the mantle to the surface. [After Maaløe (1985).] The diagram is not to scale, because the vertical elevation is 40–50 km.	29
Figure 4–5	Schematic illustration of the phenomenon of dilation. [Adapted from Park (1989).]	30
Figure 4–6	Schematic illustration of the bending of Karoo rocks by a linear dolerite dyke.	31
Figure 4–7	Bending of the Karoo formations by a laccolith, in a cutting on the N1 highway, between Philippolis and Trompsburg.	31
Figure 4–8	Schematic illustration of how an intruding laccolith will bend the sediment layers in a Karoo aquifer. [Derived from the gelatin model of Pollard and Johnson (1973).]	32
Figure 4–9	Photograph of cores from borehole CH6 on the Campus Test Site. The borehole is inclined at an angle of 45°.	33
Figure 4–10	Photographs of thin sections of (a) a fine-grained and (b) a coarse-grained dolerite dyke at Philippolis.	34

Chapter 5

Geology of the Campus and Dewetsdorp Test Sites

Figure 5–1	South-western view of the Karoo landscape near Bloemfontein. The first hill in the back-ground is the dolerite-capped Brandkop and the farthest one Leeuberg.	39
Figure 5–2	Sites studied in establishing the Beaufort Stratigraphy around Bloemfontein. The arrows represent cross-bedding directions in the Spitskop (thin) and Musgrave (broad) sandstone units.	40
Figure 5–3	Distribution of outcrops of the Musgrave and Spitskop Sandstones for eight of the sites are shown in Figure 5–2.	41
Figure 5–4	Generalised stratigraphic column of the Beaufort Group near Bloemfontein.	42
Figure 5–5	Outcrops of Musgrave Sandstone, beneath dolerite sills in the hills around Langenhoven Park, west of Bloemfontein.	43
Figure 5–6	Thin conglomerate bed at the base of the Musgrave Sandstone, in Musgrave Hill.	43
Figure 5–7	Stacked channel deposits of sandstone and grit in the Musgrave Sandstone.	44
Figure 5–8	Ferruginized and leached rock next to joints in the Spitskop Sandstone at Tafelkop.	45
Figure 5–9	Alternating layers of siltstone and mudstone (rhythmite) overlying the Campus Sandstone.	46
Figure 5–10	Northerly trending section south-west of Bloemfontein illustrating the geometry of dolerite intrusions and sediments of the Adelaide Subgroup.	47
Figure 5–11	Megascopic dome and basin structures deforming the Karoo Supergroup between Bloemfontein and Thaba Nchu.	48
Figure 5–12	Details of the longitudinal section, <i>AB</i> , in Figure 5–11, between Bloemfontein and Thaba Nchu.	49
Figure 5–13	Stereographic projection of poles and planes illustrating the regional fracture geometry of the Musgrave and Spitskop Sandstones in the Bloemfontein area.	50
Figure 5–14	Position of the Campus Test Site at the University of the Orange Free State.	51
Figure 5–15	Plan view of the boreholes and geological map of the sandstones on the Campus Test Site.	52
Figure 5–16	Geological profiles of the 24 percussion boreholes drilled on the Campus Test Site.	53
Figure 5–17	Geological profiles of the two inclined core-boreholes drilled on the Campus Test Site.	54
Figure 5–18	Contours of the Campus Test Site's topography.	57
Figure 5–19	Description, interpretation and correlation of drill-core data from the core-boreholes CH2, CH3 and CH4 on the Campus Test Site.	58
Figure 5–20	Distribution of structures, rock strength characteristics and alteration zones in the interpreted lithofacies of the Adelaide Subgroup on the Campus Test Site.	59
Figure 5–21	Contour maps of (a) the top and (b) the thickness of the Campus Sandstone on the Campus Test Site.	61
Figure 5–22	Contours for the top of the mudstones that underlie the Campus Sandstone on the Campus Test Site.	62
Figure 5–23	Conical shear fractures that developed in a palæosol within the mudstones of lithofacies 2. The white mineral coating on the surface of the fracture is baryte.	62
Figure 5–24	Photograph of a part of the core from Borehole CH3. Notice in particular the fracture marked with the comment 'total water loss'.	63
Figure 5–25	Photograph of microfractures in 0,25 mm quartz grains, from a core sample of the Campus Sandstone.	64
Figure 5–26	Detailed view of the fracture in Figure 5–24. Substantial water loss was incurred along this 80 mm fracture zone during the drilling.	64
Figure 5–27	Surface contours of the elevation of the Mode I fracture in the Campus Sandstone on the Campus Test Site.	65
Figure 5–28	Acoustic scanner images of the Campus Sandstone in (a) core-borehole CH1, and (b) percussion borehole UO5. The orientation of the oblique fracture above 23 m in Borehole UO5 is 085 65.	66
Figure 5–29	A 360° calliper diagram of the eccentricity of Borehole UO5, at a depth of 23,8 m.	66
Figure 5–30	Schematic diagram of the different geological formations and aquifers present on the Campus Test Site.	67
Figure 5–31	Presently known areal extent of the active part of the Mode I water-bearing fracture, in the	

	Campus Sandstone on the Campus Test Site.	68
Figure 5–32	Location of the three experimental sites at Dewetsdorp.	69
Figure 5–33	Plan view of the percussion borehole positions and a vertical cross-section through Experimental Site 1 at Dewetsdorp.	70
Figure 5–34	Plan view of the percussion and core borehole positions and a vertical cross-section through Experimental Site 2 at Dewetsdorp.	70
Figure 5–35	Plan view of the percussion and core-borehole positions and a vertical cross-section through Experimental Site 3 at Dewetsdorp.	71
Figure 5–36	Geological logs of the percussion boreholes on the experimental sites at Dewetsdorp. ...	72

Chapter 6

The Physical Behaviour of Karoo Aquifers

Figure 6–1	Schematic representation of a slab-shaped, dual-porosity medium. [After (Moench, 1984).]	76
Figure 6–2	Schematic illustration of the parallel plate model for a fracture.	77
Figure 6–3	Water-level contours of the aquifers on the Campus Test Site before and after repeating the constant rate test where Borehole UO5 was pumped at $2,25 \text{ m}^3 \text{ h}^{-1}$ for the third time. (Depth of pump = 22 m.)	78
Figure 6–4	Drawdowns observed in boreholes UO4, UO8 and UO12 during a series of five constant rate tests performed on the Campus Test Site.	79
Figure 6–5	Dependence of the Theis-fitted S -value ratios on the inverse ratio, of the distance between the observation and perturbed borehole. (Subscripts 1 and 2 denote members 3 and 5 of the tests, in which boreholes UO5 and UP16 were pumped at a rate of $2,25 \text{ m}^3 \text{ h}^{-1}$.)	80
Figure 6–6	Representative graphs of the Theis-fitted S - and T -values for the Class 3 boreholes as a function of the discharge rate.	81
Figure 6–7	Graphs of the horizontal hydraulic conductivities in Table 6–3.	83
Figure 6–8	Pumping rates and drawdowns observed in boreholes UO9, UP15, UP16 and UO20 during the constant rate test on Borehole UP16 at the Campus Test Site.	84
Figure 6–9	Graph of the water levels observed in Borehole D19 at Philippolis during a constant rate test carried out by Botha <i>et al.</i> (1996).	85
Figure 6–10	Graphs of the water levels in boreholes UP16 and UO5 during a constant rate test performed on 1995–05–15 with UP 16 as the perturbed borehole.	86
Figure 6–11	Graphs of the water levels in boreholes UO5, UO11, UP15 and UO20 during a constant rate test performed on 1995–06–01 with Borehole UP15 as the perturbed borehole.	86
Figure 6–12	Behaviour of the water levels in Borehole D20 at Philippolis during a constant rate test and the fourth step of a step drawdown test. (The step drawdown test's time scale is shown on the upper time axis.)	87
Figure 6–13	Graphs of the piezometric heads, in the three aquifers on the Campus Test Site, as measured in Piezometer UO18, during the constant rate test of 1995–05–15 on Borehole UP16. ...	88
Figure 6–14	Drawdowns observed during a constant rate test on a high-yielding borehole at Kokstad. ($Q = 46,8 \text{ m}^3 \text{ h}^{-1}$.)	89
Figure 6–15	Least square fits of Equations (6.4) and (6.5) to the drawdowns observed in Borehole G39973 at Calvinia.	92

Chapter 7

A Numerical Model for the Campus Test Site

Figure 7–1	Comparison of the hydraulic and geological properties of the upper rhythmite layers in boreholes UO4 and UP16 on the Campus Test Site.	97
------------	---	----

Chapter 8

Implementation of the Numerical Model

Figure 8–1	Approximation of discontinuities in the Galerkin finite element method, with quadrilateral elements.	104
Figure 8–2	Schematic diagram of the hypothetical aquifer used in the study of the finite boundary	

	problem.	106
Figure 8–3	Comparison of the Muskat solution with the Neumann and Dirichlet surface source approximations as a function of the distance (r), at the time steps 0,5 and 2 h.	107
Figure 8–4	Comparison of the Muskat solution with the Neumann and Dirichlet surface source approximations, for different finite element sizes.	108
Figure 8–5	Schematic representation of the hypothetical aquifer used to study the behaviour of the Dirichlet method, when the borehole is represented as a line source.	108
Figure 8–6	Comparison of the Muskat and line source approximation of a borehole, for the different finite element grids.	109
Figure 8–7	Convergence of the Dirichlet surface source approximation as a function of the time step, at different distances (r) from the borehole.	110
Figure 8–8	Convergence of the Dirichlet line source approximation, as a function of the time step, at different distances (r) from the borehole.	110
Figure 8–9	Plan (a) and side (b) views of the initial finite element grid used to study the convergence properties of the Dirichlet surface source approximation.	111
Figure 8–10	Errors in the Dirichlet surface source approximation as a function of the maximum angular element size, at different distances (r) from the borehole.	111
Figure 8–11	Errors in the Dirichlet line source approximation as a function of the maximum radial element size, at different distances (r) from the borehole.	112
Figure 8–12	Behaviour of the true and associated homogeneous piezometric head of the Dirichlet surface source approximation as a function of the time step (Δt).	112
Figure 8–13	Convergence of the Dirichlet line source approximation as a function of the maximum element size, at different distances (r) from the borehole.	113
Figure 8–14	Sketch of the upper right-hand quarter of the hypothetical aquifer used to study the behaviour of a fracture in a Karoo aquifer.	114
Figure 8–15	The three-dimensional finite element grid used to study the behaviour of the hypothetical aquifer, in Figure 8–14.	114
Figure 8–16	Changes in the piezometric heads of the hypothetical aquifer with elevation, at distances of (a) 0,5 m and (b) 16 m from the borehole, for different times.	115
Figure 8–17	Volumetric visualization of the 19,8 m piezometric contour in the aquifer, when pumping boreholes 1, 3 and 4 simultaneously, after (a) 8 h and (b) 72 h.	116

Chapter 9

Modelling the Campus Test Site

Figure 9–1	Finite element grid used in modelling the aquifer on the Campus Test Site.	120
Figure 9–2	Comparison of the observed and simulated piezometric heads in Piezometer UO18, for the constant rate test performed on 1995–06–01 with UP 15 as the perturbed borehole.	122
Figure 9–3	Comparison of the observed and simulated piezometric heads in piezometers UO1 and UO18, for the hydraulic test of 1995–05–15 on Borehole UP16, with Dirichlet boundary conditions on the four vertical sides of the aquifer.	123
Figure 9–4	Comparison of the observed and simulated piezometric heads in piezometers UO1 and UO18, for the hydraulic test of 1995–05–15 on Borehole UP16, with zero-flux Neumann boundary conditions on the four vertical sides of the aquifer.	124
Figure 9–5	Comparison of the observed and simulated piezometric heads in piezometers UO1 and UO18, after pumping Borehole UP16 for 0,5 and 1 h.	125
Figure 9–6	Comparison of the observed water levels and simulated piezometric heads, in boreholes UP16 and UO5, after pumping Borehole UP16 for 0,5 and 1 (h).	126
Figure 9–7	Comparison of the observed water levels and simulated piezometric heads in borehole Borehole UP15 and Piezometer UO18, after pumping Borehole UP15 for 0,5 and 1 h at a rate of $9,72 \text{ m}^3 \text{ h}^{-1}$	127
Figure 9–8	Piezometric heads in the fracture plane and a plane 1 (m) above the fracture in the sandstone layer, across a vertical cross-section through Borehole UP16, after pumping Borehole UP16 at $3,6 \text{ m}^3 \text{ h}^{-1}$ for 0,25 and 1 h.	128
Figure 9–9	Piezometric heads in (a) the fracture, and (b) a plane 1 m above the fracture, across a vertical cross-section through Borehole UP15, after pumping Borehole UP15 at rates of 3,6, 7,2 and $9,72 \text{ m}^3 \text{ h}^{-1}$ for 1 h.	129

Figure 9–10	Comparison of the simulated piezometric heads, at the centre of the fracture, and the water levels in Borehole UP16, for the first step of a multi-rate test as a function of the time. 130
Figure 9–11	Comparison of the simulated piezometric heads, at the centre of the fracture, and the water levels in Borehole UP16, for the first step of a multi-rate test as a function of \sqrt{t} 130

Chapter 10

Analysis of Hydraulic Test Data from Karoo Aquifers

Figure 10–1	The two-layered aquifer used to represent the aquifer on the Campus Test Site in the vertical two-dimensional numerical model. 135
Figure 10–2	Computed drawdowns in the piezometric heads at various distances, along the centre planes of the two layers in Figure 10–1, with the new program and Program SAT3. 136
Figure 10–3	Drawdowns in the piezometric heads at various distances, along the centre horizontal planes of the two layers in Figure 10–1, computed with the vertical two-dimensional model. . 136
Figure 10–4	Contours of the computed drawdowns in piezometric heads after 48 h. 137
Figure 10–5	Influence of the thickness of Layer 2 and the aquifer, expressed as the ratio (x : y), on the drawdowns of a hypothetical aquifer. 139
Figure 10–6	Comparison of the observed and fitted drawdowns for the Kokstad hydraulic test, with aquifer radii of 528, 1 024 and 2 048 m. 140
Figure 10–7	Comparison of the observed and fitted drawdowns for the Kokstad hydraulic test, with the default aquifer radius of 1 024 m, and the force fitted drawdowns of the 528 and 2 048 m radii data. 141
Figure 10–8	The effect of zero-flux and constant head boundary conditions on the fitted drawdowns for the hydraulic test at Kokstad ($R = 1\,024\text{ m}$). 142
Figure 10–9	Comparison of the observed and fitted drawdowns for: (a) Borehole UP15 on the Campus Test Site, and (b) boreholes D19 and D20 at Philippolis. 143
Figure 10–10	Observed and fitted drawdown curves for the step test on A14 at Philippolis district, with an aquifer thickness of 40 m and Layer 2 thicknesses of 6 and 8 m. 144
Figure 10–11	Graphs of the storativities in Table 10–8 as a function of the inverse distance from the perturbed borehole. 145
Figure 10–12	Differences between the drawdowns observed in Borehole UO7 and those fitted with RPTSOLV. 146

Appendix A

The Intrusion of Laccoliths

Figure A–1	Gilbert’s model for the intrusion of magma. 156
Figure A–2	Relation between the driving pressure of the magma and height of a fracture, in an overburden 40 m thick, for a given density. 157
Figure A–3	Schematic representation of the intrusion of magma into an overburden consisting of different strata. 157
Figure A–4	Two common plan shapes described by Equation (A.4). 158
Figure A–5	Cross-sections of the displacements caused by (a) an anticlinal and (b) a circular laccolithic intrusion. 159
Figure A–6	Linear pressure distribution over an anticlinal laccolithic intrusion. 159
Figure A–7	Displacement profiles of the layers over an anticlinal laccolith subject to: (a) a uniform, (b) a linear and (c) a discrete driving pressure. 160
Figure A–8	Distribution of the maximum shear stresses in a layer overlying a laccolithic intrusion. (a) Theoretical distribution for a layer, with a length to thickness ratio of 4. (b) Contours of the isochromatics determined from a photo-elastic gelatin model. [Redrawn from Pollard and Johnson (1973).] 161
Figure A–9	Schematic representation of a non-uniform pressure distribution over a laccolithic intrusion. The driving pressure, with a constant magnitude, p'_d acts out only over the distance l in the x -direction. 162
Figure A–10	Schematic representation of the stretching in the centre plane of a layer displaced to its maximum, w_m , by an intruding laccolith. 162
Figure A–11	Schematic representation of the longitudinal bending strains across a layer deformed by a

	laccolith.	163
Figure A-12	Formation of a peripheral dyke in experimental gelatin models. [Redrawn from Pollard and Johnson (1973).]	163

Appendix B

Description of Equipment used in the Hydraulic Tests

Figure B-1	Graphical illustration of the pumping system used in most of the hydraulic tests described in the report.	165
Figure B-2	Calibration curve for one of the transducers used in the project.	166

Appendix C

Mathematical Reduction of Dimensions

Figure C-1	Schematic representation of the unit vectors associated with two orthogonal co-ordinate systems.	167
Figure C-2	Diagrammatic illustration of the relation between the Cartesian co-ordinates, (x, y, z) , and cylindrical co-ordinates (r, ϕ, z)	169

LIST OF TABLES

Chapter 3

The Karoo Supergroup

Table 3–1	Porosities of the Clarens Formation. [After Beukes (1969).]	21
-----------	---	----

Chapter 4

Magmatic Intrusions

Table 4–1	Summary of the characteristics of dolerite dykes, at Philippolis and Rouxville, and the yields of boreholes, which intersected them.	35
-----------	--	----

Chapter 5

Geology of the Campus and Dewetsdorp Test Sites

Table 5–1(a)	Geological profiles of the core-boreholes CH1 and CH2, drilled on the Campus Test Site.	55
Table 5–1(b)	Geological profiles of the core-boreholes CH3 and CH4, drilled on the Campus Test Site.	56
Table 5–2	Order of competency of the lithofacies in Figure 5–20, arranged from the highest to lowest (bottom to top).	57
Table 5–3	Variation in grain size, within the stacked facies units of Figure 5–20 from bottom to top.	60

Chapter 6

The Physical Behaviour of Karoo Aquifers

Table 6–1	Behaviour of drawdowns in boreholes UO1 – UP16 on the Campus Test Site.	78
Table 6–2	Hydraulic parameters for the Class 3 boreholes obtained from a fit of the drawdowns observed when Borehole UO5 was pumped at a rate of $2,25 \text{ m}^3 \text{ h}^{-1}$, with the pump installed at depths of 22 and 30 m.	80
Table 6–3	Averaged values of the horizontal hydraulic conductivities, K_h , for the more important formations on the Campus Test Site as determined from double-packer tests.	83
Table 6–4	Transmissivities of Borehole UO5 on the Campus Test Site, derived from student slug tests.	89

Chapter 7

A Numerical Model for the Campus Test Site

Table 7–1	Comparison of the collar height and elevations of the sandstone and mudstone layers of Aquifer 3 with the piezometric heads in piezometers UO1 and UO18, as measured on 1995–05–15.	96
Table 7–2	Piezometric heads of the three aquifers as measured on 1995–05–15 in piezometers UO1 and UO18.	98

Chapter 8

Implementation of the Numerical Model

Table 8–1	Radial intervals used to generate the finite element grid in the horizontal plane.	106
Table 8–2	Hydraulic parameters of the aquifer used in the study of the Dirichlet surface and line source approximations.	106
Table 8–3	Distances of the nodes (from the bottom up), in the vertical plane of the finite element grid in Figure 8–15.	114
Table 8–4	Hydraulic conductivity and specific storativity values of the rock matrix and fracture, used in the numerical model.	117

Chapter 9

Modelling the Campus Test Site

Table 9–1	Principal components of the hydraulic conductivity tensor and storativities, used in modelling the Campus Aquifer.	121
-----------	---	-----

Chapter 10

Analysis of Hydraulic Test Data from Karoo Aquifers

Table 10–1	Comparison of the hydraulic parameters and source terms required by a three-dimensional, a horizontal two-dimensional and a vertical two-dimensional flow model.	134
Table 10–2	Aquifer parameters of the hypothetical aquifer used to compare the vertical flow program and the three-dimensional Program SAT3.	134
Table 10–3	Hydraulic parameters and least squares error (χ^2) for the three fits of the Kokstad data in Figures 10–6 and 10–7.	140
Table 10–4	Comparison of the hydraulic conductivities and specific storativities obtained from Program RPTSOLV for the Kokstad data with Dirichlet and Neumann boundary conditions.	141
Table 10–5	Aquifer parameters for the two field tests, determined with the two-dimensional vertical flow model.	142
Table 10–6	Summary of the step drawdown test performed on Borehole A14 at Philippolis.	143
Table 10–7	Fitted hydraulic parameters for Borehole A14 at Philippolis.	144
Table 10–8	Comparison of the hydraulic parameters derived from fitting drawdowns, observed during a constant rate test on Borehole UP16, with RPTSOLV and the Theis equation.	144

LIST OF SYMBOLS

1 LATIN SYMBOLS

A	= An $N \times N$ matrix	
a	= Intercept of a straight line	
a	= Length of an undeformed layer's centre plane	[L]
a	= Set of parameters	
a	= Width of a fracture	[L]
$\mathbf{A}(u, v, w)$	= Vector-valued function in the co-ordinates u	
a'	= Length of a deformed layer's centre plane	[L]
a_{ij}	= The ij -th element of A	
B	= An $N \times N$ matrix	
b	= Aperture of a fracture	[L]
b	= Slope of a straight line	
B	= Elastic modulus of a single-layered overburden	[M L ⁻¹ T ²]
B_i	= Elastic modulus of the i -th layer in a multi-layered overburden	[M L ⁻¹ T ²]
b_{ij}	= The ij -th element of the matrix B	
c_i	= Series expansion coefficients	
D	= Flexural rigidity of a plate	[M L ² T ²]
d	= Thickness of an aquifer, or overburden	[L]
D_e	= Effective flexural rigidity of a set of n free-sliding layers	[M L ² T ²]
$Df(t)$	= Derivative of f with respect to t	
d_i	= Thickness of the i -th layer in a multi-layered aquifer	[L]
D_t	= Partial derivative with respect to t	
du	= Elementary distance vector in the co-ordinates u	[L]
D_x	= Derivative with respect to x	[L ⁻¹]
dx	= Elementary distance vector in the co-ordinates x	[L]
E	= Young's modulus	[M L ⁻¹ T ²]
e_{xx}^b	= Longitudinal strain of a layer due to bending	[1]
e_{xx}^s	= Longitudinal strain of a layer due to stretching	[1]
e_u, e_v, e_w	= The set of orthogonal unit vectors in the co-ordinate system u	
F	= The $N \times 1$ finite element source vector	[T ⁻¹]
$f(\mathbf{x}, t)$	= Strength of a source or sink	[T ⁻¹]
f_i	= The i -th element of the vector F	[T ⁻¹]
g	= Acceleration of gravity	[M L T ⁻²]
$g_i(\mathbf{x})$	= Functions of the spatial co-ordinates x	
h	= Height of a fracture above the source	[L]
h	= Water pressure in calibration curve of pressure transducer	[L]
$h(\mathbf{x}, t)$	= Pressure head	[L]
h_u, h_v, h_w	= Scaling factors of the u co-ordinate system	[1]
I	= Electric current in calibration curve of pressure transducer	[A]
i, j, k	= The set of orthogonal unit vectors in the co-ordinate system x	
J	= The Jacobian matrix of the transformation from x to u	
J	= The Jacobian, i.e. the determinant of J	
$J_0(z), J_1(z)$	= Zero and first order Bessel functions	
K	= Hydraulic conductivity tensor	[L T ⁻¹]

K	= Magnitude of the hydraulic conductivity tensor	$[L\ T^{-1}]$
K_d	= Directional hydraulic conductivity	$[L\ T^{-1}]$
K_h	= Horizontal hydraulic conductivity	$[L\ T^{-1}]$
K_i	= Hydraulic conductivity of the i -th layer in a multi-layered aquifer	$[L\ T^{-1}]$
l	= Sealed off length in a packer test	$[L]$
\mathbf{L}	= Symbolic differential operator	
M	= Number of finite element nodes on the boundary of the borehole	
\mathbf{N}	= Normal force acting in a vertical plane	$[M\ L^1\ T^{-2}]$
N	= Number of finite element nodes	
\mathbf{n}	= Unit normal vector	
p	= Fluid pressure	$[M\ L^{-1}\ T^{-2}]$
p	= Pressure of a magma	$[M\ L^{-1}\ T^{-2}]$
p_0	= Lithostatic pressure	$[M\ L^{-1}\ T^{-2}]$
p_0	= Pressure at reference plane	$[M\ L^{-1}\ T^{-2}]$
$p_d(\mathbf{x}, y)$	= Driving pressure for intruding magma	$[M\ L^{-1}\ T^{-2}]$
p_i	= Inner pressure	$[M\ L^{-1}\ T^{-2}]$
p_m	= Overpressure in a magma chamber	$[M\ L^{-1}\ T^{-2}]$
p_o	= Outer pressure	$[M\ L^{-1}\ T^{-2}]$
p_z	= Pressure difference between a magma and a dyke	$[M\ L^{-1}\ T^{-2}]$
\mathbf{Q}	= Discharge rate of a fracture, or pump	$[L^3\ T^{-1}]$
Q	= Magnitude of \mathbf{Q} , or injection rate	$[L^3\ T^{-1}]$
\mathbf{Q}	= The $N \times 1$ finite element flux vector	$[L^3\ T^{-1}]$
$Q(t)$	= Recharge (+) or discharge (–) rate of a borehole	$[L^3\ T^{-1}]$
$\mathbf{q}(\mathbf{x}, t)$	= Darcy velocity	$[L\ T^{-1}]$
$q(\mathbf{x}, t)$	= Magnitude of the Darcy velocity	$[L\ T^{-1}]$
\mathbf{Q}_D	= Finite element flux vector for Dirichlet boundary conditions	$[L^3\ T^{-1}]$
Q_D	= Recharge or discharge rate for Dirichlet boundary conditions	$[L^3\ T^{-1}]$
q_{Di}	= Darcy velocity across the side of an element, containing node i	$[L\ T^{-1}]$
q_i	= The i -th element of \mathbf{Q}	$[L\ T^{-1}]$
r	= Radial distance	$[L]$
R	= Radius of an aquifer	$[L]$
r	= Scaling ratio	$[1]$
\mathbf{r}	= The position vector from the \mathbf{x} to the \mathbf{u} co-ordinate system	$[L]$
$r_{1,2}$	= Radii of curvature	$[L]$
r_b	= Radius of section sealed-off with packers	$[L]$
R^n	= Dimension of the Euclidean space	
S	= Magnitude of the total shearing force	$[M\ L\ T^{-2}]$
S	= Storativity of an aquifer	$[1]$
\mathbf{S}	= Total shearing force	$[M\ L\ T^{-2}]$
$s(t)$	= Drawdown in a borehole	$[L]$
$S(\mathbf{x})$	= Storativity of a confined aquifer	$[1]$
$S_0(\mathbf{x})$	= Specific storativity of an aquifer	$[L^{-1}]$
$S_{0i}(\mathbf{x})$	= Specific storativity of the i -th layer in a multi-layered aquifer	$[L^{-1}]$
S_i	= Storativity of the i -th layer of a multi-layered aquifer	$[1]$
t	= Time	$[T]$
T	= Transmissivity of an aquifer	$[L^2\ T^{-1}]$
\mathbf{T}	= Transmissivity tensor of an aquifer	$[L^2\ T^{-1}]$
T_e	= Effective thickness of an n -layered overburden	$[L]$
T_i	= Transmissivity of the i -th layer of a multi-layered aquifer	$[L^2\ T^{-1}]$
\mathbf{u}	= A three-dimensional set of orthogonal co-ordinates (u, v, w)	$[L]$
u	= Prescribed nodal function	
W	= Magnitude of \mathbf{W}	$[M]$
\mathbf{W}	= Weight of rock mass	$[M]$
$w(x, y)$	= Vertical displacement in a single layer above the laccolith	$[L]$
w_m	= Maximum vertical displacement of a layer above a laccolith	$[L]$
\mathbf{x}	= Cartesian co-ordinates of a point = (x, y, z)	$[L]$
z	= Elevation above a datum level	$[L]$

2 GREEK SYMBOLS

∇	= Gradient operator	[L ⁻¹]
α	= Intercept of a straight line	
β	= Slope of a straight line	
Δ	= Small increment	
$\delta(x - x_0)$	= Dirac delta function	[1]
$d\Gamma$	= Elementary volume element in the space Γ	[L ³]
$d\Omega$	= Elementary volume element in the domain spanned by co-ordinates \mathbf{x}	[L ³]
$\Phi(u, v, w)$	= Scalar function in the co-ordinates \mathbf{x}	
$\phi_j(\mathbf{x}, t)$	= The j -th finite element basis function	
Γ	= Space spanned by the co-ordinates \mathbf{u}	[L ³]
ξ	= A three-dimensional set of orthogonal co-ordinates (ξ, η, ζ)	[L]
κ	= A unit Cartesian vector	
λ	= A constant in the Dirichlet approximation of a borehole	
μ	= Viscosity of a fluid	[M L ⁻¹ T ⁻¹]
ρ	= Density of a fluid	[M L ⁻³]
ρ_m	= Density of a magma	[M L ⁻³]
ρ_r	= Density of rock mass	[M L ⁻³]
σ	= Poisson's ratio	[1]
σ	= Shearing force over an area	[M L ⁻¹ T ⁻²]
σ	= The surface tension of water	[M T ⁻²]
$\sigma_{xx}, \sigma_{xz}, \sigma_{zz}$	= Components of normal and shear stresses in the (x, z) plane	[M L ⁻¹ T ⁻²]
Ω	= Domain of differential equation	[L ³]
Ω	= Space spanned by the by co-ordinates \mathbf{x}	[L ³]
$\varphi(\mathbf{x}, t)$	= Piezometric head	[L]
$\varphi(\mathbf{x}_j, t_n)$	= Exact value of $\varphi(\mathbf{x}, t)$ at the finite element node j and time step Δt_n	[L]
φ_0	= Prescribed piezometric heads	[L]
φ'	= Finite element approximation of homogeneous piezometric head	[L]
φ_b	= Arbitrary set of piezometric heads on boundary of a borehole	[L]
φ_D^{n+1}	= Finite element approximation of Dirichlet piezometric head	[L]
φ^n	= Finite element approximation of $\varphi(\mathbf{x}, t_n)$	[L]
ε	= Porosity of a medium	[1]
$\partial\Omega$	= Boundary of Ω	[L ²]

CHAPTER 1

INTRODUCTION

1.1 GENERAL

Water, particularly fresh or potable water, is indispensable for all man's activities on earth. Approximately 75% of the total volume of fresh water on earth is frozen in glaciers, while rivers and lakes hold approximately 0,33%. The remaining 24,67% occurs as groundwater (Chorley, 1969; Zumberge and Nelson, 1984). Since the water in glaciers is not available for general consumption, groundwater forms the largest source of fresh water available to man.

The situation in South Africa, however, is complicated because of the nature of the aquifers. Here groundwater is usually regarded as an unreliable source of water. The result is that groundwater contributes only 10% to the national water budget (Department of Water Affairs, 1986). The surface water resources, however, have now almost been exploited to their limits. South Africa, therefore, will have to make greater use of its groundwater resources in the future, to meet the demand of the growing population, and also in a more efficient manner. This is especially true in the semi-arid and arid central and western regions of South Africa, which cover approximately 66% of the country (Department of Water Affairs, 1986), where there are no major rivers, or other surface sources. The majority of the inhabitants in these areas therefore depend on groundwater for their water supply. A large part of these regions, and approximately 50% of the country as a whole, is underlain by the so-called *Karoo Supergroup* of geological formations (see Figure 1–1). The potential thus exists that aquifers in the Karoo Supergroup can make a significant contribution to the water budget of the country. Unfortunately, Karoo aquifers have a very complex and unpredictable behaviour. The general view is thus that Karoo aquifers are not reliable sources of water, although there are boreholes which have provided the residents of farms and towns sustainably with water for many years.

A major characteristic of the Karoo Supergroup, which consists mainly of sandstones, mudstones, shales and siltstones, is their low permeability. The majority of boreholes drilled in the Karoo formations therefore have very low yields ($< 3,6 \text{ m}^3 \text{ h}^{-1}$). Indeed, the common view is that Karoo aquifers do not contain large quantities of groundwater, hence the name Karoo, which is the Hottentot word for dry. However, large volumes of groundwater are pumped from mines and the basements of buildings daily in areas underlain by the Karoo formations, which is not what one would expect from aquifers with a limited yield. A number of studies, of which the one by Kirchner *et al.* (1991) was perhaps the most detailed, were therefore undertaken in the past in an attempt to utilize these aquifers more efficiently.

1.2 BACKGROUND OF THE STUDY

The main objective in the study of Kirchner and co-workers was to determine the recharge potential of the Karoo aquifers. To achieve this, they had to know the storage capacity of the aquifers. Two approaches were used for this purpose. The first was to determine the storativity of the aquifers through hydraulic tests, and the second to study the water balance of the aquifers. Since the Karoo Supergroup consists of sedimentary rocks, they assumed that their hydraulic tests could be analysed with the classical Theis equation. However, this yielded storativity values $\sim 10^{-6}$, three orders of magnitude smaller than that obtained from the water balance studies. Since the result of the water balance studies agreed more with the historical operation of the aquifers, Kirchner and his co-workers assumed that the result from the hydraulic tests was wrong, and neglected it.

Although there exist other methods with which the hydraulic parameters of an aquifer can be determined, the hydraulic (or pumping) test still remains the much preferred method. In this method, one first observes a series of water levels, and then tries to fit them to a so-called *type curve*, which depends on the hydraulic parameters. The main reason for the popularity of the method is that there exist a large number of graphical techniques that can be used in fitting the data (Kruseman and De Ridder, 1991), although automated techniques are now available (Duffield and Rumbaugh, 1991). However, the method does not differ essentially from the classical method of curve-fitting. The danger thus always exists that the data can be

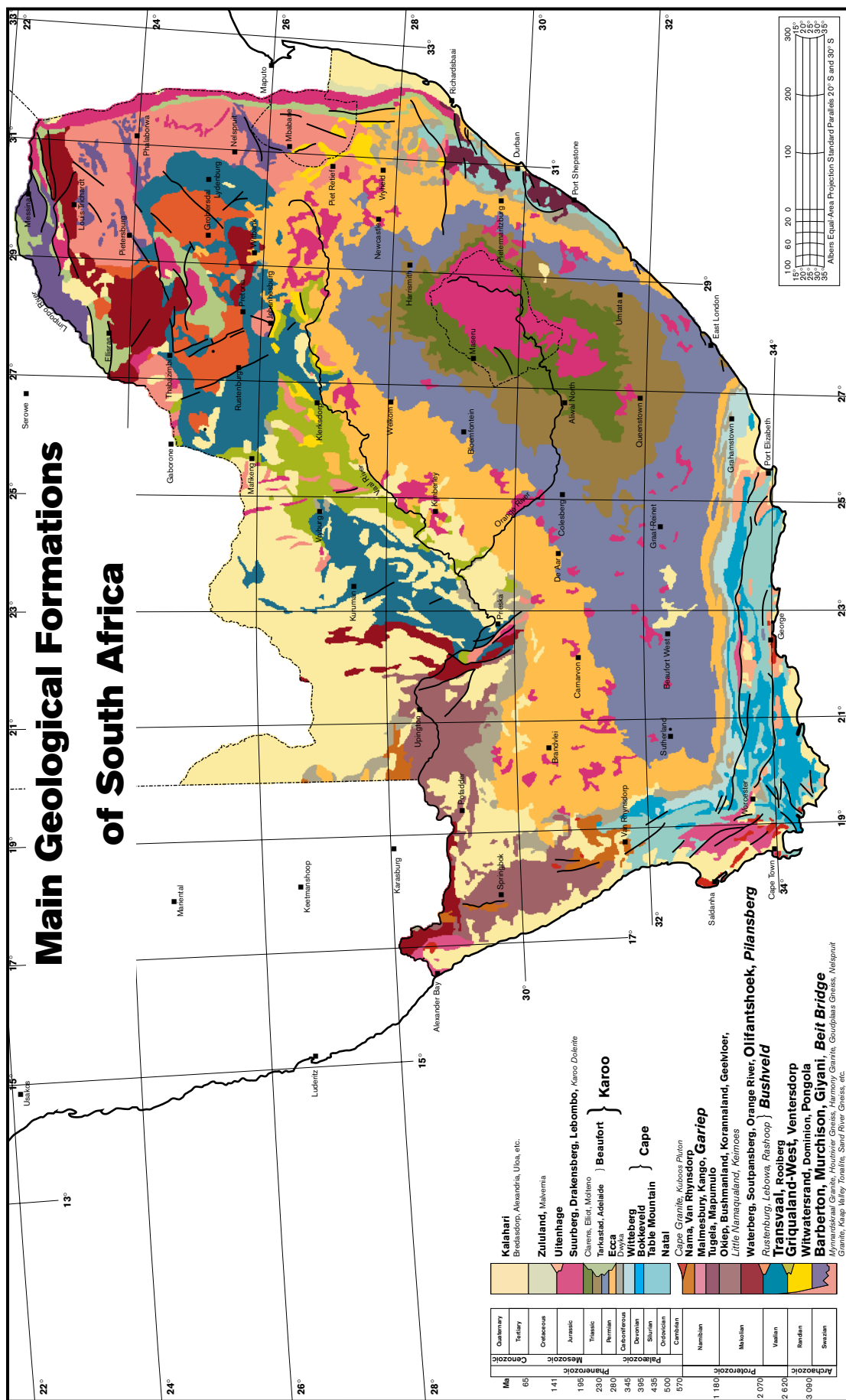


Figure 1-1 Geological map of South Africa with the main Karoo basin.

fitted to a wrong type curve as illustrated in Figure 1–2. The application of these methods is thus not as straightforward as textbooks would like one to believe. This applies particularly in cases where the behaviour of the aquifer may deviate from the basic assumptions made in the derivation of the type curve. It is thus imperative that the practitioner of the method should make sure that the type curve he or she is using, is indeed applicable to the aquifer, as illustrated by the work of Boehmer and Boonstra (1986) on intrusive dykes in the Karoo sediments.

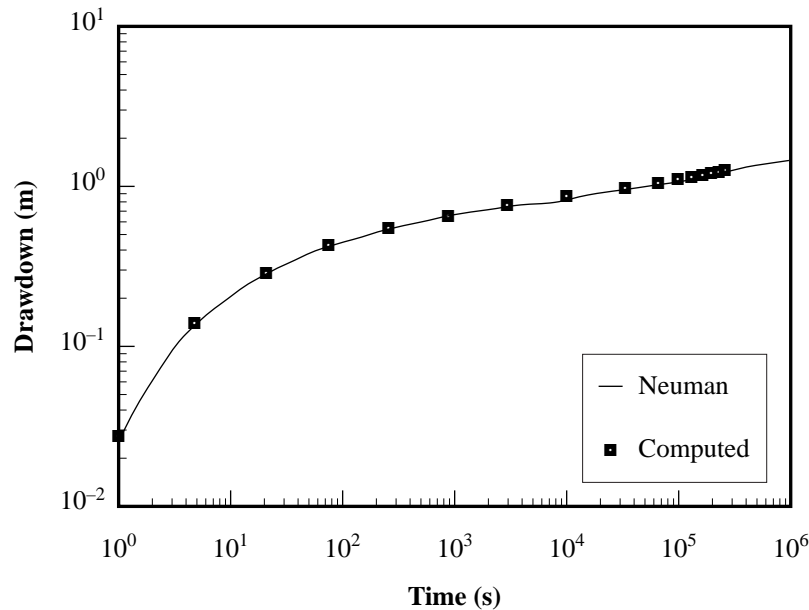


Figure 1–2 Example of the fit between water levels, in a two-layer confined aquifer and the Neuman type curve for a phreatic aquifer, taken from Botha and Verwey (1992).

There was therefore a strong possibility that the methods Kirchner *et al.* (1991) used to analyse their hydraulic tests, misrepresented the aquifers' properties and physical behaviour. It was thus quite natural for them to doubt the results of their hydraulic tests. Unfortunately, too little information was available at that stage on the nature of Karoo aquifers to try to determine precisely what the problem was. The Water Research Commission was thus approached with the request to fund a more detailed investigation of these and other hard-rock aquifers in South Africa.

1.3 OBJECTIVES OF THE STUDY

The objectives of the present study as set out in the original project proposal to the Water Research Commission were as follows:

- An investigation of the nature and behaviour of secondary aquifers, with special reference to the applicability and reliability of existing conceptual models for the description and analysis of hydraulic tests, conducted in these aquifers.
- The development of improved and/or new techniques for the implementation and analysis of hydraulic tests in secondary aquifers.
- Integration of the improved and/or new techniques, developed in (b), into a user-friendly computer package for the analysis of hydraulic tests in secondary aquifers.

The original idea was to cover all the major secondary aquifers that occur in South Africa—Karoo, dolomitic, igneous and metamorphic—in the project. Since Karoo aquifers were the most accessible to the project team, it was natural to start the investigations with these. However, it soon became clear that the behaviour of these aquifers does not conform to the behaviour of conventional aquifers as described in the literature. This presented the project team with a difficult decision—abandon Karoo aquifers and continue with the others, or concentrate exclusively on Karoo aquifers and try to understand their behaviour. Since Karoo aquifers are the most extensive type of aquifer present in South Africa, the latter alternative was put to the Steering Committee of the project, who accepted it. The discussion in this report is therefore limited to Karoo aquifers, to which the research effort was thereafter restricted.

A Technical Committee appointed by the Steering Committee decided during a field visit in March 1994, that the project could benefit from a more detailed analysis of the structural and geological aspects of Karoo formations. They therefore requested that Dr. W.P. Colliston and Mr. J.C. Looek of the Department of Geology at the University of the Free State should become active co-workers on the project, and that the duration of the project be extended by one year. The objectives of this extension as set out in the revised final contract with the Water Research Commission were as follows:

- (a) To provide an integrated geological working model for the sandstone/shale aquifer(s) at the Campus Test Site of the Institute for Groundwater Studies. This model may be used to supplement and test the current and future numerical models for fractured aquifers as for example those developed by the Institute for Groundwater Studies at the UOFS.
- (b) To determine and assess the association of structural geological planar structures (e.g. joints, fractures and faults) and sedimentology (palaeoflow direction, grain framework and microstructure) with potential groundwater reservoirs in the competent rocks of the Karoo Supergroup.
- (c) Representation of the aquifers' geometry by means of fractals.
- (d) The development of hydraulic tests that will also reflect the geometry of the aquifer and not only its relational parameters, as is the case with existing methods.

The attainment of these objectives was, unfortunately, hampered by two unexpected developments. The first was a considerable delay in the approval for the continuation of the project, and the second the resignation of Mr. J.P. Verwey, the key researcher responsible for the field investigations. The result was that the field work had to be restricted to the Campus Test Site, and that none of the more esoteric aquifer tests envisaged in the motivation for the continuation of the project, could be performed. However, this loss was somewhat offset by the information gained during the co-operation with the Consulting Engineers, Cahi De Vries, in the development of a new well-field for the Municipality of Philippolis, and later also for the Municipality of Rouxville.

1.4 METHODOLOGY USED IN THE INVESTIGATIONS

1.4.1 The Nature of Groundwater Motion

Groundwater does not exist in a vacuum, but in the interstices that occur naturally in all geological formations on earth. There are thus essentially three research fields that need to be considered in a scientific study of groundwater phenomena.

- (a) The environment, i.e. the geological formations in which groundwater flow occurs.
- (b) A study of the interactions between the water and the geological formations.
- (c) The formal description of the interactions.

The first step in the study of any aquifer should thus be to understand the geology of the area in which it occurs. Although the behaviour of the aquifer will mainly be determined by the current state of the geology, this state is the result of an evolutionary process that took place over many years, even millions of years, as is the case with Karoo aquifers. It was thus thought worthwhile not to concentrate on the present state of the Karoo Supergroup alone, but also to look at its historical evolution, as this may explain some features in the current state that would be difficult to explain otherwise.

The interactions between the water and the geological formations will obviously be controlled by the laws of physics and chemistry. These laws are embedded in physical theories and described in the conventional language of physics—mathematics. Any discussion of groundwater motion must consequently refer to elements from these three subjects at one time or another.

A theory is in essence an abstract and general description of a natural phenomenon, or a group of such phenomena. To apply it to a particular object of study, such as a specific aquifer, requires that one must develop what Botha (1994) calls a *conceptual model* for the object. A conceptual model is nothing more than a mental interpretation of the object, and can be expressed in any convenient form. However, the easiest method to relate the model to the underlying theory is to couch it also in the mathematical language of physics.

1.4.2 Experimental Sites

The geology and the behaviour of the aquifers were mainly studied at five experimental sites, developed specifically for this project, and during the development of water supply schemes for the Municipalities of Philippolis and Rouxville. The first experimental site, henceforth referred to as the Campus Test Site, is situated on the Campus of the University of the Free State in Bloemfontein, and the other four at Dewetsdorp,

77 km east of Bloemfontein.

Five percussion boreholes, scattered across the Campus Test Site, existed at the beginning of the project in 1992. These boreholes were drilled by the Department of Geohydrology at the University of the Free State, to whom the site belongs. The first step was thus to drill an additional 11 percussion boreholes on the site. The first 10 of these boreholes were drilled with funds from the Water Research Commission, while the other one was drilled by the Department of Geohydrology. Six of these boreholes were drilled specifically with the view to perform cross-borehole packer tests, since the work at Atlantis (Botha *et al.*, 1990) suggested that it is an ideal method to use in the investigation of hard-rock aquifers. The other five boreholes were drilled mainly to try to clarify anomalies, observed in the water levels of the newly drilled six and the existing five boreholes. An additional 15 boreholes have since been drilled on the site. Seven of these additional boreholes are core-boreholes, drilled by the Department of Water Affairs and Forestry and the other eight percussion boreholes drilled by the Department of Geohydrology. The Department of Geohydrology also installed piezometers in three of the percussion boreholes on the Campus Test Site.

There are 19 percussion boreholes on the test sites at Dewetsdorp. Eleven of these were drilled as part of this project, while seven were drilled by the Department of Water Affairs and Forestry as part of the project of Kirchner *et al.* (1991). The other borehole, for which no information is available, has been used for years by the Municipality of Dewetsdorp for production purposes. The Department of Water Affairs and Forestry also drilled two core-boreholes on two of the sites.

The results for the Rouxville project have not been published, but the investigations and the various production fields at Philippolis have been described by Botha *et al.* (1996), to which the reader is referred for more detailed information.

1.5 STRUCTURE OF THE REPORT

Geohydrologists have always assumed that fractures play an important role in the behaviour of Karoo aquifers. A logical conclusion is thus that one should study these aquifers with the methods devised for fractured aquifers. However, the picture that emerged from the cores of the core-boreholes drilled on the Campus Test Site and Dewetsdorp differs substantially from the conventional interpretation of fractured aquifers. This applies especially to the orientation and distribution of fractures, and the role they play in the movement of water through the aquifer.

As pointed out in Chapter 2, the behaviour of an aquifer is primarily determined by the geometry of the voids in the rock matrix of the aquifer. It is therefore of the utmost importance that methods should be found with which the void geometry of an aquifer can be studied. Three complementary methods that seemed to be particularly useful for this purpose: detailed geological studies of the aquifer, geophysical surveys and mathematical models are consequently also discussed in Chapter 2.

There can be little doubt that the physical properties of Karoo aquifers are related to the palæo-environment that existed at the time when the various Karoo formations were deposited. This deposition, which occurred during the Carboniferous, Permian, Triassic and early Jurassic ages (300 to 193 million years ago), and the glacial, marine, deltaic and fluvial to aeolian environments in which took place, is described in Chapter 3. These palæo-environments were responsible for a major characteristic of Karoo formations—the presence of alternating layers of mudstones, sandstones, siltstones and shales.

The Karoo sedimentation was ended by widespread volcanism that occurred during the late Triassic to early Cretaceous age, 204–120 million years ago. This magmatic activity, which can be related to the tectonic movement of Gondwanaland, is discussed in Chapter 4, where it is argued that the numerous ring dykes in the Karoo Landscape were caused by the intrusion of magma in the form of laccoliths. This interpretation may be controversial, but provides a natural explanation for the existence of the structures, something that the conventional interpretation cannot explain, without invoking some rather esoteric mechanisms. The interpretation also suggests that the Karoo formations should have another characteristic that may be very important for the flow of groundwater—the presence of fractures, or weakened zones, along the bedding planes of the alternating layers.

The geology of the five test sites is discussed in Chapter 5. This study revealed that bedding-parallel fractures do indeed occur in the Karoo formations, as envisaged in Chapter 4. These fractures have apertures of 1 mm or less, but can cover areas extending over several thousands of square metres, or perhaps even several square kilometres. However, the fractures are very sparsely spaced and weakly connected. The geometry of Karoo aquifers therefore deviates considerably from that of the media commonly considered in the literature on groundwater.

An interesting feature that emerged from the structural-stratigraphic mapping of Bloemfontein and its

immediate surroundings, which is also discussed in Chapter 5, is the north-easterly trending megascopic domal structure on which Bloemfontein is situated. This structure is very reminiscent of what one would expect of a laccolithic intrusion.

The information in Chapter 5 is combined with field observations in Chapter 6 to try to understand the behaviour of Karoo aquifers better. This exercise showed that the yields of boreholes in these aquifers are ultimately controlled by the bedding-parallel fractures and layered nature of the Karoo formations. This means that it will be difficult to describe the behaviour of these aquifers without the use of a three-dimensional representation of the aquifer.

Another rather disturbing result that emerged from this study is that Karoo formations, and thus aquifers, may readily be deformed by pumping water from them. This will not only affect the ability of these aquifers to store and yield water, but can also have a considerable impact on mass transport in the aquifers. Unfortunately, very little is known about these deformations at the moment.

Three-dimensional mathematical models of groundwater flow are not very popular in geohydrological circles, mainly for two reasons. The first is that such models require considerably more field data and sophisticated computer resources than an equivalent two-dimensional model. The second is that in field investigations very little attention is usually paid to those factors that are important in three-dimensional flow, such as the geometry and structure of the aquifer. However, the discussion in Chapter 6 shows that it will be difficult to explain the fracture-controlled behaviour of boreholes in Karoo aquifers without a three-dimensional numerical model. The three-dimensional computer program, SAT3, developed in a previous contract with the Water Research Commission (Verwey and Botha, 1992), was therefore adapted and used to develop a numerical model for the Campus Test Site. The development of the model is discussed in Chapter 7, and its practical application, calibration and verification in Chapter 8.

The actual application of the model to the Campus Test Site is described in Chapter 9. Two very interesting results that emerged from this model are: (a) flow towards a borehole is restricted to the plane of the fracture, and (b) the water-yielding fracture can be completely dewatered near the borehole without affecting the piezometric levels farther away adversely. There is thus a possibility that the water-yielding fracture can be deformed if the discharge rate of a production borehole is too high.

Although the three-dimensional computer program provides an excellent tool for studies of the general behaviour of a Karoo aquifer, the program is too complex to use on a routine basis. This applies in particular to situations where one wants a good, but not necessarily accurate, estimate of the hydraulic parameters of an aquifer. The field observations and the numerical model of the Campus Test Site in Chapter 9 have shown that groundwater flows mainly in the vertical direction in a stressed Karoo aquifer. This suggested that some of the major features in the behaviour of a Karoo aquifer could be described with a two-dimensional vertical flow model. This model, derived from the three-dimensional model by integrating the radial direction in the three-dimensional flow equation out, is described in Chapter 10, and used in the estimation of hydraulic parameters for Karoo aquifers with satisfactory results.

The report concludes with a few comments on the behaviour of Karoo aquifers observed during the project, but which could not be investigated fully, as well as recommendations for future work in Chapter 11.

CHAPTER 2

THE PHYSICAL BEHAVIOUR OF AN AQUIFER

2.1 INTRODUCTION

The physical behaviour of an aquifer is ultimately determined by the interactions between the water and the rock matrix in which the aquifer occurs. Although other interactions exist, there is no doubt that the adhesive force between the water molecules and the boundaries of the voids in the rock matrix is the most basic interaction. This force can be described mathematically by Laplace's equation (Bear, 1972)

$$(p_o - p_i) = \sigma \left(\frac{1}{r_1} + \frac{1}{r_2} \right) \quad (2.1)$$

where σ is the surface tension of water, p_o and p_i the outer and inner pressure on the water surface, and r_1 and r_2 the radii of curvature of the water surface, which is determined by the void's geometry. The flow of water through an aquifer is thus in the first place determined by *the geometry of the voids in the rock matrix* of the aquifer. A good knowledge of the void geometry is therefore of the utmost importance in the study of an aquifer's behaviour.

The dependence of an aquifer's behaviour on the void geometry is so basic that it is rarely mentioned in groundwater literature. The most common approach is simply to assume that the rock matrix can be represented as a porous medium, and then forget it (Black, 1993). It is only when the observations cannot be reconciled with the behaviour of a porous medium, that other media are considered. However, such a change in the representation of the rock matrix should be made, not merely because the observations cannot be reconciled, but rather on sound physical evidence. The first step to take in the study of any aquifer should therefore be to determine the geometry of its voids.

A major reason for the neglect of the void geometry in aquifer studies is that there do not exist very efficient methods that can be used for this purpose. Indeed, there are only two classes of methods available for this purpose—geological methods and geophysical methods. These methods are discussed in more detail in Section 2.2 below.

The modern scientist is usually not satisfied with mere observations of a given phenomenon. What he or she really wants to do, is try to relate the various observations with one another, and predict the behaviour of the phenomenon under various conditions in the future. In the exact sciences, this objective is achieved by developing a suitable theory for the phenomenon. A similar approach is also applied in geohydrology, but instead of referring to a theory, geohydrologists seem to prefer the word *model*, without specifying precisely what they mean by the term. This aspect together with some problems associated with one of the most basic tools used to investigate the behaviour of an aquifer—hydraulic tests—are discussed further in Section 2.3.

2.2 DETERMINATION OF AN AQUIFER'S VOID GEOMETRY

2.2.1 Geological Methods

The geometry of voids at any point in the earth's subsurface is closely related to the geological formation present at that point. The easiest way to get an idea of the void geometry of an aquifer is therefore to know the geology of the area in which the aquifer is situated. The first step to determine the behaviour of an aquifer must thus always be to determine the geology of the formation, or formations, in which the aquifer occurs.

The geological methods, commonly used to determine the geology of an area—field surveys, geological maps, aerial photography and satellite imagery—unfortunately tend to concentrate more on properties of the earth's surface. Such surveys can certainly provide useful information on the areal extent of an aquifer, and on the influence man may have on the behaviour of the aquifer, but not the geometry of the voids in the aquifer, since aquifers generally occur at depth. It is thus important to supplement areal surveys with surveys in depth.

One in-depth method that can be applied quite easily, is to compile a geological profile of a borehole. There are basically two approaches that can be used for this purpose. The first is to use the drill chips ejected during the drilling of a borehole, and the second is to drill core-boreholes. Although drill chips cannot yield the same detailed information as cores, they are always present at the drilling of a borehole. The compilation of geological profiles should thus really be a standard practice in the drilling industry. Unfortunately, this is not the case in South Africa. Core-boreholes, on the other hand, are very expensive to drill. Nevertheless, they provide such useful information that it is always worthwhile to try and drill a few of them, especially when developing a well-field in an unknown formation. In fact, it would have been impossible to explain the behaviour of Karoo aquifers, were it not for the core-boreholes the Department of Water Affairs and Forestry drilled on the Campus Test Site and two of the test sites at Dewetsdorp.

Another way in which geology can contribute towards a better knowledge of an aquifer's behaviour, is through an understanding of the origin and evolution of the formations that contain the aquifer. This aspect is so basic, yet geohydrologists do not seem to pay particular attention to it if one looks at the existing literature. Although such an approach is understandable, information of this kind should not be neglected in the study of an aquifer's behaviour. Indeed, it was only when the history of the Karoo Supergroup was taken into account that the behaviour of Karoo aquifers could be explained in logical and physically acceptable terms.

2.2.2 Geophysical Methods

It is not unfair to say that Geology is a science of observation when one compares it with some of the more exact sciences such as Physics and Chemistry. To circumvent this deficiency, geologists often turn to the latter subjects for more exact measurements. This applies especially in those situations where information is needed below the soil surface. Geophysical techniques are consequently often employed in groundwater investigations.

Magnetic airborne surveys are very useful in the structural mapping of an area, particularly to determine the dominant direction of tectonic movement, and the location of features such as faults, dykes and fracture zones. However, the majority of geophysical surveys (magnetic, electromagnetic, electric and gravitational), used in groundwater investigations, are surface-based. These methods can yield valuable information on the global geometry of an aquifer, but not of the void geometry. The results are also often ambiguous, especially in Karoo aquifers with its numerous layers of mudstones, sandstones and siltstones. It may thus be necessary to use a combination of these techniques, to overcome the ambiguities (Partridge and Hubert, 1993). Unfortunately, The methods are very tedious, time-consuming and thus expensive. Geophysical surveys are consequently often conducted very superficially and then only to site boreholes.

Two new geophysical techniques that seem especially promising for groundwater investigations in the Karoo formations, are high resolution radio and seismic tomography. In these techniques, one observes the attenuation of radio and seismic waves by the intervening rock masses between two boreholes. Results from Karoo aquifers (Wedepohl *et al.*, 1995) indicate that seismic tomography provides excellent information on the geometry of the intervening rock masses. Radio tomography, on the other hand, can be used to determine the flow pattern of the groundwater, although not for distances exceeding 50 m.

2.3 GROUNDWATER MODELS

2.3.1 Definition of the Term Model

The word model has so many interpretations in groundwater literature, that it is sometimes not clear what is meant by it (Konikow and Bredehoeft, 1992). This confusion is discussed by Botha (1994), who ascribes it to the lack of a theory for groundwater motion. It may thus be worthwhile to briefly discuss the term 'theory' and how it relates to the word 'model', as used in groundwater literature, before proceeding with the discussion on the application of models.

The South African Oxford Dictionary describes the word theory as: 'a supposition or system of ideas explaining something, especially one based on general principles *independent of particular things to be explained* (e.g. the atomic theory). A theory in the exact sciences thus usually consists of two components: non-trivial observations of a phenomenon and man's ability to reason abstractly (Botha, 1994).

It is quite common in establishing a theory for a phenomenon to come across quantities, or *interactions*, to borrow a term from physics, that play a basic role in the theory, but cannot be measured directly in general. What is usually done in such cases, is to relate the interaction to a more directly observable quantity, or

observable, through a number of *constitutive parameters* (Botha, 1994). A well-known example of such an interaction in the theory of groundwater motion is Darcy's law

$$\mathbf{q} = -\mathbf{K}\nabla\varphi(\mathbf{x}, t)$$

where $\mathbf{q}(\mathbf{x}, t)$ is the Darcy velocity, \mathbf{K} the hydraulic conductivity tensor and $\nabla\varphi(\mathbf{x}, t)$ the gradient of the piezometric head.

The results derived from a theory usually take the form of mathematical equations, which may have to be transformed further before they can be applied to observations of a particular phenomenon. For example, one has to prescribe suitable boundary conditions, and then solve the equation, either analytically or numerically, before the results can be applied to a particular phenomenon if the equation is a differential equation. It is these transformations, commonly known as the application of a theory in the exact sciences, that are usually described by the term *model*, or more specifically, *conceptual model*, in groundwater literature. The ideal would thus have been to discard the term *model* completely, and just use the term *theory* also in groundwater. However, the term *model* is so entrenched in the literature on groundwater, that this will be difficult. This situation has led Botha (1994) to introduce four types of models.

- (a) **Mathematical models**—used when one wants to refer to the general equations governing the motion of groundwater.
- (b) **Conceptual models**—used to denote the governing equations in a mathematical model and the auxiliary conditions (e.g. boundary conditions) needed to solve the governing equations for a specific aquifer.
- (c) **Analytical models**—used to denote analytical solutions of conceptual models.
- (d) **Numerical models**—used to denote numerical solutions of conceptual models.

This nomenclature will be used exclusively in the discussion that follows.

The main advantage of a theory is that it supposedly represents the best description of a phenomenon's physical behaviour, at a specific moment. The question thus arises of what to do with observations that do not agree with the theory. The approach, normally followed in the exact sciences, is to repeat the observations, and discard them if they do not yield consistent results. It is only when the results are repeatedly inconsistent with the existing theory that scientists begin to doubt the validity of the theory. Experience has taught that this situation usually arises because the existing theory neglects one or more of the basic interactions that controls the phenomenon. Since a theory is nothing more than a product of the human intellect, it is usually possible to adapt the theory to the inconsistent new results, or to develop a new theory that can account for the new and all previous results. A theory may thus never be complete, but can be very helpful in understanding the behaviour of a physical phenomenon.

As mentioned in Section 2.1, the flow of water in an aquifer is controlled mainly by the geometry of its voids. An ideal theory for groundwater motion should therefore include a description of the void geometry, which, unfortunately, is usually not known. A common practice in the literature on groundwater phenomena is thus to *assume* that the geometry of an aquifer can be represented as a porous matrix in one form or another. The majority of conceptual models used today in groundwater investigations, are consequently based on the theory of flow through a porous medium, although not often appreciated as such.

2.3.2 Hydraulic Tests

One reason for the popularity of porous flow models is that the influence of the matrix geometry on the flow can be described by a few constitutive parameters, commonly known as *hydraulic parameters* (Bear, 1972). The possibility therefore exists that one can describe the flow of a fluid in a porous medium without any reference to the actual geometry of the matrix if these parameters can be determined experimentally. This is probably the main reason why the geometry of an aquifer is so often neglected in groundwater studies.

It should not be too difficult to determine the hydraulic parameters of a true porous matrix in which the flow is not influenced by other factors. Unfortunately, there are not many geological formations whose geometries compare favourably with that of the hypothetical porous media, usually considered in the physics of flow through a porous medium. Moreover, the flow in natural aquifers is often controlled by a number of other factors. Some of the more important of these are: the reaction of the voids to stresses and strains, variations in the concentrations of dissolved solids, heterogeneity of geological formations, disturbances caused by man and the rate at which the aquifer is recharged or discharged. Since it is difficult to measure these factors directly, geohydrologists often try to derive their influence from observations of the pressure distribution in the aquifer. This quantity is not only easy to measure, but its behaviour must clearly also reflect the influence of the other factors. This led to the introduction of perhaps the most widely used obser-

vational method in groundwater literature—the *hydraulic test*.

The first step in a hydraulic, or pumping, test (as it is more commonly, but erroneously, called), is to stress the aquifer. This is usually done by disturbing the water level in a chosen borehole, henceforth referred to as the *perturbed borehole*, and then observe the response of the water levels in suitably placed *observation boreholes*. The hydraulic parameters are then derived by fitting the observed responses of the water levels to a suitable analytical model for the aquifer (Kruseman and De Ridder, 1991).

There are three basic difficulties inherent in this approach. The first is: how does one know that the chosen analytical model represents the aquifer's geometry and thus physical behaviour accurately? This question is particularly important when the modeller relies only on a compendium of analytical methods, such as Kruseman and De Ridder (1991), to choose an analytical model. For, although the authors give a detailed description of the constraints of each of the models, the constraints are mainly mathematical in nature. Nowhere is there any mention of the geometry of the voids, or other factors, that may influence the fit.

Kruseman and De Ridder (1991) admittedly divide their models into two broad classes of aquifers: those whose matrices can be represented by a porous medium, and those whose matrices can be represented by a dual porous medium. However, there are no guide-lines that can be used to decide whether an aquifer can indeed be represented by the chosen medium, except by looking at the various drawdown curves—a procedure fraught with difficulties. The possibility therefore always exists that the hydraulic parameters derived from a hydraulic test may not be representative of an aquifer (Botha and Verwey, 1992), or contain large unknown errors (De Marsily, 1986).

One approach to ensure that the hydraulic parameters are representative of the aquifer is to make sure that there does not exist more than one analytical model that fits the data with the same accuracy. However, this approach can be time-consuming, and not very productive. It is thus imperative that the analyst of a hydraulic test should always ensure that the chosen analytical model satisfies the basic physical properties of the aquifer for which the analytical model is used.

A second approach, which is essential if none of the existing numerical models fits the observations, is to go back to the basic theory and derive a new conceptual model for the aquifer. However, this approach is not without difficulties either, for the following reasons.

- (a) There may not be enough observations, especially field observations, to determine the physical and geometrical properties of the aquifer precisely—a prerequisite to derive a new and successful conceptual model for the aquifer.
- (b) It may not always be clear how to formulate a mathematical model for the specific type of aquifer.
- (c) The appropriate conceptual model may not have an analytical model, even for regular boundaries, in which case one has to resort to a numerical model.

The approach is nevertheless the only one possible if one wants accurate results.

Another difficulty with conventional hydraulic tests is that the analytical models, known today, require that the aquifer can be represented by a *regular and homogeneous domain*, usually a sphere (Muskat, 1937; Theis, 1935). One consequence of this assumption, and the heterogeneity of natural geological formations, is that the observed drawdowns usually deviate from the analytical model, especially at early times. It is thus often said that hydraulic tests produce better results if performed over a long time. However, there is no mathematical function, even those that contain the time as an independent variable, that will suddenly change shape without a change in its constitutive parameters. The real reason why a long time seems to be more appropriate for the performance of a hydraulic test, follows briefly. The flow of groundwater is governed by the law of mass conservation, which can be described mathematically by a parabolic partial differential equation (Bear, 1979; Verwey and Botha, 1992). It is not difficult to show (Weideman, 1980) that the solution, $u(\mathbf{x}, t)$, of any parabolic partial differential equation can always be expressed in the form

$$u(\mathbf{x}, t) = c_0 + \sum_{i=1}^{\infty} c_i \exp(-\lambda_i t) g_i(\mathbf{x}) \quad (\lambda_i > 0, \lambda_1 \leq \lambda_2 \leq \dots) \quad (2.2)$$

where, the c_i are constants and the $g_i(\mathbf{x})$ functions of the spatial co-ordinates \mathbf{x} . The drawdown at large times will therefore tend towards the constant value

$$u(\mathbf{x}, t) \Big|_{t \rightarrow \infty} = c_0$$

Any information contained by the Fourier terms under the summation sign in Equation (2.2) will therefore be lost if the analysis of the drawdowns is restricted to large times. Deviations of the observed drawdowns

from the chosen analytical model must therefore be regarded as an indication that the model is incorrect when analysing hydraulic test data. It is thus gratifying to see that conceptual models, more concerned with the accurate representation of the aquifer's geometry rather than the ease of evaluation, begin to appear in the literature (Caças *et al.*, 1990).

The third and final difficulty with hydraulic tests is more subtle and applies whether the user uses an analytical or a numerical model. To show this, it is sufficient to notice that the parabolic partial differential equation which describes the flow of groundwater, can be expressed in symbolic form as

$$\mathbf{L}[\mathbf{a}]\varphi = f$$

where φ is the piezometric head, \mathbf{a} the hydraulic parameters of the aquifer, $\mathbf{L}[\cdot]$ the parabolic partial differential operator and f the strength of sources or sinks. The common procedure in applications of differential equations is to specify the parameters \mathbf{a} , prescribe suitable initial and boundary conditions and then solve for φ . However, the procedure is exactly the opposite in a hydraulic test. Here one tries to recover values for the parameters, \mathbf{a} , from the solution φ . This type of problem is consequently known in the mathematical literature as the *inverse problem*.

One difficulty of the inverse problem is that its solution is ill-posed (Sahimi, 1995; Sun, 1994). This means that the problem has an infinite number of solutions. The fact that a set of hydraulic parameters satisfies a given set of piezometric heads, thus does not necessarily mean they are representative of the aquifer. This can only be assured if one knows beforehand that the differential equation, and the prescribed boundary and initial conditions, truly represent the physical behaviour of the aquifer.

2.4 CONCLUSION

It is common practice to describe the physical behaviour of an aquifer with a conceptual model. These models contain certain hydraulic parameters, the number and type of which are determined by the aquifer's void geometry. *The void geometry must therefore be known before the model can be applied in practice with confidence*. Unfortunately, this is usually not the case. To circumvent this lack of knowledge, two assumptions are often made in studying the behaviour of an aquifer. The first is that the rock matrix can be represented as a porous medium, and the second that the hydraulic parameters can be determined by fitting a conceptual model inversely to drawdowns observed during a hydraulic test.

Judging from the discussion above, this approach suffers from two serious disadvantages. The first, and most serious one, is that the porous matrix may not represent the geometry of the aquifer's voids. Since the results of applying a wrong conceptual model to an aquifer will be meaningless, care should be taken to avoid it at all costs. One approach to prevent this situation is to look for deviations between drawdowns, observed during a hydraulic test, and the conceptual model. Any deviations that occur at early times are particularly important in this regard.

The previous approach may not always yield acceptable results, however. The reason for this is that the solution of the inverse problem is not unique. The possibility thus exists that a wrong conceptual model may fit the observed drawdowns perfectly, as has been illustrated by Botha and Verwey (1992). It is therefore dangerous to rely solely on hydraulic tests to determine the hydraulic parameters of an aquifer, particularly those based on unconfirmed inverse models.

The best approach to study the behaviour of an aquifer is to establish its true geometry, by whatever geological and geophysical methods are available, and then derive a suitable conceptual model for the aquifer. This will not only ensure that the hydraulic parameters are representative of the aquifer, but may also indicate how one can determine them, perhaps without invoking an inverse model. Judging from the experience gained during the present investigation, core-boreholes can be of considerable value in this regard, especially if one wants an accurate description of the aquifer's geometry. However, as Botha and Magda (1993) have shown, much can sometimes be learnt from more common observations, provided one does not have preconceived notions about the geometry of the aquifer.



CHAPTER 3

THE KAROO SUPERGROUP

3.1 GENERAL

As pointed out in Chapter 2, it is always advantageous to have some knowledge of the historical development of the formations in which aquifers occur. Since the Karoo aquifers of South Africa occur within the so-called Karoo Supergroup, this chapter will be devoted to a brief discussion of this Supergroup's development.

The available information indicates that the Karoo Supergroup was formed when sediments filled an intracratonic, foreland basin on Gondwanaland, during the Carboniferous, Permian, Triassic and early Jurassic ages, 300 to 160 million years ago (Truswell, 1970). Since Gondwanaland drifted from polar to tropical latitudes during this period, the sedimentation occurred under different depositional environments (Tankard *et al.*, 1982). The result is that one can clearly distinguish between different groups of sediments, each with its own physical properties, within the Supergroup today (see Figure 3–1).











Drakensberg Volcanics			Basalt	Jurassic
Stormberg Group	Clarens		Cross-bedded sandstone	Triassic
	Elliott		Red mudstone and sandstone	
	Molteno		Sandstone, conglomerate and mudstone	
Beaufort Group	Tarkastad Subgroup		Burgersdorp Formation	Permian
			Katberg Sandstone	
	Adelaide Subgroup		Green, grey and purple mudstones	
		Sandstone		
Ecca Group			Shale and sandstone	
Dwyka Group			Tillite and diamictite	Carboniferous

Figure 3–1 The Karoo Supergroup. [Adapted from Tankard *et al.* (1982).]

The main Karoo Basin overlies the central and eastern parts of South Africa, with its deepest parts in the southern part of the Northern Cape Province and Lesotho (Du Toit, 1954), as shown in Figure 3–2. Smaller isolated subsidiary basins also occur in Gauteng, Mpumalanga and Namibia (Visser, 1989). However, these subsidiary basins do not contain the Dwyka, Beaufort or lower Stormberg Groups (Truswell, 1970).

The structure of the different groups in the main basin and the influence this structure has on the hydrological properties of the aquifers in the Karoo Supergroup are discussed in Sections 3.3 to 3.6 below. This is followed by a discussion of a few processes that transformed the original sediments in Section 3.7, and recent formations in Section 3.8. However, it may be worthwhile to first discuss another phenomenon—the formation of the Cape Fold Belt—that had a significant influence on the structure of the Karoo Supergroup, as it is known today.

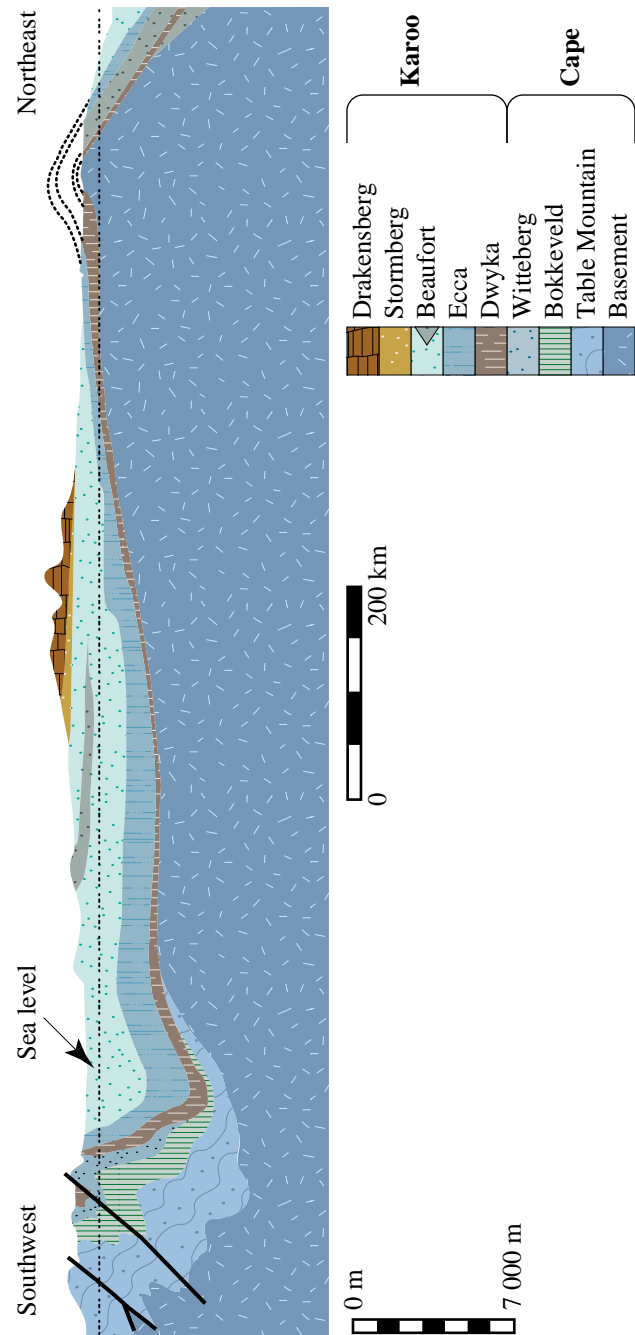


Figure 3–2 Schematic cross-section through the Karoo Basin. [After Rowsell and De Swardt (1976).]

3.2 THE CAPE FOLD BELT

It is known that an island arc (an arcuate chain of islands located and aligned in relation to an orogenic belt and characteristically having a deep trench on the convex side) began to develop south of the present-day coastline of Africa, even before the Karoo sedimentation began. It is difficult to explain the development of the island arc. One possible explanation is to relate it to the great, unexplained cataclysm, that struck the earth towards the end of the Permian Age and may have been responsible for the break-up of Pangaea. What the cataclysm did, was to fracture the once solid Gondwana Plate into a number of proto-plates, that began to collide with one another. The island arc, under discussion, seems to have been caused by compressional forces created by the collision of the proto-African plate and the proto-southern plate, associated with the Falkland plateau (Tankard *et al.*, 1982). This island arc eventually developed into a volcanic mountain range, that gave rise to the Cape Fold Belt, and thus a second source of orogenic material for the Karoo sedimentation.

The transformation of the island arc into the Cape Fold Belt caused an enormous folding of the Karoo strata, as can be seen from the cross-section through the Karoo Basin in Figure 3–2. Folds and faults are consequently quite common in the south and south-western Karoo Basin. The formation of these structures must certainly have caused the development of secondary porosities in the aquifers, but at the same time at least partially destroyed their primary porosity. A good knowledge of structural geology may thus be necessary to try to understand the geometry and behaviour of aquifers in the area subjected to the folding.

3.3 THE DWYKA FORMATION

3.3.1 Deposition

The Dwyka sediments, which are situated at the base of the Karoo Supergroup, have been deposited on older Precambrian granitic rocks in the north and sedimentary rocks, associated with the Cape Fold Belt in the south. This sedimentation took place when Gondwanaland migrated over the South Pole during the Carboniferous Age.

Visser and Kingsley (1982) use an east-west line, representing a palæo-coastline, to divide the Dwyka Formation into a northern and southern facies. The northern facies was mainly deposited in deep valleys, eroded by glaciers that moved from topographical high areas towards a sea, while the southern facies was deposited in glaciomarine conditions on a sea-bed. This interpretation is consistent with the observation that the thickness of the deposits in the northern facies varies considerably over short distances (0 – 700 m) in an east-west direction, while the thickness of the southern facies is more uniform. These properties and the fact that the Dwyka sediments wedge out from a thickness of 800 m in the south, to 100 m in the north (Tankard *et al.*, 1982), suggest that the Dwyka sediments were deposited along the coastline of a palæo-sea, under conditions of glaciation.

The Dwyka Formation consists mainly of Dwyka diamictite—angular to rounded clasts of the basement rocks, embedded in a clay and silt matrix. However, varved shales, sandstone layers and conglomerates, typical of a fluvio-glacial environment, are also present. The diameters of clasts in the Dwyka diamictite of the northern facies (~3 m) are often larger than those of clasts in the southern facies (~1,5 m), which moreover tend to fine upwards. This suggests that the intensity of flows decreased with time.

The Dwyka Formation is ordered vertically in cycles that persist laterally in the southern and western parts of the Karoo Basin. These cycles, four of which have been identified in the west, contain massive tillite followed by bedded diamictite and linear to sheetlike bodies of sandstones deposited by outwash and floating ice (Tankard *et al.*, 1982).

3.3.2 Hydrological Properties of the Dwyka Formation

The Dwyka diamictite, shales and tillites have very low hydraulic conductivities [$\sim 10^{-11}$ to 10^{-12} m s⁻¹ (Driscoll, 1986)], and virtually no primary voids. They therefore tend to form more aquitards than aquifers (Freeze and Cherry, 1979). The few sandstone bodies deposited in the glacial valleys of the northern facies are very limited in extent, and sealed off by the diamictite. The aquifers in them are therefore limited and often only contain fossil water. Since the Dwyka sediments were deposited mainly under marine conditions, the water in these aquifers tends to be saline. Exploitable aquifers thus only exist in a few places, where sand and gravel were deposited on beaches or where the Dwyka Formations are fractured significantly. The Dwyka Formation is thus not an ideal formation for the development of aquifers.

3.4 THE ECCA GROUP

3.4.1 Deposition

In its continued drift northwards, Gondwanaland entered a more temperate region during the Permian Age (286–248 Ma). The Dwyka ice cap thus began to melt, leaving a deep basin in the south and incised glacial valleys in the north, as illustrated in Figure 3–3.

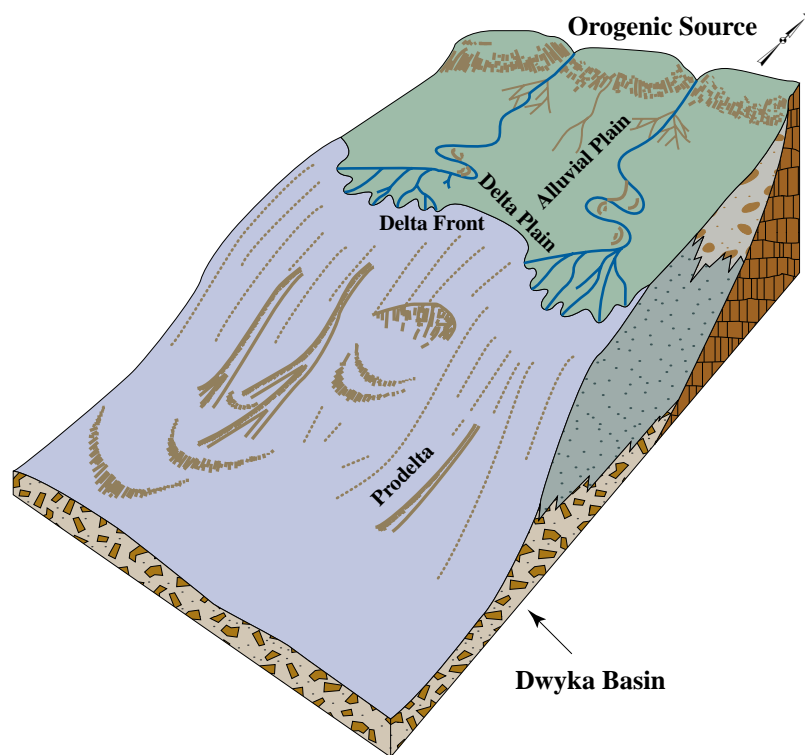


Figure 3–3 Diagrammatic sketch of the Ecca Group's deposition. [Adapted from Reineck and Singh (1973).]

The melting of the ice slowly began to erode the exposed bedrock formations to form rivers in the glacial valleys. The more temperate climate caused the flood-plains of these rivers to be covered by mats of swamp vegetation—the sources of the coal-seams often found on top of the coarse, fluvial channel sandstones in the Ecca Group (Tankard *et al.*, 1982).

The island arc south of the Dwyka basin began to develop into the Cape Fold Belt at this time. The compression resulting from the formation of the Belt, caused the original basin to shrink considerably and to form a southern shore-line. This allowed streams to also flow from the elevated areas of the island arc towards the basin. These streams deposited sheetlike sandstone bodies (~25 m thick), overlain by fine-grained sediments, along the southern shore of the basin (Tankard *et al.*, 1982).

Some of these fluvial systems must have been quite extensive, judging from the width of sandstone bodies (500 m to 30 km), associated with the Ecca Group. These bodies are especially prominent in Mpumalanga, which is situated on the northern part of the basin. This suggests that the largest fluvial systems occurred along the glacial Dwyka valleys on the northern shore-line of the basin.

As the waves eroded the cliffs at the contact of the flood-plains and the basin, the larger fluvial systems began to form deltas along the shallow parts of the basin's shore-line, thereby prograding the strand-plain and shore-line. This gave the rivers the opportunity of building their deposits slowly forward and to create so-called *prodeltas*.

The progradation of the delta systems led to the formation of shallow lagoons, on a stable shelf, along the shore-line of the basin (see Figure 3–3). This resulted in the deposition of sheetlike sandstone bodies, over wide areas of the stable shelf. The base of the Vryheid Formation near Durban, which consists primarily of sediments derived from lagoon deposits, is a good example of these strand-plain deposits.

The physics of sedimentary transport requires that coarser particles in the flow settle first, while finer particles are transported deeper into the basin. The coarse fractions of the sediment load were therefore

deposited on the banks of the main channels as levees, while the finer grained sediments were carried out further into the delta front. The fine to very fine-grained sediments were deposited on the prodeltas, illustrated in Figure 3–3, as silt and clay. This explains why the sediments in the Ecca Group tend to coarsen upwards. However, the interfingering of large sheetlike sandstone bodies and Ecca shales, as can be observed at Bothaville in the Northern Free State for example, indicates that the transgression of the basin's water level and wave action reworked the Ecca sediments a number of times. In fact, Tankard *et al.* (1982) recognised as much as eight periods of delta progradation and transgression. The coarseness of Ecca formations thus often changes considerably with depth, particularly along the palæo-shore-line of the basin.

An interesting feature of the Ecca period is the deep trough, with an east-west trend, that developed in the southern parts of the basin. The origin of the trough is not known, but it was possibly caused by downwarping or subsidence. The trough, which had a maximum thickness of approximately 2 000 m in the Eastern Cape, was filled with mud and silt that accumulated in the sediment starved basin (Tankard *et al.*, 1982). The succession in the trough therefore consists mainly of Ecca shales.

Gravity flows, associated with deltas that prograded from the north, south and west near the end of the Ecca period, led to the deposition of turbidite sandstones, in the deeper parts of the basin. These sandstones are usually very dense, and thus unable to transmit large quantities of water.

The preceding discussion shows that the Ecca Group was mainly deposited under deep marine conditions. However, the presence of layered tuffs in the Collingham Formation indicates that there was also some distant volcanic activity during this period.

3.4.2 Hydrological Properties of the Ecca Group

The Ecca Group consists mainly of shales, with thicknesses that vary from 1 500 m in the south, to 600 m in the north. Since these shales are very dense, they were often neglected as sources of groundwater in the past. However, as illustrated in Figure 3–4, their porosities tend to decrease from ~0,1 north of latitude 28° S, to < 0,02 in the southern and south-eastern parts, while their bulk densities increase from ~2 000 to >2 650 kg m⁻³. The possibility thus exists that economically viable aquifers may exist in the northern parts of the areas underlain by the Ecca shales. It is thus rather surprising to find that there are areas, even in the central parts, where large quantities of water are pumped daily from the Ecca shales. The Petrusburg district in the central Free State, where 4 500 ha are irrigated from boreholes drilled into the Ecca shales, compared to the 2 000 ha irrigated from the Modder River that flows through the district is a prime example of such an area. One should therefore not neglect the Ecca shales as possible sources for groundwater.

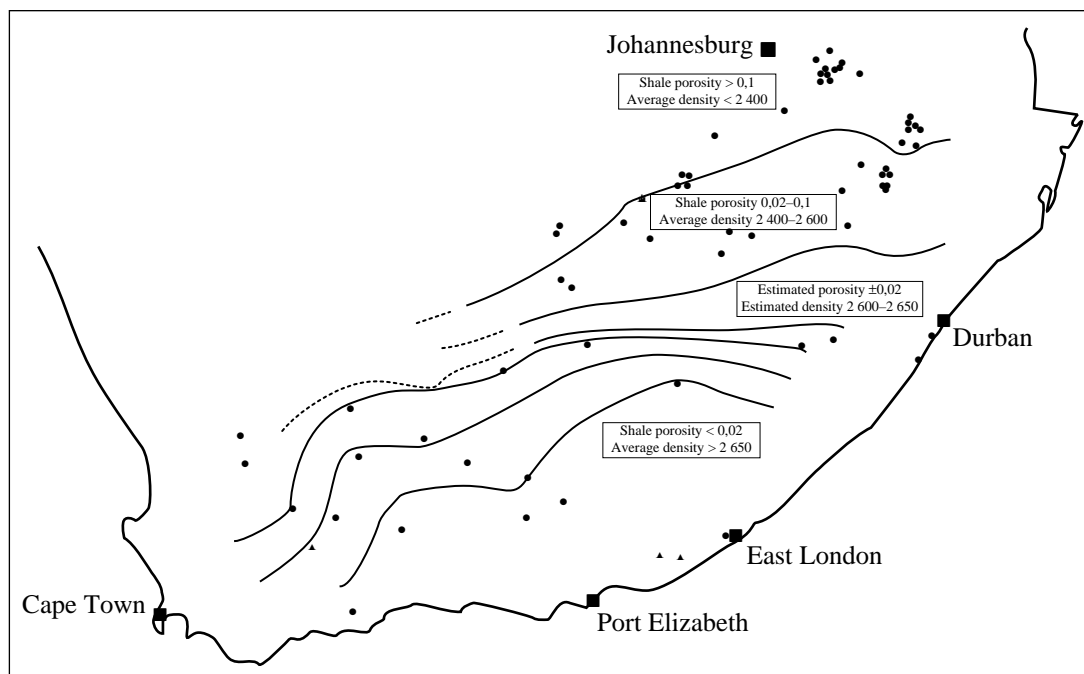


Figure 3–4 Contour map of the porosities and bulk densities of the Ecca shales in South Africa. [Redrawn from the map in Rowsell and De Swardt (1976).]

The prodelta sandstones represent another formation of the Eccca Group in which one would expect to find high-yielding aquifers. Unfortunately, Rowsell and De Swardt (1976) have found that the permeabilities of these sandstones are also usually very low. The main reason for this is that the sandstones are usually poorly sorted, and that their primary porosities have been lowered considerably by diagenesis.

Sand grains tend to orientate themselves with their longest axis parallel to the flow direction in fluvial processes. One can therefore expect that sedimentary rocks will exhibit preferential flow paths, and that their hydraulic conductivities will be larger in the direction of the palæoflow, than perpendicular to it. Such rocks are said to be *anisotropic*. Since the Eccca Group was deposited in a fluvial environment, one would expect Eccca aquifers to be anisotropic. The methods used to analyse hydraulic tests from these aquifers must therefore be able to account for this anisotropy.

3.5 THE BEAUFORT GROUP

3.5.1 General

The continued deep-water sedimentation and delta growth filled the original Karoo Basin almost completely towards the end of the Eccca period. However, at this stage the Cape Fold Belt experienced a renewed uplift. This caused an isostatic subsidence along an east-west axis that developed into a foreland basin and a new cycle of sedimentation. This sedimentation led to the deposition of what is now known as the Beaufort Group (Rowsell and De Swardt, 1976; Theron, 1970). This Group achieves a thickness of approximately 3 000 m in the Eastern Cape Province, and underlies an area of approximately 200 000 km². The Group therefore constitutes the major member of the Karoo Supergroup in South Africa today, as can be seen in Figure 1-1.

The Beaufort Group is stratigraphically divided into two major units, the upper Tarkastad Subgroup and the lower Adelaide Subgroup. The Tarkastad Subgroup is subdivided into the upper Burgersdorp Formation with its brightly coloured red, blue and green mudstones and the lower Katberg Formation, that can be up to 900 m thick. The Katberg Formation also contains brightly coloured shales and mudstones, but consists mainly of thick layers of coarse-grained sandstone.

The Adelaide Subgroup consists mainly of green, bluish, grey and red mudstones and fine-grained sandstones that form thick lens-shaped units (Du Toit, 1954). The subgroup is further divided into the Teekloof, Abrahamskraal and Balfour Formations. The Balfour Formation consists of coarse sediments at its base, which change upwards into red and purple mudstones and fine-grained sandstones.

3.5.2 Deposition

Two fluvial processes were responsible for the deposition of the Beaufort Group: *braided and meandering streams*, illustrated in Figure 3–5. Braided streams tend to develop on steep slopes, have high stream velocities and consist of a number of channels, while meandering streams usually consist of a single channel, have low stream velocities and develop on relatively flat terrain (Davis, 1983). A stream can therefore be braided along some parts of its length and meandering on the rest, depending on the topography of the terrain through which it flows.

Deposits on the beds of braided streams consist mainly of coarse sediments, conglomerates and patches of finer grained material on their banks, while meandering streams deposit mainly fine-grained sand, mud and silt with little or no conglomerates (Visser, 1989).

The channels of streams are not stationary, but tend to migrate laterally. In braided streams, this migration often extends over large areas but is restricted in meandering streams to a small, sandy meander-belt next to the vegetated banks and their associated muddy sediments (Scholle and Spearing, 1982). This lateral migration of the channels tends to produce cycles in which the coarse-grained channel deposits are overlaid by fine-grained deposits. The sheetlike, wedge-shaped sandstone layers intermingled with shale lenses often found in the Beaufort Group can therefore be ascribed to braided streams. However, the horizontal layers of alternating sandstone, siltstone and mudstone are due to meandering streams (Tankard *et al.*, 1982).

3.5.3 Hydrological Properties of The Beaufort Group

The major source areas of the Beaufort rocks were far from the basin, especially in the north. The coarser rocks in the Beaufort Group are therefore found near the Cape Fold Belt, which forms the

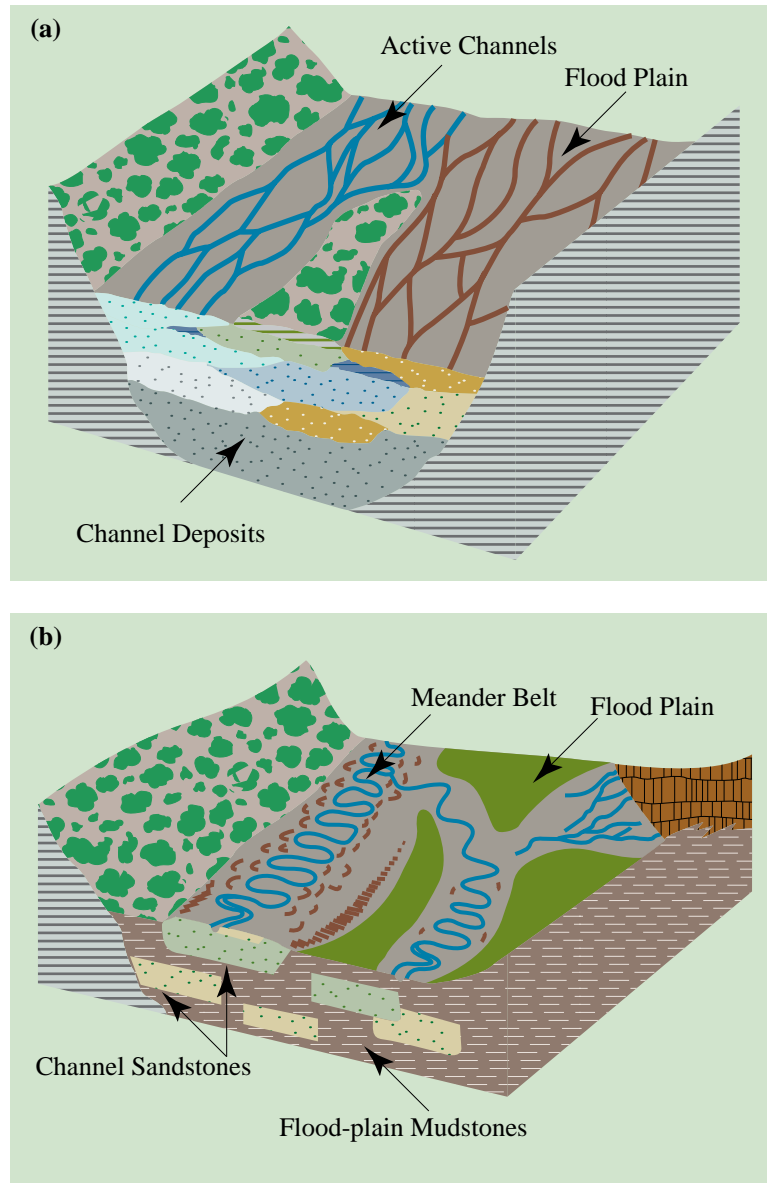


Figure 3-5 Models of (a) a braided river environment, and (b) a meandering river environment. [Redrawn from Scholle and Spearing (1982).]

southern border of the Beaufort Group, while those in the central basin consist mainly of mudstones, shales and fine-grained sandstones. These fine-grained sediments were mainly deposited where the braided rivers began to meander. The sedimentary units in the Group therefore usually have very low primary hydraulic conductivities.

Since the Beaufort Group was also deposited in a fluvial environment, one can expect that aquifers in these formations will, like those in the Eccia Group, be anisotropic. The geometry of these aquifers, however, is further complicated by the migration of the braided and meandering streams. Aquifers in the Beaufort Group will therefore not only be multi-layered, but also multi-porous with variable thicknesses.

The contact plane between two different sedimentary layers will cause a discontinuity in the hydraulic properties of an aquifer. The pumping of a multi-layered aquifer will thus cause the piezometric pressure in the more permeable layers to drop faster than those in the less permeable layers. It is therefore possible to mine the more permeable layers of the multi-layered Beaufort aquifers completely, without materially affecting the piezometric pressure in the less permeable layers. This complex behaviour of aquifers in the Beaufort Group is further complicated by the fact that many of the coarser, and thus more permeable, sedimentary bodies are lens-shaped. The life-span of a high-yielding borehole in the Beaufort Group may therefore be limited if the aquifer is not recharged frequently.

3.6 THE STORMBERG GROUP

3.6.1 The Stormberg Basin

During the Triassic (230–193 Ma), sediments again began to accumulate in four smaller basins in Southern Africa, caused by a renewed uplift of the Cape Fold Belt. The relic of one of these basins, known as the Stormberg Basin, covers an elliptic area that stretches from the northern parts of the Eastern Province into the Free State, Lesotho and KwaZulu-Natal (see Figure 1–1). The other three basins are situated in Zimbabwe, Namibia and Botswana (Visser, 1984), and will not be discussed here.

The formations deposited in the Stormberg Basin, collectively referred to as the Stormberg Group, form the upper formations in the Karoo Supergroup. These formations are: the Molteno Formation, that directly overlies the Beaufort Group, the Elliot Formation and the Clarens Formation (see Figure 3–1). The formations form a clastic wedge towards the source areas in the south, while their strata are mainly horizontal to sub-horizontal with a dip towards Lesotho (Visser, 1984). The sediments in these formations range from conglomerates to mudstones.

3.6.2 The Molteno Formation

The Molteno Formation forms a wedge with a maximum thickness of 640 m at Maclear, in the south-east, and 30 m at Bethlehem in the north-eastern Free State (Tankard *et al.*, 1982; Visser, 1984). The Formation, which resembles the Katberg sandstone unit of the Beaufort Group, forms a single sandstone unit herewith prominent topographical high areas. Pebbles often found at the contact of the Molteno Formation and Beaufort Group indicate that the base of the Molteno Formation is an erosional surface. This implies that the Molteno sediments eroded the Beaufort sediments before deposition took place (Theron, 1970).

Six depositional cycles, tectonically related to renewed uplifts of the Cape Fold Belt, have been identified in the Molteno Formation (Tankard *et al.*, 1982). Each of the cycles starts with conglomerates and coarse sandstones at the base, followed by fine-grained sandstones and shales with coal-seams. The coarse sediments in the cycles were deposited by braided streams, and the finer sediments by meandering streams (Visser, 1984). The coal-seams indicate that a rich and varied plant growth existed in swamps on the flood-plains during the Molteno era. The cycles are laterally uniform over large areas, but tend to be coarser towards the source areas in the south.

3.6.3 The Elliot Formation

The Molteno sedimentation was followed by the Elliot sedimentation. At this stage, Gondwanaland has drifted more northwards and entered an area where the climate was hotter and drier than in any of the preceding ages. Sediments transported from the source areas eroded and lowered these areas considerably, while filling the Stormberg basin at the same time. The basin thus became shallower with time. The Elliot sediments were therefore mainly deposited under highly oxidizing conditions by meandering streams with reduced energies (Visser, 1989).

The Elliot Formation forms, like the Molteno Formation, a wedge with a maximum thickness of 500 m in the south and 20 m in the north (Tankard *et al.*, 1982; Visser, 1984). The contact between the two formations is transitional and easily recognisable as the first succession of red mudstone. This is followed by medium to fine-grained sandstones—the so-called ‘red beds’ of the Eastern Free State.

The Elliot Formation is characterized by a succession of alternating sandstone, siltstone and mudstone layers, with sandstones dominating in the east and south, and mudstones in the north-west (Theron, 1970). Although the whole formation thins out to the north, all three zones are present throughout. The mudstones are often 100 m thick with thin lenses of fine-grained sandstone (Tankard *et al.*, 1982). The prominent sandstone bodies in the south can be up to 15 m thick, but tend to pinch out laterally (Visser, 1984).

The Elliot Formation was deposited by the same processes as the Beaufort Group. Its geometry therefore much resembles that of the Beaufort Group. The only significant difference is that the Elliot Formation contains more red mudstones and less sandstones.

3.6.4 The Clarens Formation

After the deposition of the Elliot sediments, Gondwanaland was situated at approximately 45° S. The conditions were therefore very similar to the wind-blown Gobi desert of today. The sediments in this formation are

therefore related to æolian sand, playa lakes and sheetflood deposits (Beukes, 1969; Tankard *et al.*, 1982). The majority of these deposits occurred along a north-south belt through Lesotho. Although the Clarens Formation, or Cave Sandstone as it is sometimes called, reaches a maximum thickness of 300 m in the Orange River valley, its average thickness is approximately 145 m (Eriksson, 1981).

Because æolian processes can only move fine-grained particles, sandstones in the Clarens Formation are fine to very fine-grained, with cross-bedded units that can be up to 10 m thick. Stormfloods led to the formation of wadies, in which medium- to fine-grained sandstones were deposited. Wadi deposits are typically upward fining with coarse-grained sandstone at the base, followed by finer grained cross-bedded and planar-bedded sandstone. Intercalated sand and silt were also deposited in the playa lakes. The fine-grained sandstones, resulting from these playa lakes have a high clay content in their matrix (Beukes, 1969).

3.6.5 Hydrological Properties of The Stormberg Group

The characteristics and depositional history of the Molteno Formation indicate that the Formation could form an ideal aquifer. This applies not only to the pebble conglomerates and coarse-grained sandstones at the base of the Formation, but also to the other sedimentary bodies. These sedimentary bodies are more persistent than those of the Beaufort Group and also sheetlike (Theron, 1970)—the ideal geometry for an aquifer. Unfortunately, the Formation does not occur over a large area and tends to form topographical highs. It is thus difficult to site high-yielding boreholes in the Molteno Formation and determine its hydrological behaviour. Nevertheless, it may still be worthwhile to study the groundwater potential of this formation in more detail, particularly if one takes its favourable geometric properties into account.

The largest part of the Elliot Formation consists of red mudstones. The Formation thus represents more of an aquitard than an aquifer. One approach to exploit the groundwater potential of these relatively impermeable but highly porous rocks, is to drill boreholes through the Elliot Formation into the Molteno Formation and restrict the pumping of water to the latter, more permeable formation. This will allow water from the Elliot Formation to leak towards the Molteno Formation. However, the procedure will require more detailed knowledge of both the Molteno and Elliot Formations than is presently available.

The Clarens Formation consists almost entirely of well-sorted, medium- to fine-grained sandstones, deposited as thick consistent blankets (Visser, 1984). It is thus more homogeneous than any of the other Karoo formations. With this type of geometry, the Formation should be an ideal aquifer. Although the Formation has a relatively high and uniform porosity, as shown in Table 3–1, it is poorly fractured and has a very low permeability. The Formation may therefore be able to store large volumes of water, but unable to release it quickly.

Table 3–1 Porosities of the Clarens Formation. [After Beukes (1969).]

Type of Sandstone	Porosity (%)
Very fine grained	6,19–9,82
Cross-bedded	8,87–10,75
Average	8,46

The previous conjecture is supported by the large number of springs that constantly flow from the Clarens Formation. The best approach to use aquifers in the Formation efficiently, will then be to follow the springs and withdraw water very slowly. However, this can only be achieved by using methods other than boreholes to withdraw water from these aquifers. The ancient Persian qanats (Issar, 1985) is one approach that satisfies these demands.

3.7 TRANSFORMATIONS OF THE ORIGINAL SEDIMENTS

3.7.1 Lithification, Compaction and Cementation

The Karoo sedimentation was ended by the outpour of the Drakensberg lavas. This event buried the sediments completely at depths of approximately 2 500–3 000 m, in the case of the Beaufort Group (Rowse and De Swardt, 1976). The increase in pressure and temperature caused by this overburden compacted and lithified the layers of sand, silt and mud to form the sand-, silt- and mudstone layers of today. Some of the deeper buried sediments underwent a slight metamorphism, which indicates that the diagenesis and compaction of the original sediments have been quite severe. The sediments consequently must have lost a large part of

their primary porosity at this stage. This applies especially to the clays, which compact considerably more than sands (Blatt *et al.*, 1980).

Indications are that the Karoo sediments have not been disturbed significantly after the end of the Jurassic Period (141 Ma). This gave groundwater the opportunity to deposit secondary minerals containing carbonates and silica into the open voids, thereby reducing the porosity of the sediments even further. This cementation is especially noticeable in the sandstones, which are usually more permeable than silt- and mudstones, and therefore more subject to cementation (Selley, 1976).

Lithification, compaction and cementation reduced not only the porosity of the Karoo rocks, but also their elasticity. Since the ability of an aquifer to yield water depends on both these properties and its hydraulic conductivity, boreholes in Karoo aquifers may not have high yields. However, this does not imply that the aquifers do not contain significant volumes of water. What it does mean is that one cannot expect to frequently drill very high-yielding boreholes in these formations.

3.7.2 Isostatic Uplift and Development of Fractures

Once formed, the Karoo Supergroup began to weather and erode almost immediately. This process was considerably faster than sedimentation. Large volumes of rock were therefore eroded down quickly in the geological sense. One result of this rapid erosion of the 2 500–3 000 m overlying rock mass was to cause the underlying rocks to uplift isostatically. Such an uplift has a number of consequences for the underlying strata (Price, 1966). However, the most important one, from a geohydrological point of view, is the formation of fractures, which will improve both the porosity and permeability of the strata.

Fractures presumably develop in all the formations of the Karoo Supergroup and all three directions, but more likely in the relatively inelastic sandstones than the elastic shale and mudstone layers. The difference in the elasticity of the various formations may also have favoured the development of fractures along their bedding planes during the uplift. However, the overburden's weight caused some of the deeper lying bedding-parallel fractures to close again once the rate of erosion declined.

3.8 RECENT FORMATIONS

The original Karoo Formations are not the only sources of groundwater in areas underlain by the Karoo Supergroup. The more recent formations, alluvium, colluvium and calcrete, often form extensive aquifers. For example, the town of Ficksburg in the Eastern Free State obtains approximately 50% of its water from alluvial beds in the Caledon River.

Calcrete is usually formed in arid and semi-arid areas and from the weathering of dolerites that are rich in calcium. Since the recharge rate of calcrete aquifers from rain is higher than the 2% average of Karoo aquifers (Kirchner *et al.*, 1991), some of the best Karoo aquifers are situated in calcrete deposits. Farmers in the central Free State district of Petrusburg, for example, often tap calcrete aquifers up to 30 m thick for irrigational purposes. Weaver *et al.* (1993) also targeted valley calcretes with good results after boreholes sited along dolerite dykes failed to yield enough water for the town of Strydenburg in the Northern Cape Province.

3.9 CONCLUSIONS

There can be no doubt that the properties of Karoo aquifers will depend strongly on the deposition and properties of sedimentary rocks in the Karoo Supergroup. One can therefore expect the aquifers to be multi-layered, highly heterogeneous and anisotropic, while their permeabilities will be relatively low and highly variable—not only horizontally, but also in depth. These properties are so much at variance with the media, commonly considered in the derivation of conceptual models for aquifers, that it is difficult to see how the behaviour of these aquifers can be described with existing conceptual models. This applies in particular to the analytical models, often used in the analysis of hydraulic tests performed on aquifers in these formations.

Since many of the Karoo formations are more porous and elastic than other rocks, their small permeabilities may be compensated for to some extent by their specific storativities, as is the case with the Clarens Formation. Unfortunately, the original porosities and specific storativities of the other formations have been reduced considerably by lithification, compaction and cementation. It is thus very difficult to drill boreholes with significant yields into the primary formations. However, this does not imply that the aquifers do not contain significant volumes of water, but rather that they will not readily yield water. *This can only be achieved if one is willing to adapt the rate and volume of water withdrawn to the physical and geometric properties of*

the aquifers and to manage them properly. This is definitely not the case today.

The more recent formations (alluvium, colluvium and calcrete) often form extensive aquifers in areas underlain by the Karoo Supergroup. It will thus be a mistake to disregard these formations when developing production fields in these areas.



CHAPTER 4

MAGMATIC INTRUSIONS

4.1 INTRODUCTION

The Karoo sedimentation was ended by widespread volcanism at the beginning of the Jurassic Age (Tankard *et al.*, 1982). The magmatic activity responsible for this event is presumably related to the tectonic movement of Gondwanaland during the late Triassic to early Cretaceous ages (204–120 Ma). This magmatic activity, whose centre shifted northwards over the period, seems to have occurred in pulses with variable intensities (Fitch and Miller, 1984).

The magmatic activity is commonly divided into two phases—an extrusive and an intrusive phase. The extrusive phase is conventionally associated with the outpour of the Drakensberg lavas. This event probably occurred during the second pulse of the magmatic activity discussed above, when its centre was situated below Lesotho and the northern parts of the Eastern Cape Province (Fitch and Miller, 1984). The event is discussed in Section 4.2, where it is linked with the intrusion of the ring-shaped dyke structures and sills, which are common in large parts of the Karoo landscape.

The continuous shifting of the magmatic activity's centre implies that its later pulses would have less influence on the Karoo sediments. However, some of the pulses may still have enough energy to cause the intrusive phase. The numerous linear dolerite dykes and kimberlites in the Karoo formations probably intruded during one or more of these pulses. These structures are discussed in Sections 4.3 and 4.4, respectively.

The influence that the various intrusions had on the geology and geohydrology of Karoo aquifers is discussed in Section 4.5.

4.2 THE DRAKENSBERG LAVAS

4.2.1 General

The extrusive phase of the magmatic activity must have been extremely active, judging from the thickness of the lavas in Lesotho. The lavas, which are still 1 400 m thick in some places, cover approximately 80% of Lesotho and a significant area of the Eastern Cape Province. No wonder that Fitch and Miller (1984) refer to this event, which they date to around 193 Ma, as '*one of the most sudden, extensive and important events in the Mesozoic history of Africa.*'

Although the fragmentation of Gondwanaland must have been on a much larger scale than an ordinary earthquake, it is not unreasonable to assume that the event was also followed by a series of less energetic tectonic events. This assumption implies that the outpouring of the Drakensberg lavas was followed by further, less extensive phases; a conclusion supported by the work of Fitch and Miller (1984), who identified seven such phases between 204 Ma and 120 Ma.

The thickness of the Drakensberg lavas and the extent of the area they covered suggest that this catastrophic event has been accompanied by huge extensional forces. It is thus difficult to imagine that the forces responsible for the event were restricted to Lesotho, since the intensities of natural catastrophes usually decrease with distance from their centres. The effect that the event had on nearby regions would therefore have been less severe than in Lesotho. The outpouring of the Drakensberg lavas must therefore be regarded as incongruous, from the physical point of view, unless evidence can be found for less extensive intrusions in the areas surrounding Lesotho.

The theory of magmatic intrusions in Appendix A indicates that magma can intrude into the earth's crust either through existing fractures or matrix melting. It is natural to associate the outpouring of the Drakensberg lavas with the intrusion of magma, into fractures that penetrated the earth's crust fully, or could be opened by the intruding magma. However, intrusions in the surrounding areas would have been restricted to fractures that penetrated only the deeper layers of Gondwana's crust. This would certainly have been the case for most of the fractures. This may explain why related intrusions have not

been observed in the surrounding areas. The possibility also exists, of course, that some of the known intrusions in these areas are indeed related to the Drakensberg lavas, but that their origin had been misinterpreted previously.

Magma that intrudes into partially developed fractures has two options: it can solidify immediately, or begin to lift and deform the upper layers. As shown by the discussion in Appendix A, it will be quite natural for the magma to form laccolithic bodies in the latter situation. The possibility therefore exists that the crust of the area, surrounding Lesotho will contain magmatic structures in the form of laccoliths.

4.2.2 Ring Dykes

One of the most prominent features in the Karoo landscape today is the large number of ring-shaped dyke structures present in the southern Free State and the northern parts of the Eastern and North Cape Provinces. A closer examination of these structures reveals that they are positively weathered dolerite structures in the form of a cup. Since this form very much resembles that of a peripheral dyke associated with a laccolith (see the discussion in Appendix A), it is natural to associate them with the widespread volcanism that must have accompanied the outpour of the Drakensberg lavas. This interpretation has the advantage that it provides a simple physical explanation for the existence of these structures and the otherwise incongruous extrusion of the Drakensberg lavas. However, the structures are conventionally regarded as undulating dolerite sills (Meyboom and Wallace, 1978).

Although it is always possible to deform a sheet into a cup form mathematically, the physical process will require extraordinary physical conditions. Moreover, it is not clear from the mathematics of the deformation why the dykes should in this case always dip towards a point at their centres. It was this observation that led Burger *et al.* (1981), who mapped the ring dykes in the southern Free State and adjacent areas extensively, to conclude that the structures are laccoliths and not undulating dolerite sills. *Ring dykes will therefore be interpreted as laccolithic structures in this report.*

The laccolithic structures are not restricted to surface features alone. Indeed, two of the largest of these structures, one at Ingeli and the other at Insizwa, occur at considerable depths, as illustrated by the vertical cross-section for the one at Insizwa, in Figure 4–1.

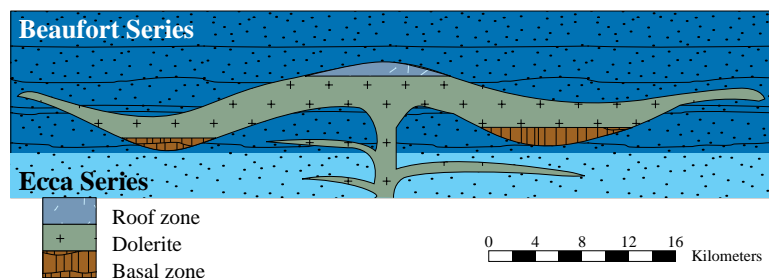


Figure 4–1 Vertical cross-section through the laccolithic body at Insizwa. [Redrawn from Truswell (1970).]

The association of the ring dykes with the outpour of the Drakensberg lavas is supported by two other observations. The first is that the areal density and size of the structures decrease with distance from Lesotho, as can be seen on any satellite image of the area. The second is that the structures appear especially in those areas where the Karoo basin was very deep.

Two arguments are usually advanced to reject the interpretation of ring dykes as laccolithic structures: (a) the ‘horns’ (peripheral dykes) of laccoliths are too small to represent the observed ring structures, and (b) the stems of the laccoliths have never been observed. However, it must be remembered that the pictures of laccoliths in Appendix A and other publications are based on the classical gelatin models of Pollard and Johnson (1973), which certainly do not represent the field situation accurately. Moreover, as shown by Equation (A.10), the final form of the ‘horns’ will ultimately be controlled by the *elastic properties* of the magma and its immediate surroundings. Since the theory of elasticity, unlike quantum mechanics, does not place implicit restrictions on the behaviour of elastic materials, the ‘horns’ can in principle assume almost any circular form imaginable. The ‘horns’ of ring dykes may therefore extend for hundreds of metres, perhaps even kilometres, below the surface (Burger *et al.*, 1981).

The previous property of the ‘horns’, incidentally, explains why the stems of laccoliths have not been observed so far—they are simply too deep. Moreover, there is no reason to believe that the peripheral dyke

will be symmetric with the stem of the laccolith. It will thus be very difficult to establish the exact position of the stem from observations of its associated peripheral dyke alone.

4.2.3 Dolerite Sills

Sills in the Karoo formations are sheetlike forms of dolerite intrusions that tend to follow the bedding planes of the formations concordantly. These structures, whose thicknesses vary from less than a metre to hundreds of metres, represent the dominant form in which dolerite is emplaced in the Karoo Supergroup (Walker and Poldervaart, 1949). It is thus important to know how the sills were emplaced and how they may influence the geohydrology of the Karoo Supergroup.

The theory of magmatic intrusions in Appendix A shows that the driving force of the magma must exceed a critical limit to form a laccolith. Laccoliths will thus not always form when magma intrudes the overburden. Indeed, the theory shows that it may be more common for the magma to fracture the overburden along bedding planes, and then flow along the fracture to form a sill—a possibility that increases as the viscosity of the magma decreases. It is therefore not unrealistic to interpret sills as laccoliths without the characteristic peripheral dyke structure. This view is supported by the extent of the sills, which indicates that considerable forces were responsible for their emplacement. Moreover, it also provides a natural explanation why sills are the dominant form in which dolerite was emplaced in the Karoo Supergroup. It is therefore not unreasonable to assume that the sills were emplaced at the same time as the ring dykes and the outpour of the Drakensberg lavas.

Of course the possibility exists that some of the sills intruded during the very active third pulse in the fragmentation of Gondwanaland, which Fitch and Miller (1984) date to 178 Ma. This age agrees very much with the age of 180 Ma that Reid and Rex (1994) assign to sills in the north-western parts of the Northern Cape Province.

Dolerite sills in the Karoo Supergroup often have very complex forms. Some of them are transgressive, a further indication that they are related to laccoliths, while others tend to be sinuous (see Figure 4–1). This variation in the shapes of sills, which is not foreign to laccolithic intrusions (Rubin, 1995), is probably the reason why Meyboom and Wallace (1978) interpreted ring dykes as undulating sills.

4.3 LINEAR DOLERITE DYKES

It is possible that some ring dykes and sills intruded during the magmatic pulses that occurred after the pulse of 178 Ma. However, judging from the discussion in Appendix A, it is more probable that these pulses caused the intrusion of another set of magmatic intrusions present in the Karoo sediments—*linear dolerite dykes*. An important consequence of this interpretation is that linear dolerite dykes must be younger than the ring dykes and sills—a conclusion supported by a number of observations. For example, Reid and Rex (1994) date the Mehlberg Dyke, in the northern Richtersveld, to the Cretaceous period (134 Ma), which is considerably younger than the Jurassic age (180 Ma) of the sills in the area.

Another indication that the linear dykes are younger than ring dykes and sills, is that they frequently cut the latter structures, as illustrated in Figure 4–2. The linear dykes are also usually thinner than ring dykes and are confined to the Ecca and Beaufort Groups (Walker and Poldervaart, 1949). This is a clear indication that the magmatic activity at the time the linear dykes intruded was less than when the ring dykes and sills intruded.

The insight into the intrusion of linear dykes is fairly limited at the moment (Rubin, 1995). It is however known that linear dykes are usually associated with linear conduits that feed magma to the earth's surface (Hargraves, 1980). In his discussion of the magmatic activities on Hawaii, Ryan (1990) also notes that the magma erupts from linear fissures for periods ranging from a few hours to a month.

As mentioned in Appendix A, the form of linear dykes suggests that they intruded by the mechanism of matrix melting. In this case, the intrusion is driven by a difference in the magma pressure at the top and bottom of the dyke. No existing fracture is thus needed for the magma to intrude.

To describe the mechanism of matrix melting, consider a magma with density ρ_m . As shown in Section A.2 of Appendix A, there exists a pressure difference, p_d , between the magma at the top of the dyke and its bottom. If there is also an overpressure, p_m , in the magma chamber, the tip of the dyke will experience an excess pressure

$$P = p_m + p_d$$

If large enough, this excess pressure may fracture the overburden and allow the magma to propagate in the vertical direction, as shown in Figure 4–3.

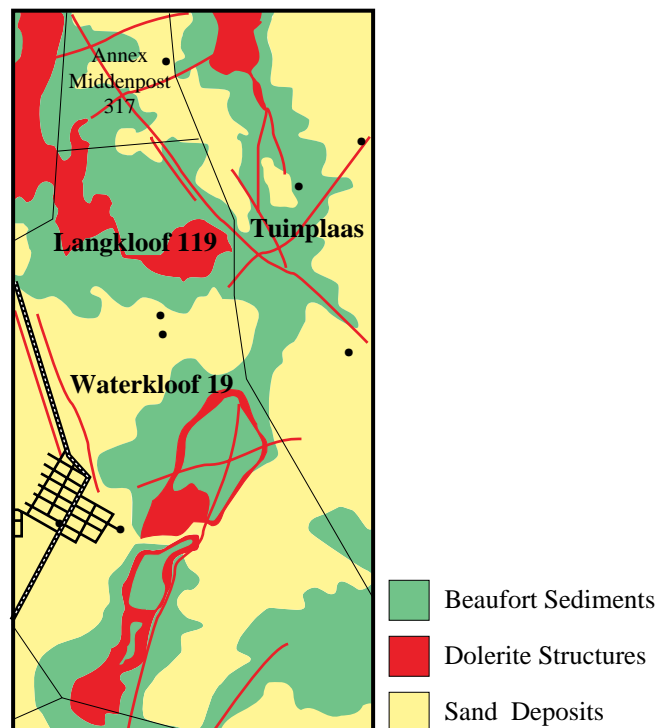


Figure 4–2 Examples of linear dolerite dykes that cuts ring dykes and sills near Philippolis. [After Burger *et al.* (1981).]

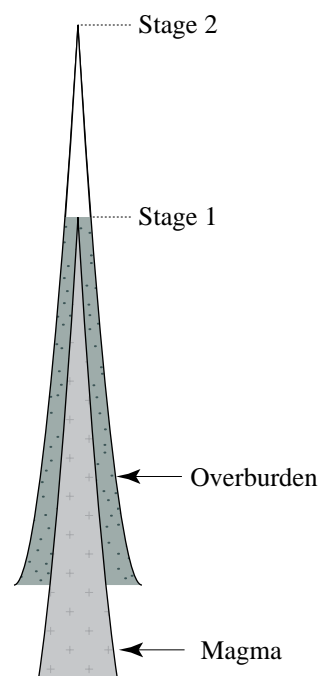


Figure 4–3 Hypothetical shape of an intruding dyke, adapted from Maaløe (1985). The magma has reached Stage 1, where it caused the overburden to fracture to Stage 2, into which it will intrude in a fraction of a second.

Seismic observations suggest that linear dykes are formed at depths of 40–50 km (Maaløe, 1985). Since the mantle is ductile at these depths, the dyke will probably propagate by creep fracture. However, since the overlying rocks are less elastic, the velocity of fracture propagation increases to a few kilometres per second near the surface. This velocity is so high that the fracture begins to thin out and the magma starts to lag behind as the fracture propagates upwards. The effect of this high velocity is that the magma intrudes in jerks with a frequency of 1–10 Hz (Maaløe, 1985). It is not impossible that parts of the host rock may be dislocated during these jerks, and transported upwards by the intruding magma. This phenomenon may have been responsible for the inclusion of sandstone in a core sample, from a dolerite dyke at Dewetsdorp. The characteristic sinusoidal seismic activity, called *harmonic tremors*, often observed during volcanic eruptions, is probably also related to these jerks (Maaløe, 1985).

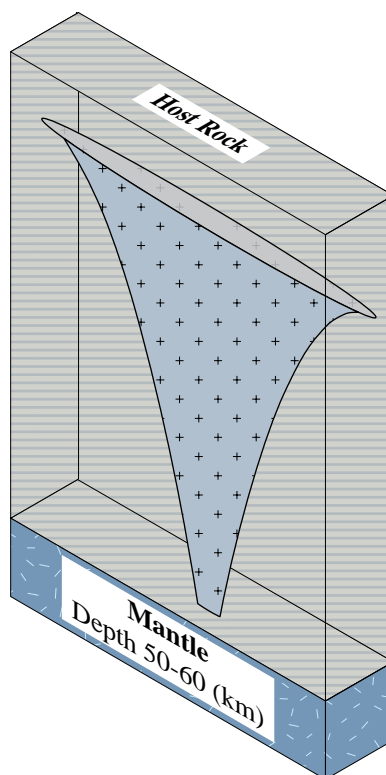


Figure 4-4 Possible shape of a dyke, extending from the mantle to the surface. [After Maaløe (1985).] The diagram is not to scale, because the vertical elevation is 40–50 (km).

The exact form of the dyke during the intrusion is not known. However, the increase in fracture velocity will tend to deform its shape. A dyke that starts out with an elliptical cross-section may thus end as an elongated narrow fracture as shown in Figure 4-4. The form of the Gap dyke in the Transkei, which can be followed for several kilometres before it narrows down and disappears (Walker and Poldervaart, 1949), much resembles this geometry.

4.4 KIMBERLITES

Kimberlites present another type of magmatic intrusion into the Karoo sediments. The gaseous magmas responsible for these structures intruded very rapidly into the earth's crust to form pipes, dykes and sills. These magmas were often responsible for the formation of breccias and tuffs, depending on the volume of gases they contained (Tankard *et al.*, 1982). There is thus a possibility that high-yielding boreholes can be sited along kimberlites, as shown by the Free State towns of Jagersfontein and Fauresmith, that obtain all their water from the abandoned diamond mine at Jagersfontein. However, the overall contribution of kimberlites to groundwater in the Karoo sediments is relatively low. Moreover, recent investigations have shown that the water from the diamond mine at Jagersfontein contains large quantities of arsenic, which may be related to the composition of kimberlites. Kimberlites will therefore not be considered further in this discussion.

4.5 THE GEOHYDROLOGY OF DOLERITE INTRUSIONS

4.5.1 GENERAL

Linear dolerite dykes have always been regarded as the major source of groundwater in the Karoo Supergroup. One important reason for this belief is that dolerite dykes are the only structures in the Karoo Supergroup that can be located relatively easy with existing geophysical techniques. The density of fractures, usually regarded as the main source of water in Karoo formations, is also higher near linear dykes than in the undisturbed sedimentary rocks.

The classical explanation for the existence of the fractures near linear dykes is that the hot magma baked the Karoo rocks during the intrusion. However, the question then arises: why are dolerite sills and ring dykes not regarded as good sources of groundwater?

As explained above, sills possibly intruded with the ring dykes and Drakensberg lavas during the extremely active magmatic phase of 193 Ma. Basaltic magma is generated at depths of 60–80 km and thus have an extremely high temperature, 900–1 200°C (Maaløe, 1985). The magma partaking in the intrusion of the sills and laccoliths was therefore so hot that, instead of merely baking the Karoo sediments, they actually metamorphosized them. Linear dykes, on the other hand, intruded during the less active phases of Gondwanaland's fragmentation, and thus would have less energy, some of which was used to fracture the overburden. Linear dykes therefore did not have enough energy to metamorphosize the Karoo sediments significantly. This explanation is supported by the experience gained at Philippolis. The 26 successful boreholes drilled there, were all sited along linear dykes, except for two redeveloped boreholes, originally sited by Burger *et al.* (1981) along a ring dyke, and another two that did not intersect any dyke. The boreholes sited by Burger had blow-yields of 14,4 and 25 m³ h⁻¹, while the highest blow-yield in the other boreholes sited along ring dykes was only 3,6 m³ h⁻¹.

An interesting difference between the ring dykes at Philippolis is that the dyke of Burger *et al.* (1981) has weathered negatively (i.e. down to the soil surface), while the ring dykes Botha *et al.* (1996) investigated, have all weathered positively. Highly weathered ring dykes should therefore not be neglected as borehole sites. However, it must be remembered that the ring dyke forms the boundary of the associated aquifer. A production borehole situated next to and on the inside of a ring dyke may therefore not be able to tap the resources of the aquifer in full (Bakkes, 1977).

4.5.2 Mechanical Deformation of Karoo Rocks

The baking and metamorphosizing of the host rocks were not the only effects that the intrusion of dolerites had on the Karoo sediments. Other effects, particularly mechanical deformation, may also have influenced the geohydrological properties of the rocks.

Judging from the experience gained in drilling the boreholes at Dewetsdorp and Philippolis, two of the most important mechanical deformations of the host rock are: bending and dilation. However, there are indications that not more than 50% of the linear dykes in the Karoo formations were deformed mechanically. This may be a further indication that the dykes intruded by matrix melting.

Dilation occurs when the intruding dyke, particularly inclined dykes, shifts the overburden on top of it, as shown in Figure 4-5. The magma in an intruding dyke tends to cool off more rapidly at its contact with the host rock, thereby forming a chilled edge. Dykes that caused dilation are therefore often accompanied by slickensides, usually slickensided quartz, in the Karoo formations. It is interesting that on the three occasions where bore-

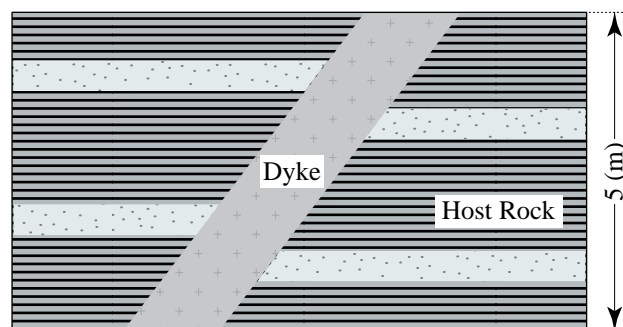


Figure 4-5 Schematic illustration of the phenomenon of dilation. [Adapted from Park (1989).]

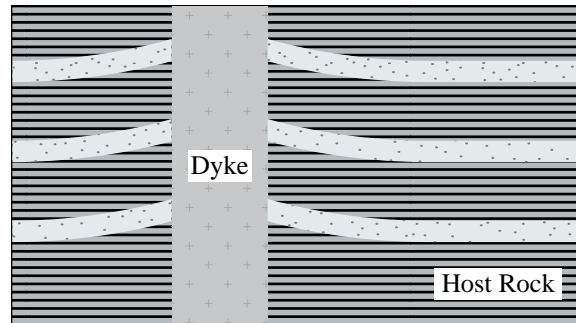


Figure 4-6 Schematic illustration of the bending of Karoo rocks by a linear dolerite dyke.

holes were drilled through such dykes at Dewetsdorp and Philippolis; more water was struck at the upper contact of the dyke than at the lower contact. One possible explanation for this behaviour is that the upper surface of the dyke was stripped of its chilled edge during the intrusion, thereby exposing the country rock to the hotter magma for a longer time, and thus the possibility of fracturing (Walker and Poldervaart, 1949).

Observations have shown that the intrusion of dolerites caused two types of bending in the host rocks of the Karoo formations. The first type, illustrated schematically in Figure 4-6, is where the surrounding rocks were bended concavely by an intruding linear dyke. It is not difficult to see that this type of bending was caused by frictional forces that existed between the dolerite and the surrounding rock. The bending is consequently usually restricted to relatively small distances (~20 m) on both sides of the dyke. This type of bending, nevertheless, can fracture the host rock considerably near the dyke. The highest yielding borehole Botha *et al.* (1996) drilled at Philippolis, indeed intersected such a fractured region near a linear dyke. One should be careful, however, not to confuse this type of fracturing with that caused by a dyke that intruded into a pre-existing fault.

The second type of bending that can be observed quite often in the Karoo formations, is where the host rock was bended in the form of an arch, as illustrated in Figure 4-7. A preliminary attempt to explain this type of bending quantitatively, has shown that the simplest explanation is to assume that the dolerite intruded as a laccolith. The existence of these arch-shaped formations therefore supports the hypothesis that laccoliths did intrude into the Karoo formations at some time in the past. However, the physical interesting feature of Figure 4-7 lies not so much in that it illustrates that laccoliths have intruded into the Karoo formations, but rather that such intrusions do bend the overburden in the form predicted by the simple theory of laccolithic



Figure 4-7 Bending of the Karoo formations by a laccolith, in a cutting on the N1 highway, between Philippolis and Trompsburg.

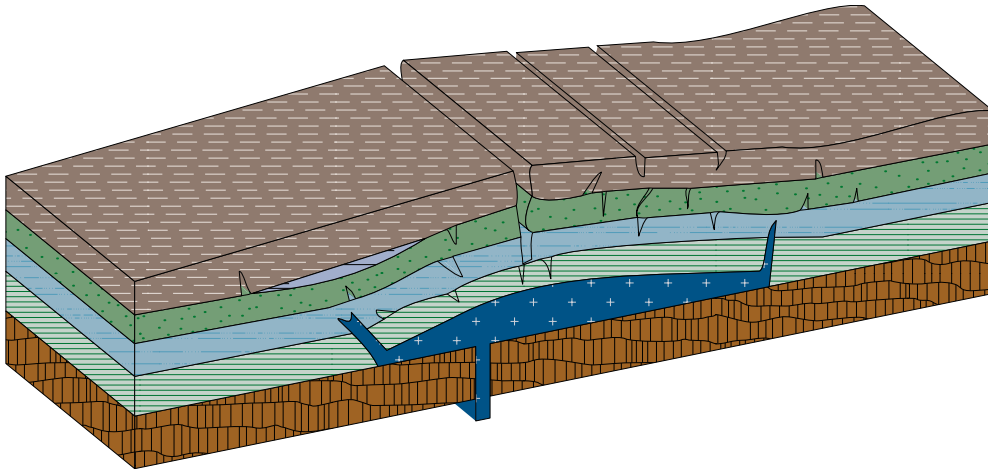


Figure 4–8 Schematic illustration of how an intruding laccolith will bend the sediment layers in a Karoo aquifer. [Derived from the gelatin model of Pollard and Johnson (1973).]

intrusions in Appendix A.

The discussion in Section A.4.4.2 and the illustration in Figure 4–8 show that laccolithic intrusions will cause two sets of fractures in the overburden—one that opens downwards and the other that opens upwards. The fractures that open upwards should be free from dolerite, and thus form receptacles for groundwater, unless closed later by other processes. Such areas will clearly be ideal recharge areas for Karoo aquifers, or even form aquifers on their own if they did not develop too deeply within the earth’s surface. Rocks bended by laccoliths can therefore play a prominent role in the geohydrological behaviour of aquifers. It may thus be important to pay more attention to the areas enclosed by ring dykes in future studies of Karoo aquifers.

The discussion in Section A.4.5 is based on the assumption that multiple layers in the overburden will slide across one another during the intrusion of a laccolith. The Karoo formations, however, are highly stratified with alternating layers of partially bonded sandstones, mudstones, siltstones and shales, each with its own elastic modulus. It will therefore be difficult for the layers to simply slide across one another, without weakening or fracturing their contact planes when displaced by a laccolith. The intrusion of laccoliths may thus have been responsible, or at least have contributed, to the existence of another major feature of Karoo formations—bedding-parallel fractures. The frequency with which bedding-parallel fractures occur in Karoo formations and their sizes can be judged from the photograph of the core from Borehole CH6, situated on the Campus Test Site, in Figure 4–9.

All the high-yielding boreholes, drilled during this project intersected at least one bedding-parallel fracture. This observation suggests that bedding-parallel fractures act as the main conduits of water in Karoo aquifers. A major prerequisite to drill a successful borehole in the Karoo formations is thus to strike one of these bedding-parallel fractures. There must therefore be areas in the Karoo landscape, *away from dolerite dykes*, where high-yielding boreholes can be drilled, if the previous interpretation is correct. This conclusion is supported by the hydrocensus of Burger *et al.* (1981), who surveyed 1 245 boreholes in the districts of Bethulie, Springfontein and Trompsburg. As shown by their census results and the accompanying maps, 63% of these boreholes are situated on laccoliths, and not near dolerite dykes. It is also interesting to observe that none of the 32 boreholes drilled on the Campus Test Site to date intersected a dolerite dyke.

It is, of course, possible that bedding-parallel fractures may have been created by other processes, such as the uplift caused by the weathering of the formations. The simplicity of the physics involved, however, favour the intrusion of laccoliths. The bending of Karoo formations by laccolithic intrusions may thus have played a very important part in the geohydrology of Karoo aquifers.

4.5.3 Weathering of Dolerite Dykes

One surprising observation made during the drilling programs at Philippolis and Rouxville, was the influence that the weathering of a dyke had on the success rate of boreholes. The dykes, near which high-yielding boreholes have been drilled, were all highly weathered and exhibited *exfoliating* weathering patterns. The boreholes drilled near all the other dykes were either dry, or had very low yields.

The general belief is that coarse-grained dolerite tends to weather more intensely than fine-grained



Figure 4-9 Photograph of cores from borehole CH6 on the Campus Test Site. The borehole is inclined at an angle of 45°.

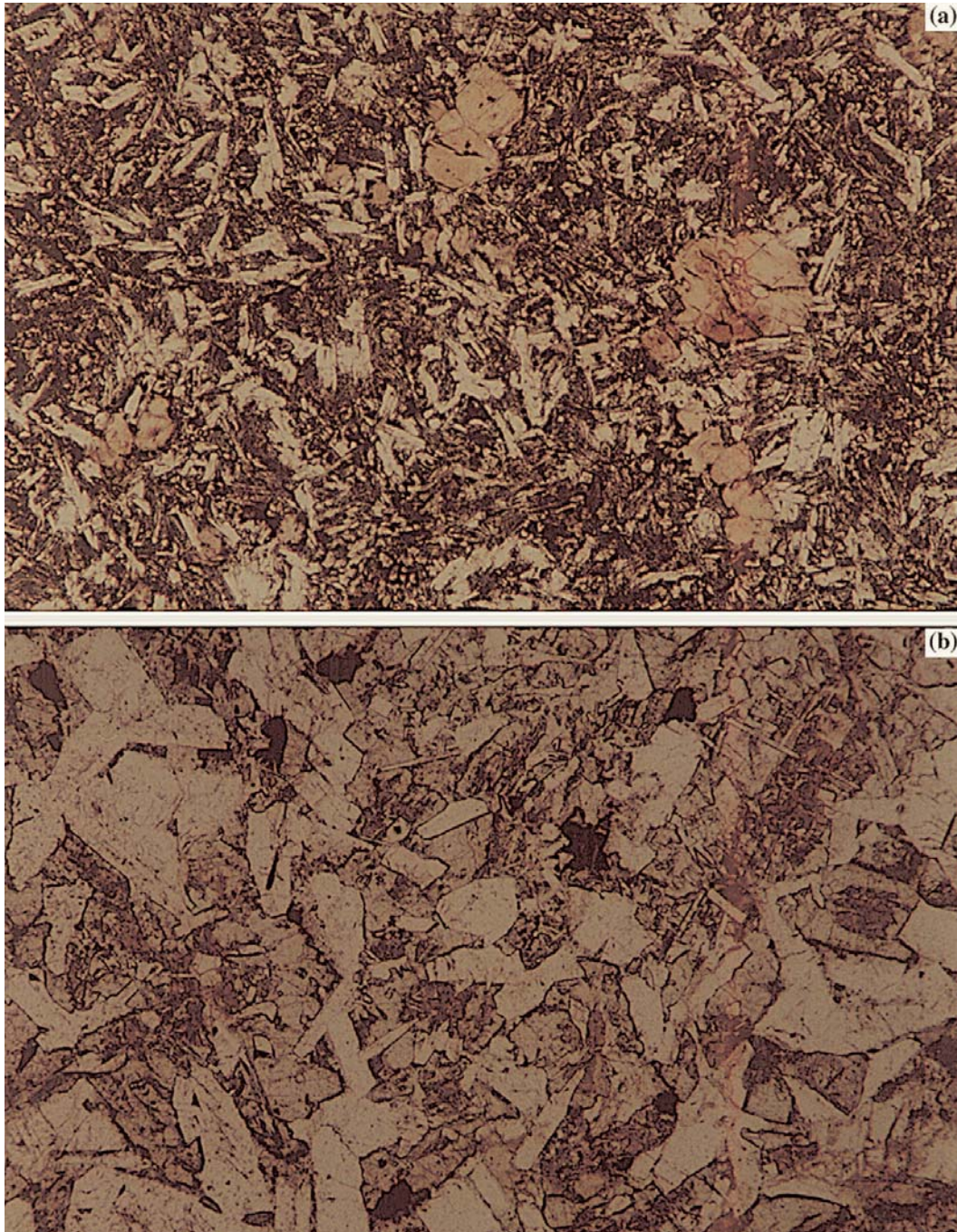


Figure 4–10 Photographs of thin sections of (a) a fine-grained and (b) a coarse-grained dolerite dyke at Philippolis.

dolerite. However, a visual inspection of highly weathered dykes at Philippolis and Rouxville indicated that they were fine- to medium-grained. Thin sections, two of which are shown in Figure 4–10, were therefore made from samples of the dykes, and analysed microscopically. The results, summarized in Table 4–1, confirmed that the dykes were indeed fine- to medium-grained. A dyke's grain size and state of weathering can thus be important indicators of the yields one can expect from boreholes drilled near linear dykes.

4.6 DISCUSSION

One of the most characteristic features of the Karoo landscape is the ring-shaped dyke structures that are especially noticeable in the southern Free State and adjacent areas. These structures are conventionally re-

Table 4–1 Summary of the characteristics of dolerite dykes at Philippolis and Rouxville, and the yields of boreholes which intersected them.

Sample	Grain Size	State of Iron Oxides	Weathering	Borehole Yield (m ³ h ⁻¹)
D15	Coarse	Highly leached	Highly weathered	6,0
RC3	Coarse	Leached	Not weathered	Dry
RB1	Medium	Not leached	Not weathered	0–1
RF	Medium	Not leached	Not weathered	1,5
RB2	Medium	Leached	Not weathered	3,0
D21	Medium	Leached	Highly weathered	2,5
D19	Fine	Leached	Highly weathered	9,0
F32	Fine	Leached	Highly weathered	12,0
SS1	Fine	Leached	Highly weathered	18,0
RA1	Fine	Not leached	Not weathered	6,0

garded as partially weathered dolerite sills. However, the present discussion shows that it makes more physical sense to regard them, and the dolerite sills that occur even more frequently in the landscape, as laccolithic structures. A particular advantage of this interpretation is that it provides a natural explanation of the observed complex geometry and behaviour of Karoo aquifers, discussed more fully in Chapter 6. This interpretation is, admittedly, based on very little field data. It is thus important that efforts should be made to elucidate the intrusion of these structures. More detailed information on their age may be particularly useful in this regard.

Linear dolerite dykes have always been considered as very important for the geohydrology of Karoo aquifers, particularly as places where successful boreholes can be drilled; a view that is fully supported by the present investigation. This situation can be ascribed to two properties of the dykes: (a) they are highly magnetic and can thus be traced easily with existing geophysical methods, and (b) they only baked the host rock, thereby creating ideal conditions for the formation of fractures. The latter property is particularly important as successful boreholes in Karoo aquifers have always been associated with fractures in the aquifer. However, linear dykes do not seem to play an important role in the physical behaviour of the aquifers, except that they form internal boundaries within the aquifers, thereby limiting the domain from which a borehole can receive water.

An interesting phenomenon observed at Philippolis, is that the majority of high-yielding boreholes are situated near highly weathered fine- to medium-grained dolerite dykes, in particular those that show an exfoliating weathering pattern. No explanation can be given for this phenomenon at this stage, except to note that it is mainly found in the younger linear dykes and not the older laccolithic ring dykes.



CHAPTER 5

GEOLOGY OF THE CAMPUS AND DEWETSDORP TEST SITES

5.1 INTRODUCTION

The physical behaviour of Karoo aquifers was studied at five experimental sites in the Free State. The sites are located on different stratigraphic sequences in the Beaufort Group and represent some of the variable characteristics to be expected in Karoo aquifers. The Campus Test Site at the University of the Orange Free State in Bloemfontein was developed first. This site is located on the Adelaide Subgroup of the Beaufort Group, while the four other sites, situated at Dewetsdorp, are located on the Tarkastad Subgroup.

The original purpose of the experimental sites was to acquire data on the behaviour of the aquifers by analysing data from hydraulic tests with existing analytical models. A series of percussion boreholes was therefore drilled on each site. However, a new approach had to be adopted when the results of the initial hydraulic tests made it clear that the existing analytical models were inadequate for the analysis of hydraulic test data from Karoo aquifers.

The first step in this direction was to supplement the percussion boreholes with core-boreholes. The cores from the first of these boreholes indicated that the geometry of these aquifers differs completely from that used in the derivation of the analytical models available at the time and even from the customary interpretation of Karoo formations. The aquifers' present geometry must obviously be related to the genesis of the Karoo formations. Two steps were therefore taken to try to explain the observed geometry of the aquifers. The first was to review the genesis of the Karoo formations, described in Chapters 3 and 4, and the second to try to confirm the results of the review with field observations. The existing information on the geology of the central Free State was too limited for this purpose, unfortunately. The only way to achieve the objective was thus to investigate the geology of the area in greater detail. Since the resources available for this purpose were limited, the investigation had to be limited to the area around Bloemfontein, and to the following three objectives.

- (a) Provide a regional perspective for the clastic aquifers at the Campus Test Site.
- (b) Study the stratigraphy, sedimentology and structure through a multi-disciplinary approach.
- (c) Determine the aquifer potential of rocks in the Karoo Supergroup in this area.

The discussion that follows therefore begins with the geology of Bloemfontein in Section 5.2. This is followed by a discussion of its stratigraphy, structure and geomorphology in Section 5.3 and its structural geology in Section 5.4. The geology and geohydrologic features of the Campus Test Site are discussed in Section 5.5, while that of the Dewetsdorp sites are discussed in Section 5.6. The main results of the investigation are summarised in Section 5.7.

5.2 GEOLOGY OF THE BLOEMFONTEIN AREA

5.2.1 Previous Studies and Sources of Information

The Karoo strata of the central Free State and more specifically the area around Bloemfontein, are not very well-known, because stratigraphers and palaeontologists prefer to study the better exposed sections in the incised and mountainous areas along the eastern border of the province. It is known though that Bloemfontein is situated on the upper beds of the Adelaide Subgroup, near the western border of the Beaufort Group, except for a few small isolated outliers. Beds of the Tarkastad Subgroup crop out 30–40 km south and east of the city.

A careful scrutiny of Sheet 2926 Bloemfontein (Geological Survey, 1966) and an examination of contacts in the field showed that the existing map of the basal contacts of the Adelaide Subgroup is not very consistent. For example, Kingsley and Theron (1964) discovered a coarse-grained sandstone containing feldspar and pebbles in the Adelaide Subgroup near Bloemfontein, with a cross-bedding directed to the west and north-west. Theron (1970) subsequently investigated the unit in more detail and carefully examined the extra-basinal pebbles and cobbles. He came to the conclusion that the unit is a separate entity because of its texture and

primary structures, and gave it the informal name of Northern Beaufort Formation. Theron (1970) considers the unit separate from, but contemporaneous with, the Tarkastad Subgroup. Unfortunately, he omitted to give a stratigraphic column or a thickness for the unit. In this report, the unit is called the Musgrave Sandstone.

Theron (1975) later extended his palaeocurrent studies to the full area where the Beaufort Group crops out in the Free State. Although his studies are interesting, their usefulness is limited by the lack of stratigraphic control.

The discovery of uranium in rocks of the Beaufort Group, shortly after 1970, led to a massive exploration programme in the Southern Karoo (Cole *et al.*, 1991). The uraniferous rocks were later traced north-eastwards along a narrow zone up to a farm 40 km south-south-west of Bloemfontein. Although the reports mention a few other, smaller radiometric anomalies in the lowermost Beaufort rocks of the area, their exact stratigraphic position and nature of the host rock are not described.

A useful method to establish stratigraphic control is to use biostratigraphic markers, since they provide definite evidence for the age, position and correlation of stratigraphic assemblages. For example, it is known that *Daptocephalus* Zone (*Dicynodon* Assemblage Zone) fossils mark the Adelaide Subgroup, while *Lystrosaurus* Zone fossils mark the Tarkastad Subgroup. The map of Kitching (1977) shows that *Daptocephalus* Zone fossils occur in an area near the Modder River, but also shows four *Lystrosaurus* Zone localities north and south of Bloemfontein. Unfortunately, these localities are not described in the text and the precise positions where the fossils were found, are not known. No *Lystrosaurus* fossils were found in or near the city during the present study, however.

Geologists and diviners have sited numerous boreholes over the years in and near Bloemfontein, but there are very few records of their geological profiles and yields. The borehole data used in the following discussion were therefore restricted to that of the boreholes on the Campus Test Site.

5.2.2 Regional Survey

The regional survey of the area was based on a continuous feed-back system in that data obtained on a regional scale were always compared with that obtained on a local scale. This technique yielded a broad geological perspective of the palaeo-environmental system of deposition, the magmatic intrusion of dolerites and the effects of later tectonic forces on the deposition of the strata.

The first step was to investigate suitable exposures in hillslopes, road-cuttings and dongas, in an area of approximately 20×20 km around Bloemfontein, and to compile geological columns for the Beaufort strata observed in them. The thickness, lithology, fossil content, texture, primary structures and nature of contacts were therefore noted for each bed and at each locality. The strata from one site to the other were then correlated by using characteristic and easily recognisable marker beds. Unfortunately, dolerite intrusions, scree and a surficial cover made it impossible to establish complete columns for some of the localities. This study benefited considerably from the work of Dr. Johan Welman, palaeontologist of the National Museum in Bloemfontein, who helped to identify the Karoo vertebrate fossils and determine their exact stratigraphic position.

5.3 GEOMORPHOLOGY OF THE CENTRAL FREE STATE

5.3.1 General

As discussed in Chapter 3, the sediments of the Karoo Supergroup were deposited in a foreland basin from the late Carboniferous to the early Jurassic Periods. The strata around Bloemfontein represent the platform facies of the basin, whose trough lay 400 km to the south. This platform facies rests on the Cape-Vaal Craton, an ancient stable part of Southern Africa. The result is that the Karoo strata are still horizontal or nearly so. Slight departures from the horizontal bearing, and the reasons for them, are discussed in Section 5.4.

A major feature of the landscape around Bloemfontein is the hills of dolerite and Beaufort strata, the latter often capped by dolerite, separated by wide plains with pediments and bahadas, as shown in Figure 5–1. Outcrops are rare between the hills, because of the surficial cover of calcrete, windblown sand, alluvium and soil. A shallow watershed runs north-south, just west of the city centre. The surface drainage to the west is towards Kaal Spruit, and to the east through rivulets that run first eastwards and eventually northwards before joining the Modder River.

The presence of *Dicynodon* fossils in the sediments indicates that the age of the strata around Bloemfontein belongs to the upper part of the Adelaide Subgroup (see Figure 3–1). The Eccia Group is present at a projected depth of roughly 200 m, and crops out 40 km west of the city. The Tarkastad Subgroup of the Beaufort Group crops out to the east and south-east. Before the onset of the post-Jurassic erosion, the upper units of



Figure 5–1 South-western view of the Karoo landscape near Bloemfontein. The first hill in the background is the dolerite-capped Brandkop and the farthest one Leeuberg.

the Karoo Supergroup extended to the west of the city.

An examination of contacts in the field shows that the mapping of the Ecce-Beaufort contact, as reported on the Sheet 2926 Bloemfontein, is inconsistent and even misleading from a geohydrological point of view. The reason for this inconsistency is the absence of stratigraphical-structural data for the area. Aquifers in Beaufort sediments were thus often associated with Ecce sediments in the past. This caused a considerable difficulty for the stratigraphic classification of the core-boreholes drilled to depths of 100 m on the Campus Test Site.

According to Sheet 2926 Bloemfontein, the Ecce Group is represented by shales in this area. The argillaceous rock that occurs below a prominent medium-grained sandstone on the Campus Test Site was consequently interpreted as Ecce shales. Based on his analysis of the lithology and palaeocurrents, Ryan (1967) relates the Ecce in this part of the Karoo to the Central Facies of the Group, which represents *deposition in an inland sea*. However, the detailed stratigraphic analysis of the cores revealed that the argillaceous rock was grey and red mudstone and siltstone *deposited in a fluvial system*. Moreover, the cores give no indication of a ‘break’ in palaeo-environment, as one would expect from the description of the Ecce and Beaufort sedimentation in Chapter 3. The previous interpretation of the argillaceous rock as Ecce shales is thus incorrect; it is mudstone and siltstone deposited in the fluvial systems associated with the Beaufort Group.

5.3.2 Beaufort Stratigraphy

The positions of the hills, road-cuts and dongas, used to compile a stratigraphic column for the Beaufort Group, are shown on the map in Figure 5–2. The geological columns for the Beaufort strata at eight of the sites are shown in Figure 5–3 and the column in Figure 5–4. The beds overlying the Musgrave Sandstone in the column are only present at Leeuberg, and do not occur in or near Bloemfontein. They are included here only for reference purposes.

The list of vertebrate fossils in the column of Figure 5–4 shows that the *Dicynodon* Assemblage Zone occurs at least to a position 20 m above the Musgrave Sandstone. The three major sandstone units (Musgrave, Spitskop and Campus) in the area are thus situated in the Adelaide Subgroup of the Beaufort Group. No contact between the *Dicynodon* and *Lystrosaurus* Assemblage Zones has been observed near the city.

Sandstone units are usually considered to be the main aquifer units in sedimentary formations (Botha, 1996). The rest of the discussion will consequently concentrate on the three major sandstone units in Figure 5–4.

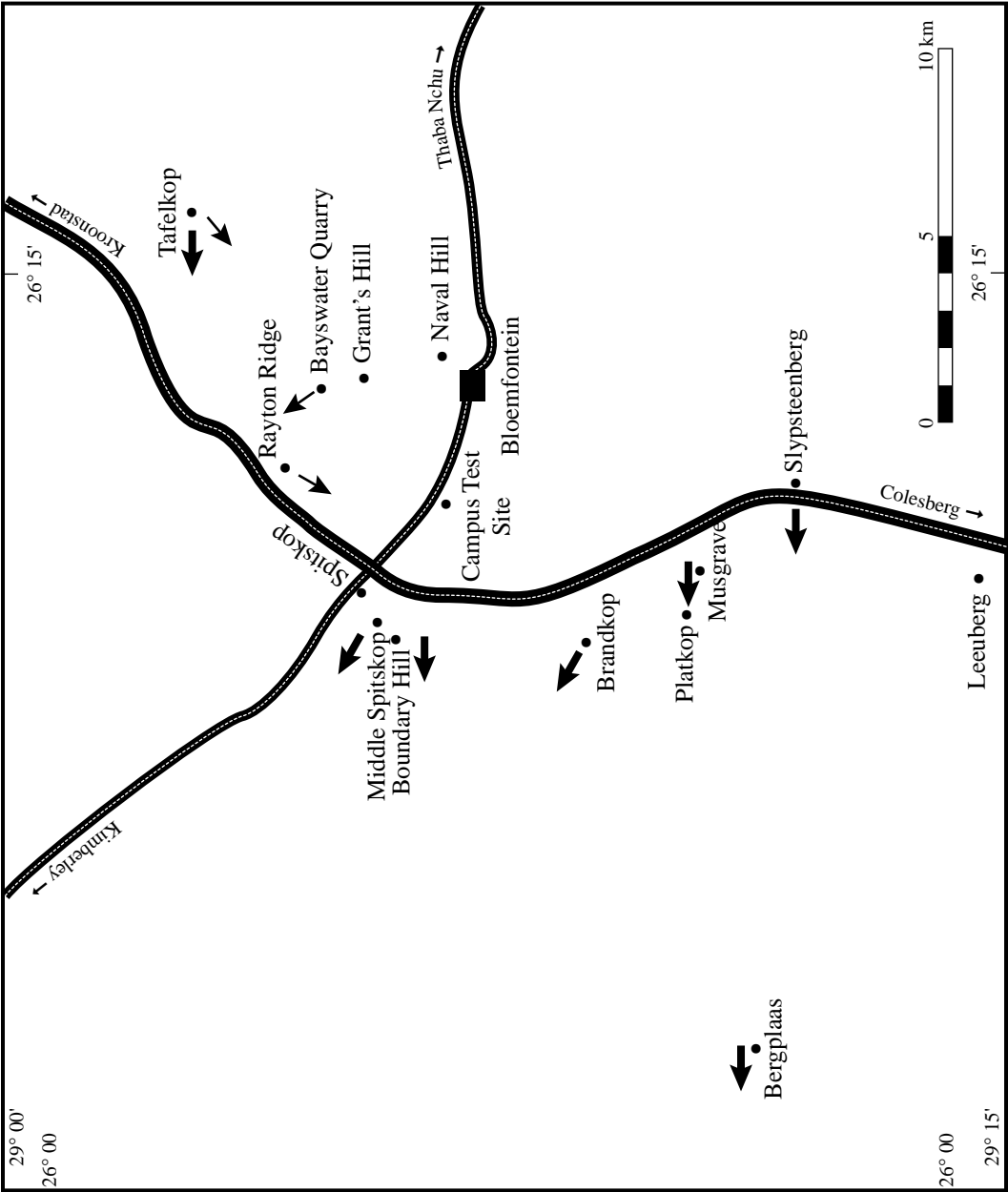


Figure 5-2 Sites studied in establishing the Beaufort Stratigraphy around Bloemfontein. The arrows represent cross-bedding directions in the Spitskop (thin) and Musgrave (broad) sandstone units.

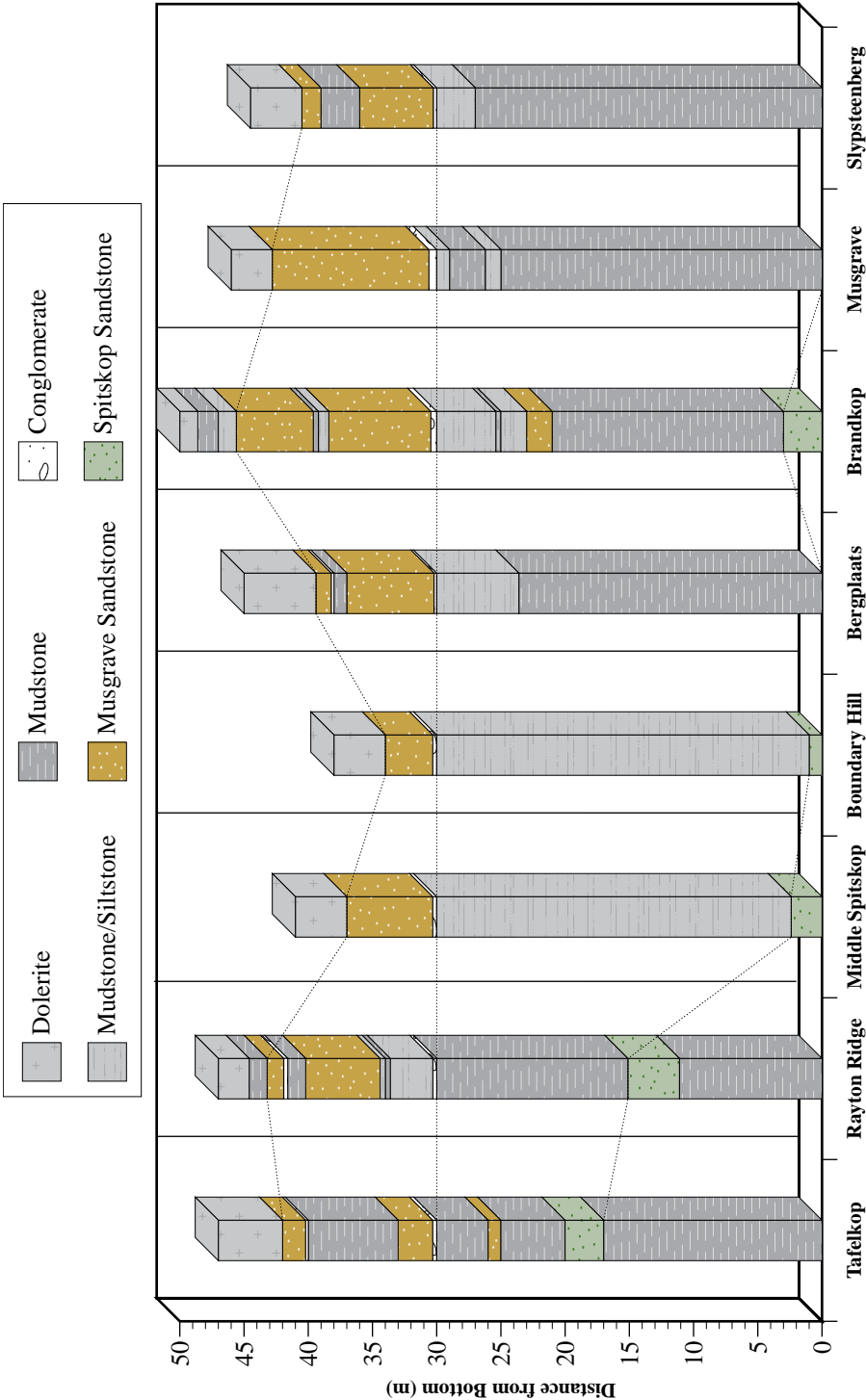


Figure 5-3 Distribution of outcrops of the Musgrave and Spitskop Sandstones for eight of the sites are shown in Figure 5-2.

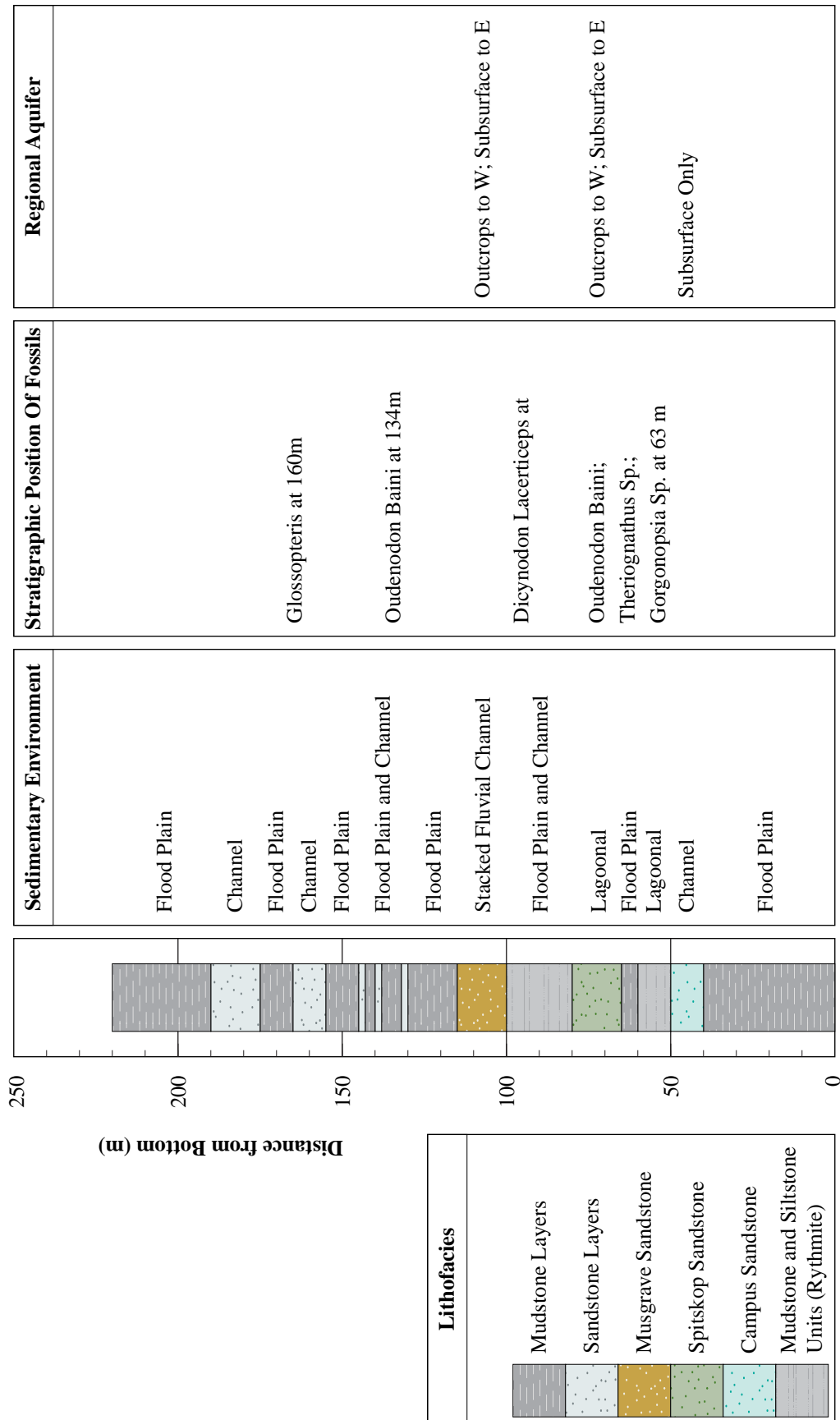


Figure 5-4 Generalised stratigraphic column of the Beaufort Group near Bloemfontein.

The Musgrave Sandstone unit usually crops out below dolerite sills in the hills around Bloemfontein, as shown in Figure 5–5. Complete sections of the unit are therefore rare. The lithology of the unit varies from a medium sandstone to a grit and sometimes a conglomerate. Pebbles and cobbles of clear quartz, milky quartz, microcline, quartz porphyry, granite, granite gneiss and quartzite occur either in conglomerate beds, layers of conglomerate, as in Figure 5–6, or as isolated finds in a coarse bed. A stacking of these structures in Musgrave Hill, shown in Figure 5–7, occurs in an incised channel filled in by sandstone and grit. Spectacular examples of cross-bedding occur in most outcrops of Musgrave Sandstone.

There are a number of factors that have to be considered, when interpreting the environment in which the Musgrave Sandstone was deposited. These are: the coarse nature of the sandstone, isolated cobbles in a



Figure 5–5 Outcrops of Musgrave Sandstone, beneath dolerite sills in the hills around Langenhoven Park, west of Bloemfontein.



Figure 5–6 Thin conglomerate bed at the base of the Musgrave Sandstone, in Musgrave Hill.

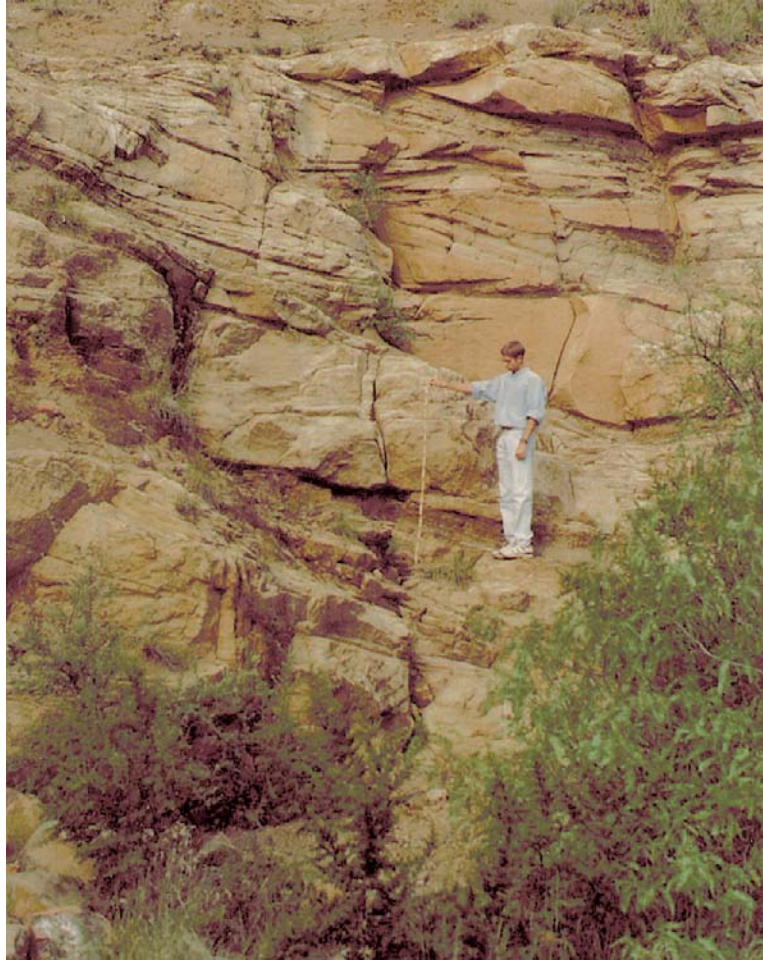


Figure 5–7 Stacked channel deposits of sandstone and grit in the Musgrave Sandstone.

coarse sandstone bed, matrix-supported conglomerates, thin layers of conglomerate which lie on an erosional surface over many kilometres and the unidirectional cross-bedding shown in Figure 5–2. This suggests that the unit was deposited by a braided river system, illustrated in Figure 3–5(a), with channels separated by expanses of sand and sand bars, occasionally covered by thin deposits of grit and conglomerate left by flash floods. The Musgrave Sandstone thus differs completely from the deposits of meandering rivers lower down in the stratigraphic column.

A major feature of the Musgrave Sandstone, clearly shown in Figure 5–7, is the vertical joints, often enlarged by surface and near surface weathering. Major aquifers could thus exist in the Musgrave Sandstone, if these joints appear throughout the unit. This may particularly be the case in the areas east of Bloemfontein, where the unit is rarely exposed.

The medium-grained feldspathic Spitskop Sandstone usually crops out at the base of hills in and around the city. The unit is completely free of grits and pebbles at all sites investigated, except for Tafelkop. The absence of coarse beds, the parallel bedding, micro cross-lamination and the wide dispersal of trough cross-bedding directions in Figure 5–2 indicates that the unit was deposited in the channel of a meandering river.

The Spitskop Sandstone often forms very thick layers, to such an extent that it was quarried extensively a century ago in the now abandoned Bayswater Quarry, where massive sandstones can still be seen today. The ferruginized and leached nature of the rock, visible near joints in Figure 5–8, suggest that the unit may contain well-developed aquifers.

The mudstone and siltstone units that overlie the Spitskop Sandstone, are rarely exposed because of scree along the slopes of hills. The lithology of the visible outcrops generally varies from pure mudstone to a mudstone/siltstone rhythmite. A skull of the reptile *Oudenodon baini* from the *Dicynodon* Assemblage Zone, which was discovered in a maroon mudstone on the slopes of Tafelkop, shows that these units form part of the Adelaide Subgroup.

The Campus Sandstone unit does not crop out in the study area. The study of its properties therefore had



Figure 5-8 Ferruginized and leached rock next to joints in the Spitskop Sandstone at Tafelkop.

to be restricted to cores from the core-boreholes on the Campus Test Site. This feldspathic sandstone is medium-grained and contains parallel bedding, ripple-drift lamination and trough cross-bedding in specific zones. A black mudstone that sharply overlies this sandstone is followed in turn by thin coarse grit beds. This suggests that the Campus Sandstone is related to a channel deposit in a meandering river that eventually abandoned one loop to form an oxbow lake, in which black mudstones accumulated under euxinic conditions. The oxbow lake was later partially filled in by coarse grits that overspilled from an adjacent channel.

The siltstone-mudstone facies overlying the Campus Sandstone consists of a siltstone-mudstone assemblage with mudstone dominant near the base and siltstone in the upper beds. The well-bedded nature of this unit, illustrated in Figure 5-9, and the ripple-drift cross-lamination in the silty layers, suggest that the unit is related to the deposit in a lagoonal-ephemeral lake on a flood-plain. A number of fossils of Karoo reptiles were recovered from these mudstones which lie immediately below the Spitskop Sandstone unit in Figure 5-4.

The Campus Sandstone is underlain by layers of mudstones. About 40 m of these grey and maroon mudstones were studied in a number of the core-boreholes drilled on the Campus Test Site. The mudstones, which often contain small nodules of palaeocalcrete and occasional thin layers of siltstone, can readily be interpreted as floodplain deposits. The sedimentary process, responsible for the deposition of the rocks underlying the Campus Test Site, thus reminds one very much of the meandering river system illustrated in Figure 3-5(b).

5.4 REGIONAL STRUCTURAL GEOLOGY

5.4.1 Structural-Stratigraphic Mapping

The main objective of this study, which was also based on the 400 km² region around the Campus Test Site in Figure 5-2, was to establish the regional distribution and geometry of the main sandstone bodies and dolerite on a 1:10 000 and 1:30 000 scale. The geometry and correlation of the sandstones and dolerite structures were studied by using marker units, geometric analysis of bedding and the drawing of structurally controlled sections across the area. All occurrences of surface sandstones in the hills in and around Bloemfontein were mapped and correlated with either the Musgrave or Spitskop Sandstone bodies. These sandstones, which vary in thickness from 2 to 20 m, occur only in the subsurface to the east of Bloemfontein. The geometry of fractures in the sandstones was also documented at various outcrops throughout the area.

The stratigraphic correlation was complicated considerably by the occurrence of curvilinear dolerite structures on three stratigraphic levels that displaced the lithologies perpendicular to the plane of intrusion, both vertically and laterally. Asymmetric open folds with north-easterly trending axial traces on a hectometre scale were observed at Brandkop, Rayton Ridge and Tafelkop in Figure 5-2, for example. The dips of these fold limbs, which



Figure 5–9 Alternating layers of siltstone and mudstone (rhythmite) overlying the Campus Sandstone.

vary between 5° and 15° , have a dramatic effect on the local position of the various stratigraphic units.

The areal distribution, correlation and understanding of the complex geometry of the dolerite intrusions were established, using structural section reconstructions and the spatial positions of established stratigraphic marker sequences. The intrusions that interdigitate with the Adelaide sediments represent a single megascopic unit known as the Rayton Ridge Sill. The Sill that bifurcates to the south and east has a synintrusive folded morphology locally, resembling dome and basin structures, as illustrated in Figure 5–10. The locations of the sites used in constructing this northerly trending 4 km section can be found in Figure 5–2.

The full extent of the megascopic fold development is borne out by the structural contours for the top of the Musgrave Sandstone in Figure 5–11. The contours define an oval-shaped domal structure with most of the city of Bloemfontein situated on the core of the structure. The dips around the domal structure are less than one degree and the anticlinal axial trace trends north-easterly. A synclinal trace occurs some 35 km to the east of Bloemfontein.

The existence of this domal structure is very interesting for two reasons. The first is that it is exactly the type of structure one would expect to be formed by laccolithic intrusions. The second is its influence on both the surface and subsurface directions of flow. It is clear from Figure 5–11 that the main drainage system for surface water has not been affected by the domal structure, but the minor streams feeding into the main system appear to be controlled by the structure. The minor systems therefore possibly represent a younger drainage system.

It is known that groundwater levels and the direction of groundwater flow tend to follow the topographic surface (Van Sandwyk *et al.*, 1992). This means that the flow of groundwater will be directed away from the domal core towards the synclinal axes situated on either side of the domal structure. The synclinal structure therefore represents a sink and a potential regional groundwater resource area.

The easterly trending longitudinal section, AB, in Figure 5–12, illustrates that the Musgrave Sandstone is mostly in the subsurface for the part east of Bloemfontein. It could thus represent a major groundwater resource in this region. However, leakage into the Modder River will take place where the Musgrave Sandstone is exposed in the core of the syncline.

5.4.2 The Rock Mass Structure

The general shape of the sandstone bodies in the area investigated is irregular sheet-like to tabular. The lithofacies and palaeocurrent analysis (see Figures 5–2 and 5–3) showed that the sandstone bodies thin locally away from channel centres and regionally to the west, with the presumed source area situated east of Bloemfontein.

Extensional fractures (Mode I) and shearing fractures (Mode II) are pervasively developed in both the sediments and dolerite intrusives. Fractures in the dolerites were probably caused by the original thermal cooling stress and later isostatic uplift through erosion. A stereographic projection of poles and planes for the

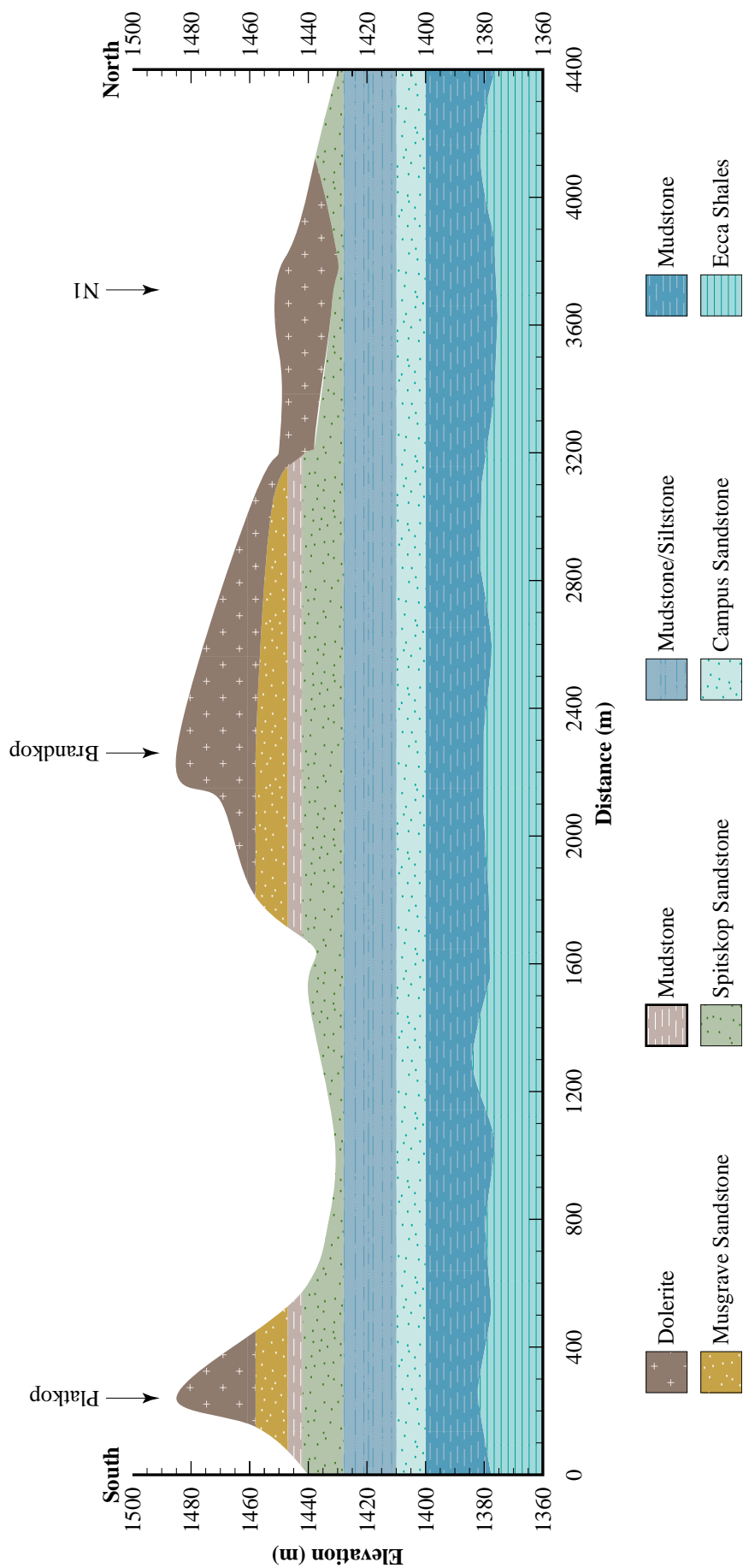


Figure 5–10 Northerly trending section south-west of Bloemfontein illustrating the geometry of dolerite intrusions and sediments of the Adelaide Subgroup.

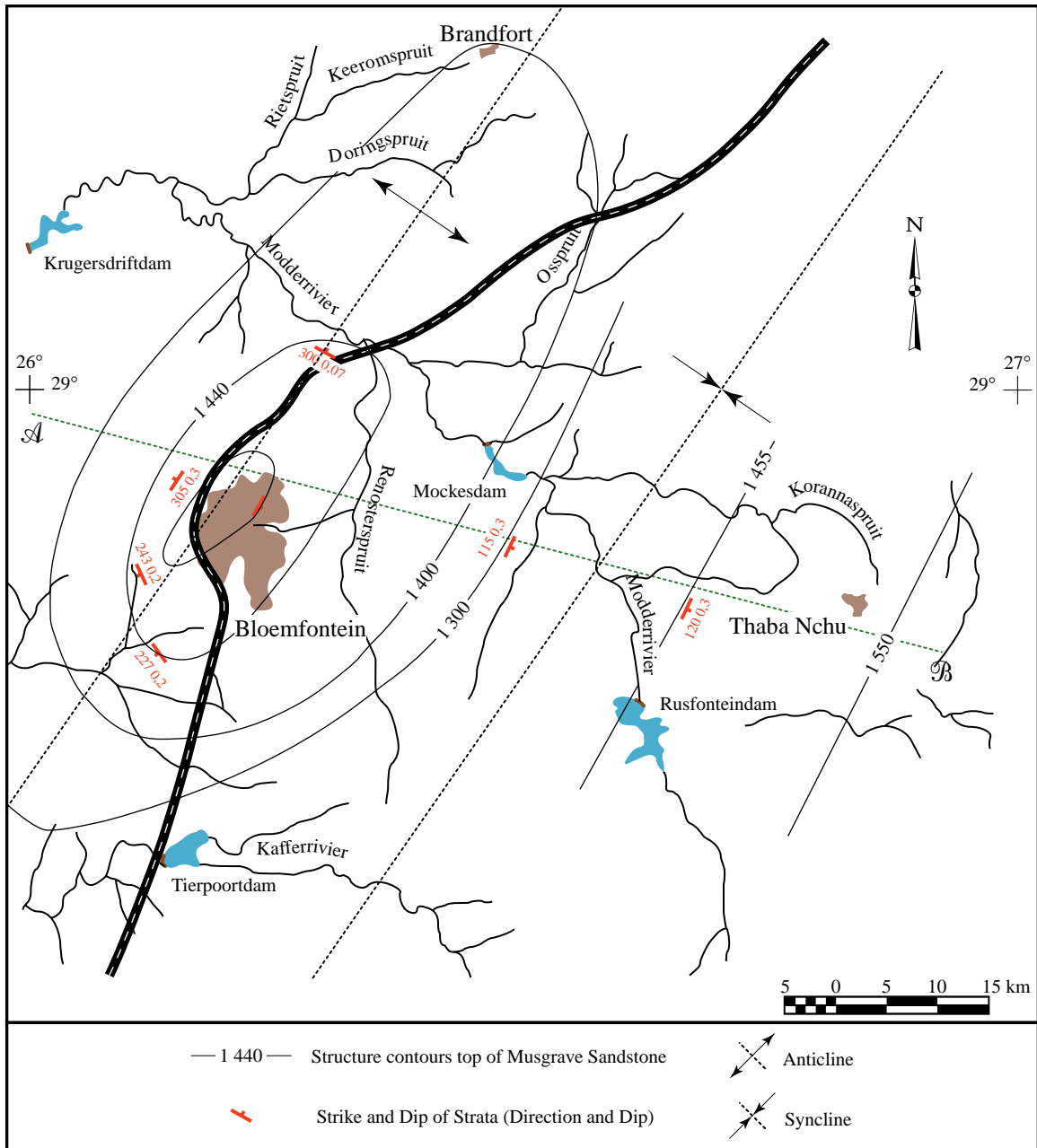


Figure 5-11 Megascopic dome and basin structures deforming the Karoo Supergroup between Bloemfontein and Thaba Nchu.

dominant types of fractures recognised in the sediments is given in Figure 5-13. These include: sub-horizontal bedding-parallel fractures and orthogonal and diagonal fractures with dominant north-west, north-east and east-west regional trends. The latter fractures appear to be of a compressional origin, but now appear in tension (open fractures), probably as a result of uplift and erosional unloading.

5.5 THE CAMPUS TEST SITE

5.5.1 General

The Campus Test Site at the University of the Free State (see Figure 5-14) covers an area of approximately $180 \times 192 \text{ m}^2$, and was originally intended as a test site for postgraduate students. The positions of the 24 percussion and 7 core-boreholes that have been drilled on the site to date are shown in Figure 5-15. Five of the seven core-boreholes were drilled vertically and two at an inclination of 45° in an attempt to intersect all

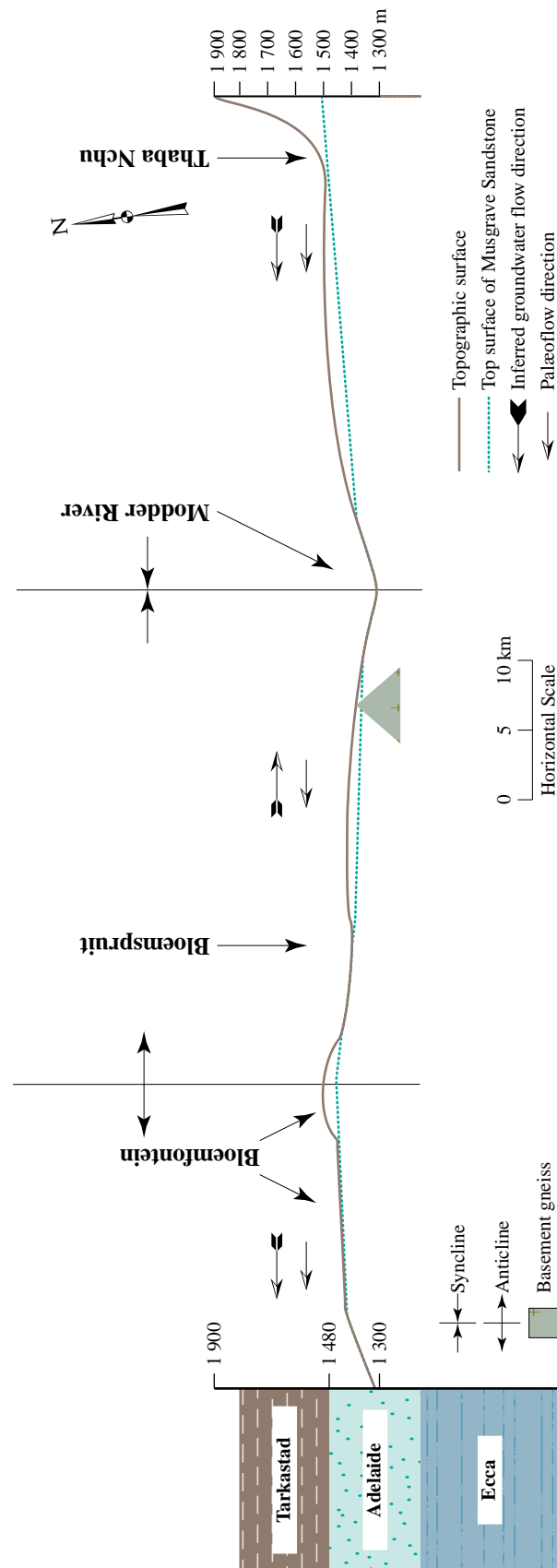


Figure 5-12 Details of the longitudinal section, \mathcal{AB} , in Figure 5-11, between Bloemfontein and Thaba Nchu.

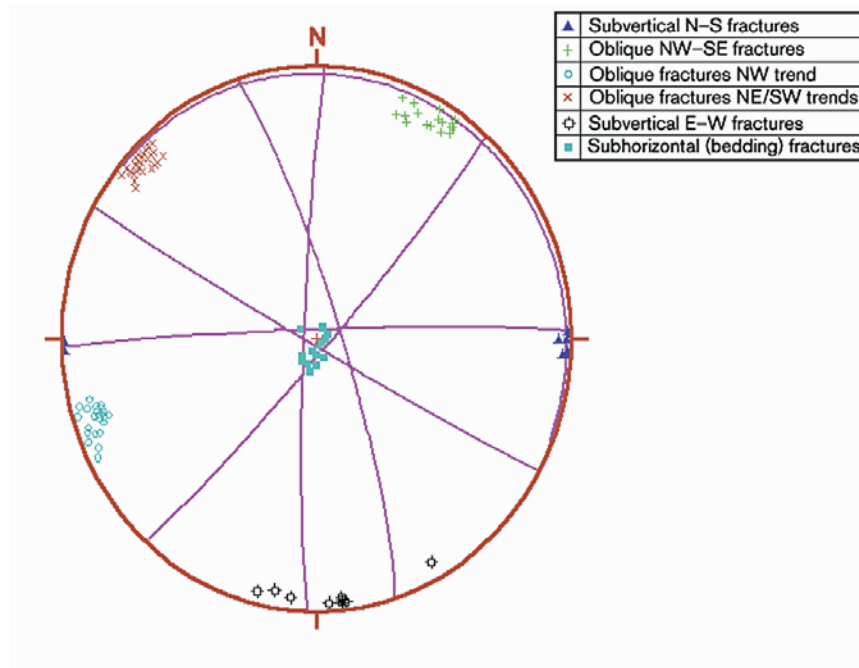


Figure 5-13 Stereographic projection of poles and planes illustrating the regional fracture geometry of the Musgrave and Spitskop Sandstones in the Bloemfontein area.

possible orientations of fractures in the lithologies. The Department of Geohydrology installed permanent pumps in Boreholes UP15 and UP16, which were very useful for the hydraulic tests, which are described later.

The geology of the Site was studied using geological mapping, vertical sedimentological-structural profiling of borehole cores and wireline logging of selected boreholes. These data were very useful in the interpretation of the Site's depositional environment, stratigraphy and characterization of the aquifers. A microscopic study of selected cores provided very interesting information on the nature of the zones of chemical alteration and microfractures.

The geological profiles of the percussion and two inclined core-boreholes (CH5 and CH6) are shown in Figures 5-16 and 5-17 respectively while those for the vertical core-boreholes, CH1-CH4, are given in Table 5-1.

5.5.2 Mapping and Macroscopic Bedding Orientation

The geological map of the Campus Test Site in Figure 5-15 shows that the Site is situated partially on a basal outcrop of the Spitskop Sandstone, but mainly on the underlying Campus Sandstone. Outcrops of the mudstones that overlie the Campus Sandstone are superficially covered by soil and clay. A macroscopic dolerite sill defines the southern border of the Site. The two north-easterly trending subvertical fracture zones, detected in the cores of boreholes CH6 and CH7, are the only subvertical structures intersected when the core boreholes were drilled. However, the zones are not present in any of the other boreholes.

The contours in Figure 5-11 suggest that the Karoo strata in this part of Bloemfontein should dip towards the south-east, on the regional scale. However, the topography of the Campus Test Site dips towards the north-east, as shown in Figure 5-18.

5.5.3 Stratigraphy and Sedimentology

The geological column of the Campus Test Site can be subdivided into five different easily recognisable rock units, each characterised by a unique assemblage of rock types and primary structures. These lithological units may be subdivided into different lithofacies types, as shown in Figures 5-19 and 5-20. A characteristic feature of the lithofacies is the cross-lamination present in lithofacies 2, the upper part of lithofacies 3, and lithofacies 4 and 5. Cross-bedding occurs in different directions (as viewed in the vertical) in the sandstone lithofacies.

The vertical lithofacies represent vertical accretion of deposits in flood-plains (mudstone and mudstone/siltstone facies), shallow lakes (rhythmite facies) and channels (sandstone facies). The palaeosols and

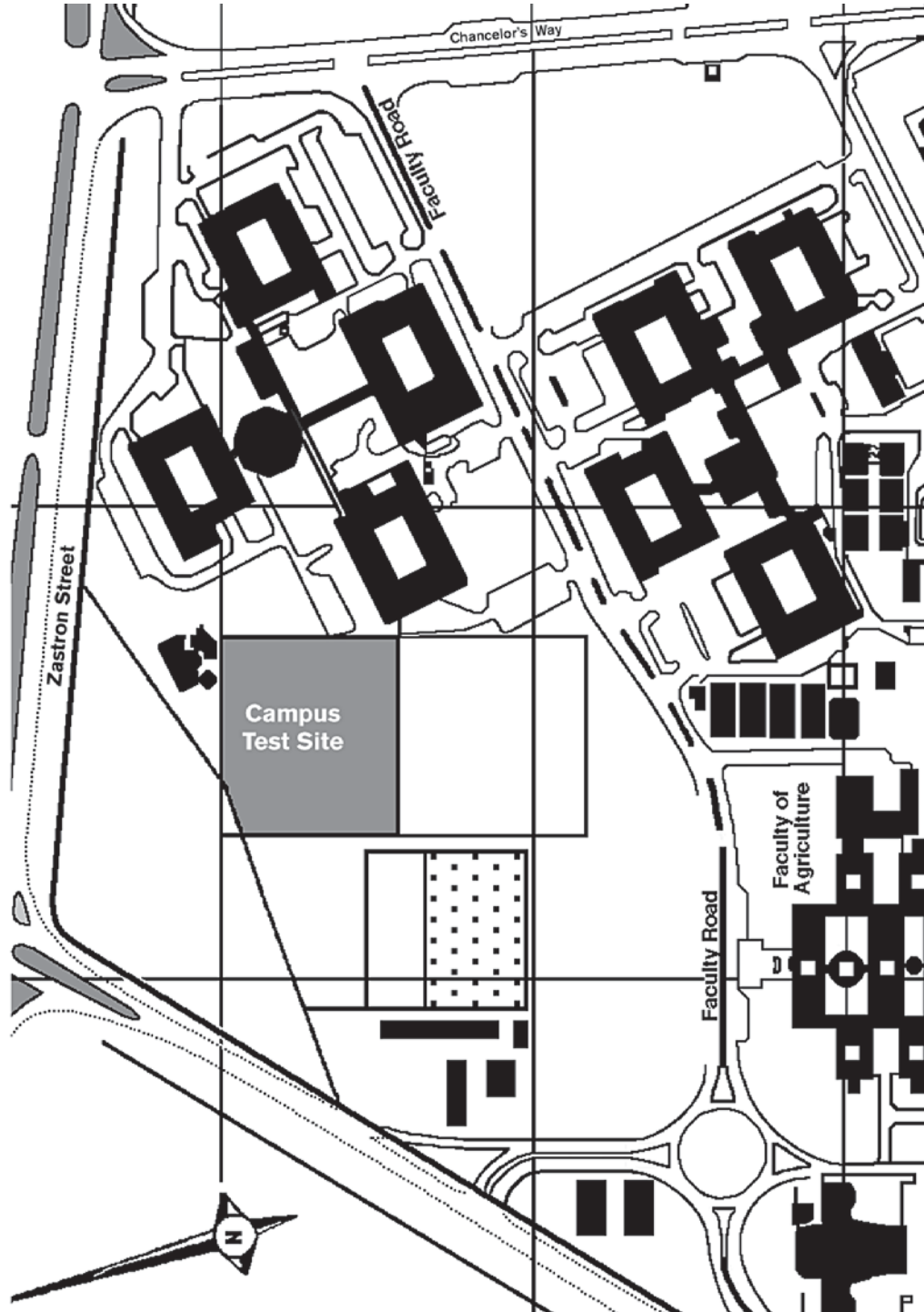


Figure 5-14 Position of the Campus Test Site at the University of the Orange Free State.

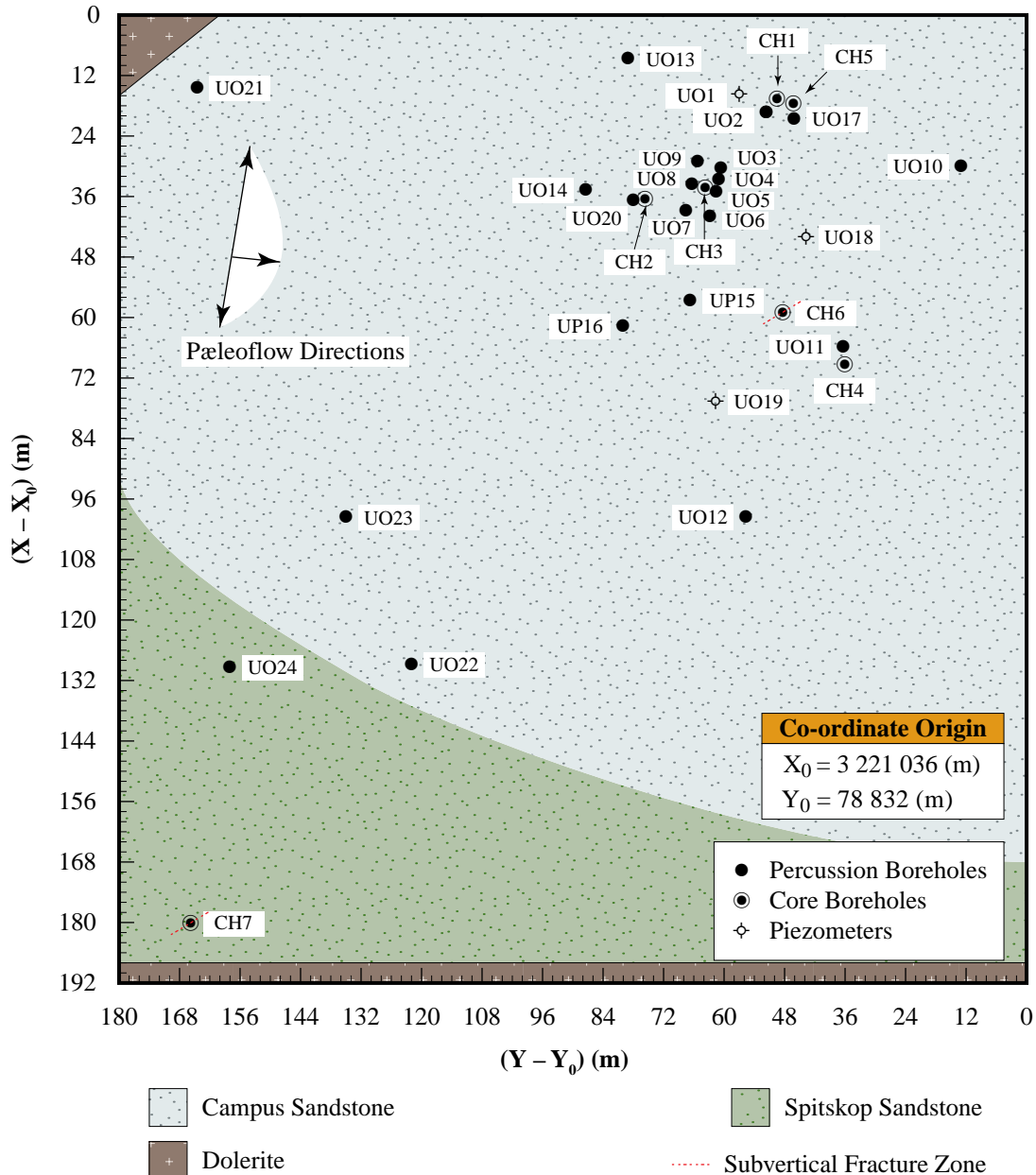


Figure 5-15 Plan view of the boreholes and geological map of the sandstones on the Campus Test Site.

palæocretes in mudstone/siltstone facies represent periods of sub-aerial emergence and bioturbative activity, and fluid flow in the Karoo basin respectively. This confirms the view expressed earlier, that the deposition was related to the fluvial environment of the Adelaide Subgroup, rather than the lacustrine environment of the Ecca Group. An examination of the cross-lamination and cross-bedding orientation derived from dipmeter and acoustic scanner logs, showed that the palæoflow direction varied from north-north-east (010°) towards south-south-west (190°), as indicated in Figure 5-15.

The diagram on the right side of Figure 5-20 shows that there is a considerable variation in competency of the various lithofacies and even within lithofacies, caused by the variations in the composition of the lithofacies themselves. For example, at the base of the sandstone facies, 50 to 300 mm thick coarse conglomerate bands occur that alternate with coarse-grained (0,5 to 1 mm) cross-bedded sandstone. The sandstone fines upwards with the development of cross-lamination and interbedded laminae of mudstone. A similar variation exists in the lateral facies and rock strengths. The order of competency for the lithofacies in Figures 5-19 and 5-20 is summarised in Table 5-2.

The entire lithological sequence is characterized by a primary mechanical anisotropy in competency, caused by the well-developed external and internal layering and bedding of the lithofacies units. The ordering of the

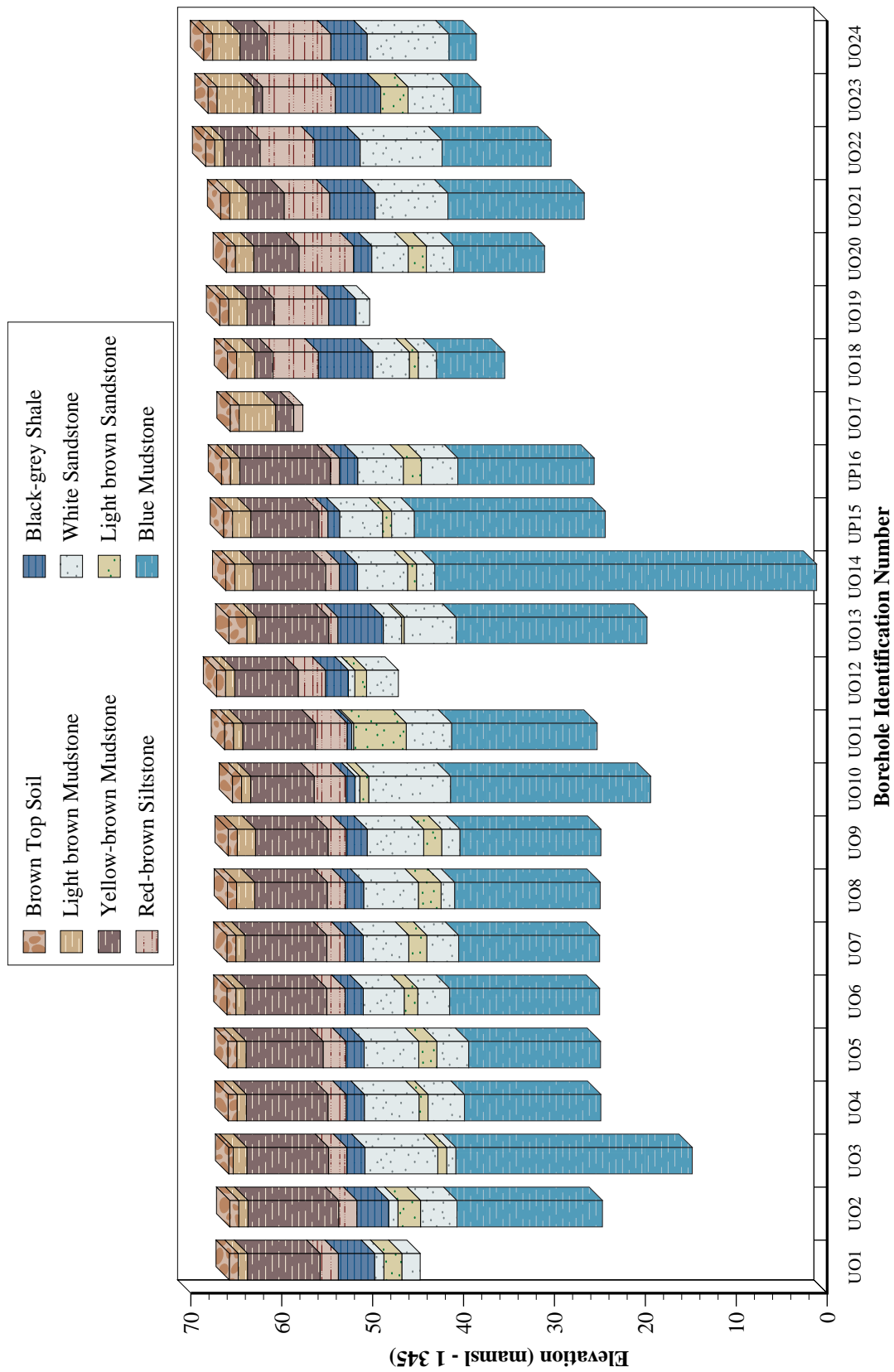


Figure 5-16 Geological profiles of the 24 percussion boreholes drilled on the Campus Test Site.

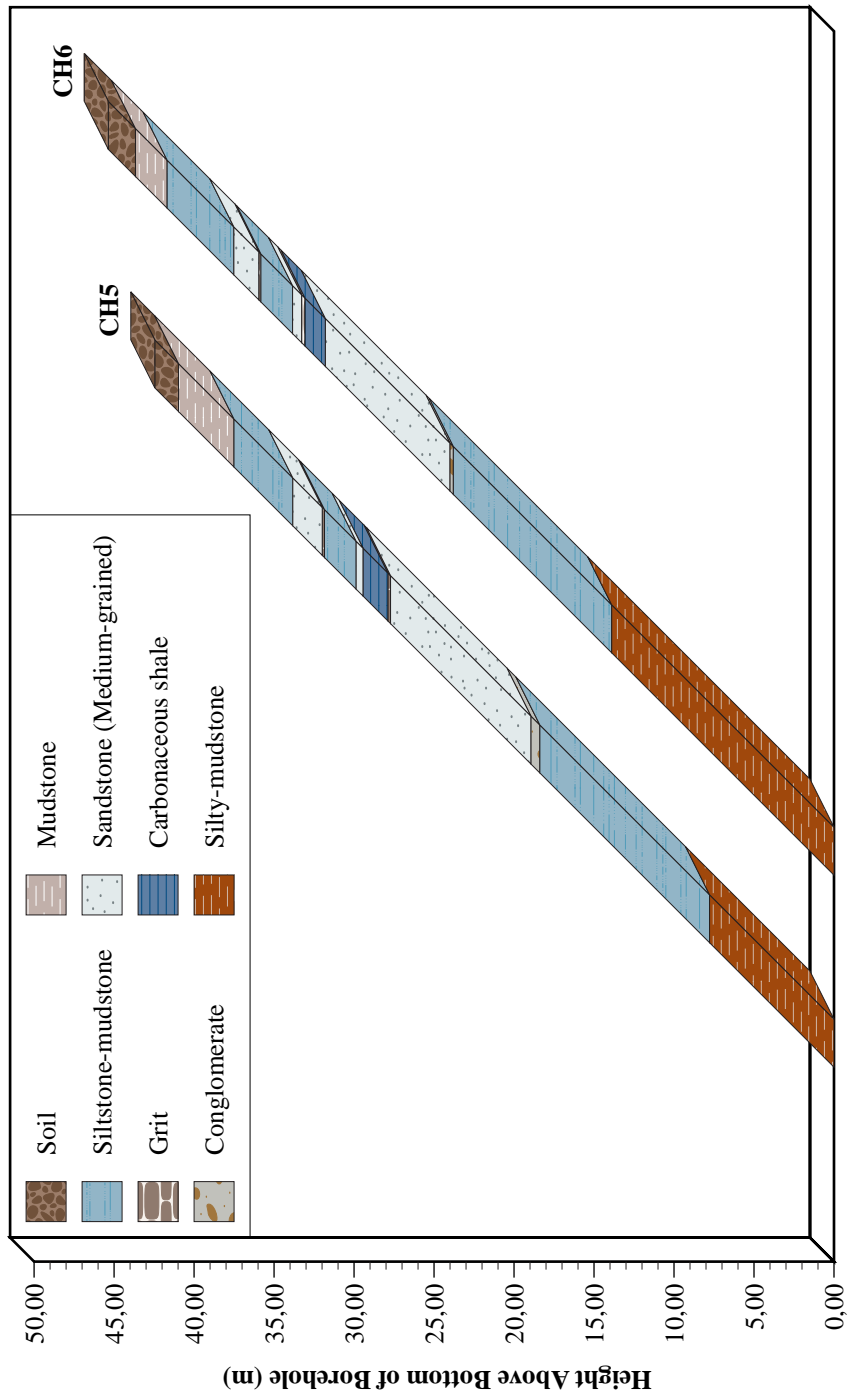


Figure 5-17 Geological profiles of the two inclined core-boreholes drilled on the Campus Test Site.

Table 5-1(a) Geological profiles of the core-boreholes CH1 and CH2, drilled on the Campus Test Site.

Borehole CH1				Borehole CH2			
Lithology	Core Length (m)	Thickness (m)	Elevation (mamsl)	Lithology	Core Length (m)	Thickness (m)	Elevation (mamsl)
Soil	0,000	1,700	1410,690	Soil	0,000	0,270	1411,040
Mudstone	1,700	3,300	1408,990	Mudstone	0,270	0,270	1410,770
Siltstone-mudstone	5,000	2,160	1405,690	Siltstone-mudstone	3,540	8,410	1407,500
Sandstone (medium-grained)	7,160	3,270	1403,530	Sandstone (medium-grained)	11,950	0,230	1399,090
Grit	10,430	0,020	1400,260	Sandstone-mudstone	12,180	0,040	1398,860
Siltstone-mudstone	10,450	1,950	1400,240	Sandstone (medium-grained)	12,220	0,100	1398,820
Grit	12,400	0,400	1398,290	Carbonaceous shale	12,320	1,240	1398,720
Carbonaceous shale	12,800	0,280	1397,890	Grit	13,560	0,010	1397,480
Grit	13,080	0,040	1397,610	Carbonaceous shale	13,570	0,140	1397,470
Carbonaceous shale	13,120	1,160	1396,410	Grit	13,710	0,010	1397,330
Carbonaceous shale	14,280	0,020	1396,390	Carbonaceous shale	13,720	0,010	1397,320
Grit	14,300	0,080	1396,310	Grit	13,730	0,280	1397,310
Carbonaceous shale	14,380	0,020	1396,290	Siltstone-mudstone	14,010	0,770	1397,030
Grit	14,400	0,090	1396,200	Grit	14,780	0,040	1396,220
Carbonaceous shale	14,490	0,040	1396,160	Siltstone-mudstone	14,820	0,260	1396,260
Grit	14,530	0,020	1396,140	Sandstone (medium-grained)	15,080	8,130	1395,960
Carbonaceous shale	14,550	0,020	1396,120	Conglomerate	23,210	0,150	1387,830
Grit	14,570	0,560	1395,560	Mudstone	23,360	1,270	1387,680
Carbonaceous shale	15,130	0,020	1395,540	Siltstone	24,630	0,530	1386,410
Grit	15,150	8,120	1387,420	Sandstone (fine-grained)	25,160	0,470	1385,880
Sandstone (medium-grained)	23,270	0,480	1386,940	Mudstone	26,710	1,080	1384,330
Conglomerate	23,750	0,730	1386,210	Silty-mudstone	28,110	1,400	1382,930
Mudstone	24,480	0,690	1385,520	Sandstone (fine-grained)	28,310	0,200	1382,730
Siltstone	25,170	1,080	1384,440	Silty-mudstone	32,270	3,960	1378,770
Mudstone	26,250	1,650	1382,790	Sandstone (fine-grained)	32,510	1,050	1377,480
Sandstone (fine-grained)	27,900	0,220	1382,570	Siltstone	33,810	0,250	1377,230
Mudstone	28,120	3,710	1378,690	Sandstone (fine-grained)	40,610	6,800	1370,430
Sandstone (fine-grained)	28,290	1,580	1377,110	Sandstone (fine-grained)	41,130	0,520	1369,910
Mudstone	32,000	4,420	1372,690	Silty-mudstone	45,410	4,280	1365,630
Sandstone (fine-grained)	33,580	1,000	1371,690				
Mudstone	38,000	1,080	1370,610				
Siltstone	39,000	3,950	1366,660				
Sandstone (fine-grained)	40,080	1,600	1365,060				
Silty-mudstone	44,030	6,430	1358,630				
Sandstone (fine to medium-grained)	45,630	1,940	1356,690				
Silty-mudstone	52,060	7,830	1348,860				
Sandstone (fine-grained)	54,000	0,750	1348,110				
Silty-mudstone	61,830	1,420	1346,690				
Sandstone (fine-grained)	62,580						
Silty-mudstone	64,000						

Table 5–1(b) Geological profiles of the core-boreholes CH3 and CH4, drilled on the Campus Test Site.

Borehole CH3				Borehole CH4			
Lithology	Core Length (m)	Thickness (m)	Elevation (mamsl)	Lithology	Core Length (m)	Thickness (m)	Elevation (mamsl)
Soil	0,000		1410,950	Soil	0,000		1411,300
Mudstone	2,300	2,300	1408,650	Mudstone	2,500	2,500	1408,800
Siltstone-mudstone	4,300	2,000	1406,650	Siltstone-mudstone	4,350	1,850	1406,950
Siltstone (medium-grained)	9,470	5,170	1401,480	Siltstone (medium-grained)	7,700	3,350	1403,600
Siltstone-mudstone	9,530	0,060	1401,420	Siltstone-mudstone	9,660	1,960	1401,640
Sandstone (medium-grained)	10,820	1,290	1400,130	Siltstone-mudstone	12,450	2,790	1398,850
Sandstone (medium-grained)	13,370	2,550	1397,580	Grit	12,720	0,270	1398,580
Carbonaceous shale	14,540	1,170	1396,410	Carbonaceous shale	14,150	1,430	1397,150
Grit	14,560	0,020	1396,390	Grit	14,540	0,390	1396,760
Carbonaceous shale	14,650	0,090	1396,300	Carbonaceous shale	14,650	0,110	1396,650
Grit	14,720	0,070	1396,230	Sandstone (medium-grained)	23,800	9,150	1387,500
Carbonaceous shale	14,840	0,120	1396,110	Conglomerate	23,950	0,150	1387,350
Grit	14,900	0,060	1396,050	Siltstone	24,580	0,630	1386,720
Mudstone	15,160	0,260	1395,790	Mudstone	24,980	0,400	1386,320
Sandstone (medium-grained)	23,780	8,620	1387,170	Siltstone	28,200	3,220	1383,100
Conglomerate	24,070	0,290	1386,880	Mudstone	28,300	0,100	1383,000
Mudstone	25,570	1,500	1385,380	Sandstone (fine-grained)	28,900	0,600	1382,400
Siltstone	26,190	0,620	1384,760	Mudstone	34,800	5,900	1376,500
Sandstone (fine-grained)	27,470	1,280	1383,480	Sandstone (fine-grained)	36,000	1,200	1375,300
Mudstone	31,980	4,510	1378,970	Mudstone	40,200	4,200	1371,100
Sandstone (fine-grained)	32,280	0,300	1378,670	Sandstone	41,300	1,100	1370,000
Mudstone	32,930	0,650	1378,020	Mudstone	41,800	0,500	1369,500
Sandstone (fine-grained)	33,460	0,530	1377,490	Sandstone (fine-grained)	43,100	1,300	1368,200
Mudstone	37,460	4,000	1373,490	Silty-mudstone	45,400	2,300	1365,900
Sandstone (fine-grained)	37,760	0,300	1373,190	Sandstone (fine-grained)	46,150	0,750	1365,150
Mudstone	38,180	0,420	1372,770	Silty-mudstone	48,650	2,500	1362,650
Silty-mudstone	39,860	1,680	1371,090				
Sandstone (fine-grained)	40,790	0,930	1370,160				
Silty-mudstone	41,630	0,840	1369,320				
Sandstone (fine-grained)	41,960	0,330	1368,990				
Silty-mudstone	45,450	3,490	1365,500				

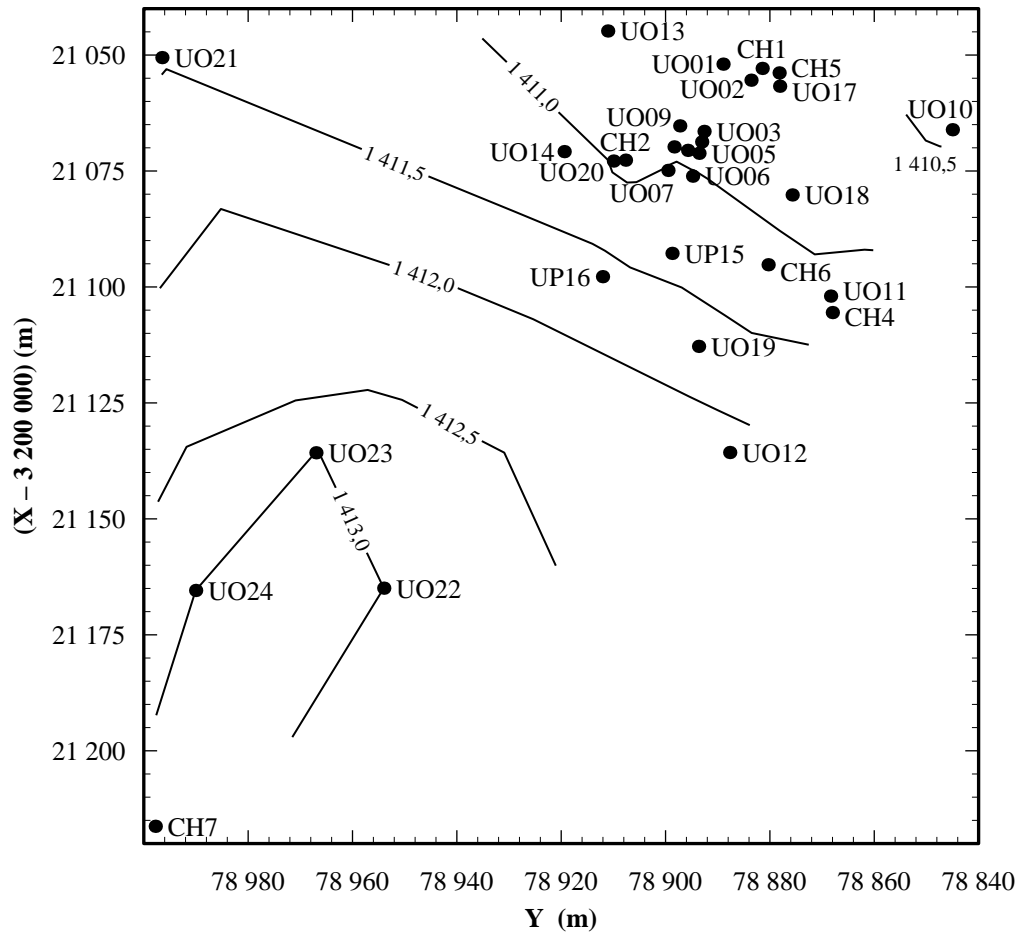


Figure 5–18 Contours of the Campus Test Site's topography.

Table 5–2 Order of competency of the lithofacies in Figure 5–20, arranged from the highest to lowest (bottom to top).

Lithofacies	Description
1	Mudstone
5	Black Shale
2	Cross-laminated Mudstone and Siltstone
4	Cross-laminated Rhythmite Sequence
3	Cross-bedded Sandstone

anisotropy, beginning with the lithofacies with the highest frequency of lamination and bedding, is as follows:

$$\text{Lithofacies } 4 > 5 > 3 > 2 > 1$$

Another characteristic of the lithological sequence is the vertical variation in grain size. A broad description of this variation from bottom to top of the stacked facies units, is given in Table 5–3.

5.5.4 Rock Mass Structure

The shape of the Campus Sandstone body on the Test Site was determined by analysing the elevations at which the upper and lower contacts of the sandstone body occur in the percussion and core logs. The sedimentologic interpretation suggests that the shape is irregular sheetlike to tabular. Contours of the sandstone's top surface in Figure 5–21(a) indicate that the sandstone body has a domal shape around Borehole UP15, with a main axial trace that trends from the south-east to north-west. An interesting feature of the sandstone body, revealed more clearly by its isopach contour map in Figure 5–21(b), is the relation between

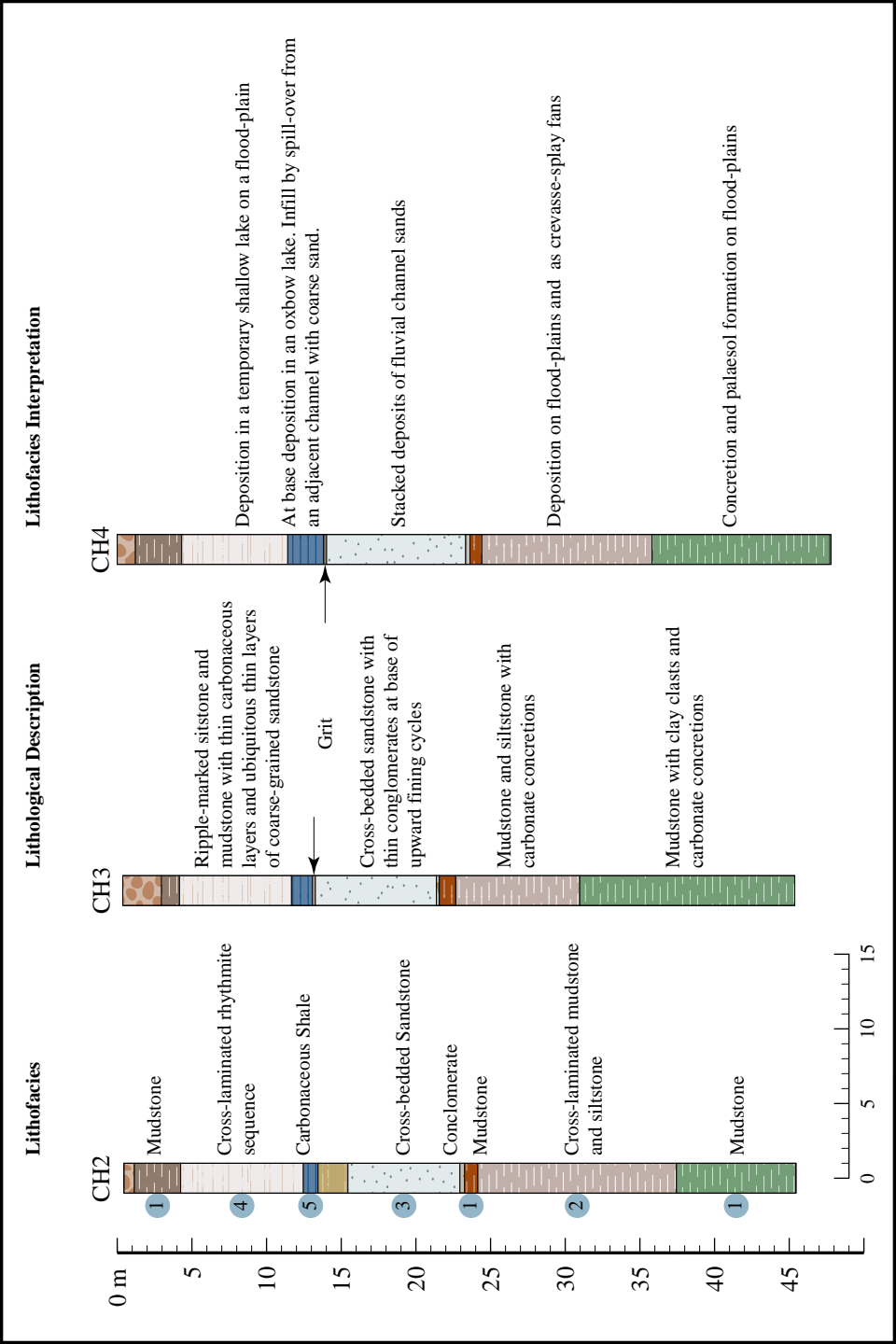


Figure 5-19 Description, interpretation and correlation of drill-core data from the core-boreholes CH2, CH3 and CH4 on the Campus Test Site.

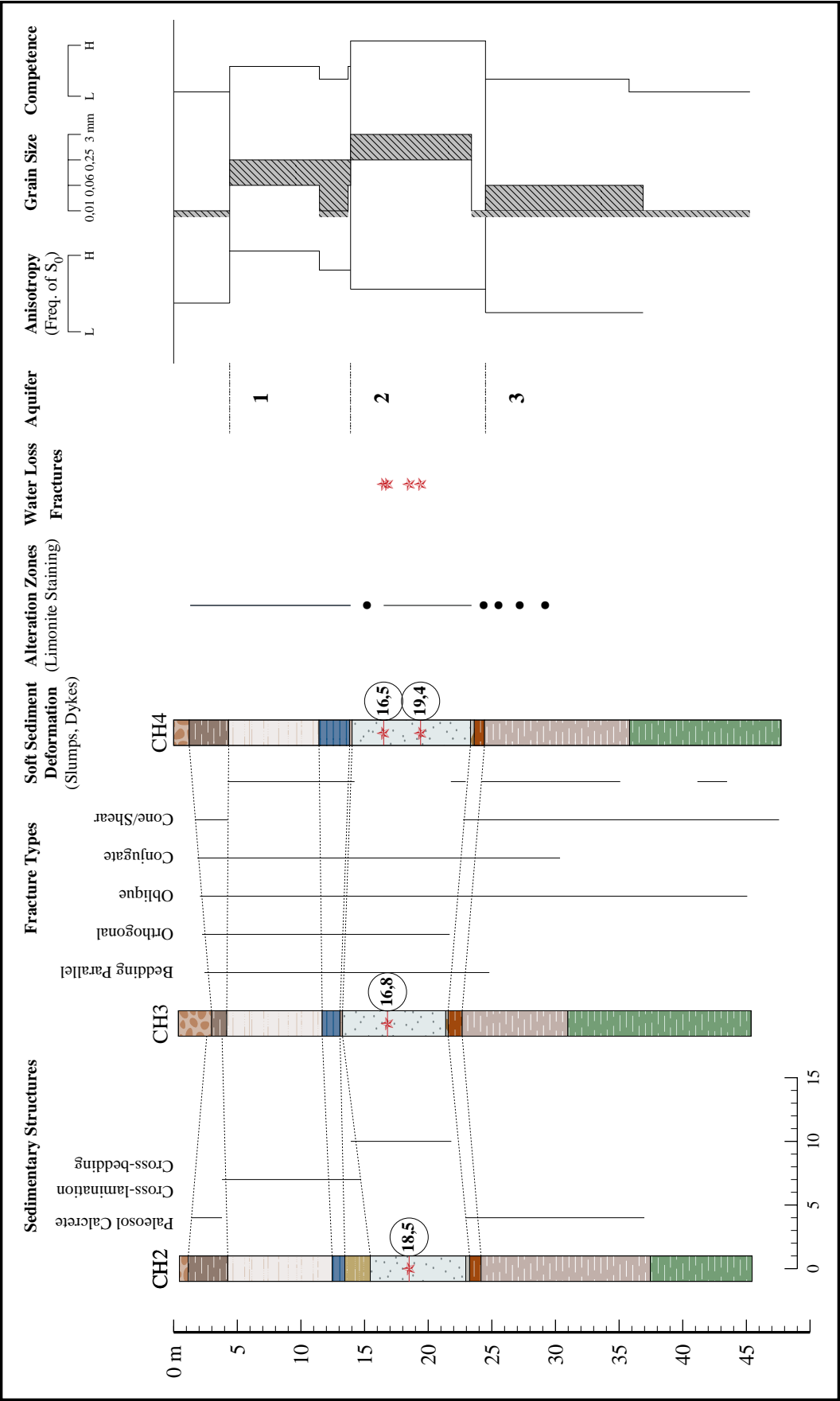


Figure 5-20 Distribution of structures, rock strength characteristics and alteration zones in the interpreted lithofacies of the Adelaide Subgroup on the Campus Test Site.

Table 5–3 Variation in grain size, within the stacked facies units of Figure 5–20 from bottom to top.

	Lithofacies	Grain Size (mm)
Top	1	0,01
	4	0,06 to 0,125
	5	0,01 (Interbanded between 0,06 and 0,125)
	1	0,01
	3	3 to 0,25
	1	0,01
	2	0,01 to 0,06
Bottom	1	0,01

the thickness of the sandstone and the high-yielding boreholes, particularly boreholes UO5 and UP16.

The domal shape of the sandstone body is also present in the mudstone lithofacies below the sandstone facies. However, these facies contain an additional domal structure north-west of Borehole UO14, as illustrated by the contours in Figure 5–22. However, the domal shapes are not present in the lithofacies sequence overlying the sandstone facies. Indeed, some members of the sequence wedge out against the domal structure at Borehole UP15, as can be seen in Figure 5–16.

The overall structure of the vertical lithofacies at the Test Site is consistent with what one would expect from a fluvial environment. However, there is a possibility that hydraulic fracturing, caused by the build-up of high pore-pressures in the post-depositional saturated argillaceous sediments, may also have played a role. The presence of conical shear fractures in a core sample from the mudstone lithofacies below the Campus Sandstone shown in Figure 5–23, supports this suggestion.

A major feature of the core samples is the large number of fractures, particularly bedding-parallel fractures, whose frequency decreases downwards from the upper more weathered zone, as thicker and more competent units are encountered. However, their large-scale development is restricted to the upper part of the sandstone facies, as shown in Figure 5–24. The bedding-parallel fractures in the upper, more weathered zone, are often transected by large numbers of orthogonal, oblique and diagonal fractures. These fractures clearly represent secondary fracturing of the rock mass, caused by the post-lithification processes described in Chapters 3 and 4.

Microscopic studies of thin sections from the sandstone facies, of which an example is shown in Figure 5–25, showed that the grains of quartz and feldspar can also be fractured. The dark red bands in the figure are clay minerals that have been deposited in permeable areas between quartz and feldspar grains by groundwater flow along the cross-bedding in the sandstone.

The Mode I fracture, marked ‘*total water loss*’ in Figure 5–24, is the most significant fracture on the Campus Test Site. A close-up view of the fracture situated completely in the sandstone facies of Figure 5–19 is shown in Figure 5–26. The fracture has an estimated areal extent of 5 000 m² and an aperture that varies between 0,5 and 1,0 mm, as measured in the core. An idea of the fracture’s geometry can be obtained from the contours of its elevation in Figure 5–27, derived from dipmeter, acoustic scanner and calliper surveys. The fracture follows the contours of the Campus Sandstone in Figure 5–21 so closely that there can be no doubt that it is a bedding-parallel fracture.

A more detailed view of the fractures in the Campus Sandstone can be obtained from the June 1996 acoustic scanner logs of core-borehole CH1 and high-yielding percussion borehole UO5 in Figure 5–28. The orientations of the fractures are shown by the tadpoles on the right, and their position and vertical extent by the yellow calliper trace on the left. Green tadpoles represent bedding-parallel fractures, and red tadpoles oblique fractures. The Mode I fracture occurs at a depth of 20,9 m in CH1, and within the fractured zone at 23,0 – 23,3 m in Borehole UO5. The direction of dip and dip for these fractures are 300 07 and 320 07 respectively, where the first three numerals represent the azimuth of dip and the last two the angle of dip.

An interesting feature of the acoustic scanner image for Borehole UO5 in Figure 5–28(b) is the presence of a second ‘fracture’ zone at a depth of 23,8 m. The orientation of the zone’s top is 264 08 and that of its bottom 362 18. However, the absence of any tadpoles in the region and the acoustic calliper image of the area in Figure 5–29 show that the zone does not represent a fracture, but an elastic deformation of the borehole. It is therefore important to note that this ‘fracture’ zone was not detected in two previous geophysical surveys of the borehole, whose identical calliper traces are displayed by the red line on the far left of Figure 5–28(b). The first of these surveys was carried out in June 1992, shortly after the borehole was drilled, and the second in December 1993. The only conclusion is thus that this highly warped zone, indicative of failure along a pre-

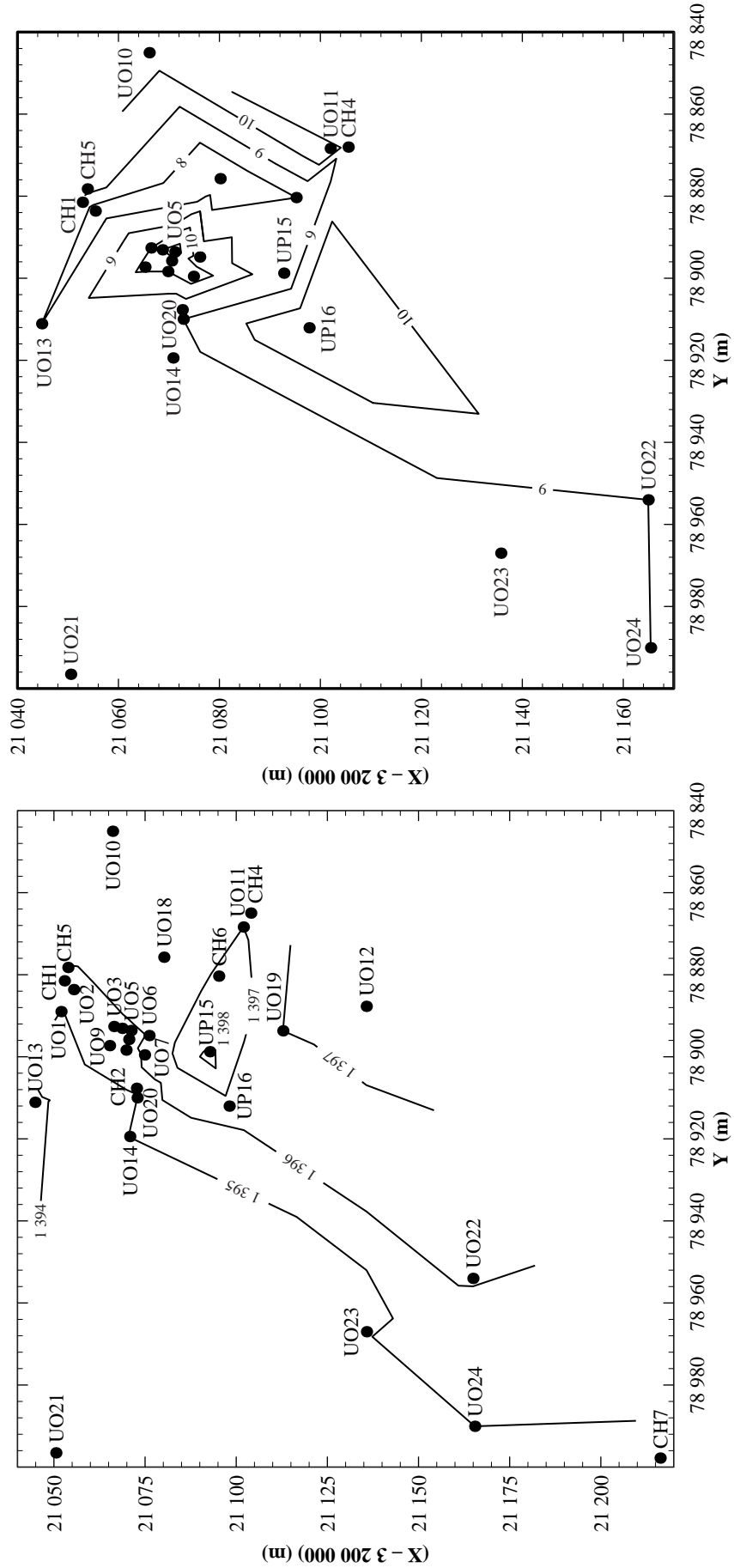


Figure 5-21 Contour maps of (a) the top and (b) the thickness of the Campus Sandstone on the Campus Test Site.

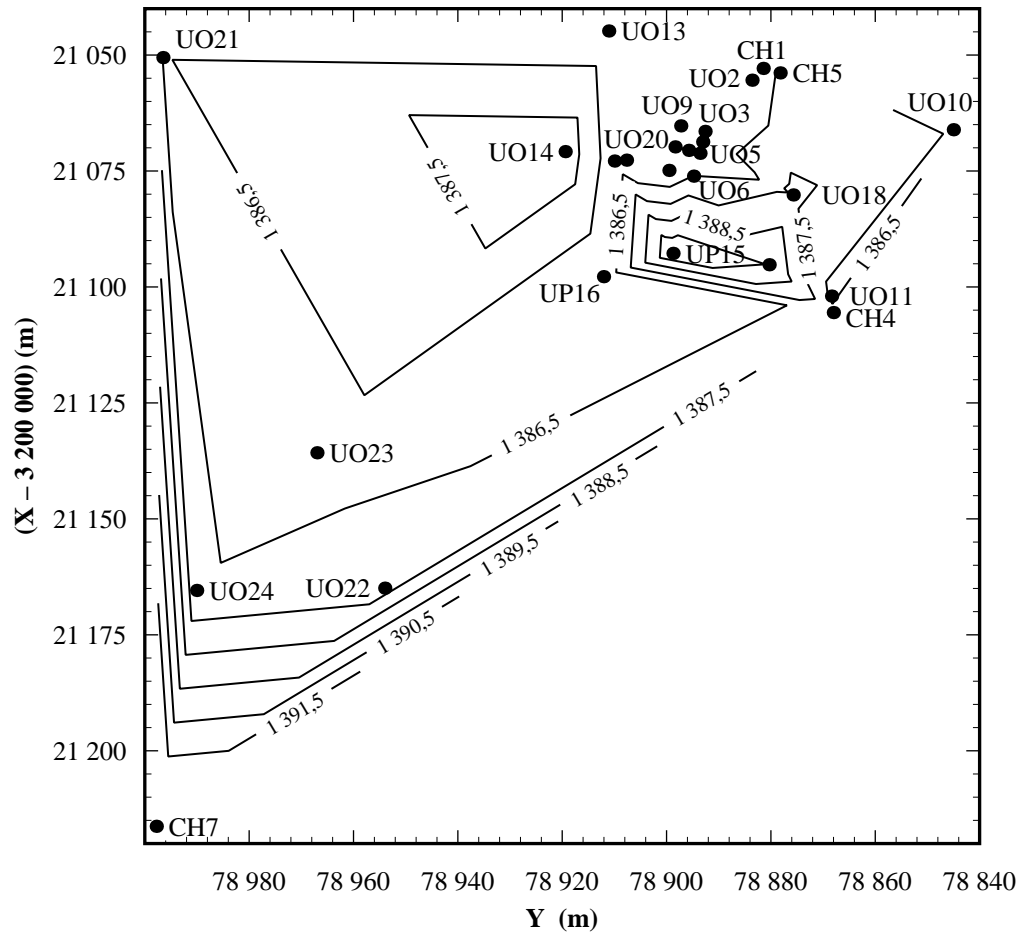


Figure 5-22 Contours for the top of the mudstones that underlie the Campus Sandstone on the Campus Test Site.

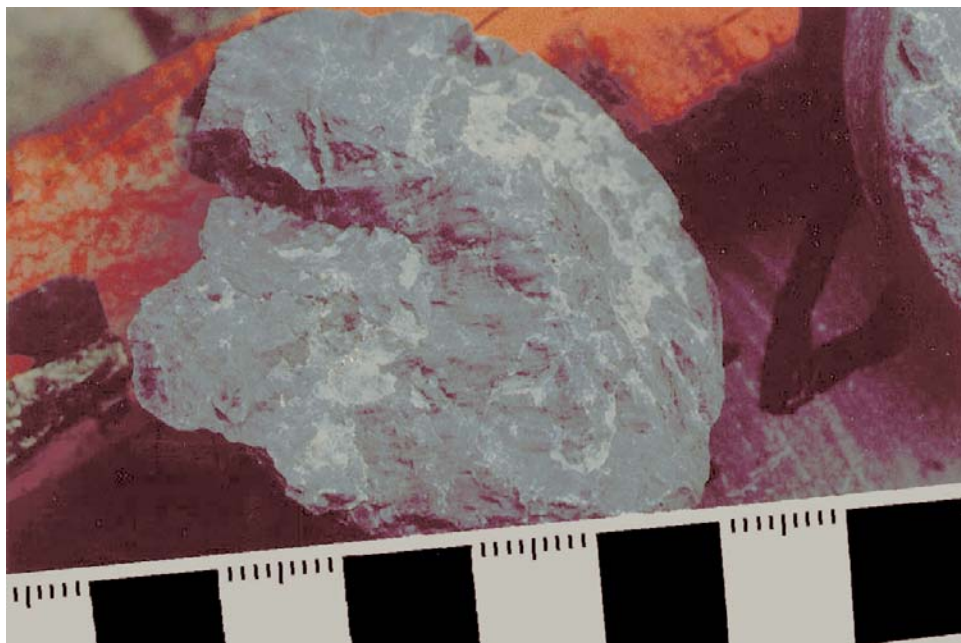


Figure 5-23 Conical shear fractures that developed in a palæosol within the mudstones of lithofacies 2. The white mineral coating on the surface of the fracture is baryte.



Figure 5–24 Photograph of a part of the core from Borehole CH3. Notice in particular the fracture marked with the comment ‘total water loss’.

existing plane of weakness, developed after December 1993. The zone was thus probably caused, when a plane of weakness was activated by hydraulic tests performed on the borehole after December 1993.

The red bands that demarcate the fracture zones on the images in Figure 5–28, are limonite-stained alteration zones, usually associated with matrix diffusion from oxygen-rich water into the formations surrounding the fractures. The zones extend for approximately 1 mm around the smaller fractures to more than 1 m around the Mode I fracture. This phenomenon has two important consequences for Karoo aquifers—it shows that the aquifers are recharged from time to time, and what is perhaps more important, that Karoo formations are particularly susceptible to matrix diffusion. *This property and the small permeabilities of the Karoo rocks will make it very difficult to ever clean up a polluted Karoo aquifer.*

5.5.5 Geometry of the Aquifer

There are three aquifers present on the Campus Test Site, as shown in Figure 5–20 and Figure 5–30. The first aquifer is a phreatic aquifer that occurs in a laminated alternation of mudstones and siltstones (6–9 m thick) and a fine-grained, cross-laminated rhythmite sequence (1–6 m thick). A black carbonaceous shale layer (0.5–4 m thick) separates the first aquifer from the second and main aquifer. This aquifer occurs in the 8–11 m thick Campus Sandstone layer, and is confined. The third aquifer, also a confined aquifer, occurs in a succession of interbedded mudstone, siltstone and a fine-grained sandstone.

A rather interesting and surprising result at the time the boreholes were drilled, was the difference in water levels and blow-yields between the high-yielding and low-yielding boreholes. For example, the blow-yields of boreholes UO5 and UO3 (which are only 5 m apart) were 30 and 0.5 m³ h⁻¹ respectively, while the

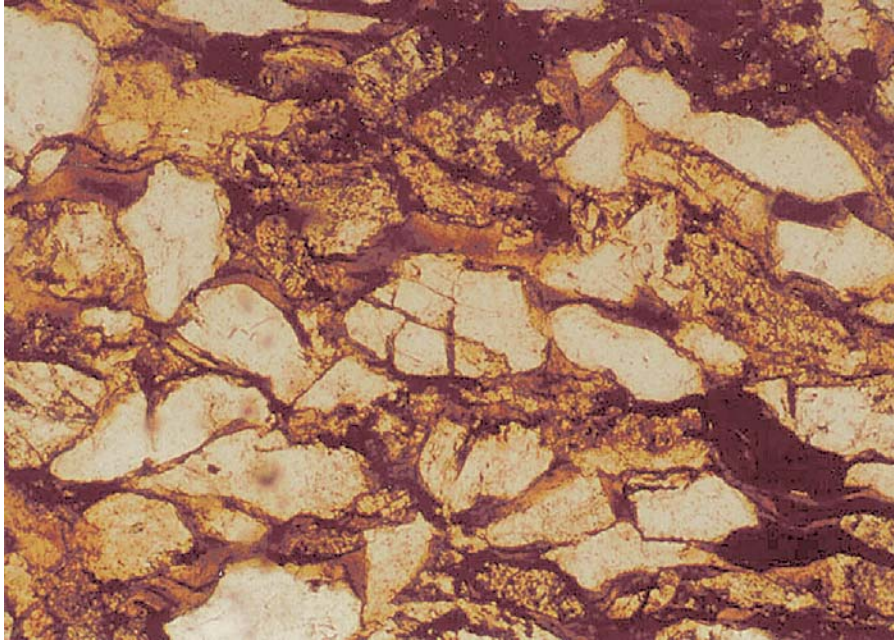


Figure 5–25 Photograph of microfractures in 0,25 mm quartz grains, from a core sample of the Campus Sandstone.



Figure 5–26 Detailed view of the fracture in Figure 5–24. Substantial water loss was incurred along this 80 mm fracture zone during the drilling.

water level in Borehole UO5 was 7 m lower than that of Borehole UO3. The boreholes were consequently surveyed geophysically to try to understand that behaviour. This survey showed that all the high-yielding and none of the low-yielding boreholes intersect the Mode I fracture of Figure 5–26. It is thus quite logical to assume that *a borehole in a Karoo aquifer only has a significant yield if it intersects a bedding-parallel fracture*. The same behaviour has since been observed in boreholes drilled at Dewetsdorp, Philippolis and Rouxville. The phenomenon is thus certainly not restricted to the Campus Test Site. *It is therefore not unreasonable to expect that bedding-parallel fractures play a very important role in the hydraulic behaviour of Karoo aquifers.*

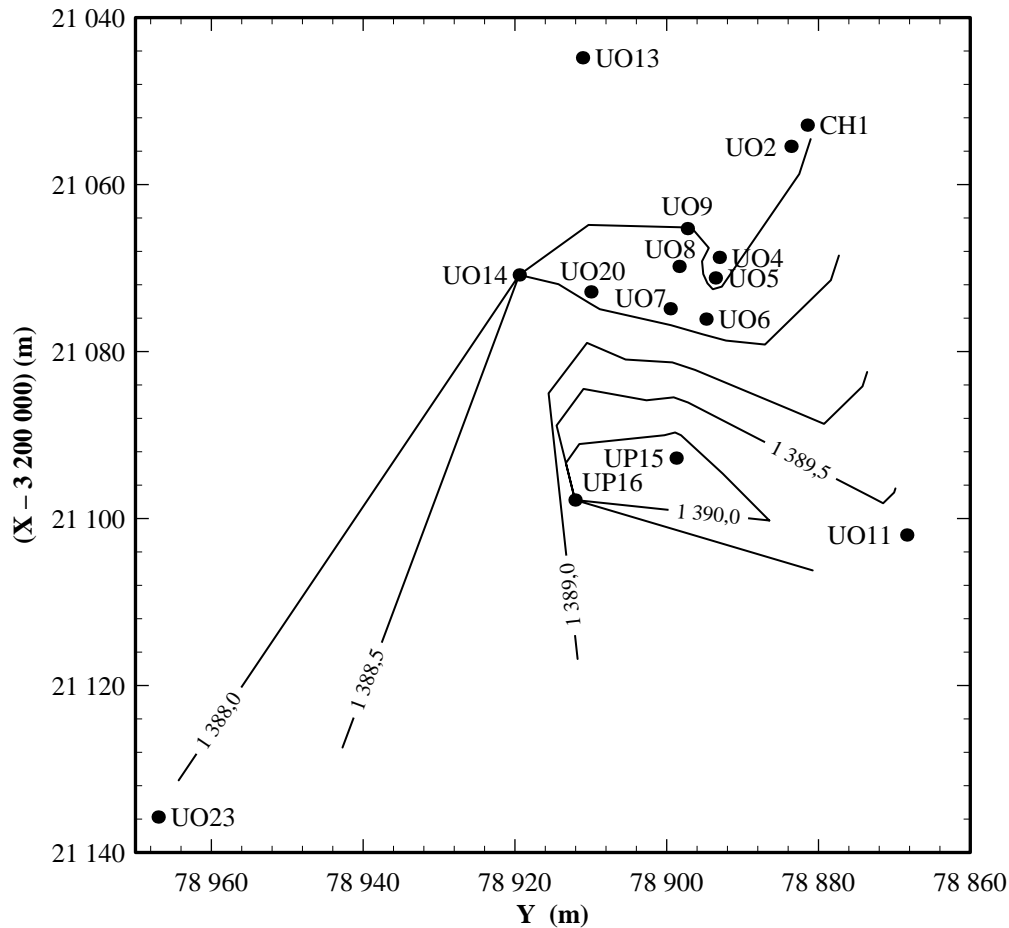


Figure 5-27 Surface contours of the elevation of the Mode I fracture in the Campus Sandstone on the Campus Test Site.

The conventional view, of course, has always been that fractures play an important part in the hydraulic behaviour of Karoo aquifers, particularly in the sense that they represent the main water-bearing units. Although the exact extent of the Mode I fracture is not known, there are indications that it is restricted to a domain, with a radius of not more than 100 m, centred on the area shown in Figure 5-31. The fracture, whose aperture is not larger than 1 mm, can therefore store at most $7,854 \text{ m}^3$ of water, which means that it can only supply Borehole UO5 with its yield of $30 \text{ m}^3 \text{ h}^{-1}$, with water for approximately 16 minutes. The fracture can therefore not serve as the main storage unit of water on the Campus Test Site. Since the sandstone and shales surrounding the fracture are the only other storage units available on the site, they must be the main suppliers of water to the boreholes. To see if this is possible, assume that the vertical hydraulic conductivity of the sandstone is 10^{-6} m s^{-1} and that the hydraulic gradient between the sandstone and fracture is 1. In other words, assume there is no pressure difference between the fracture and sandstone, and that the water flows towards the fracture under gravity. In this case, water can percolate into the fracture at a rate of $56,549 \text{ m}^3 \text{ h}^{-1}$. *Groundwater in Karoo aquifers must therefore be stored mainly in the sedimentary rocks and not in the fractures.* This result was confirmed by tests performed on cores during the drilling of the core-boreholes. Fractures in Karoo aquifers are therefore not storage units for water, but serve as conduits that transport the water from the sedimentary rock matrix towards the borehole. The simplest geometrical representation of a Karoo aquifer is therefore that of a fractured, perhaps multi-fractured, multi-porous medium.

The photograph of the core from Borehole CH3, in Figure 5-24, shows that there are subvertical fractures present in the aquifers on the Campus Test Site. However, they are mainly restricted to the upper mudstone layers, and typical of a weathering zone, where expansive stress is at a premium.

The microfractures in the quartz grains and bedding planes of the sandstone and mudstones will certainly increase the storativity of Karoo aquifers, but they are too small to increase the hydraulic conductivity of the aquifers significantly. Since the dimensions of these fractures are very similar to that of the formations' primary pores, they will not be considered separately in this discussion.

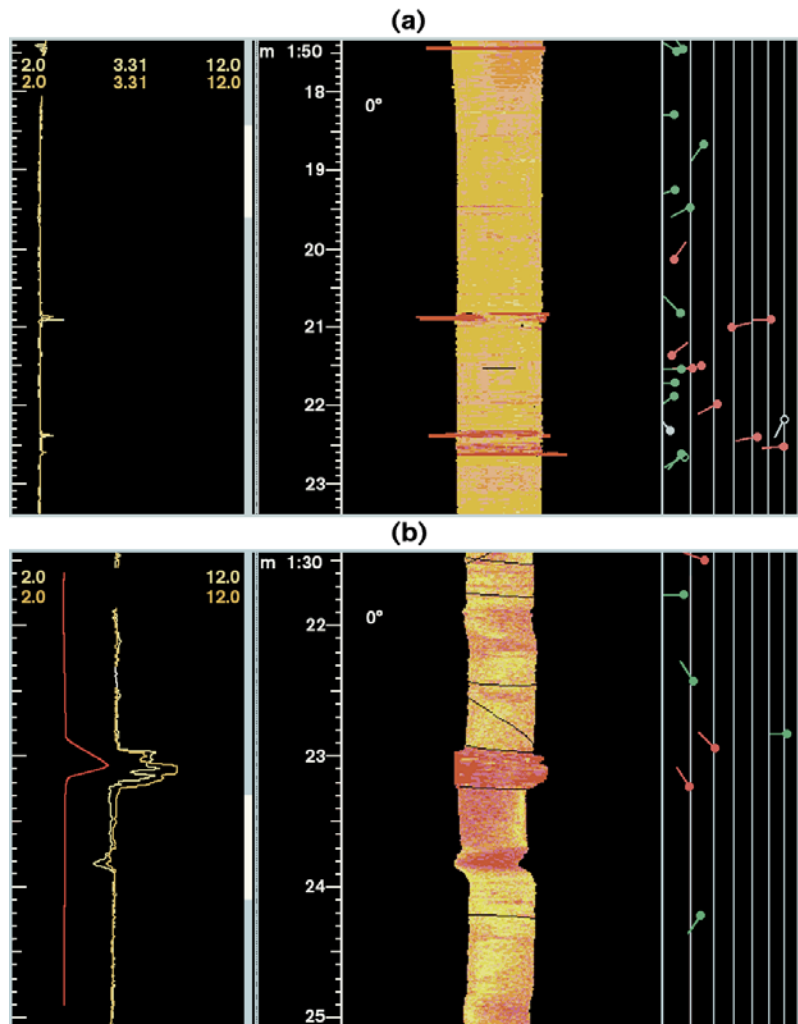


Figure 5–28 Acoustic scanner images of the Campus Sandstone in (a) core-borehole CH1, and (b) percussion borehole UO5. The orientation of the oblique fracture above 23 m in Borehole UO5 is 085 65.

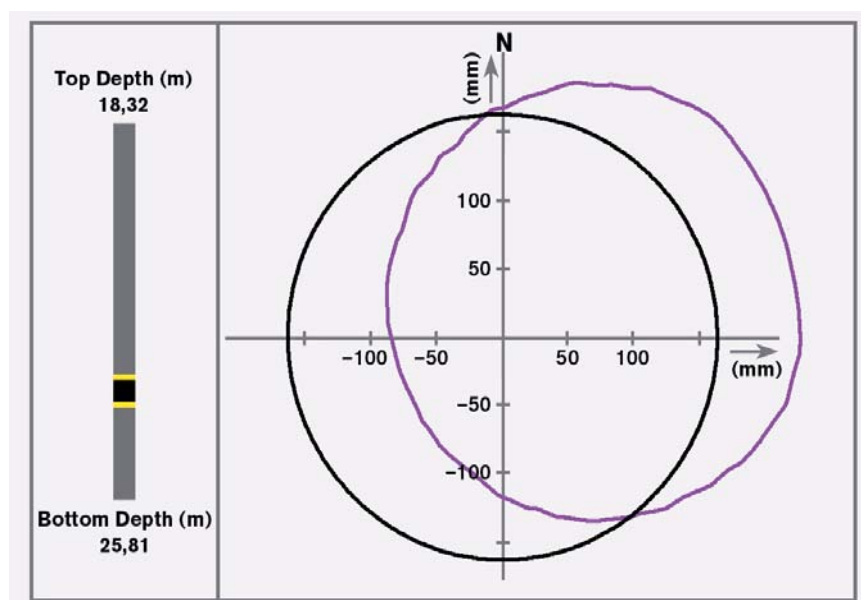


Figure 5–29 A 360° calliper diagram of the eccentricity of Borehole UO5, at a depth of 23,8 m.

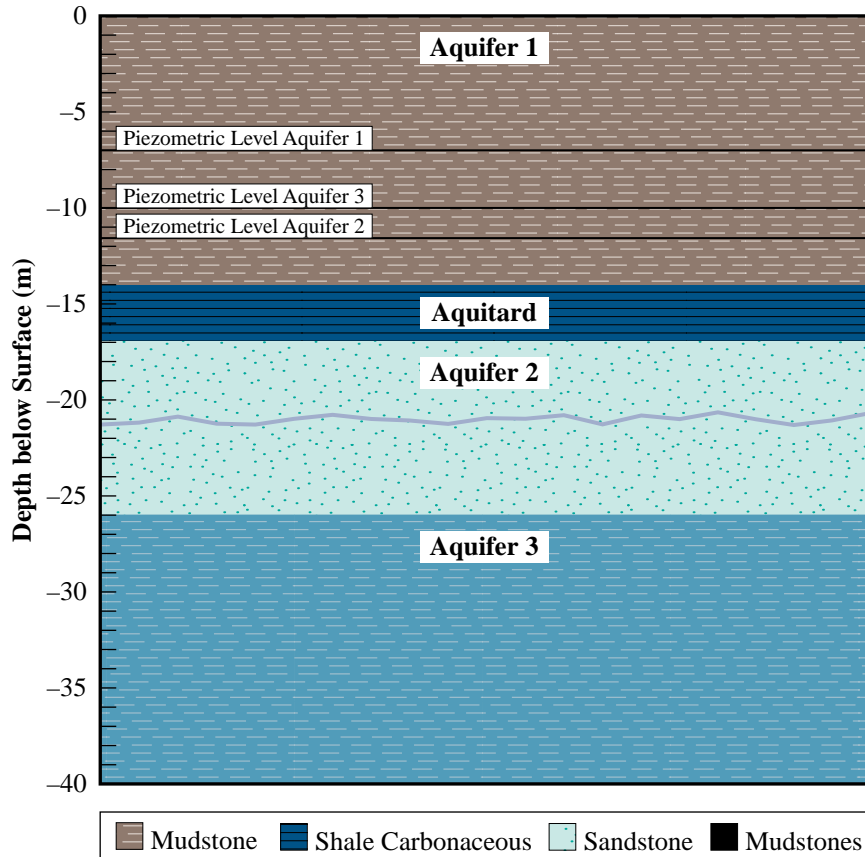


Figure 5-30 Schematic diagram of the different geological formations and aquifers present on the Campus Test Site.

5.6 THE DEWETSDORP TEST SITES

5.6.1 Introduction

Dewetsdorp is situated 77 km south-east of Bloemfontein in the Free State. The aquifers on the farms Kareefontein 66, Frankfurt 602 and Jouberts Rust 456, surrounding the town, were investigated previously by Kirchner *et al.* (1991), as part of their study on the exploitation potential of Karoo aquifers. The availability of this information suggested that these aquifers could be used to test results from the aquifer on the Campus Test Site, and interpolate them to a wider range of aquifers in the Karoo formations.

Kirchner *et al.* (1991) originally drilled 40 boreholes in the aquifers of which only three had yields more than $3,6 \text{ m}^3 \text{ h}^{-1}$. However, the positions of these boreholes were not suitable for cross-borehole packer tests. An additional 12 percussion boreholes were therefore drilled for this project on three of the Kirchner sites, shown in Figure 5-32. Three of these boreholes had yields more than $21,6 \text{ m}^3 \text{ h}^{-1}$. These percussion boreholes were later supplemented with two core-boreholes drilled by the Department of Water Affairs and Forestry.

5.6.2 Geology

Dewetsdorp is underlain by both the Tarkastad and Adelaide Subgroups of the Beaufort Group, in particular the Katberg Formation of the Tarkastad Subgroup and the Balfour Formation of the Adelaide Subgroup (Kirchner *et al.*, 1991). The Katberg Formation that forms the lower contact between the Tarkastad- and Adelaide Subgroups is very prominent in the area, probably because it is more resistant to weathering than the underlying Balfour Formation. Although the Katberg Formation consists mainly of sandstone, it tends to form cliffs and is thus not a promising formation in which to site boreholes. The sediments in the formation also tend to form lens-shaped bodies with the result that it is difficult to correlate the layers in borehole logs. The geometry of these aquifers differs in this sense from that of the Campus Test Site aquifer with its parallel layers.

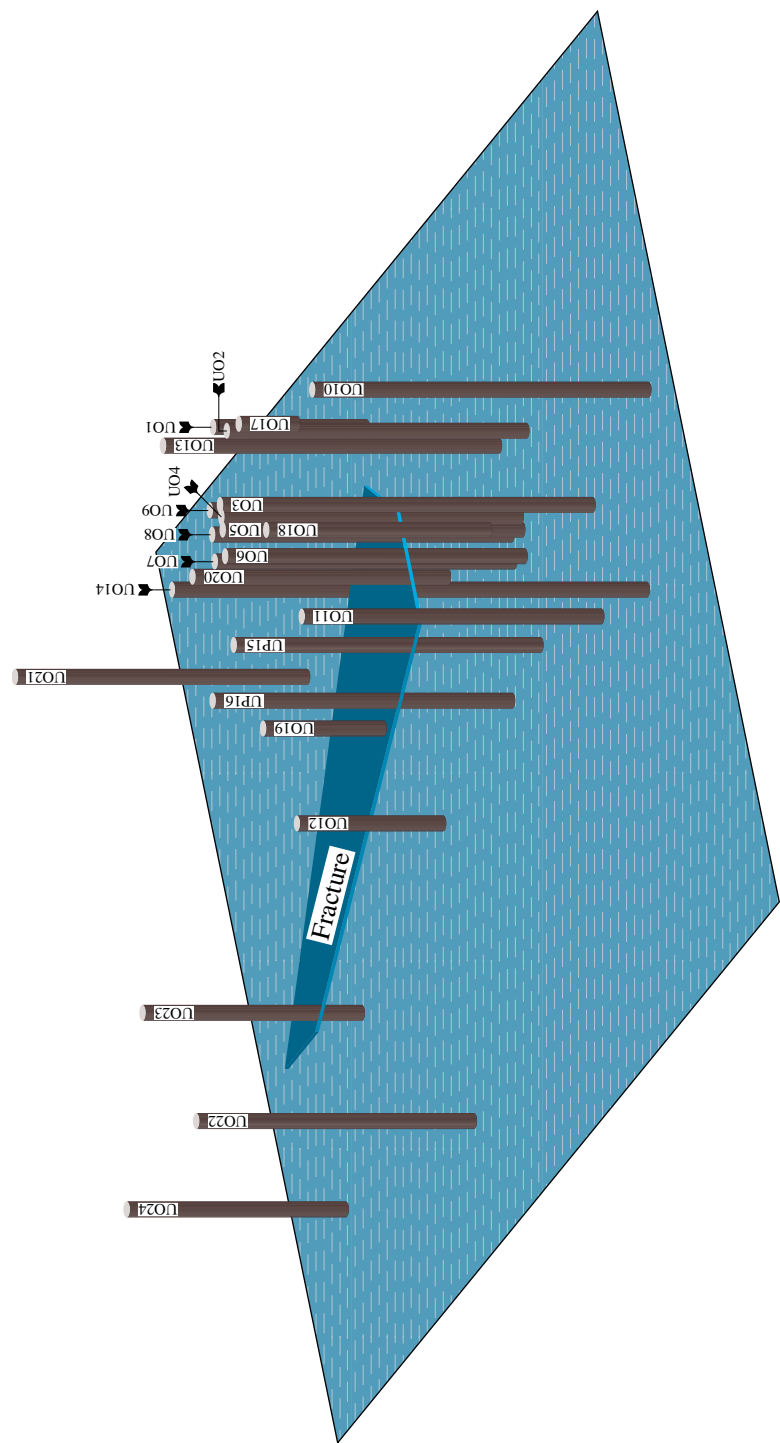


Figure 5–31 Presently known areal extent of the active part of the Mode I water-bearing fracture, in the Campus Sandstone on the Campus Test Site.

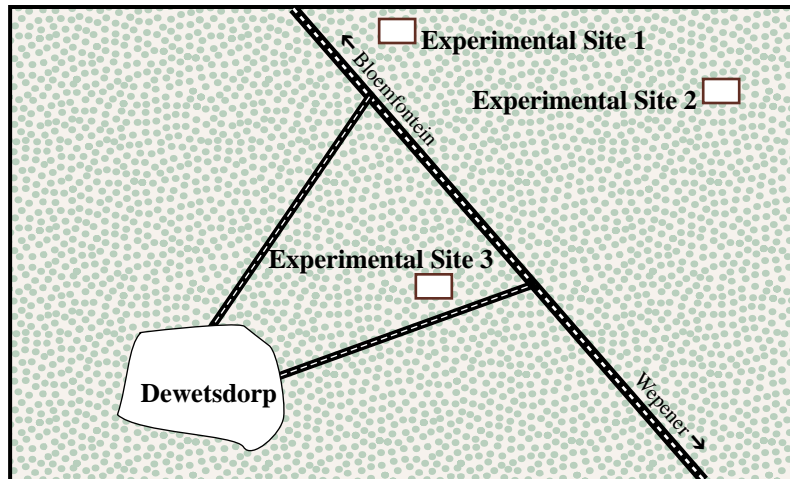


Figure 5–32 Location of the three experimental sites at Dewetsdorp.

The area in the north-east is underlain by the Balfour Formation with its fine-grained, cross-bedded sandstone, coarse arkose layers and mudstones. The mudstones, that vary in colour from green to red, represent the cyclic sedimentation of channel and flood-plain deposits.

There are a number of circular dolerite hills present in the area that represent ring dykes (Theron, 1970). A circular outcrop of dolerite to the west of Dewetsdorp, which is clearly visible on the 1:30 000 areal photograph of the area, also resembles a ring dyke.

The numerous linear dolerite dykes in the area are so intensely weathered in the low-lying areas that they can hardly be detected with surface magnetic methods. The dykes that occur at Sites 2 and 3 are fine-grained, less than 1 m thick and inclined towards the west. These dykes are very similar to the dykes at Philippolis where high-yielding boreholes have been sited.

5.6.3 Geohydrology of the Experimental Sites

Site 1 is situated north of the Bloemfontein-Wepener road (see Figure 5–32). Kirchner *et al.* (1991) drilled four boreholes on the site, of which only Borehole G36461 had a significant yield ($2,16 \text{ m}^3 \text{ h}^{-1}$). The water level of this borehole was 3 m lower than that of the other, which reminds one very much of the situation on the Campus Test Site. An additional four boreholes, B1, B2, B9 and B10 in Figure 5–33, were consequently drilled on the site with the view to perform packer tests there. Unfortunately, the yields of these boreholes were too low for such tests.

Site 2 is located directly north of Dewetsdorp and to the east of Site 1. Two boreholes G36430 and G36464 were drilled on the site by Kirchner *et al.* (1991). Borehole G36430 had a yield of $9,72 \text{ m}^3 \text{ h}^{-1}$, but G36464 was virtually dry.

Three new boreholes were drilled on the site. The first, B3, with a blow-yield of $21,6 \text{ m}^3 \text{ h}^{-1}$, intersected a north-east striking dolerite dyke that dips to the west, as indicated in Figure 5–34. The dyke, which is fine-grained and weathered to such an extent that it can hardly be traced with a magnetometer, is highly fractured and jointed at a depth of 35 m. The slickensided calcite and quartz (blown out during the drilling) and the fact that water was struck above and not below the dyke, suggest that the dyke intruded by dilation.

The second borehole, B4, did not intersect the dyke, and had a blow-yield of only $1,08 \text{ m}^3 \text{ h}^{-1}$. Another borehole, B11, was therefore drilled on the eastern side of the dyke to see if the dyke does not form a boundary between two aquifers, but was virtually dry. Only the two boreholes that intersected the dyke on the site therefore had significant yields. This may be an indication that the area away from the dykes is less fractured here than at the Campus Test Site or Philippolis. One possible explanation for this is that Dewetsdorp lies higher on the Beaufort Group than the other two sites. The intrusion of dolerites therefore fractured the upper layers of the Karoo formations at Dewetsdorp less than at the Campus Test Site and Philippolis.

Site 3 is situated to the north-east of the town, near the bed of a brook. Two percussion boreholes, A1 and C5, in Figure 5–35, were drilled on the site before the present investigation. Borehole C5 was drilled by Kirchner *et al.* (1991) in 1985, while the Department of Water Affairs and Forestry drilled A1 as a production borehole for the Municipality, at an unknown date. This borehole is situated on a north-east striking dyke that dips to the west at an angle of approximately 70° and has an estimated yield of $5 \text{ m}^3 \text{ h}^{-1}$.

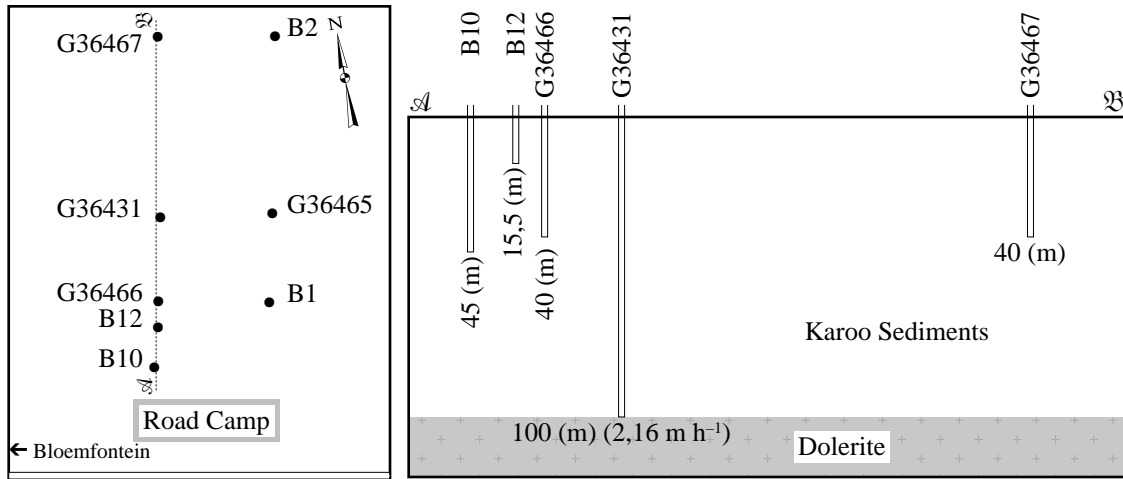


Figure 5-33 Plan view of the percussion borehole positions and a vertical cross-section through Experimental Site 1 at Dewetsdorp.

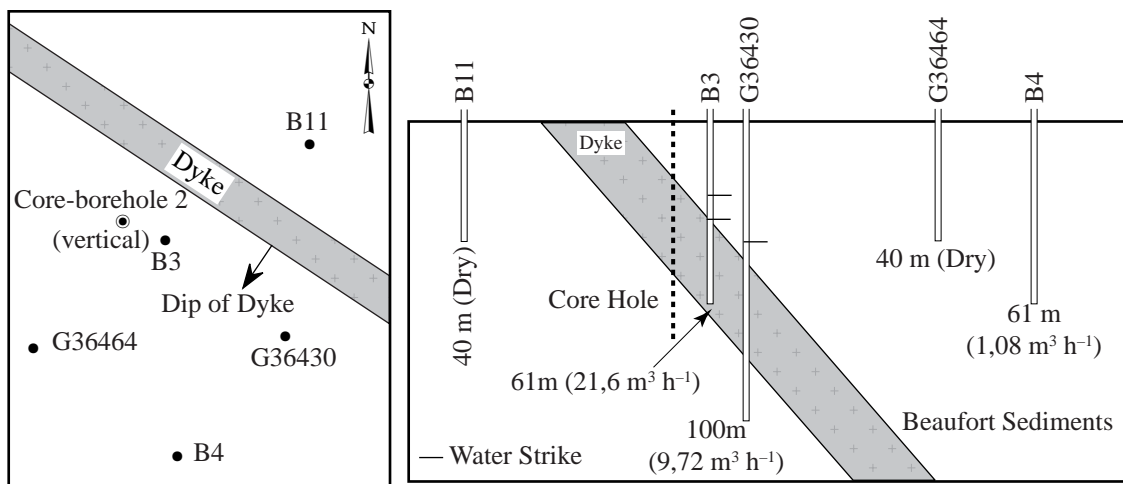


Figure 5-34 Plan view of the percussion and core borehole positions and a vertical cross-section through Experimental Site 2 at Dewetsdorp.

The dyke crops out on one of the brook's banks where it is totally weathered. It was thus thought a good site to investigate the influence that dykes may have on the behaviour of Karoo aquifers. Four additional percussion boreholes and one core-borehole were therefore drilled on the site. Boreholes B5 and B6 intersected the dyke from 24–28 m, while B7 and B8 intersected it from 17–23 m and 30–35 m, respectively. Boreholes B5 and B6 had blow-yields of only $1,08 \text{ m}^3 \text{h}^{-1}$, but B7 had a blow-yield of $25,2 \text{ m}^3 \text{h}^{-1}$ and B8 a blow-yield of $36 \text{ m}^3 \text{h}^{-1}$. This confirms the observations at the Campus Test Site that the yields of Karoo boreholes can differ substantially, even over small distances.

A structure intersected at a depth of 30,5 m in B8, is probably a fault as mylonitic quartz (26 mm thick) with slickensides was regained from the drill samples. It is interesting that the structure was intersected in the dyke and not its contact with the Karoo formations. This suggests that the dyke may have been fractured by some form of post-intrusion activity.

A comparison of the geological profiles for the boreholes at Dewetsdorp in Figure 5-36, and those of the Campus Test Site in Figure 5-16, shows that the Dewetsdorp sites are underlain by more and thinner geological units than the Campus Test Site. The chances of striking a well-developed aquifer at Dewetsdorp are therefore not very high. This may explain why *Kirchner et al.* (1991) were not very successful with their drilling programme.

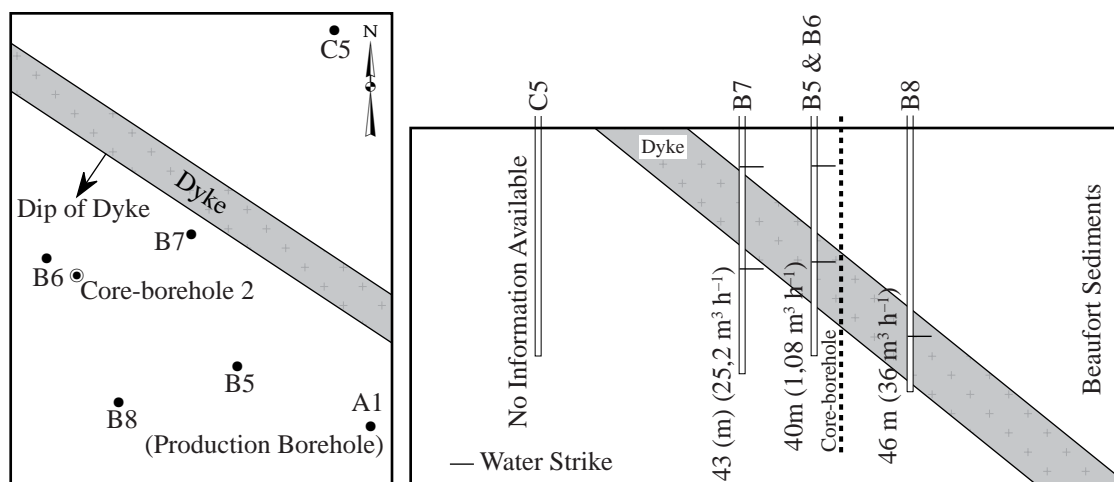


Figure 5-35 Plan view of the percussion and core-borehole positions and a vertical cross-section through Experimental Site 3 at Dewetsdorp.

5.7 DISCUSSION

The regional structural-stratigraphic investigation around the Campus Test Site provided the geological perspective for the aquifers drilled at the site. The study, which included palaeontological evidence, showed that the position of the Ecce-Beaufort contact as reported on Sheet 2926 Bloemfontein (Geological Survey, 1966) is inconsistent, and that all the lithologies drilled on the Campus Test Site were situated in the Adelaide Subgroup. Three major sandstone sheets which have regional aquifer potentials—the Campus, Spitskop and Musgrave sandstones—were identified. The Spitskop and Musgrave sandstones crop out west of the city, but the Campus Sandstone is confined to the subsurface everywhere.

A north-easterly trending megascopic domal structure that deforms the sediments, but does not influence the north-westerly trending main drainage, may act as a regional groundwater ridge. The existence of this megascopic structure has two significant consequences. The first is that it has exactly the form that one would expect of sedimentary formations displaced by the intrusion of laccoliths, and therefore supports the view expressed in Chapter 3, that dolerites intruded as laccoliths in this area. The second consequence is that the adjacent basin structures form regional sinks for groundwater accumulation. The influence of such structures on the flow of groundwater in Karoo formations should therefore not be underestimated.

The regional palaeocurrent and facies analysis of the Beaufort sediments indicated that the palaeofluvial environment is represented by argillaceous and arenaceous assemblages today. The Campus and Spitskop Sandstones represent channels from a meandering river system, while the Musgrave Sandstone is typical of channels associated with braided river systems. The coarse nature of the latter sandstone suggests that it may be a significant groundwater resource.

Interpretation of regional fracture development in the sediments indicates that the subvertical fractures in the area provide conduits for surface water, while pervasively developed bedding-parallel fractures act as the main conduits for water within the aquifers. The yields of boreholes in Karoo aquifers are therefore mainly determined by the probability that they intersect such a bedding-parallel fracture. These results, and those from the experimental sites, suggest that the siting of boreholes should be limited to those areas where bedding-parallel fractures are present. Since the chances are better to strike such fractures near dolerite dykes, and the dykes can be located relatively easy, it is logical to concentrate on these dykes when siting boreholes in the Karoo formations. One difficulty associated with this practice is that the dyke may be impermeable and act as a boundary of the aquifer. In such cases it will be difficult for the borehole to maintain an optimal yield over prolonged periods, especially during droughts. However, as shown by the Campus Test Site, and to a lesser extent Site 1 at Dewetsdorp, there are other areas where these fractures occur, and high-yielding boreholes can be drilled. Unfortunately, no surface geophysical technique exists today with which these fractures can be detected. Indeed, it seems that wireline logging techniques, using dipmeter or acoustic scanner probes are the only viable methods to detect these fractures.

It is difficult to explain the existence of the sparsely spaced bedding-parallel fractures that act as conduits for water to boreholes, at all the sites studied in this investigation without invoking the intrusion of laccoliths as conceptualized in Figure 3-9. This conjecture is further strengthened by the observation in

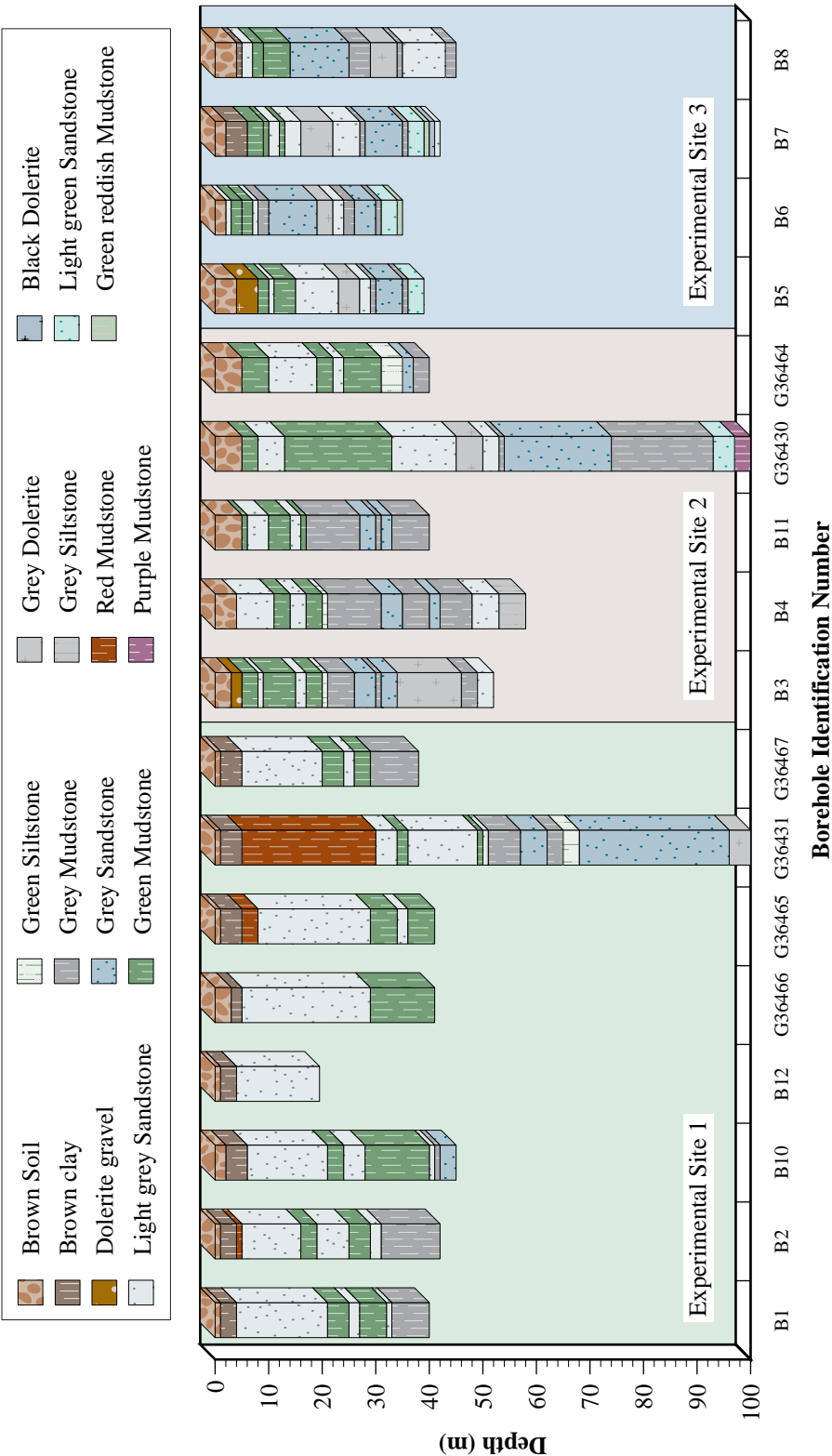


Figure 5–36 Geological logs of the percussion boreholes on the experimental sites at Dewetsdorp.

Section 5.4.2, that the fractures had a compressional origin, but now appear in tension. The discussion of the intrusion of laccoliths in Appendix A indicates that the areal extent of the fractures will depend on the size of sedimentary layers lifted by the laccolith, but that their apertures may be small. This is in agreement with the present information on these fractures, which shows that the apertures of the fractures are only of the order of 1 mm, but their areal extent can vary from a few thousand square metres to several square kilometres.

The bedding-parallel fractures' dimensions imply that Karoo aquifers have a far more complex geometry than that of the media conventionally used to describe the behaviour of aquifers. The best way to describe this geometry is that of a semi-fractured, multi-porous medium, in which the water is stored in the matrix, while the fractures present the main conduits for flow.

An important consequence of the complex geometry of Karoo aquifers is that one can expect that their hydraulic properties will vary considerably over very short distances. This variability is further enhanced by the lithology of Karoo aquifers, which consists mainly of sedimentary rocks. Since fluvial systems tend to deposit sediment particles with their long axes parallel to the flow, Karoo aquifers are highly heterogeneous and anisotropic. It is thus simply not worthwhile to try to analyse observations of Karoo aquifers with methods derived from the conventional groundwater media, such as an ordinary porous medium or even the dual porosity medium of Barenblatt *et al.* (1960). Moreover, the presence of different semi-pervious layers implies that vertical flow will be very significant in these aquifers.

The presence of microfractures in the quartz grains and bedding planes of the sandstone and shale layers has serious implications for the pollution of Karoo aquifers. One of the most important of these is that the pollutant can spread rapidly through the fractures and diffuse into the matrix, through matrix diffusion, from where it cannot be removed easily.

In summary, it can be said that the development of the Campus and Dewetsdorp sites provided valuable information on the behaviour of Karoo aquifers, especially the unpredictable behaviour of these semi-fractured aquifers. These aquifers are much more complex than the aquifers commonly considered in the literature on groundwater. Special care must therefore be taken in the siting of boreholes and waste disposal sites in Karoo aquifers. However, many of the problems experienced with Karoo aquifers today can be minimized, or even prevented, if care is taken of the aquifers' complex geometry.



CHAPTER 6

THE PHYSICAL BEHAVIOUR OF KAROO AQUIFERS

6.1 INTRODUCTION

The study of the genesis and evolution of Karoo aquifers in Chapters 3 and 4, and the information gained from the geology of the test sites on the Campus and at Dewetsdorp described in Chapter 5, show that these aquifers have a very complex geometry. One can therefore expect that their hydraulic behaviour will also be complex. The danger thus exists that such an aquifer can be damaged, or even destroyed, if not managed in accordance with its physical properties. The neglect of these properties in the management and operation of Karoo aquifers may be one of the major reasons for the present distrust in these aquifers. In this chapter an attempt will be made to combine the information gained on the properties of these aquifers in the previous chapters, with results from hydraulic tests to try to understand the physical behaviour of Karoo aquifers better.

The discussion begins with a brief description of the nature of flow in Karoo aquifers, particularly matrix- and fracture flow in Section 6.2. This is followed by a discussion of the various hydraulic tests performed on some of these aquifers in Section 6.3. These tests have shown that the local behaviour of a stressed Karoo aquifer is controlled by bedding-parallel fractures. The effect of this dependence on the ability of a Karoo aquifer to yield water is discussed in Section 6.4.

Although fractures control the local behaviour of Karoo aquifers, their global behaviour is more determined by dolerite dykes and hydrochemical actions, which is discussed in Sections 6.5 and 6.6 respectively.

The attempt to clarify the behaviour of Karoo aquifers with analytical models, in Section 6.7, has shown that the flow in these aquifers is linear and not radial. The majority of the existing conceptual models for the analysis of hydraulic test data, therefore, cannot be used for Karoo aquifers.

The main conclusion of this investigation, discussed in Section 6.8, is that the physical behaviour of Karoo aquifers is controlled by their complex geometries and elastic properties. These factors must certainly be taken into account if the aquifers are to be managed and operated efficiently.

6.2 THE NATURE OF FLOW IN KAROO AQUIFERS

6.2.1 General

Karoo aquifers have been classified in Chapter 5 as multi-layered, multi-porous aquifers in which bedding-parallel fractures form the main conduits of water. The apertures and areal extent of the fractures, however, are limited. They are therefore not able to store large quantities of water, with the result that their piezometric pressures drop rapidly when a borehole that intersects them is pumped. This drop in piezometric pressure will cause water to leak from the matrix to the fracture. There are thus two types of flow present in a Karoo aquifer: bedding-parallel fracture flow and matrix flow.

The simplest approach to Karoo aquifers is to regard them as dual-porosity aquifers. However, the existing theory of dual-porosity media (Moench, 1984) assumes that the media is infinite and cyclic, as indicated in Figure 6-1. This is clearly not the case in Karoo aquifers, which frequently contain just one water-bearing bedding-parallel fracture. As will be shown below, it is these fractures that are responsible for the unique and complex behaviour of Karoo aquifers.

There exist of course, also microfractures in the Karoo formations, as can be seen from the photographs of the cores in Figures 4-9 and 5-24, but their dimensions are the same as that of the pores. They will therefore be considered as part of the porous matrix.

6.2.2 Matrix Flow

The bedding-parallel fractures' lack of storage capacity implies that the rock matrix must be the main storage unit in Karoo aquifers. The description of the genesis of Karoo rocks in Chapter 3 has shown that these rocks

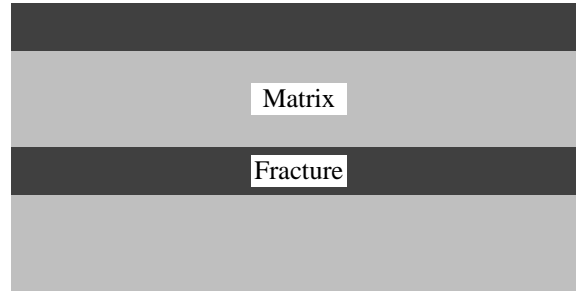


Figure 6-1 Schematic representation of a slab-shaped, dual-porosity medium. [After (Moench, 1984).]

will consist mainly of fine-grained mudstones, siltstones and shales, with interbedded sandstones, whose grain size can vary from fine to coarse. The rocks therefore originally had a very high primary porosity, but this porosity was considerably reduced by cementation and compaction. The result is that the pores and microfractures in the rocks are usually very small. It thus follows from Laplace's equation [Equation (2.1)] that the flow of water will be severely restricted by adhesive forces in these rocks. One can thus expect that the hydraulic conductivity, \mathbf{K} , of the rocks will be very small ($\sim 10^{-6}$ – 10^{-8} m s $^{-1}$). Nevertheless, it follows from Darcy's law,

$$\mathbf{q} = -\mathbf{K}\nabla\phi \quad (6.1)$$

that there will always be a flux of water, \mathbf{q} , from the matrix to the fracture, as long as there exists a piezometric pressure gradient, $\nabla\phi$, from the rock matrix towards the fracture. Although this flux may be small, the flow over a large area can be considerable. The matrix can thus supply large quantities of water to a bedding-parallel fracture with a large areal extent, as discussed in Section 5.5.5. Vertical flow through the matrix may therefore be the predominant type of flow in Karoo aquifers.

6.2.3 Fracture Flow

The flow in a fully fractured medium is largely controlled by the fracture dimension, orientation and connectivity (Odling, 1993). The bedding-parallel fractures in Karoo aquifers are mainly horizontally orientated and sparsely distributed. Since no large-scale vertical or subvertical fractures were observed in these aquifers, multiple bedding-parallel fractures will only be weakly connected through the intermediate rock matrix. The ability of a Karoo aquifer to transmit water will therefore be determined mainly by the apertures of bedding-parallel fractures, if present.

An idea to what extent the fractures' apertures may influence flow in Karoo aquifers can be obtained by looking at the expression for the discharge rate of a simple parallel plate fracture (De Marsily, 1986)

$$\mathbf{Q} = -\frac{ab^3\rho g}{12\mu} \nabla\phi$$

where ρ is the fluid density, g the acceleration of gravity, μ the viscosity of the fluid, ϕ the piezometric head in the fracture, with a the width and b thickness of the fracture, as defined in Figure 6-2. The flux of a fluid through the fracture

$$\mathbf{q} = \frac{\mathbf{Q}}{ab} = -\frac{b^2\rho g}{12\mu} \nabla\phi \quad (6.2)$$

thus depends on the square of the fracture's aperture, b . One can thus expect that the yield of a borehole in a Karoo aquifer will depend strongly on the aperture(s) of the bedding-parallel fracture(s) that it intersects.

It follows from Equation (6.2), that the yield of a borehole that depends on a bedding-parallel fracture for its water will be limited on two accounts—the aperture of the fracture and the piezometric gradient within the fracture. Although the apertures of bedding-parallel fractures in Karoo aquifers are larger than those present in more conventional fractured aquifers, they are still not very large (~ 1 mm). A borehole in a Karoo aquifer may therefore not be able to sustain a specific discharge rate, even though the piezometric level in the aquifer is still high. As will be shown below, it is precisely this property of the bedding-parallel fractures that is responsible for the complex behaviour of Karoo aquifers.

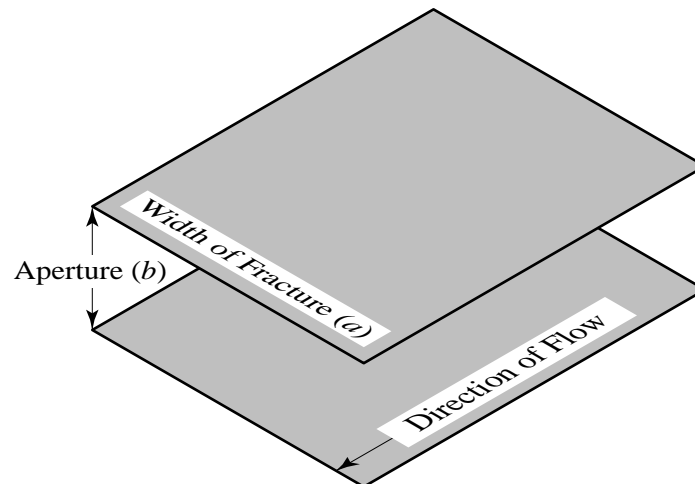


Figure 6-2 Schematic illustration of the parallel plate model for a fracture.

6.3 HYDRAULIC TESTS

6.3.1 General

Numerous hydraulic tests have been performed on the boreholes at the Campus Test Site, Philippolis and Rouxville, as part of this project, with the view to determine the physical behaviour of the aquifers. Mr. Alan Woodford from the Department of Water Affairs and Forestry's Cape Town office also kindly provided information on tests he performed on boreholes in the Calvinia area. The present discussion will, however, be limited to tests that display the complex behaviour of Karoo aquifers the best.

6.3.2 Multiple Constant Rate Tests

A series of five constant rate tests was performed from April 1993 to June 1993 on the 16 boreholes, UO1 – UP16, that existed at the time on the Campus Test Site. The main purpose of the tests was to see if the pumping rate and pumping depth may have any influence on the results of hydraulic tests. The perturbed borehole was pumped for six hours at rates of 1,125, 2,25 and 4,5 m³ h⁻¹, and allowed to recover for at least 18 h in all the tests. The tests were also repeated three times to verify the repeatability of constant rate tests in Karoo aquifers. The first four members of the series were performed with Borehole UO5 as the perturbed borehole, and the fifth one with Borehole UP16. The pump was installed at a depth of 22 m (as measured from the borehole collar) for all the tests, except for the fourth member, where it was lowered to a depth of 30 m.

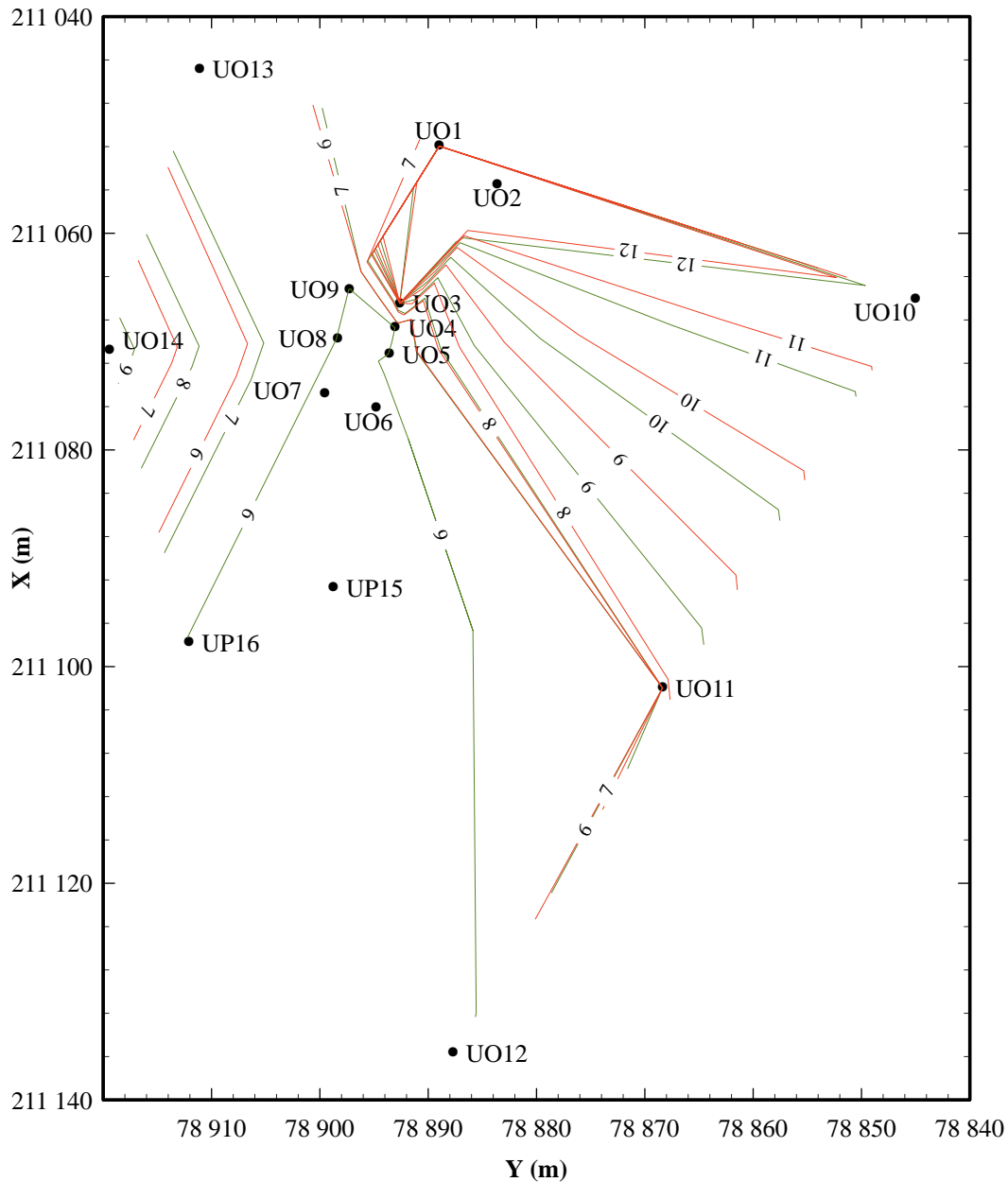
The drawdowns were all recorded electronically with the apparatus described in Appendix B. The drawdowns could thus be measured in all sixteen boreholes simultaneously, at one minute intervals and a consistent accuracy of ± 5 mm. The result was that much smaller variations in the drawdowns could be observed than would have been the case if the measurements were made by hand.

A visual inspection of the observed drawdowns showed that the boreholes can be divided naturally into three distinct classes, as indicated in Table 6-1. This behaviour remained puzzling until contours were drawn of the water levels in the aquifer before and after each of the tests, in reviewing the data for this report. As shown by the example of these contour maps in Figure 6-3, there exists a well-defined boundary, running from boreholes UO1 to UO11 through Borehole UO3, across which there is very little flow. A closer examination of the boundary shows that it coincides very much with the boundary of the Mode I fracture in Figure 5-31. A logical conclusion is thus that the behaviour of the Class 1 boreholes is caused by the fact that they do not intersect the fracture, or that the fracture is closed in that area. The *aquifer's geometry* is therefore the main reason for the observed behaviour of the boreholes, as one could have anticipated from the discussion in Chapters 3 and 5.

As Botha and Magda (1993) have pointed out, one should expect differences in the geometry of an aquifer to show up in contours of its water levels. The boundary in Figure 6-3 is thus probably more representative of the Mode I fracture's boundary than that shown in Figure 5-31, which is only based on the geological and geophysical logs of the boreholes.

Table 6–1 Behaviour of drawdowns in boreholes UO1 – UP16 on the Campus Test Site.

Class	Borehole	Behaviour of Drawdowns
1	UO1 – UO3, UO10	Inconsistent behaviour of drawdowns
2	UO14	Drawdown consistent but irregular
3	UO4 – UO9, UO11 – UO13, UP15, UP16	Drawdowns consistent and regular

**Figure 6–3** Water-level contours of the aquifers on the Campus Test Site before and after repeating the constant rate test where Borehole UO5 was pumped at $2,25 \text{ m}^3 \text{ h}^{-1}$ for the third time. (Depth of pump = 22 m.)

The absence of a geophysical log makes it difficult to explain the behaviour of Borehole UO14. The more so, because its geological log indicates that it does penetrate the fracture, although the aperture of the fracture may be very small. One rather strange, but interesting, explanation relates to the history of the borehole. This borehole is one of the five original boreholes the Department of Geohydrology drilled in 1989, and was thus already four years old at the time of the tests. The borehole had to be re-drilled about a year after the tests, because it was completely clogged by an ant nest situated over the fracture. It is thus

likely that the ant nest already existed at the time of the tests, and interfered with the yield of the fracture. This interpretation has the advantage that it provides a natural explanation not only for the irregular behaviour of the drawdowns, but also why the borehole behaved normally after the cleansing operations.

The observed drawdowns differed considerably from one observation borehole to another, and displayed minor differences within each member, as could have been expected. A statistical analysis, however, showed that differences within a given member are not significant. Constant rate tests can therefore be repeated in Karoo aquifers with confidence. This statement should not be interpreted as saying that the behaviour and properties of a Karoo aquifer will not change with time. All that it says is that one can trust the results of a single test performed at a specific time.

The first impression of the observed drawdowns for the Class 3 boreholes, of which examples are shown in Figure 6–4, was that they are very similar to drawdowns described by the classical analytical model of Theis (1935) for a confined porous aquifer. The results of the tests were therefore interpreted with this analytical model. The small differences between the observed and computed drawdowns, particularly at the end of the pumping period, were ignored in the analysis.

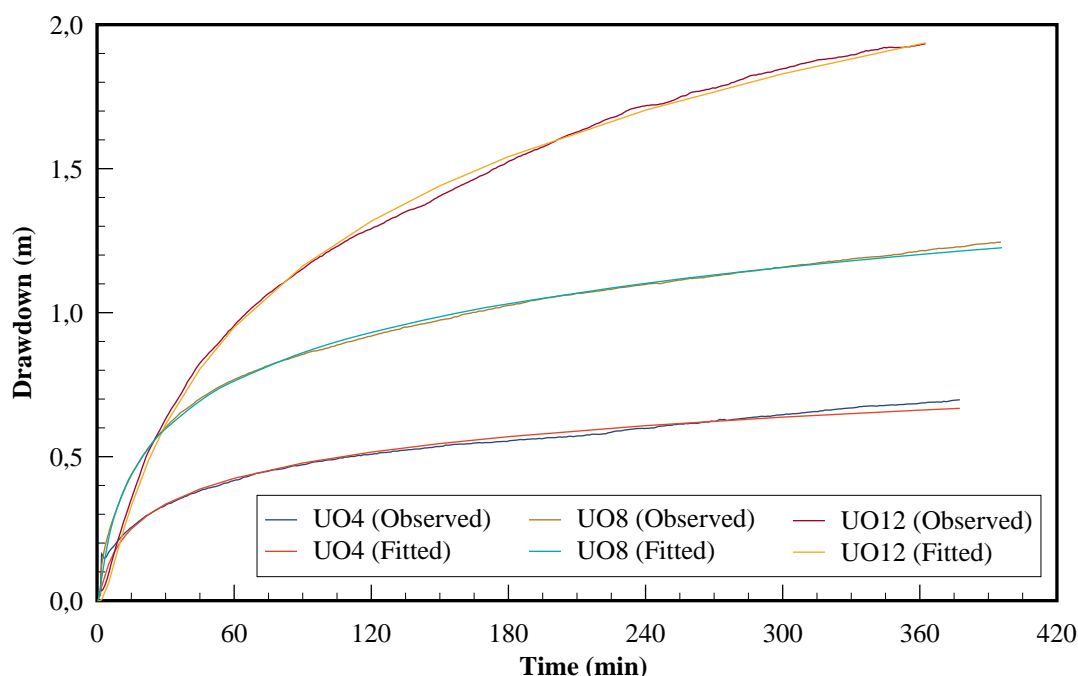


Figure 6–4 Drawdowns observed in boreholes UO4, UO8 and UO12 during a series of five constant rate tests performed on the Campus Test Site.

The Theis model is based on the assumption that the aquifer is uniform and the flow radial and horizontal. The hydraulic parameters associated with the model, the storativity (S) and transmissivity (T), therefore, *cannot* depend on the discharge rate (Q), distance from the perturbed borehole (r), and time (t). Any observed variation in the hydraulic parameters with the last three parameters should thus be regarded as an indication that the model is not applicable for the specific aquifer. This property is, unfortunately, often neglected when fitting the Theis model to observed drawdowns.

The first indication that the Theis model is not applicable to Karoo aquifers came from an analysis of the S -values, which decrease continuously as r increases. This behaviour has been observed previously in Karoo and other aquifers in South Africa by Bredenkamp *et al.* (1995). The authors recognized that the results are unrealistic, but nevertheless proceed to derive methods with which the values can be corrected, implying that one can correct inapplicable results!

The dependence of the Theis-fitted S -values on r suggests that the S -values may also depend on the position of the perturbed borehole. It was thus thought worthwhile to compare the ratios of S -values, derived from the tests performed on boreholes UO5 and UP16, with the inverse ratio of the observation boreholes' distances from the perturbed boreholes. The results, displayed graphically in Figure 6–5, clearly show that this is not the case. Theis-fitted storativities are therefore a function of a power of the inverse distance, from the observation to the perturbed borehole, but not the position of the perturbed borehole.

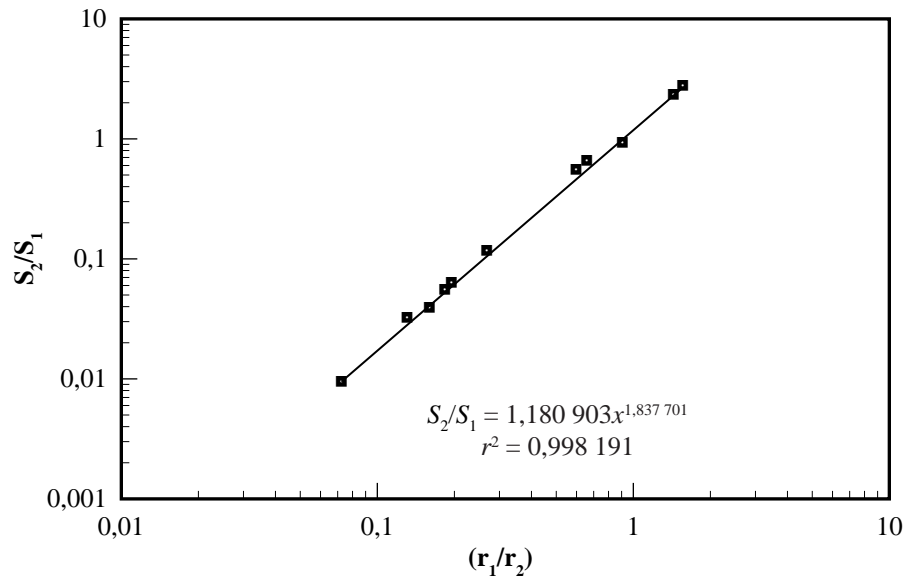


Figure 6–5 Dependence of the Theis-fitted S -value ratios on the inverse ratio of the distance between the observation and perturbed borehole. (Subscripts 1 and 2 denote members 3 and 5 of the tests, in which boreholes UO5 and UP16 were pumped at a rate of $2,25 \text{ m}^3 \text{ h}^{-1}$.)

A second indication that the Theis model is not applicable to Karoo aquifers came from an analysis of the S - and T -values for the Class 3 boreholes in Table 6–1 as a function of Q . The T -values first tend to increase and then decrease with increasing Q , while the S -values increase linearly with the discharge rate, as shown in Figure 6–6. A statistical analysis of the results revealed that the dependence of the S -values on Q is not significant, but that the dependence of the T -values on Q is highly significant. The reason the dependence of S on Q seems not to be significant, is that S also depends on r . There can thus be little doubt that the parameters derived from the Theis fit do depend on Q .

It is difficult to explain the dependence of the Theis-fitted hydraulic parameters on distance and pumping rate, except to note that it may be related to vertical flow in the aquifer—something that the Theis model neglects completely. This possibility will be discussed further in Section 6.7.

Verwey and Botha (1992) have shown that the hydraulic parameters arrived at by fitting the Theis curve to drawdowns in a fully three-dimensional aquifer will be a function of the depth at which the pump is installed. That this is indeed the case for the aquifer on the Campus Test Site is shown by the hydraulic parameters in Table 6–2, derived from four of the constant rate tests for the Class 3 boreholes. The statistical analysis of the results has shown that the dependence of the S -values on the depth is again not significant, but that the dependence of the T -values on the depth is highly significant.

Table 6–2 Hydraulic parameters for the Class 3 boreholes obtained from a fit of the drawdowns observed when Borehole UO5 was pumped at a rate of $2,25 \text{ m}^3 \text{ h}^{-1}$, with the pump installed at depths of 22 and 30 m.

Borehole	Depth 22 m		Depth 30 m		Ratios	
	$T_{22} (\text{m}^2 \text{ s}^{-1})$	S_{22}	$T_{30} (\text{m}^2 \text{ s}^{-1})$	S_{30}	T_{22}/T_{30}	S_{22}/S_{30}
UO4	$2,134 \cdot 10^{-4}$	$1,032 \cdot 10^{-2}$	$1,855 \cdot 10^{-4}$	$1,424 \cdot 10^{-2}$	$8,693 \cdot 10^{-1}$	1,380
UO6	$2,211 \cdot 10^{-4}$	$2,542 \cdot 10^{-3}$	$1,880 \cdot 10^{-4}$	$3,565 \cdot 10^{-3}$	$8,502 \cdot 10^{-1}$	1,403
UO7	$2,128 \cdot 10^{-4}$	$1,379 \cdot 10^{-3}$	$1,882 \cdot 10^{-4}$	$1,883 \cdot 10^{-3}$	$8,844 \cdot 10^{-1}$	1,365
UO8	$2,100 \cdot 10^{-4}$	$2,821 \cdot 10^{-3}$	$1,878 \cdot 10^{-4}$	$3,815 \cdot 10^{-3}$	$8,945 \cdot 10^{-1}$	1,352
UO9	$2,143 \cdot 10^{-4}$	$1,309 \cdot 10^{-3}$	$1,860 \cdot 10^{-4}$	$1,931 \cdot 10^{-3}$	$8,679 \cdot 10^{-1}$	1,475
UO11	$1,781 \cdot 10^{-4}$	$1,363 \cdot 10^{-4}$	$1,725 \cdot 10^{-4}$	$1,435 \cdot 10^{-4}$	$9,686 \cdot 10^{-1}$	1,053
UO12	$1,952 \cdot 10^{-4}$	$4,988 \cdot 10^{-5}$	$1,612 \cdot 10^{-4}$	$6,400 \cdot 10^{-5}$	$8,257 \cdot 10^{-1}$	1,283
UO13	$1,885 \cdot 10^{-4}$	$1,271 \cdot 10^{-4}$	$1,657 \cdot 10^{-4}$	$1,737 \cdot 10^{-4}$	$8,789 \cdot 10^{-1}$	1,367
UP15	$2,049 \cdot 10^{-4}$	$1,625 \cdot 10^{-4}$	$1,803 \cdot 10^{-4}$	$2,257 \cdot 10^{-4}$	$8,797 \cdot 10^{-1}$	1,389
UP16	$2,022 \cdot 10^{-4}$	$8,077 \cdot 10^{-5}$	$1,784 \cdot 10^{-4}$	$1,071 \cdot 10^{-4}$	$8,827 \cdot 10^{-1}$	1,325

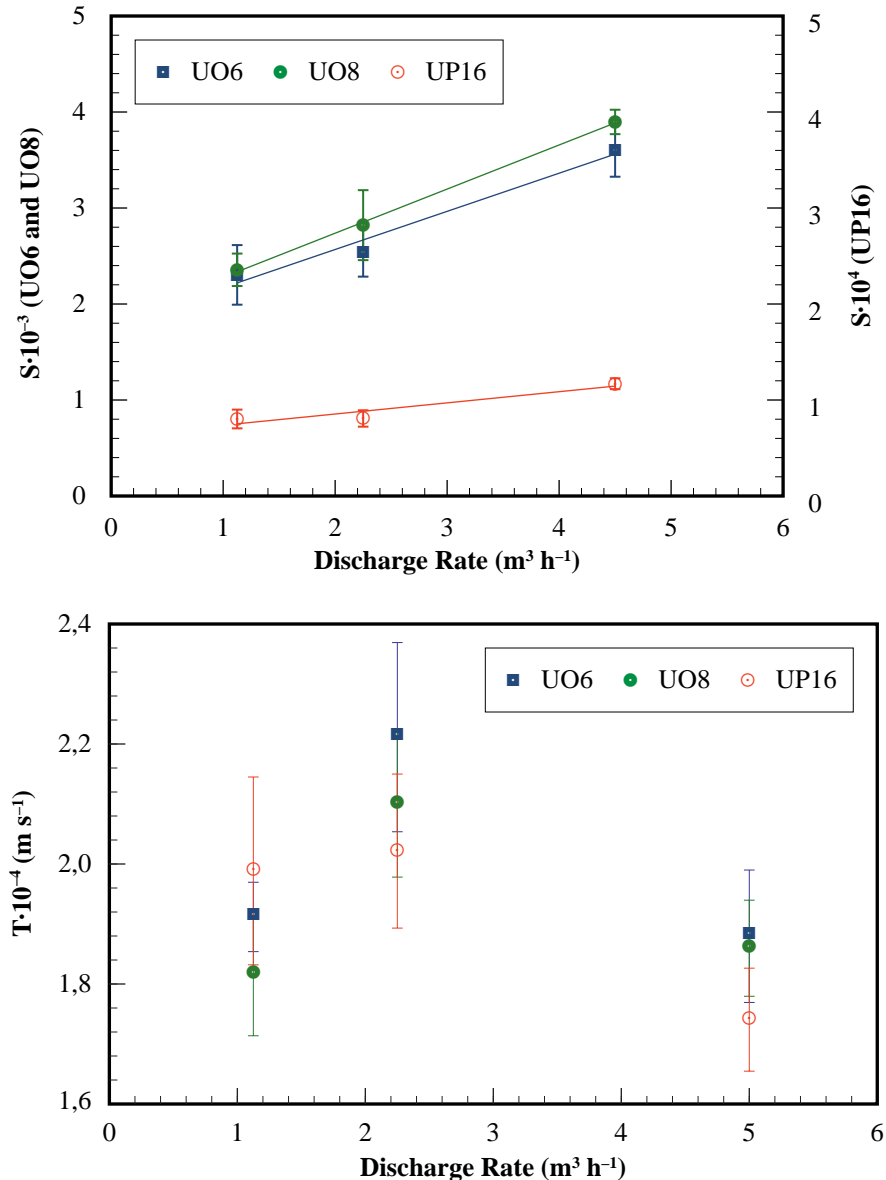


Figure 6–6 Representative graphs of the Theis-fitted S - and T -values for the Class 3 boreholes as a function of the discharge rate.

An interesting feature of the results in Table 6–2 is that the transmissivities, with the pump installed at 22 m, are always less than those with the pump installed at 30 m, while the inverse is true for the storativities. A possible explanation of this behaviour is that the hydraulic conductivity of the formation at 30 m was less than that of the formation at 22 m. This conclusion is supported by the observation that the drawdown cone observed with the pump installed at 22 m, was shallower than the one observed when it was installed at 30 m, particularly at the later times. The position at which a pump is installed in a production borehole may thus be a very important parameter in the management and operation of a Karoo aquifer.

The previous results of the constant rate tests clearly show that *the Theis model is invalid for Karoo aquifers*. Theis-fitted hydraulic parameters may be used to obtain *qualitative* information on the properties and behaviour of an aquifer, but *it will be a mistake to base a quantitative evaluation of the aquifer on them, or to use them in developing management models for Karoo aquifers*.

6.3.3 Cross-borehole Packer Tests

A major disadvantage of conventional constant rate tests is that the observed water levels always represent an average over the aquifer's thickness (Verwey and Botha, 1992). The tests can therefore not be used to

obtain information on separate layers of a multi-layered aquifer, or the vertical distribution of its hydraulic parameters. There is indeed only one type of conventional hydraulic test suitable for this purpose—packer tests. The basic principle of these tests is to seal a section of a borehole off with an inflatable device (the packer), inject (or withdraw) some water into the sealed-off section and observe the behaviour of the action in the section, or similar sections in adjacent boreholes.

There are two types of packer tests that are often applied in practice: double-packer and cross-borehole packer tests. Double-packer tests can only be performed in single boreholes, and thus provide information on the horizontal hydraulic parameters. Cross-borehole packer tests, on the other hand, can provide information on the full spatial distribution of both the hydraulic parameters.

The success achieved with cross-borehole packer tests in the Malmesbury Formation at Atlantis (Botha *et al.*, 1990) suggested that this type of test may be particularly useful in clarifying the behaviour of Karoo aquifers. Boreholes UO3 – UO9 on the Campus Test Site were therefore drilled specifically for this purpose. The series of multiple constant rate tests were consequently followed by a series of cross-borehole packer tests. The tests were all performed with Borehole UO5 as the perturbed borehole, and measurements were taken in the other six boreholes at depths that varied from 9 m to 27 m in 2 m intervals.

The results of the tests were rather disappointing, however. All the observed changes in pressure heads, Δh , satisfied the basic equation for an anisotropic medium (Hsieh *et al.*, 1983)

$$\Delta h = \frac{Q}{4\pi r} \sqrt{\frac{K_d}{D}} \operatorname{erfc} \sqrt{\frac{r^2 S}{4K_d t}}$$

where, Q is the injection rate, r the distance to the observation borehole, t the time, S the specific storativity, D the determinant of the hydraulic tensor, \mathbf{K} , and K_d the directional hydraulic conductivity (Bear, 1972), but failed to yield real-valued ellipsoids. Numerous attempts were made to try to clarify this negative result, but without any success. All the other planned tests were therefore abandoned.

One property of the aquifer not considered when the cross-borehole packer tests were abandoned, is the geometry of the aquifer, because it was not considered important at the time. However, as shown in Figure 6–3, Borehole UO5 is situated closer to the boundary of the Mode I fracture than all the observation boreholes, except Borehole UO4. The failure of the cross-borehole tests may therefore have been caused by the proximity of the fracture boundary to Borehole UO5. This observation suggests that one can only expect positive results from cross-borehole packer tests if the spacing of the boreholes takes the geometry of the aquifer into account. Since there are no methods that allow one to determine the geometry of an aquifer explicitly, cross-borehole packer tests do not appear to be very useful in studies of highly heterogeneous aquifers.

6.3.4 Double-packer Tests

The failure of the cross-borehole tests meant that double-packer tests had to be used to get some idea of variations in the hydraulic parameters with depth. The cross-borehole tests were therefore followed by a series of double-packer tests. Although double-packer tests can be used to determine a layer's specific storativity, the transient part of the reaction dies out so quickly that only its hydraulic conductivity is usually determined (Hsieh *et al.*, 1983). It must be kept in mind though that this hydraulic conductivity, henceforth denoted by K_h , will only be representative of a horizontal segment through the sealed-off section.

There exists a number of equations that can be used to compute values of K_h , (Hsieh *et al.*, 1983), but the one most commonly used is given by

$$K_h = \frac{Q}{2\pi l \Delta h} \ln \frac{l}{r_b} \quad (6.3)$$

where l is the length of the sealed-off section, r_b the radius of the sealed-off section and the meanings of the other symbols are described above. This equation was consequently also used in this investigation. Averaged values of K_h for the more prominent formations on the Campus Test Site are summarized in Table 6–3, and are displayed graphically in Figure 6–7. These results further emphasize the dominant role that the Mode I fracture plays in the geohydrology of the aquifer on the Campus Test Site.

There are indications that Equation (6.3) may yield K_h -values that depend on the injection rate, Q . Unfortunately, this dependence cannot be investigated further here, as no provision was made for such a possibility in planning the present set of tests.

Table 6–3 Averaged values of the horizontal hydraulic conductivities, K_h , for the more important formations on the Campus Test Site as determined from double-packer tests.

Layer	Depth (m)	K_h (m s^{-1})
Upper mudstone layers	8	$9,910 \cdot 10^{-7}$
	10	$6,538 \cdot 10^{-6}$
	12	$3,601 \cdot 10^{-6}$
Carbonaceous shale layer	14	$8,796 \cdot 10^{-7}$
	16	$1,350 \cdot 10^{-6}$
Sandstone matrix of the main aquifer	18	$4,055 \cdot 10^{-5}$
	20	$1,345 \cdot 10^{-4}$
Average depth of Mode I fracture	22	$2,754 \cdot 10^{-4}$
Sandstone matrix of the main aquifer	24	$7,878 \cdot 10^{-5}$
	26	$2,205 \cdot 10^{-6}$
Mudstone layers	28	$2,309 \cdot 10^{-7}$
	30	$7,970 \cdot 10^{-8}$
	32	$4,440 \cdot 10^{-8}$
	34	$1,234 \cdot 10^{-7}$
	36	$1,564 \cdot 10^{-7}$
	37	$2,497 \cdot 10^{-8}$
	38	$1,740 \cdot 10^{-8}$
	40	$4,652 \cdot 10^{-8}$
	42	$1,745 \cdot 10^{-8}$

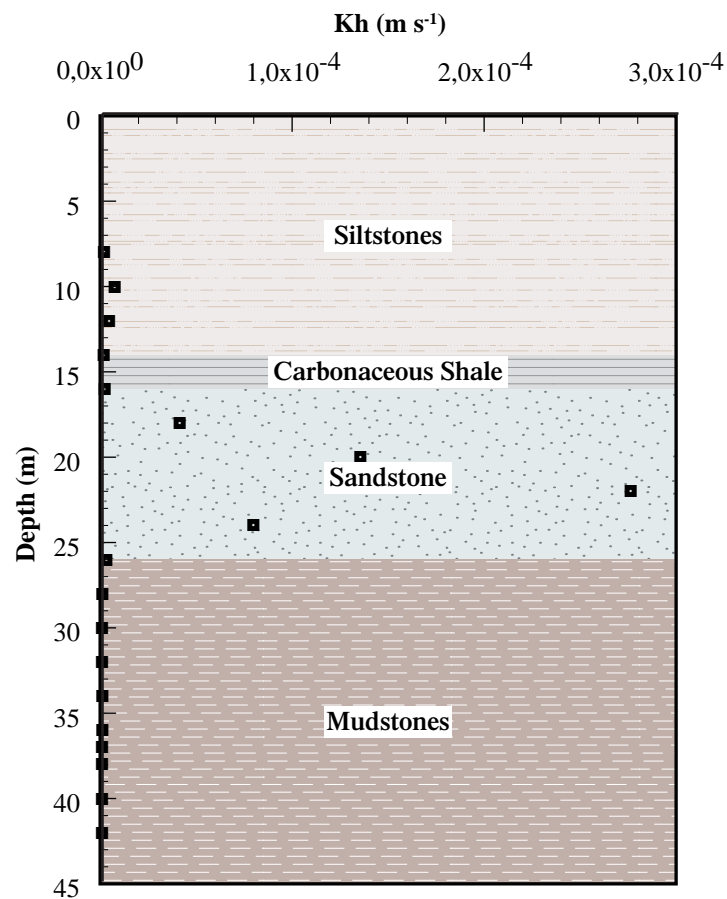


Figure 6–7 Graphs of the horizontal hydraulic conductivities in Table 6–3.

6.3.5 Other Constant Rate Tests

The results from the double-packer tests and the cores showed beyond any doubt that the aquifer on the Campus Test Site is a multi-porous, multi-layered aquifer, as envisaged in Chapter 5. It was thus considered worthwhile to carry out a new constant rate test on the aquifer after the installation of piezometers in boreholes UO1 and UO18, to try to obtain better insight into the behaviour of the aquifer.

Since the Department of Geohydrology planned to shift the pump in Borehole UP15 to Borehole UP16, a classical yield test was performed on the latter borehole at the end of 1993. This test showed that the borehole had a yield of approximately $18 \text{ m}^3 \text{ h}^{-1}$. In this test, the borehole was pumped at a discharge rate of $28,8 \text{ m}^3 \text{ h}^{-1}$, as indicated by blow tests carried out during drilling the borehole. However, the borehole was only able to support this rate for an hour, before the rate began to drop to $18 \text{ m}^3 \text{ h}^{-1}$, where it stabilized for six hours. The Department therefore installed a new pump with this capacity at a depth of 32 m (21 m below the water level) in the borehole. This borehole was consequently used as the perturbed borehole for the test to be described here.

Water levels were measured in the perturbed borehole, as well as boreholes UO2, UO3, UO6, UO9, UO10, UO11, UO13, UO14, UP15, UO20 and UO22, in the new test, while piezometric levels were measured in piezometers UO1, UO18, and temporary piezometers in Borehole UO5. (See the map in Figure 5–15 for the positions of the boreholes.) The latter piezometers were created by sealing Borehole UO5 off with an inflated packer, placed at the depth of the carbonaceous shale layer. The measurements in piezometers UO1, UO18 and Borehole UP16 were taken by hand, but the rest was registered electronically.

The test was started with a pumping rate of $11,88 \text{ m}^3 \text{ h}^{-1}$, well below the supposed yield of $18 \text{ m}^3 \text{ h}^{-1}$. However, the pumping rate immediately began to decline with the water-level in the borehole, as shown in Figure 6–8. The decline continued until the water level reached a depth of 21 m, where Borehole UP16 intersects the Mode I fracture, and then stabilized for approximately 75 minutes before resuming the decline. The high influx of water from the fracture unfortunately made it impossible to continue with the measurements in Borehole UP16 the moment when the water level reached the fracture.

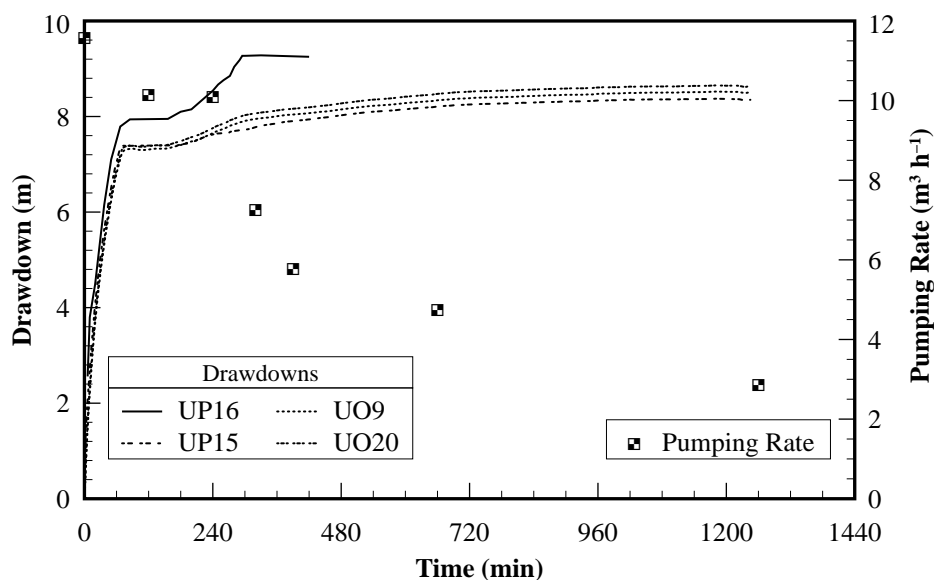


Figure 6–8 Pumping rates and drawdowns observed in boreholes UO9, UP15, UP16 and UO20 during the constant rate test on Borehole UP16 at the Campus Test Site.

The decline and stabilizing of water levels were also observed in the other Class 3 boreholes of Table 6–1, as illustrated by the drawdowns of boreholes UO9, UP15 and UO20 in Figure 6–8. Only in the Class 1 boreholes did the water levels decrease continuously throughout the test.

Since no description of a similar behaviour could be found in the available literature, the results were considered suspect and the test was ignored. However, when the same behaviour was also observed in later constant rate tests, it became clear that this may be an intrinsic property of boreholes in Karoo aquifers.

The first of these constant rate tests was performed on a proposed production borehole, D19, at Philippolis, towards the end of 1994. This borehole penetrates not just one, but three bedding-parallel fractures, at depths

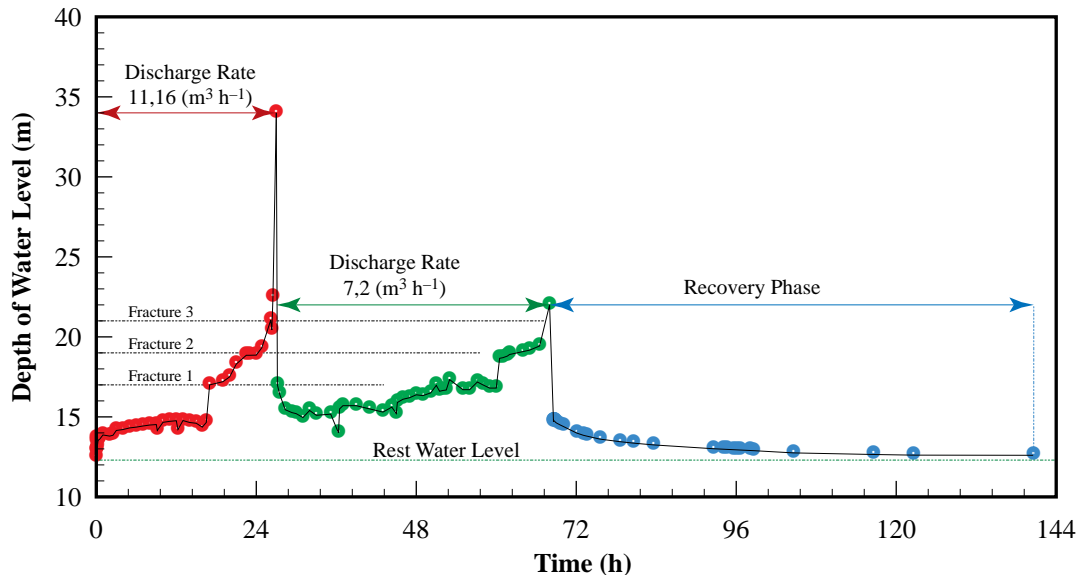


Figure 6-9 Graph of the water levels observed in Borehole D19 at Philippolis during a constant rate test carried out by Botha *et al.* (1996).

of 17, 19 and 21 m, respectively, as shown in Figure 6-9. The test started with a discharge rate of $11,16 \text{ m}^3 \text{ h}^{-1}$. This caused the water level to drop continuously for 576 minutes, and then to stabilize at a level 2 m above the first fracture for 420 minutes. The water level then dropped to a level 2 m above the second fracture at 19 m, where it stabilised for a further 144 minutes, before it dropped to a level 2 m above the third fracture at 21 m. Here, the water level stabilised again for 84 minutes, only to drop suddenly and without warning to the pump intake. At this stage, the discharge rate was lowered to $7,2 \text{ m}^3 \text{ h}^{-1}$. This caused the water level to recover within 168 minutes to a level 1,667 m above the fracture at 17 m, where it stabilized again for 816 minutes, only to repeat the previous cycle.

The similarity of drawdowns in Figures 6-8 and 6-9 immediately suggested that the drawdowns in Borehole UP16 would have shown the same behaviour had the measurements been taken for a longer time. A new constant rate test was therefore performed with Borehole UP16 as the perturbed borehole, after the field work at Philippolis was completed. In this test, the borehole was pumped at a rate of $3,6 \text{ m}^3 \text{ h}^{-1}$ for 2 800 min, while its water level and that of Borehole UO5 were measured electronically. Hand measurements of the piezometric levels in the three aquifers were also taken in Piezometer UO18 during the test. The test had to be abandoned earlier than planned because of a power failure, but were fortunately long enough to confirm the presumed behaviour of Borehole UP16, as shown in Figure 6-10. In this case, the water level also declined normally until it reached a depth of 19,6 m after approximately 12 h. Here, it stabilized for nearly 24 h before it began to decline again, first slowly and then rapidly, dropping almost instantaneously to the pump intake the moment it reached the Mode I fracture at a depth of 21 m.

A second constant rate test was performed on 1995-06-01 at the Campus Test Site. In this test Borehole UP15 was pumped, while the water levels in two other high-yielding boreholes, UO5 and UO20, and the low-yielding Borehole UO11 were monitored continuously. The test was started with a discharge rate of $9,72 \text{ m}^3 \text{ h}^{-1}$ and reduced to $3,6 \text{ m}^3 \text{ h}^{-1}$ after 140 min, before the pump was switched off 40 min later.

The comparison of the water levels in Figure 6-11 shows that the levels in boreholes UP15, UO5 and UO20 declined normally, until the level in Borehole UP15 reached a depth of ~2,5 m above the fracture after approximately 80 minutes of pumping. The level then stabilized for approximately 10 minutes, before it declined rapidly and dropped almost instantaneously to the pump intake the moment it reached the fracture. The discharge rate was then reduced to $3,6 \text{ m}^3 \text{ h}^{-1}$. This caused the level to recover rapidly to a depth of 6 m below the fracture, where it stabilized until the pump was switched off. The level then recovered quickly to a depth of approximately 2 m above the fracture, before continuing with its normal recovery.

An interesting feature of Figure 6-11 is that the water levels in boreholes UO5 and UO20, which also intersect the fracture, behaved very similarly, except for a slight difference in drawdowns that can be ascribed to the 0,7 m difference in their distances from Borehole UP15. Their water levels also dropped at the beginning, but then stabilized *at a position above the fracture for the duration of the pumping*. The observed behaviour of the water levels in the perturbed borehole is thus a characteristic of that borehole alone, and not

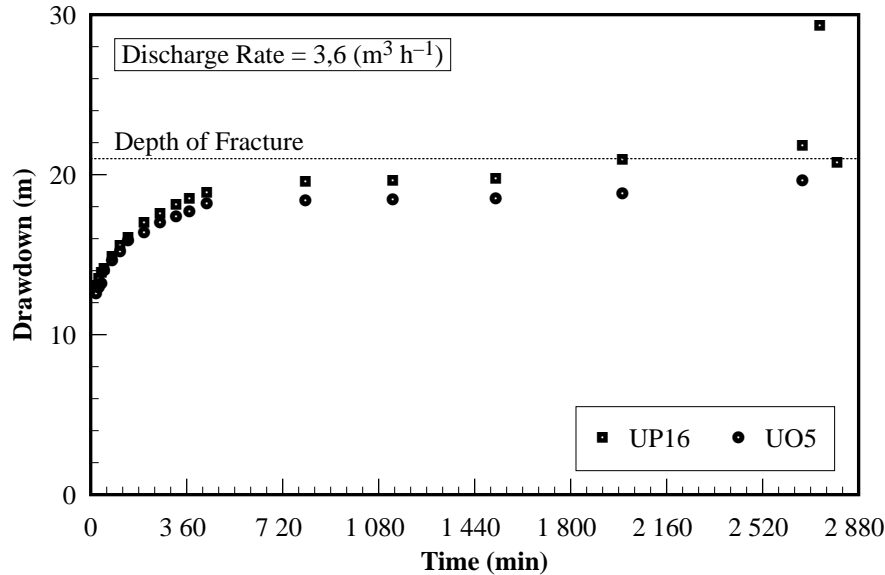


Figure 6-10 Graphs of the water levels in boreholes UP16 and UO5 during a constant rate test performed on 1995-05-15 with UP 16 as the perturbed borehole.

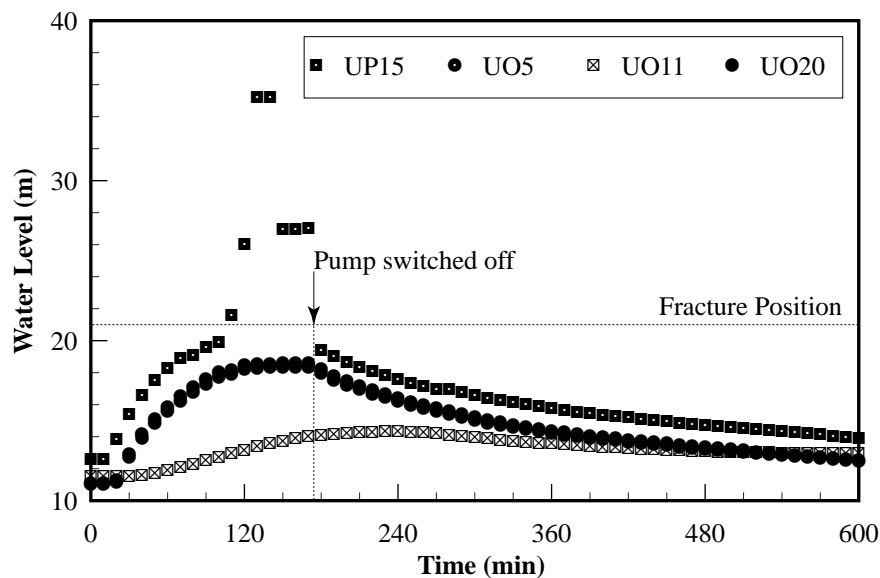


Figure 6-11 Graphs of the water levels in boreholes UO5, UO11, UP15 and UO20 during a constant rate test performed on 1995-06-01 with Borehole UP15 as the perturbed borehole.

of the aquifer as a whole.

The water level in Borehole UO11, on the other hand, remained constant for approximately 30 min before it began to decline, *and continued to decline for at least an hour after the pump was switched off*. The geological log of the borehole in Figure 5-16 shows that it intersects the sandstone layer that contains the Mode I fracture. However, the water level contours in Figure 6-3 indicate that the fracture is not present in the borehole, or is closed. Boreholes in Karoo aquifers thus not only withdraw water from fractures, but also from the Karoo rocks themselves. The commonly held view, that Karoo formations do not contain significant quantities of groundwater, is thus wrong.

There are two noteworthy differences between the water levels of the perturbed boreholes in Figures 6-10 and 6-11: the lengths of their stability phases and the depths at which their water levels stabilized. Since the tests differ only in their discharge rates, it is natural to assume that the differences were caused by the difference in the discharge rates. That this is the case, is illustrated by the drawdowns observed during the fourth step of a step drawdown test and a constant rate test on Borehole D20 at Philippolis by Botha *et al.*

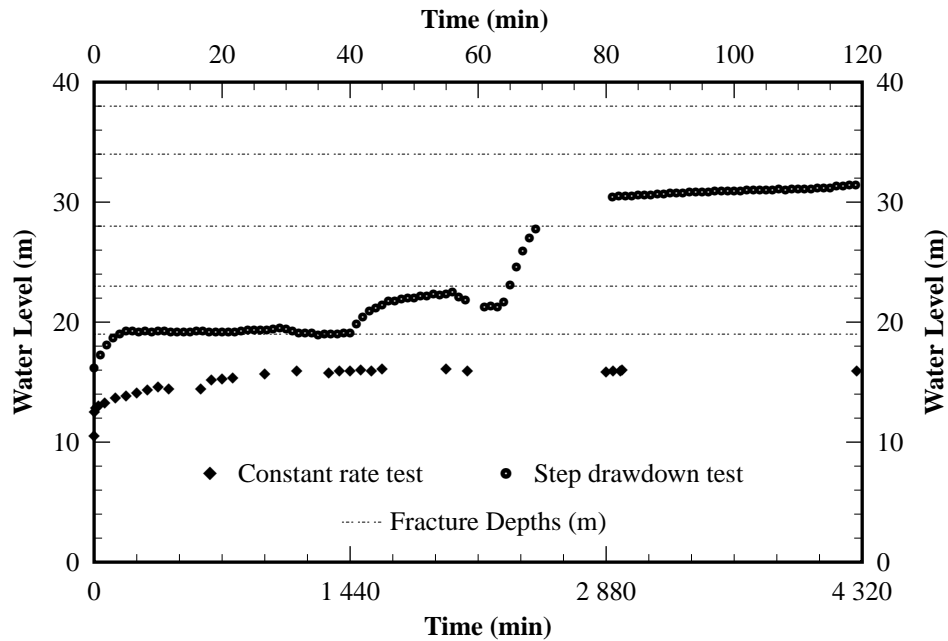


Figure 6-12 Behaviour of the water levels in Borehole D20 at Philippolis during a constant rate test and the fourth step of a step drawdown test. (The step drawdown test's time scale is shown on the upper time axis.)

(1996). In the step drawdown test, the borehole was pumped at a rate of $10,8 \text{ m}^3 \text{ h}^{-1}$ and in the constant rate test at $6,84 \text{ m}^3 \text{ h}^{-1}$.

The water level stabilized in the step drawdown test for 35 min at a depth 4 m above the second fracture, before it dropped to a depth of 5 m above the third fracture and then to a depth of 3 m above the fourth fracture, where it stabilized for the remaining 40 min of the test. (Stabilization above the first fracture occurred during the third step of the test.) However, as shown in Figure 6-12, the water level stabilized after 12 h 3 m above the first fracture and remained there for the remaining 60 h of the test. *This result suggests that there exists an upper limit on the efficiency rate at which a Karoo borehole can be pumped, if one does not want to lower its water level below the depth of a water-bearing fracture.* Bedding-parallel fractures, therefore, act not only as conduits for water to boreholes in Karoo aquifers, *but also control the behaviour of the boreholes.*

The previous behaviour of the water levels is not restricted to the aquifers on the Campus Test Site and Philippolis, but is also present in the drawdowns of constant rate tests *Kirchner et al.* (1991) performed at Dewetsdorp and De Aar. Unfortunately, their graphs are all drawn on a log-log scale, thereby masking the various effects, but the effects are clearly visible in the graphs on pages 87, 181 and 186, of the appendix volume, and the long duration test, in their Figure 4.41 on page 88. *There is thus little doubt that the yields of boreholes in Karoo aquifers are controlled by the bedding-parallel fractures they intersect.* The difficulties *Kirchner et al.* (1991) experienced in interpreting their test results can thus be ascribed to two causes. The first is that they analysed their results with a Theis curve, and the second is that they ignored the control fractures exert on the yields of boreholes in Karoo aquifers.

6.4 FRACTURED-CONTROLLED BEHAVIOUR OF KAROO BOREHOLES

6.4.1 Fracture Hydraulics

The previous results raise the question: how can one explain groundwater flow in Karoo aquifers, especially what seems to be the *fracture-controlled* behaviour of perturbed boreholes? One conclusion already reached, is that the major flow in Karoo aquifers must occur from the rock matrix to the fracture, which then supplies the borehole with water. However, Equation (6.2) shows that the flux through a fracture will be limited by its aperture and the piezometric pressure gradient across the fracture, which is determined completely by the piezometric pressure within the fracture. A highly permeable fracture will thus quickly dewater when exposed to the atmosphere, *unless recharged through its planes.* This recharge rate will, in turn, depend on the rate at which water can leak from the surrounding rock matrix to the fracture. The continuous leakage of

water to the fracture must obviously decrease the piezometric pressure in the rock matrix, and thus the piezometric gradient towards the fracture. The rate at which the rock matrix can supply water to the fracture must therefore also continue to drop, according to Darcy's law in Equation (6.1), unless leakage occurs from adjacent aquifers, thereby also decreasing their piezometric levels. *A fracture, therefore, cannot sustain the discharge rate from a borehole that exceeds the rate at which the surrounding layers can recharge it. A point will therefore be reached in such a borehole where its water level will begin to drop. There is thus a limit to the rate at which the rock-fracture system can supply water to a borehole.*

The predicted drop in the water level of a borehole may be stopped temporarily, if there exists a second fracture whose aperture is large enough, and the piezometric pressures in the layers immediately above and below are high enough to supply in the demand. This conjecture is supported by the behaviour of the piezometric levels, of the three aquifers on the Campus Test Site, during the constant rate of 1995-05-15 on Borehole UP16. As shown in Figure 6-13, Aquifer 2 entered a pseudo steady state after 12 h of pumping; the same time it took the water level in Borehole UP16 to stabilize, according to Figure 6-10. The piezometric level in Aquifer 1 continued to decline throughout the test, while that in Aquifer 3 also stabilized after a small but rapid decrease at the beginning, probably caused by the slight difference in its initial piezometric level and that of Aquifer 2.

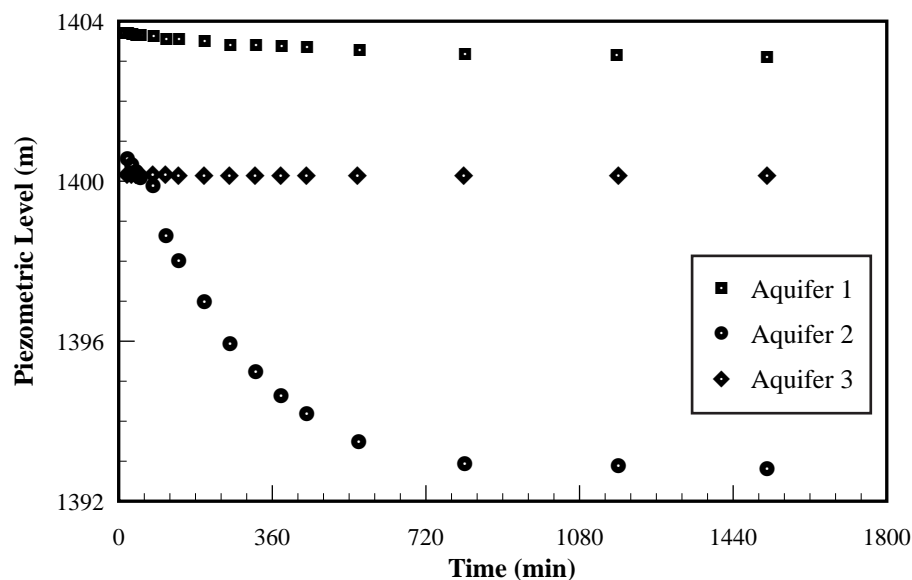


Figure 6-13 Graphs of the piezometric heads in the three aquifers on the Campus Test Site, as measured in Piezometer UO18 during the constant rate test of 1995-05-15 on Borehole UP16.

The previous discussion suggests that there may be fractures in a borehole that are not able to retard or stop a declining water level. The behaviour of the water levels for the step drawdown test in Figure 6-12 indicates that the third fracture in Borehole D20 may be such a fracture. This behaviour is illustrated even more dramatically by the drawdowns of a constant rate test on a borehole at Kokstad in Figure 6-14. Although the water level in this borehole did not experience any sharp drop, the stabilizing patterns are clearly visible, but less developed than those in Figures 6-10 and 6-11.

An interesting consequence of the previous interpretation of flow in Karoo aquifers is that the fracture-controlled behaviour of production boreholes will not be observed in a single-layered aquifer. However, such an aquifer may be very rare in Karoo formations, judging from the discussion of their general structure and the geology in Chapters 3 and 5 respectively.

A more common explanation for the fracture-controlled behaviour of water levels in perturbed boreholes would be that the drawdown reached an impermeable boundary during the test. This boundary can be either a dolerite dyke or the fracture boundary itself. There is a dolerite dyke not far from boreholes D19 and D20 at Philippolis (Botha *et al.*, 1996), but none at the Campus Test Site. That the phenomenon also occurs in boreholes on the Campus Test Site, thus rules dolerite dykes out as the cause of the phenomenon. The fracture boundary can also not be responsible for the phenomenon, for one would then expect to see it in the water levels of all boreholes connected to the fracture, which is clearly not the case with the water levels of boreholes UO5 and UO20 in Figure 6-11. The phenomenon is thus a characteristic of the perturbed borehole, *unrelated to boundary effects.*

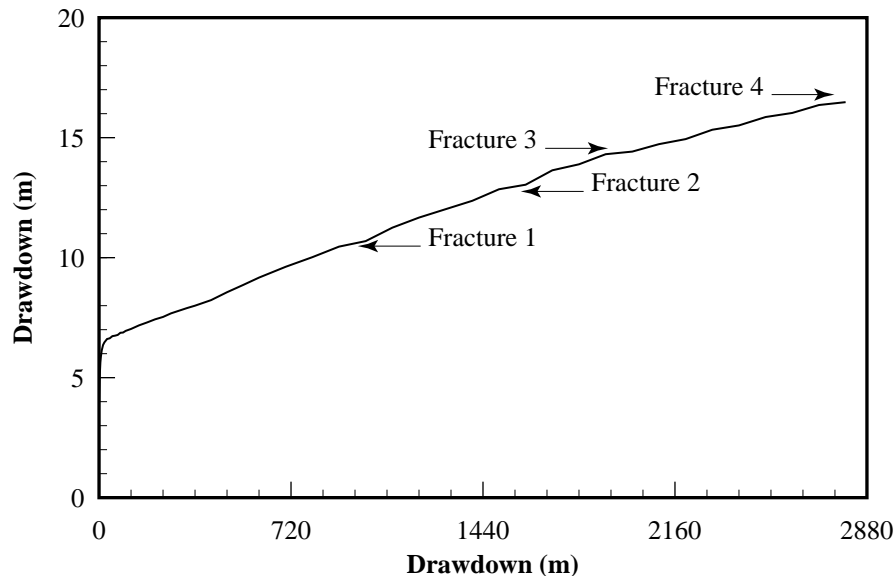


Figure 6-14 Drawdowns observed during a constant rate test on a high-yielding borehole at Kokstad. ($Q = 46,8 \text{ m}^3 \text{ h}^{-1}$.)

6.4.2 Fracture Mechanics

The water-bearing fractures intersected by boreholes drilled during this project were all bedding-parallel fractures. The possibility therefore exists that the fractures may be readily deformed, either elastically or plastically. Such a deformation, even if limited, can influence the flow through the fracture dramatically, as can be seen from Equation (6.2). For example, a decrease of 20% in the aperture of the fracture will cause a decrease of almost 50% in its yield. Any deformation of this nature will be disastrous for production boreholes that depend on fractures for their water supply.

There are a number of forces that may deform the water-bearing, bedding-parallel fractures in Karoo aquifers. The first, and most obvious one, is the weight of the overburden. The effect of this force can be considerably enhanced in a fracture dewatered by excessive pumping. Indeed, there is a possibility that such a fracture may even collapse completely. This collapse of a water-bearing fracture may be responsible for the complaint: '*my borehole has dried up*', often heard from people who depend on Karoo aquifers for their water supply. This interpretation has the advantage that it provides a natural explanation why it is often possible to drill a new successful borehole within a short distance from the one that '*dried up*'.

Another phenomenon that can be related to the '*dried up*' borehole and deformation of a water-bearing fracture, is a borehole whose yield decreases with time. The phenomenon has never been discussed in the literature to the knowledge of the authors, but discussions with farmers indicated that it is quite common in boreholes older than 10 years.

The two phenomena discussed above can also be caused by other factors, and can therefore not be considered as proof that deformations take place in Karoo aquifers. The only direct information that such deformations do occur, comes from the acoustic scanner image of Borehole UO5 in Figure 5-28(b). Of particular interest is the 'fracture' zone at a depth of 23,8 m and the subvertical fracture between 22,5 and 22,9 m, that was not present in the original calliper trace and a dip meter survey of the borehole by BPB on 1993-12-01. The features, therefore, must have developed after December 1993, as discussed in Section 5.4.4, and probably after 1994, if the decreasing transmissivities in Table 6-4 can be ascribed to the deformation. Nonetheless, there can be little doubt that Karoo aquifers are subject to deformations.

Table 6-4 Transmissivities of Borehole UO5 on the Campus Test Site, derived from student slug tests.

Year	T ($\text{m}^2 \text{ d}^{-1}$)
1991	33,0
1994	28,5
1996	8,0

Another indication that elastic deformation may play a prominent role in the behaviour of Karoo aquifers comes from the behaviour of the water level in Borehole UO11, during the constant rate test on Borehole UP15 in Figure 6–11. As pointed out above, it took the water level in this borehole about 30 min to decline, and approximately an hour to recover after the pump in Borehole UP15 was switched off. One mechanism that can explain this behaviour is that the fracture contracted in the immediate vicinity of the borehole, when the pumping started, thereby creating a pressure pulse that increased the water pressure in the adjacent formations. Since Borehole UO11 does not penetrate the fracture, according to Figure 6–3, it took some time before this increase in pressure dissipated. Exactly the opposite happened when the pump was switched off. The fracture then expanded with a corresponding drop in its piezometric pressure that had to be restored before the rock matrix could be recharged. Deformation of the fracture may thus be another cause of the fracture-controlled behaviour of water levels in perturbed boreholes, discussed above.

Dewatering and rewatering are not the only phenomena that can affect the aperture of a fracture. It is known that fractures are often kept open by asperities associated with the fracture walls, sand grains or other particles. The Mode I fracture in Figure 5–26, for example, was filled with mud, silt and fine-grained particles at the time the drill cores were recovered. The flow velocities in bedding-parallel fractures can be very high, judging from the force with which water enters a borehole when such a fracture is struck. The water could thus easily remove particles from the fracture, thereby causing the fracture to collapse, or clog the pump. Friction between the fracture surface and water could also change the flow from laminar to turbulent, thereby reducing the flux through the fracture substantially (Gilbrech, 1966).

It is difficult to say at this stage which of the previous phenomena, if any, play a significant role in the behaviour of Karoo aquifers, because they have not been considered in previous investigations of Karoo aquifers. There is thus no quantitative information available on how these phenomena may influence the yields of boreholes in general, and Karoo boreholes in particular.

6.5 DOLERITE DYKES

The preceding discussion may create the idea that bedding-parallel fractures are the most important structures in Karoo aquifers. Although this is certainly true as far as the behaviour of flow towards a borehole is concerned, the global behaviour of a Karoo aquifer is more likely controlled by dolerite dykes, as discussed in Chapter 4. One cannot therefore neglect the influence of dolerite dykes on the global behaviour of a Karoo aquifer, particularly not in the development of water-supply schemes.

The impression is often created that more boreholes have been drilled along dolerite dykes than anywhere else in the Karoo landscape, although such a conclusion is not supported by the hydrocensus of Burger *et al.* (1981). The two main reasons for this conception are probably that dykes are: (a) easy to locate with existing geophysical techniques, and (b) often surrounded by highly fractured zones. This approach is understandable, because there are no methods known today that can detect bedding-parallel fractures *in situ*. However, the approach may not always yield an optimal borehole site, since the dykes, especially the ring dykes, are often impermeable, as discussed in Chapter 4. This not only confines the aquifers to isolated compartments (Burger *et al.*, 1981), but also restricts the area from which a borehole can withdraw its water considerably.

One method to increase the yield of such a limited aquifer is to drill a production borehole through the dyke dividing two aquifers, and tap the water of both aquifers simultaneously. However, this method is not always successful, as illustrated by the experience with the boreholes on Site 2 at Dewetsdorp, discussed in Section 5.6.3.

Another disadvantage of dolerite dykes, especially linear dolerite dykes, is that they may have destroyed bedding-plane fractures that existed at the time of their intrusion. Boreholes along linear dykes therefore withdraw their water mainly from the dyke's baked and fractured zone, as hydraulic tests at Philippolis have shown. These mostly vertically inclined fractures usually have a high density, and are orientated parallel and perpendicular to the dyke. Boreholes drilled along the same dyke therefore often interfere with one another, even when spaced as far as six kilometres apart! The yields of boreholes drilled next to dolerite dykes, are thus often highly variable.

6.6 HYDROCHEMICAL ACTION

Hydrochemical action is another factor that may influence the hydraulics of Karoo aquifer, in general, and fracture flow in particular. The motion of groundwater through the original palæo-sediments caused the individual grains to cement during lithification, while the motion of recent groundwater tends to dissolve the

cement, especially near fractures. The latter of these processes depends strongly on the chemistry of the groundwater. If the water is saturated with carbonate precipitation may take place, which can seal the fractures, while oxygen-rich water may oxidize iron minerals that diffuse into the matrix and colour the sedimentary rocks. The brown colour of the sandstone around the water-yielding fracture in Figure 5–24, is an example of the latter process.

It is known that the solubility of CaCO_3 depends strongly on the partial pressure of the dissolved CO_2 . A drop in this pressure will cause calcite to precipitate. Since the pressure in the rock matrix is usually higher than in the fractures, the fractures in Karoo aquifers are very much vulnerable to calcite precipitation, especially when pumping an aquifer. Since this may lead to the formation of a so-called fracture skin and a considerable reduction of flow from the rock matrix to the fracture (Moench, 1984), such situations must be avoided as far as possible. This phenomenon may explain why many fractures in the core samples from both the Campus Test Site and Dewetsdorp, are totally closed by calcite.

6.7 ANALYTICAL MODELS FOR KAROO AQUIFERS

The discussion in Section 5.5.5 shows that Karoo boreholes receive their water mainly from bedding-parallel fractures. Since the storage capacity of these fractures is limited, they will be unable to supply water to a high-yielding borehole, unless recharged from the surrounding rock matrix. The permeability of the rock matrix is very low, however, and will not release water easily, unless there exists a high piezometric pressure gradient. This will certainly be the case if there is a sudden drop in the piezometric pressure of an adjacent bedding-plane fracture. Since these fractures are mainly horizontally inclined, the flow *will be predominantly vertical*. No conceptual model based on horizontal flow, will therefore be able to fit drawdown data from these aquifers accurately.

A major problem with vertical flow is that it can only be described by complex mathematical models, with the result that geohydrologists neglect them completely, as was done in the discussion of the multiple constant rate tests in Section 6.3.2. It was therefore thought worthwhile to conclude this discussion on the behaviour of Karoo aquifers, with an explicit demonstration of the difference between an analytical horizontal flow model, represented by the well-known Cooper-Jacob method, and a more realistic analytical model. The Cooper-Jacob method is an approximation of the Theis model and therefore strictly only valid for drawdowns in observation boreholes. However, the method is often applied to perturbed boreholes, with the assumption that the observed water level is measured at its circumference.

The basic premise of the Cooper-Jacob method is that the drawdown, s , in a borehole at some ‘late time’, t , can be described by an equation of the form

$$s = a + b \ln(t) \quad (6.4)$$

Since this equation is linear in $\ln(t)$, one only needs two data points to determine its intercept, a , and slope, b . It is thus possible to fit the equation to any set of data points where two or more points lie in a straight line on a semi-logarithmic graph of the points. One result of this simplicity is that the Cooper-Jacob method is the first method many geohydrologists turn to when faced with the problem of analysing the results from a constant rate test. However, the equation has an added connotation in geohydrology, not often appreciated by users. As any textbook on well-hydraulics, e.g. Bear (1979), will show, the Theis equation describes the drawdown in a homogeneous, horizontal aquifer with a *radial flow* pattern. The same therefore applies to Equation (6.4). Since it is not easy to transform other types of equations into the form of Equation (6.4), one can be sure that the flow is radial and horizontal if the equation fits a ‘large’ number of points from a hydraulic test.

Unfortunately, no simple analytical model could be found for vertically saturated flow in the literature. The best known example of vertical flow in groundwater is probably unsaturated flow, which exhibits a *linear* flow pattern. Dr. Paul Hsieh therefore suggested that one may consider linear saturated flow instead. This type of flow must satisfy an equation of the form

$$s = \alpha + \beta \sqrt{t} \quad (6.5)$$

according to Milne-Home (1988). Since it is impossible for a large set of data points to satisfy Equations (6.4) and (6.5) simultaneously, the two equations can be used to decide whether the flow in Karoo aquifers is radial or linear. Although numerous examples of such fits can be given, the example in Figure 6–15 will suffice for this discussion. These data were supplied to the authors by Alan Woodford, from the Office of the Department of Water Affairs and Forestry in Cape Town. In this test, Borehole G39973 at Calvinia was

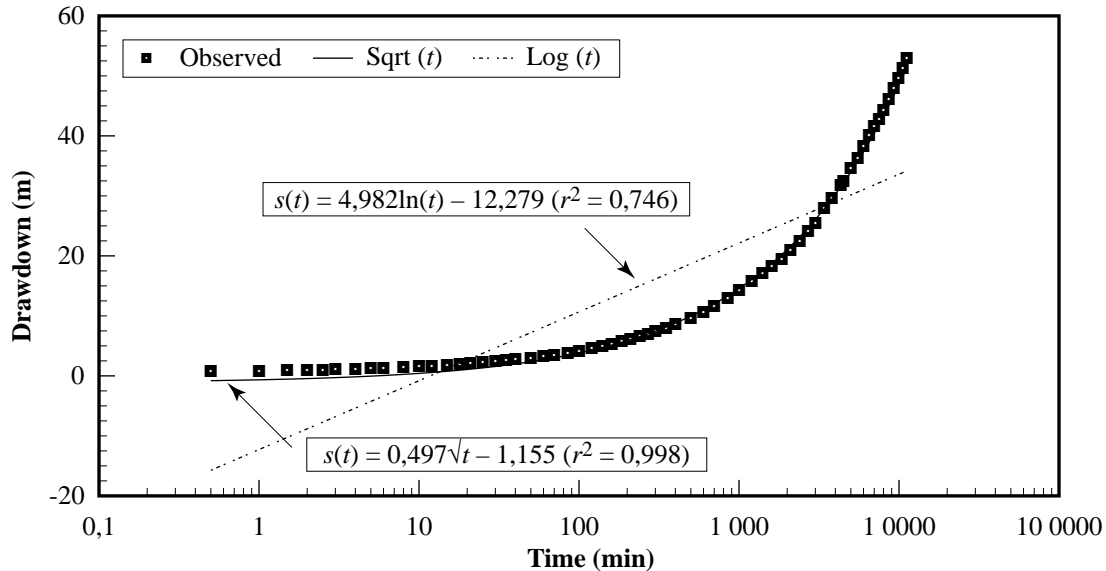


Figure 6-15 Least square fits of Equations (6.4) and (6.5) to the drawdowns observed in Borehole G39973 at Calvinia.

pumped for 11 200 min at a rate of $87,84 \text{ m}^3 \text{ h}^{-1}$, which is an extremely high-yielding borehole for Karoo standards.

It is, of course, possible to obtain a better fit of the data in Figure 6-15 to Equation (6.4), by varying the number of points considered in the fit. However, there is no way in which Equation (6.4) can fit *all the data* as perfectly as Equation (6.5). Flow in Karoo aquifers is therefore predominantly *linear and not radial*. Hydraulic parameters derived from the Theis model, or any other model that is based on radial flow, will thus be *useless* in the case of Karoo aquifers, as Kirchner *et al.* (1991) experienced. This constraint effectively restricts the number of analytical models that can be used in the study of Karoo aquifers to the horizontal fracture model of Gringarten and Ramey (1974). This quite complex analytical model was unfortunately discovered only recently, with the result that it could not be analysed in detail for this report.

The association of the vertical flow field with bedding-parallel fractures implies that this type of flow only exists when the fracture is stressed. Flow in undisturbed Karoo aquifers may thus still be mainly horizontal. Unfortunately, there is no method that allows one to determine hydraulic parameters for an undisturbed aquifer.

6.8 DISCUSSION

The main conclusion that can be drawn from the previous discussion is that the behaviour of Karoo aquifers is ultimately determined by their unusual geometry, particularly the occurrence of bedding-parallel fractures. These features provide not only the conduits for water to boreholes in Karoo aquifers, but also play a prominent role in the interactions responsible for the behaviour of these aquifers. One very important consequence of these interactions is that flow in Karoo aquifers is not radial and horizontal, but linear and vertical. This property differs so much from that of the media usually considered in the literature on aquifer mechanics, that the existing conceptual models are useless for the analysis of hydraulic tests performed on Karoo aquifers. Indeed, a survey of the conceptual models has shown that the horizontal fracture model of Gringarten and Ramey (1974) may be the only analytical model that can be applied to Karoo aquifers. However, the mathematics of the model is rather complex. It is thus doubtful if it will require less effort to implement than the numerical models that will be discussed in the following chapters.

An interesting feature of Gringarten and Ramey's horizontal fracture model is that the water level in a borehole will display four distinct stages, whose lengths are determined by the radius of the fracture. The model further predicts that the second phase, during which the water level behaves as a function of \sqrt{t} , becomes more dominant as the radius of the fracture increases. The near perfect fit of Equation (6.5) to the observed water levels of Borehole G39973 at Calvinia, in Figure 6-15, therefore suggests that this borehole withdraws its water from a very extensive fracture—a conclusion supported by its very high yield.

Another rather disturbing result that emerged from the previous discussion is that Karoo formations,

and thus aquifers, may readily be deformed by pumping water from them. This will not only affect the ability of these aquifers to store and yield water, but can also have considerable impact on mass transport in the aquifers. *Unfortunately very little is known about these deformations at the moment. It is thus imperative that more attention should be given to this aspect, if the aquifers are to be used for water-supply schemes and protected from pollution.*

Boreholes are, without any doubt, the most cost-effective method to withdraw water from an aquifer. The dependence of a borehole's yield on the presence and properties of a fracture, however, again raises the question if boreholes are the best method with which to withdraw water from Karoo aquifers. Although some of the effects can be limited by pumping and spacing the boreholes judiciously, the conclusion in Section 3.6.5, that it will be better to withdraw water from aquifers in the Clarens Formation by methods other than boreholes, thus seems to apply to all Karoo aquifers.



CHAPTER 7

A NUMERICAL MODEL FOR THE CAMPUS TEST SITE

7.1 INTRODUCTION

The absence of any reference to the fractured-controlled behaviour of boreholes in the available literature makes it difficult to quantify the influence that the physical properties of the aquifer have on the phenomenon. The first and best approach to achieve this goal would have been to study the phenomenon in more detail through further field observations and measurements. However, the lack of suitable equipment and financial resources made this approach impossible. Fortunately, there is another approach. The discussion in Chapters 3, 4 and 5 shows that the physical properties of Karoo aquifers will not vary much globally, although there may be large local variations. The behaviour of the aquifers can thus also be studied with a suitable numerical model. This approach has the added advantage that it can show directly which physical properties of the aquifer play an important part in the phenomenon, thereby avoiding unnecessary field work. These considerations led to the development of a numerical model for the aquifer on the Campus Test Site.

The discussion in Chapter 2 shows that the first and major step in developing a numerical model for any physical phenomenon is to decide which physical properties of the medium and phenomenon must be included in the underlying conceptual model. As shown by the discussions in Chapters 5 and 6, there is one property that cannot be neglected in developing such a model for a Karoo aquifer—that is its geometry. The implementation of this property in the model for the aquifer on the Campus Test Site is discussed in Section 7.2.

Karoo formations are best conceptualized as multi-layered, multi-porous media, according to the discussion in Chapter 5. This implies that the well-known saturated flow equation can be used as the mathematical model for the aquifer. This model, its associated initial and boundary conditions and hydraulic parameters are discussed in Section 7.3.

Boreholes are commonly represented in numerical models for two-dimensional groundwater flow as a point source (Pinder and Gray, 1977), thereby creating a logarithmic singularity in the solution. This causes a severe difficulty for three-dimensional groundwater flow models. An elegant method to circumvent the difficulty is to represent the borehole as a Dirichlet boundary. This method was consequently introduced in the numerical model, as discussed in Section 7.4.

7.2 GEOMETRY OF THE AQUIFER

7.2.1 Spatial Geometry

The discussion in Chapter 5 has shown that the aquifer on the Campus Test Site is essentially a three-layered aquifer. Since the carbonaceous shale layer is relatively impermeable, it was thought that Aquifer 1 will not influence flow in Aquifer 2. Although there does not exist a similar clearly defined geological boundary between Aquifers 2 and 3, the horizontal hydraulic conductivities of the aquifer in Table 6-3 suggested that this aquifer may also be neglected in the proposed model. The original idea was therefore to restrict the model to Aquifer 2, or develop a separate model for each of the three aquifers. However, the piezometric levels in Figure 6-13 show that all three aquifers respond simultaneously. Any model for the site therefore had to include all three aquifers. An attempt was made to obtain more information on the interaction between the three aquifers from the hydraulic test data, which could be used in a layered model for the Site, but the available data were not sufficient for this purpose. This left only two options for the development of a suitable model. The first was to use a two-dimensional model along a vertical plane through the three aquifers, and the second a full three-dimensional model. The easiest option would have been to use the two-dimensional vertical model, were it not that such an approach could hide important features in the behaviour of this anisotropic Karoo aquifer. A full three-dimensional model was therefore used in this investigation.

There are numerous difficulties associated with the use of a three-dimensional groundwater flow model (Verwey and Botha, 1992). The most difficult decision to take in developing the present model, was decide

how to represent the three aquifers in the model. The reason for this is that Aquifer 1 is probably a phreatic aquifer, while Aquifers 2 and 3 are confined aquifers, as shown by the data in Table 7–1. The correct approach to model the aquifer would thus be to use an unsaturated-saturated flow model. However, this would complicate the model considerably, without necessarily providing more insight into the physical behaviour of the aquifer. Moreover, there was no information available on the moisture retention curves for the various formations, as required by an unsaturated flow model (Verwey and Botha, 1992). All three aquifers were therefore represented as confined aquifers in the present model. The model may therefore not represent the aquifer perfectly, but this was not the main purpose in developing the model. What was required of the model is that it should provide insight into the behaviour of Karoo aquifers, and guide-lines to what other effects must be included in a more comprehensive model.

The assumption that all three aquifers are confined, had one simplifying consequence—one can take the soil surface as the top of the aquifer. The bottom of the aquifer, however, was more difficult to determine. The geological profile of the deepest percussion borehole (UO14), and the cores from Borehole CH7, indicate that the mudstone layers of Aquifer 3 are present to a depth of at least 100 m. The available computer resources could, unfortunately, not accommodate a model that incorporates layers this deep. The piezometric levels in Figure 6–13, however, show that Aquifer 3 has such a high storage capacity that most of the flow will probably be restricted to its upper layers. The lower boundary was consequently placed at a depth of 40 m below the collar height of Borehole UO18.

Table 7–1 Comparison of the collar height and elevations of the sandstone and mudstone layers of Aquifer 3 with the piezometric heads in piezometers UO1 and UO18, as measured on 1995–05–15.

Piezometer	Elevation (mamsl)			Piezometric Levels (mamsl)		
	Collar	Sandstone	Mudstone	Aquifer 1	Aquifer 2	Aquifer 3
UO1	1 411,07	1 394,77		1 403,91	1 399,70	
UO18	1 410,97	1 394,97	1 387,970	1 403,72	1 400,42	1 400,07

The two most prominent features of the aquifer are the Mode I fracture at a depth of 21–25 m and the carbonaceous shale layer at a depth of 14–18 m. Since all indications are that the fracture is the hydrological most active feature of the aquifer, special care was taken to represent it as accurately as possible in the model. The carbonaceous shale layer, however, was grouped with the upper mudstone layers of Aquifer 1, because its hydraulic and geological properties do not differ too much from those of the other layers as illustrated in Figure 7–1.

7.2.2 The Void Geometry

The void geometry considered in most groundwater flow models can be related to three types of media: the classical porous medium (Bear, 1972), the dual porosity medium (Moench, 1984) and the fully fractured medium (Caças *et al.*, 1990). This presented somewhat of a problem for the aquifer on the Campus Test Site, since its void geometry does not correspond fully with one of these media. A special void geometry had therefore to be constructed for the Campus Test Site.

The discussion of Karoo formations in Chapter 3 shows that these formations can be represented as porous media with different porosities and hydraulic parameters. The real difficulty was thus how to represent the fracture. The correct approach would probably be to model flow in the fracture as pipe or parallel plate flow, but this would introduce internal boundary conditions, which would complicate the model considerably. However, an examination of the fracture in the core samples (see for example Figures 4–9 and 5–24) indicated that the fracture is not fully open, but partially filled with silt, mud and fine-grained sand particles. The fracture will therefore also be considered as a porous medium, but with its own porosity and hydraulic properties in this preliminary model for a Karoo aquifer.

7.3 THE MATHEMATICAL MODEL

7.3.1 The Saturated Flow Equation

The assumptions that the fracture can be represented as a porous medium, and that Aquifer 1 is a confined aquifer, imply that the aquifers on the Campus Test Site can be modelled with the saturated flow equation for

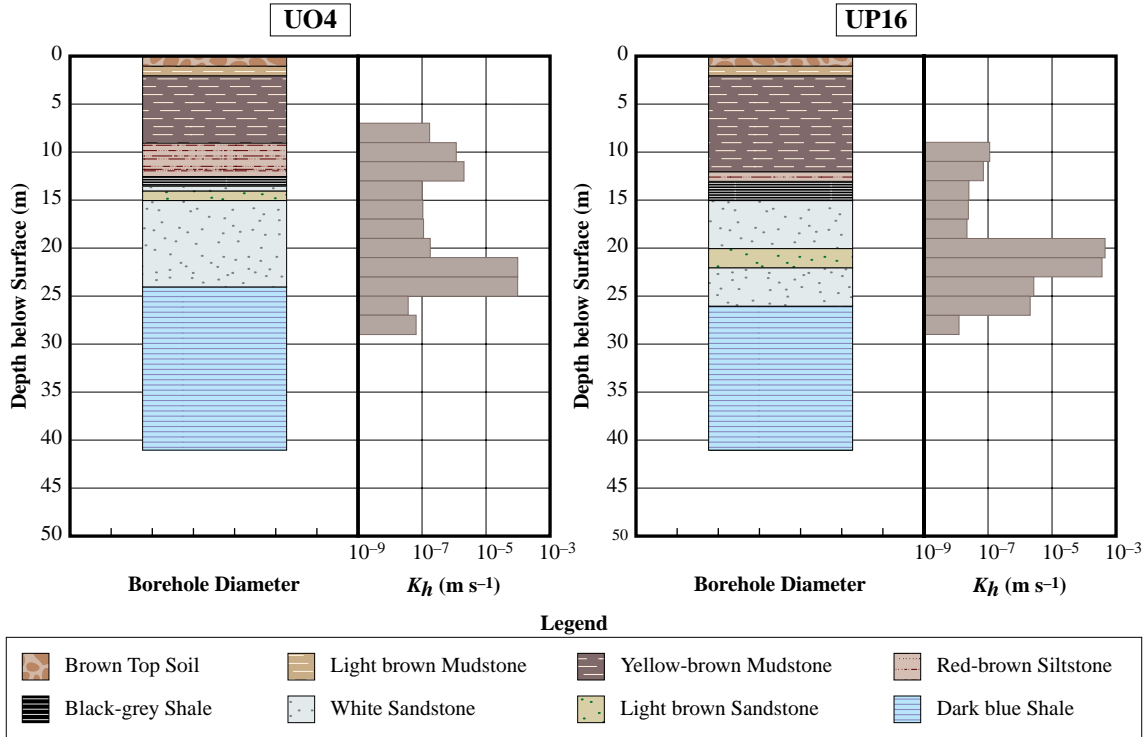


Figure 7-1 Comparison of the hydraulic and geological properties of the upper rhythmite layers in boreholes UO4 and UP16 on the Campus Test Site.

a porous medium. Since the aquifer is not polluted, one can restrict the model to the density-independent groundwater flow equation (Bear, 1979)

$$S_0 D_t \varphi(\mathbf{x}, t) = \nabla \cdot \mathbf{K}(\mathbf{x}, t) \nabla \varphi(\mathbf{x}, t) + f(\mathbf{x}, t) \quad (7.1)$$

where

- S_0 = the specific storativity of the aquifer,
- $\mathbf{K}(\mathbf{x}, t)$ = the hydraulic conductivity tensor of the aquifer,
- $f(\mathbf{x}, t)$ = the strength of any sources and sinks,
- \mathbf{x} = the three spatial co-ordinates (x, y, z),
- t = the time,
- $\varphi(\mathbf{x}, t)$ = the piezometric head in the aquifer, defined by (Bear, 1979) as

$$\varphi(\mathbf{x}, t) = z + \int_{p_0}^p \frac{dp}{\rho g} = z + h(\mathbf{x}, t)$$

with

- p = the water pressure,
- p_0 = the water pressure at a suitably chosen reference plane (z_0),
- ρ = the density of water,
- g = the acceleration of gravity,
- $h(\mathbf{x}, t)$ = the pressure head.

An important difference between Equation (7.1) and the equation conventionally used to describe the flow of groundwater in a horizontal plane (Botha, 1996)

$$S(x, y, t) D_t h(x, y, t) = \nabla \cdot [\mathbf{T}(x, y, t) \nabla h(x, y, t)] + Q(t) \delta(x - x_0) \delta(y - y_0) \quad (7.2)$$

is that Equation (7.1) contains the piezometric head as independent variable, while Equation (7.2) contains the pressure head. Equation (7.2) also uses the transmissivity tensor, \mathbf{T} , and storativity, S , instead of their three-dimensional counterparts, \mathbf{K} and S_0 , while the source term, expressed as the product of the discharge rate, $Q(t)$, and the Dirac delta functions, $\delta(x - x_0)$ and $\delta(y - y_0)$, is represented as a point source.

The piezometric head varies with depth, and can thus only be observed with piezometers. This is the main reason why a three-dimensional model requires (and generates) considerably more data than a two-dimensional model. A three-dimensional model thus places severe constraints on the computer resources and the observational network.

Equation (7.1) is a parabolic partial differential and can only be solved if a suitable initial condition and boundary conditions are prescribed (Botha and Pinder, 1983). Since these conditions determine the solution of Equation (7.1) completely, they must represent the conditions on the aquifer's boundary as accurately as possible. The choice of boundary and initial conditions has thus always been a difficult problem in constructing numerical models for aquifers. The methods used to establish suitable boundary conditions for the Campus Test Site will consequently be described in greater detail.

7.3.2 Initial Condition

The piezometric levels in the aquifers on the Campus Test Site were monitored with five piezometers, two installed in Borehole UO1 and three installed in Borehole UO18, at the time the numerical model was developed. Initial conditions for the model could therefore be derived from observations of the piezometric heads observed in these piezometers. The piezometric levels in Table 7–2 were specifically used as the initial conditions for the simulations discussed in Chapter 9.

Table 7–2 Piezometric heads of the three aquifers as measured on 1995–05–15 in piezometers UO1 and UO18.

	UO1 - 1	UO1 - 2	UO18 - 1	UO18 - 2	UO18 - 3
Aquifer	1	2	1	2	3
Piezometric Head (m)	1403,91	1399,70	1403,72	1400,42	1400,07

Since no method was available to measure the piezometric head in the fracture directly, it was assumed that its piezometric head is the same as that in Aquifer 2. The simulated piezometric heads for the fracture may thus not be fully representative of the fracture.

7.3.3 Boundary Conditions

The boundary conditions required for the solution of Equation (7.1) can be one of three types:

Dirichlet conditions where one prescribes suitable piezometric heads on the boundary.

Neumann conditions where one prescribes a flux across the boundary.

Mixed conditions where one prescribes a linear combination of Dirichlet and Neumann conditions on the boundary.

All the hydraulic tests performed thus far at the Campus Test Site had a negligible influence on the water levels of boreholes UO10, UO21 and UO22. This suggests that Dirichlet boundary conditions can be prescribed on the vertical boundaries of the aquifer, provided that the boundaries include these boreholes.

A more difficult decision was what type of boundary condition to prescribe on the top and bottom sides of the aquifer, especially to the bottom, since the exact depth of the aquifer is unknown. However, the high storage capacity of Aquifer 3 seems to limit the flow to the upper layers of the aquifer, as already noted in Section 7.2.1. Experiments with the cores and the double-packer tests also indicated that the mudstone layers are very dense at depths > 40 m. This, and the fact that there was no recharge during the time for which the simulations in Chapter were performed, suggested that homogeneous Neumann boundary conditions be placed on the top and bottom of the aquifer.

7.3.4 Hydraulic Parameters

The solution of Equation (7.1) requires not only a knowledge of the initial and boundary conditions, but also of the hydraulic conductivity tensor, \mathbf{K} , and the specific storativity, S_0 . There are essentially three methods that can be used to determine these quantities in three dimensions:

- cross-borehole packer tests (Hsieh *et al.*, 1983),
- in situ* measurement of flow velocities (Hess *et al.*, 1991), and
- tracer tests (Dverstorp *et al.*, 1992).

The determination of these parameters had to be restricted to the double-packer tests discussed in Section 6.3.4, since there was no suitable apparatus available to apply the last two methods, and the cross-borehole packer tests did not behave as expected.

The original analysis of the cross-borehole packer tests showed that the vertical component of hydraulic conductivity in Aquifer 2 is approximately five times larger than the horizontal components, but failed to yield meaningful results for Aquifers 1 and 3. Since the horizontal components of the tensor agreed very much with the horizontal hydraulic conductivities in Table 6–3, the values in the table were used for all three aquifers, while the vertical component was taken to be five times larger. The same analysis indicated that the specific storativity of the sandstone layer in Aquifer 2 was approximately $1.0 \cdot 10^{-4} \text{ m}^{-1}$, while that of the fracture was approximately $1.0 \cdot 10^{-5} \text{ m}^{-1}$. Since no information was available for the specific storativities of the other two aquifers, the value of $1.0 \cdot 10^{-4} \text{ m}^{-1}$ was also used for them.

7.4 THE NUMERICAL MODEL

7.4.1 Discretization of the Flow Equation

The first step in any numerical model is to discretize the various equations that appear in the mathematical model. The present model is based on the Galerkin finite element method, as described by Botha and Pinder (1983), and Huyakorn and Pinder (1983). This allows one to approximate Equation (7.1) with a set of linear equations given by

$$\int_{\Omega} S_0 (\hat{\phi}^{n+1} - \hat{\phi}^n) \phi_i d\Omega = -\Delta t \int_{\Omega} \nabla(\mathbf{K} \nabla \hat{\phi}^{n+1}) \cdot \nabla \phi_i d\Omega + \Delta t \int_{\partial\Omega} \mathbf{n} \cdot (\mathbf{K} \nabla \hat{\phi}^{n+1}) \phi_i dS + \Delta t \int_{\Omega} f \phi_i d\Omega$$

where Ω is the domain of the differential equation, \mathbf{n} a unit vector normal to the boundary $\partial\Omega$ of Ω , and

$$\hat{\phi}^n = \hat{\phi}^n(\mathbf{x}, t_n) \simeq \sum_{j=1}^N \varphi(\mathbf{x}_j, t_n) \phi_j(\mathbf{x})$$

an approximation of $\varphi(\mathbf{x}, t)$ at the point \mathbf{x} and time step t_n , with N the number of nodes in the finite element grid, $\varphi(\mathbf{x}_j, t_n)$ the value of $\varphi(\mathbf{x}, t)$ at the node j and time step t_n , and $\phi_j(\mathbf{x})$ a set of suitable basis functions.

The approximation of Equation (7.1) above can be written more compactly in matrix notation as

$$\mathbf{A} \boldsymbol{\varphi}^{n+1} = \mathbf{B} \boldsymbol{\varphi}^n + \Delta t (\mathbf{Q} + \mathbf{F}) \quad (7.3)$$

where \mathbf{A} and \mathbf{B} are two $N \times N$ matrices with elements

$$\begin{aligned} a_{ij} &= \int_{\Omega} [S_0 \phi_i \phi_j + \Delta t (\mathbf{K} \nabla \phi_i \cdot \nabla \phi_j)] d\Omega \\ b_{ij} &= \int_{\Omega} S_0 \phi_i \phi_j d\Omega \end{aligned} \quad (i, j = 1, \dots, N) \quad (7.4)$$

\mathbf{Q} and \mathbf{F} vectors with elements

$$\begin{aligned} q_j &= \int_{\partial\Omega} \mathbf{n} \cdot [\mathbf{K} \nabla \hat{\phi}^{n+1}] \phi_j dS = \int_{\partial\Omega} \mathbf{n} \cdot \mathbf{q} \phi_j dS \\ f_j &= \int_{\Omega} f \phi_j d\Omega \end{aligned} \quad (7.5)$$

and $\boldsymbol{\varphi}^n$ the finite element approximation of $\varphi(\mathbf{x}, t_n)$. The advantage of this approach is that the model could be based on the three-dimensional computer code SAT3, developed by Verwey and Botha (1992), without having to write a new code from scratch.

7.4.2 Representation of a Borehole

A borehole is conventionally represented in horizontal two-dimensional flow models as a point source (Huyakorn and Pinder, 1983). However, the method cannot be applied directly to three-dimensional problems, except to represent the borehole as a series of point sources spread out vertically along the borehole. Since the method yields a logarithmic singularity at the position of the source (Botha and Bakkes, 1982), the

method cannot yield an accurate solution for a three-dimensional problem.

Another approach, sometimes used in two-dimensional vertical flow models, is to view a borehole as a boundary in the aquifer, and then prescribe a Neumann boundary condition along the borehole's surface (Verwey and Botha, 1992). Unfortunately, the method can, only be applied if the following conditions are satisfied (Huyakorn and Pinder, 1983):

- (a) the aquifer is uniform,
- (b) the borehole penetrates the aquifer fully,
- (c) the discharge rate, $Q(\mathbf{x}, t)$, is constant, and
- (d) the aquifer is confined.

A method that does not suffer from the limitations above, is the Dirichlet method; first introduced by Huang (1973), and modified by Huyakorn and Pinder (1983). In this method the borehole is also considered as a boundary of the aquifer. However, instead of prescribing a Neumann boundary condition, one first prescribes an *arbitrary* Dirichlet boundary condition along its surface, and later adjusts it for the correct discharge rate. Since the borehole now forms a boundary in the aquifer, one can drop the source term and rewrite Equation (7.3) in the form

$$\mathbf{A}\boldsymbol{\varphi}_D^{n+1} = \mathbf{B}\boldsymbol{\varphi}^n + \Delta t \mathbf{Q}_D \quad (7.6)$$

where the subscript D denotes a solution of Equation (7.6) obtained with the *arbitrary* Dirichlet boundary values. Assume now that there are M ($M < N$) nodes on the boundary of the borehole. The discharge (+), or recharge (−) rate, Q_D , of the borehole, associated with the prescribed Dirichlet boundary conditions, must thus satisfy the equation

$$Q_D = \sum_{l=1}^M q_{Dl} \quad (7.7)$$

where q_{Dl} is the total flux across the side of an element, containing node l , weighted by the basis function ϕ_l , as defined in Equation (7.5). Let $\boldsymbol{\varphi}_D^{n+1}$ be the solution of Equation (7.6), and $\boldsymbol{\varphi}'$ the solution of the homogeneous system of equations

$$\mathbf{A}\boldsymbol{\varphi}' = \mathbf{0} \quad (7.8)$$

Suppose now that $\boldsymbol{\varphi}^{n+1}$ is the solution of Equation (7.6), had the correct Dirichlet boundary conditions been used, that is

$$\mathbf{A}\boldsymbol{\varphi}^{n+1} = \mathbf{B}\boldsymbol{\varphi}^n + \Delta t \mathbf{Q} \quad (7.9)$$

with

$$Q = \sum_{l=1}^M q_l \quad (7.10)$$

the true discharge rate, and that $\boldsymbol{\varphi}^{n+1}$ can be expressed as

$$\boldsymbol{\varphi}^{n+1} = \boldsymbol{\varphi}_D^{n+1} + \lambda \boldsymbol{\varphi}' \quad (7.11)$$

where λ is a constant that has to be determined. To do this, notice that the difference of Equations (7.9) and (7.6) can be expressed as

$$\mathbf{A}(\boldsymbol{\varphi}^{n+1} - \boldsymbol{\varphi}_D^{n+1}) = \lambda \mathbf{A}\boldsymbol{\varphi}' = \Delta t(\mathbf{Q} - \mathbf{Q}_D)$$

If one now sums the equations that belongs to the M Dirichlet nodes along the boundary of the borehole, and uses Equations (7.7) and (7.10) to express Q_D and Q in terms of q_{Dl} and q_l , one finds that

$$\lambda \sum_{l=1}^M \sum_{j=1}^N a_{lj} \varphi_j' = \Delta t(Q - Q_D)$$

In other words,

$$\lambda = \frac{\Delta t(Q - Q_D)}{\sum_{l=1}^M \sum_{j=1}^N a_{lj} \varphi_j'} \quad (7.12)$$

The practical implementation of the method to represent a borehole as a Dirichlet boundary can now be conveniently summarized in the following steps.

- (1) Assume that the piezometric heads on the boundary of the borehole at the time step $n+1$ can be

represented by the arbitrarily chosen set of values, φ_b , that is

$$\varphi^{n+1} = \varphi_b$$

- (2) Solve Equations (7.6) and (7.8) with this set of piezometric heads for the Dirichlet boundary conditions along the surface of the borehole.
- (3) Use this solution and the element coefficients in Equations (7.4) and (7.5) to compute λ in Equation (7.12).
- (4) Substitute this value of λ and the solutions for φ_D and φ' , computed in step 2, in Equation (7.11), to obtain the solution for the correct discharge rate.

It is interesting to notice that nowhere in the derivation of the Dirichlet method, was it necessary to specify the geometrical dimensions of the borehole. The possibility thus exists that one can represent the borehole as a line source. This possibility will be investigated further in Chapter 8.

7.5 DISCUSSION

Three-dimensional groundwater models are not very popular in geohydrological circles. The most obvious reason for this is that the model requires much more field data and sophisticated computer resources than an equivalent two-dimensional model. Another reason is that two-dimensional models have been so successful in modelling groundwater phenomena, that there does not seem to be a need for three-dimensional models.

There are at least two reasons that can be advanced for the latter view. Large-scale observations are mainly restricted to economically important well-fields. The boreholes in these fields are usually approximately of the same depth, with the result that the pumping tends to create large horizontal piezometric gradients that mask the influence of the smaller vertical gradients completely. Since groundwater moves very slowly, it may take years before the influence of smaller three-dimensional interactions become noticeable in field observations. One could thus model such an aquifer quite successfully with a two-dimensional horizontal flow model for a long time, without detecting differences between the observed and simulated results. Moreover, there exists a tendency to attribute such differences to variations in the hydraulic parameters and incorporate them by simply re-calibrating the model. *Such a phenomenological model is able to systemize information on an aquifer, but it cannot describe the physical behaviour of the aquifer.* The possibility thus exists that one can completely destroy an aquifer, if a phenomenological model is used to manage or predict the future behaviour of the aquifer.

The second reason for the popularity of two-dimensional models is that very little attention is usually paid to three-dimensional factors, such as the geometry and structure of the aquifer, in groundwater investigations. There is therefore no motivation to pay attention to the influence these factors may have on the behaviour of aquifers. This influence may be negligible in the short term, but it can have devastating effects in the future; the Love Canal disaster (Princeton University Water Resources Program, 1984) is a typical example. It is thus important that these factors should be taken into account whenever their influence becomes noticeable. Judging from the discussion in Chapters 5 and 6, the geometry and structure of Karoo aquifers play an important role in their behaviour. This suggests that it will simply be a waste of time and money to apply two-dimensional horizontal models in investigations of these aquifers. It will thus be interesting to see if the three-dimensional model introduced above, can describe the behaviour of the Karoo aquifers better than a conventional two-dimensional model.

One can, of course, argue that the use of three-dimensional models simply cannot be justified economically, and that whatever other methods are available must be used in the investigations. There are two difficulties with this argument. The first is that its main proponents are often people who have their own *preconceived ideas* of how an aquifer should behave, and are therefore not interested in information that may prove them wrong. The second difficulty is that the argument depends very much on what is meant with the term 'economically justifiable'. Does it mean that the aquifers are of no economic value, or does it mean that there is a reluctance to spend more money on investigations of the aquifers? Nobody will argue that money must be spent on aquifers that are not economically viable in the long term. However, the consequences may be disastrous if the second alternative is true. For example, it may mean that considerably larger sums of money have to be spent in the future to correct previous mistakes, or that future generations will have very little groundwater resources at their disposal. *Nature behaves in its own subtle ways, and not as prescribed by man.* The statement: 'Don't have a preconceived idea of what the result should be' by John Sumpter, as quoted by Kaiser (1996), is as applicable to the behaviour of aquifers as to endocrine disrupters.



CHAPTER 8

IMPLEMENTATION OF THE NUMERICAL MODEL

8.1 INTRODUCTION

The implementation of a numerical model generally proceeds in three steps. The first is to look at the approximating equations and implement them efficiently in a computer program. The second is to decide which pre- and post-processors are necessary to ease the burden associated with the generation of the input data required by the program, and to interpret the results. The third step is to make sure that there are not any numerical, logical, or heuristic errors in the computer program.

The approximating equations used in the present program, are essentially the same as those used by Verwey and Botha (1992), and have already been discussed in Chapter 7. The discussion in Section 8.2 is thus mainly concerned with the representation of a borehole through Dirichlet boundary conditions, and discontinuities in the hydraulic parameters.

The pre- and post-processors used for the model, have been developed over the years at the Institute for Groundwater Studies. The additional processors and mesh generator needed for the model, are briefly discussed in Section 8.3. More detailed descriptions and user guides for the processors and mesh generator, are available from the Institute for Groundwater Studies.

The major effort in writing a new computer program, or revising an existing one, is to ensure that the program is, as far as possible, without errors. The convergence properties of the model, in both space and time, are therefore discussed in Section 8.4. Particular attention is paid to the situation where the borehole is represented as a line source in the Dirichlet approximation.

A multi-porous medium is essentially a domain with discontinuous hydraulic parameters. The mathematical correct way to account for discontinuities, is to prescribe suitable internal boundary conditions across the discontinuities. However, this approach complicates the programming considerably. A heuristic approach that avoids the prescribing of internal boundaries was therefore used in the program. The applicability of the approach is studied by applying it to a hypothetical fractured aquifer in Section 8.5.

8.2 PROGRAM KARO

8.2.1 General

As mentioned in Chapter 7, the numerical model for the Campus Aquifer was based on the Program SAT3, written by Verwey and Botha (1992), to simulate three-dimensional flow of groundwater in a saturated porous medium. Unfortunately, this program only allows one to specify a borehole through Neumann boundary conditions. Parts of the program therefore had to be rewritten, to account for the representation of the borehole through Dirichlet boundary conditions, as discussed in Chapter 7. The main changes were briefly the following:

- (a) Make provision for the solution, φ' , of Equation (7.8). This also meant that additional computer memory space had to be reserved for the coefficient matrix \mathbf{A} , and not to overwrite it during the solution of Equation (7.6), as is done in Program SAT3.
- (b) Provide computer memory space for those elements in \mathbf{A} , that correspond with the Dirichlet nodes on the surface of the borehole needed in the computation of λ in Equation (7.12).
- (c) The addition of a new subroutine for the computation of λ and the final solution, given by Equation (7.11).

Provision was also made for Program KARO to compute the arbitrary Dirichlet boundary conditions along the borehole boundary automatically. This was achieved by replacing the piezometric head of the previous time step along the boundary, φ_b^n , with

$$\varphi_D^{n+1} = \varphi_b^n + (Q\Delta t_{n+1})/12$$

where Q is the prescribed discharge rate and Δt_{n+1} the $(n+1)$ -th time step. Since this modified version of Program SAT3 was developed specifically for the modelling of Karoo aquifers; the program will in the future be referred to as Program KARO.

8.2.2 Discontinuous Hydraulic Parameters

A multi-porous medium is essentially a domain with discontinuous hydraulic parameters. The mathematical correct way to account for discontinuities is to let them coincide with finite element boundaries, and then prescribe suitable internal boundary conditions across the boundaries (Bear, 1972). However, there is another, and computationally more attractive, approach if differential equations with discontinuous coefficients are solved with the Galerkin finite element method based on quadrilateral or hexahedral elements.

The integrals in the approximating equations of the Galerkin finite element method, such as Equation (7.2), are conventionally computed with a Gaussian quadrature rule, which only uses nodal values of the parameters (Botha and Pinder, 1983). In quadrilateral or hexahedral elements, the quadrature points all lie within the element (Stroud and Secrest, 1966). The method will thus not recognize a discontinuity that lies on the common boundary of two adjacent elements. All that the method can do in such cases is to ‘smear’ the discontinuity across the element boundaries. However, the ‘smeared region’ can be controlled by adjusting the element sizes. The prescription of internal boundary conditions can thus be avoided in problems with discontinuous parameters, by ensuring that the discontinuity lies along element boundaries, as illustrated in Figure 8–1.

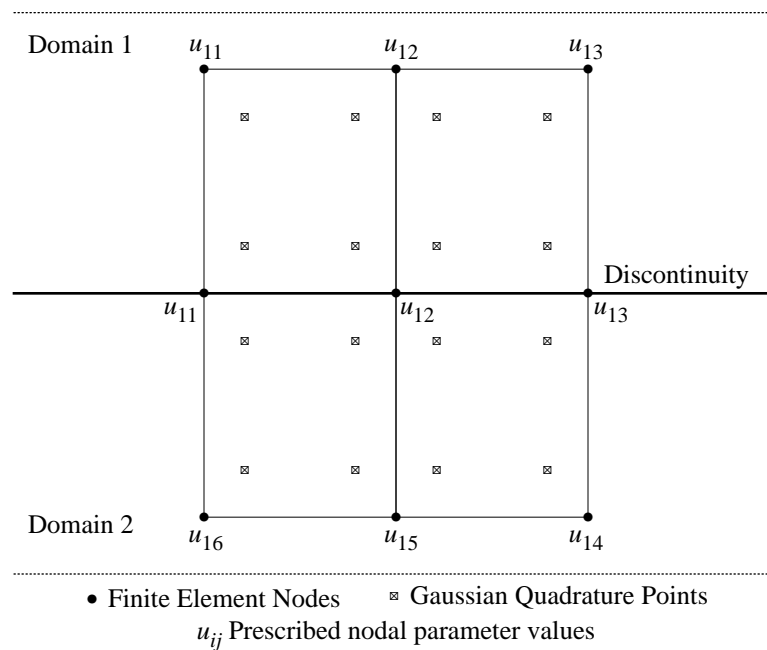


Figure 8–1 Approximation of discontinuities in the Galerkin finite element method, with quadrilateral elements.

The approximation in Figure 8–1 is particularly advantageous in those cases where the discontinuities are not sharp; a situation that arises frequently in models of groundwater flow phenomena. The approximation was consequently already implemented in Program SAT3, although not explicitly mentioned in Verwey and Botha (1992), and thus also in Program KARO.

8.3 PRE- AND POST-PROCESSORS

The generation of a finite element grid, especially when done manually, is perhaps the most time-consuming and frustrating task to perform in three-dimensional models. Verwey and Botha (1992) try to ease this task by using the grid generator QBIK—a modified version of the Program KUBIK (Pissanetzky, 1984) to generate their finite element grids. However, Program QBIK only allows one to modify elements on a horizontal plane. A new program, MESHPRO, was therefore developed for the generation of three-dimensional finite element grids.

The program first divides a given domain Ω into a number of blocks which may correspond with various properties of the domain. For example, the blocks can be chosen to coincide with the different porous domains in the case of the Campus Aquifer. The program then divides the blocks into a prescribed number of elements, numbers them and their nodal points, computes the co-ordinates of each node, and creates the necessary data files for the programs KARO or SAT3. MESHPRO will also accept data from program KARO, or program SAT3, and construct data files, ready for input to the graphic packages, TRICON (Buys, 1992) and VIS-5D (Hibbard and Saintek, 1994), used in interpreting the results.

8.4 COMPARISON OF PROGRAM KARO WITH ANALYTICAL MODELS

8.4.1 General

Although Program SAT3 has been checked extensively for numerical and approximation errors by Verwey and Botha (1992), the changes made in Program KARO influenced quite a number of the critical calculations. It was thus necessary to check the program again for numerical and approximation errors, especially the representation of a borehole by Dirichlet boundaries.

A method universally used to check for errors in a computer program for the approximate solution of a differential equation, is to compare its output with a known analytical solution of the differential equation. Unfortunately, there do not exist many analytical solutions for the groundwater flow equation, Equation (7.1). The radial symmetric Dirichlet problem of Muskat (1937) for a confined aquifer, used by Verwey and Botha (1992) in their tests of Program SAT3, was thus also used here. This solution applies to a uniform aquifer with radius R , thickness d , hydraulic conductivity K and specific storativity S_0 . The borehole is situated at the centre of the aquifer, and discharges at a rate Q , subject to the initial and boundary conditions

$$\begin{aligned}\varphi(r, 0) &= \varphi_0 \\ \varphi(R, t) &= \varphi_0 \quad (t \geq 0)\end{aligned}$$

The drawdown in such an aquifer is given by the equation

$$s(r, t) = \varphi_0 - \varphi(r, t) = \frac{Q}{\pi K d} \left[\frac{1}{2} \ln \frac{R}{r} - \sum_{j=1}^{\infty} \frac{J_0(\alpha_j r) \exp(-\alpha_j^2 \kappa t)}{\alpha_j^2 R^2 J_1^2(\alpha_j R)} \right] \quad (\kappa = K/S_0) \quad (8.1)$$

where, $J_0(z)$ and $J_1(z)$ are the zeroth and first order Bessel functions of the first kind, respectively, with $\alpha_j R$ the zeros of the equation

$$J_0(\alpha_j R) = 0 \quad (j = 1, \dots, \infty)$$

As mentioned in Chapter 7, the possibility exists that one can represent a borehole either as a surface source or a line source in the Dirichlet approximation. To distinguish between the two approximations, the former will, in future, be referred to as the *Dirichlet surface source* and the latter as the *Dirichlet line source* approximation. Since the representation of a borehole in Program SAT3 with Neumann boundary conditions also involves the surface of the borehole; this representation will be referred to as the *Neumann surface source* approximation.

Three approaches were used in the numerical experiments, performed to check program KARO for approximation and logical errors.

- (a) Comparing the analytical solution in Equation (8.1) with the surface source approximations of Programs SAT3 and KARO.
- (b) Comparing the analytical solution in Equation (8.1) with the Dirichlet line source approximation of Program KARO.
- (c) A study of the convergence properties of Program KARO for both the Dirichlet surface and line source approximations, in space and time.

8.4.2 The Dirichlet Surface Source Approximation

The main purpose of the first set of numerical experiments was simply to compare the Muskat solution in Equation (8.1) with the Neumann and Dirichlet surface source approximations of the programs SAT3 and KARO. Since the Muskat solution applies only to a uniform and radial symmetric aquifer, the finite element grid used in the study was limited to the quarter cylinder, shown in Figure 8-2. The grid consisted of two

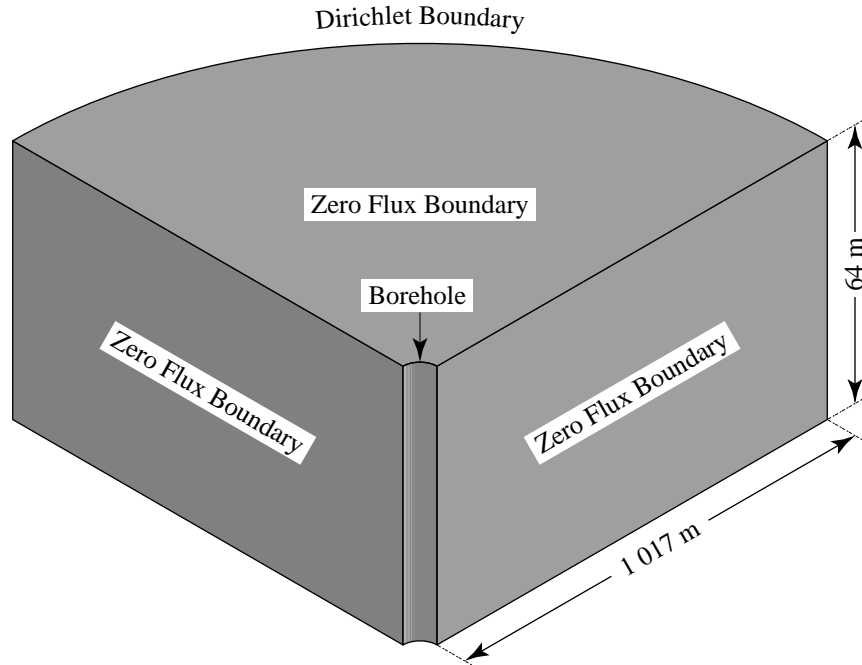


Figure 8-2 Schematic diagram of the hypothetical aquifer used in the study of the finite boundary problem.

elements, each with a height of 32 m in the vertical plane, and 12 wedges with constant angles, $\theta = 7,5^\circ$, in the horizontal plane. The wedges were divided into 512 curved elements, by subdividing each interval in Table 8-1, into 64 equally spaced subintervals.

Table 8-1 Radial intervals used to generate the finite element grid in the horizontal plane.

Distance (m)	0,1	1	9	25	57	121	249	505	1 017
--------------	-----	---	---	----	----	-----	-----	-----	-------

The hydraulic parameters of the aquifer and discharge rate used in the study are given in Table 8-2. Since the flow is radial, and Equation (8.1) applies to a confined aquifer, zero-flux Neumann boundary conditions were prescribed along the two straight vertical sides, on the top and bottom of the aquifer. A piezometric head of $\varphi_0 = 96$ m was prescribed for the initial and Dirichlet condition on the outside boundary. The boundary fluxes needed for the case where the borehole was considered as a Neumann boundary, were computed from the value of Q in Table 8-2, and Equation (7.6).

Table 8-2 Hydraulic parameters of the aquifer used in the study of the Dirichlet surface and line source approximations.

K_x (m s ⁻¹)	K_y (m s ⁻¹)	K_z (m s ⁻¹)	S_0 (m ⁻¹)	Q (m ³ s ⁻¹)
$1,0 \cdot 10^{-05}$	$1,0 \cdot 10^{-05}$	$1,0 \cdot 10^{-05}$	$1,0 \cdot 10^{-05}$	$1,0 \cdot 10^{-03}$

The main interest in this exercise was to compare the Neumann and Dirichlet approximations of a borehole and the Muskat solution. The computations were therefore limited to a total time of 2 h, but with three different time steps of 2, 1 and 0,5 h. The solutions are compared graphically in Figure 8-3.

A first impression of the results, in Figure 8-3, for both the Neumann and Dirichlet surface source approximations, is that they are not very accurate, particularly near the borehole. However, this could have been expected, since these approximations represent the borehole as a finite surface source, while the Muskat solution considers it to be a point source.

An interesting feature in Figure 8-3 is that the Dirichlet approximation for the larger time step is quite close to the Muskat solution, but then converges away from it, while the Neumann approximation converges towards it as the time step decreases. It is difficult to explain this behaviour mathematically. One possibility is that it may be associated with the way in which the domain has been discretized. A second set of numerical

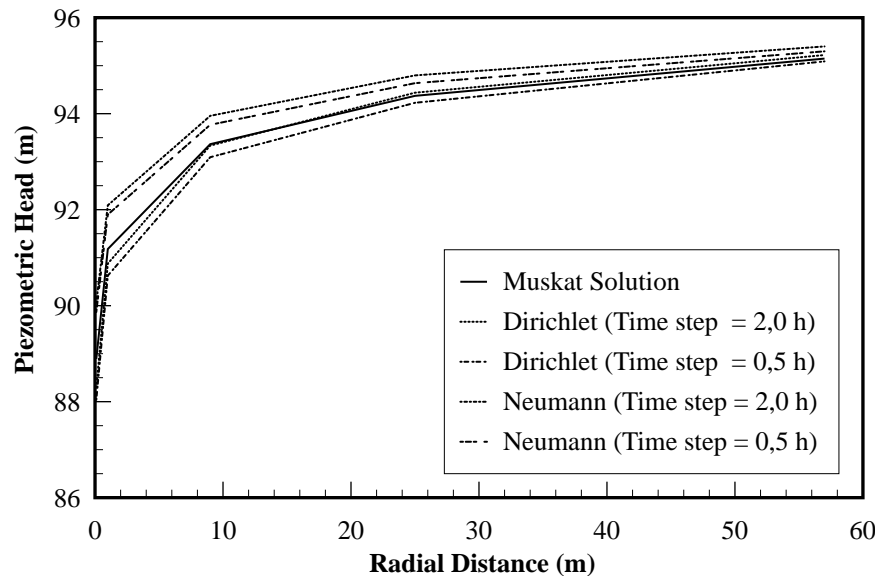


Figure 8-3 Comparison of the Muskat solution with the Neumann and Dirichlet surface source approximations as a function of the distance (r), at the time steps 0,5 and 2 h.

experiments was therefore performed with the same hydraulic parameters, but a different grid. This grid contained the same number of wedges as the previous one in the horizontal plane, but the number of elements in each wedge was restricted to 8, with nodes given by the radial distances in Table 8-1. The two elements in the z -direction were also reduced to just one. The reason for choosing this grid was that the available computer resources prevented a further refinement of the original grid.

Four series of computations were performed with the new grid. The first one was performed on the basic grid described above, but in the next three computations the elements were halved, thus doubling the number of elements each time. All computations were again performed for 2 h, but only with a time step of 0,5 h.

A comparison of the solutions from the new grid in Figure 8-4 with those in Figure 8-3, shows that the change in the grid had a considerable influence on both the Neumann and Dirichlet solutions. Not only are the Neuman approximations almost indistinguishable from one another, but also closer to the Muskat solution than the Dirichlet approximations. The Dirichlet approximations, on the other hand, now also converge towards the Muskat solution, and quite rapidly. This behaviour suggests that the convergence of the Dirichlet method depends strongly on the maximum element size, while the convergence of the Neuman method depends on the number of elements in the vertical direction. The reason for this can briefly be explained as follows: Notice that in the Neumann method one must integrate numerically over all vertical elements along the borehole boundary. The boundary surface of the borehole will remain the same for all grids, but the number of elements increases as the grid is refined. There could thus be an accumulation of approximation errors, as the sizes of the elements decrease. The Dirichlet method, on the other hand, uses piezometric heads, and these depend only on the element sizes (Botha and Pinder, 1983). The decrease in element sizes, therefore, had a considerably larger impact on the Dirichlet values than on the Neumann values. This conjecture was confirmed by further numerical experiments. The Dirichlet approximation, therefore, has a definite advantage over the Neumann approximation.

8.4.3 The Dirichlet Line Source Approximation

As mentioned in Chapter 7, there is a possibility that a borehole can be represented by a line source in the Dirichlet method. It is very difficult to generate a complete quadrilateral, or hexahedral, finite element grid for a line source with the previous radial grid. One quadrant of a new rectangular hypothetical aquifer, shown in Figure 8-5, was therefore used to investigate this possibility. The hydraulic parameters in Table 8-1 were also used with this aquifer.

The initial grid had 7 elements in the x - and y -directions, with nodes at distances of 0, 8, 24, 56, 120, 248, 504 and 1 016 m, and two elements in the z -direction. Four other grids, for which the elements in the x - and y -direction were halved each time, were also used in the computations. These grids will be referred to as Grids 1 to 5. A piezometric level of $\varphi_0 = 96$ m was prescribed for the initial condition and the Dirichlet

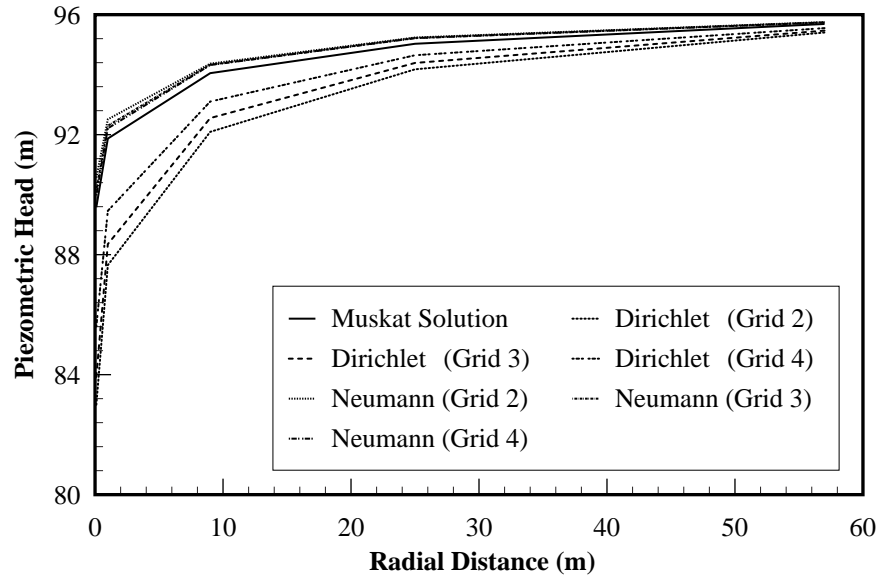


Figure 8-4 Comparison of the Muskat solution with the Neumann and Dirichlet surface source approximations, for different finite element sizes.

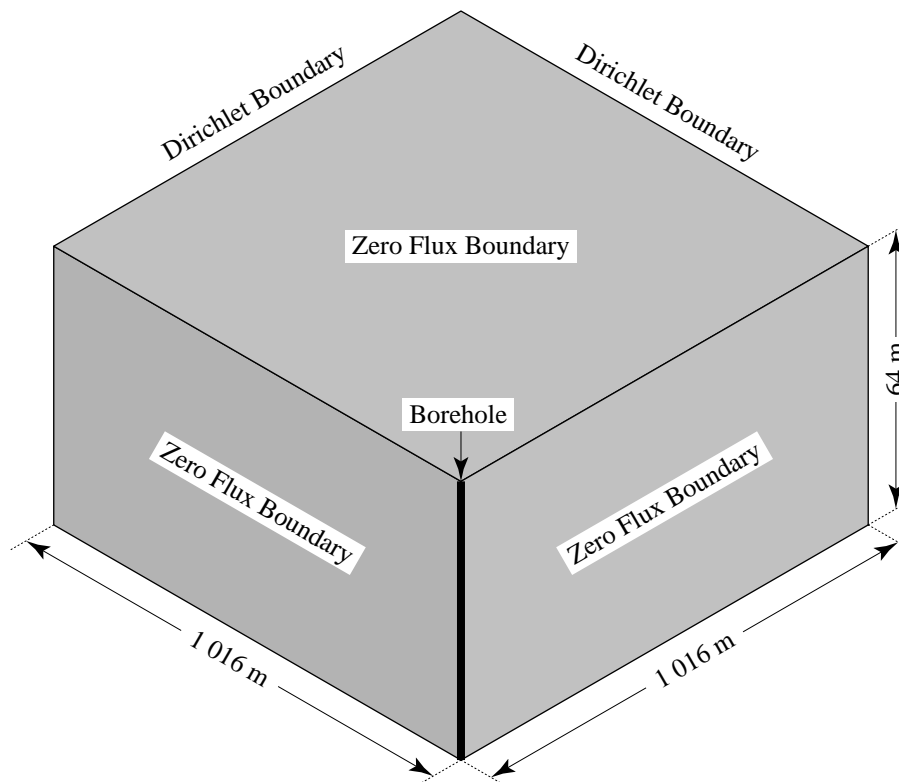


Figure 8-5 Schematic representation of the hypothetical aquifer used to study the behaviour of the Dirichlet method, when the borehole is represented as a line source.

boundaries for every one of the computations. Three of the approximations are compared graphically with the Muskat solution in Figure 8-6.

A first glance at the solutions in Figure 8-6 suggests that the line source approximation converges very rapidly, as the element sizes are reduced. However, the oscillation in the solution for Grid 1 suggests that the approximation becomes unstable if the grid is too coarse. It may thus be necessary to perform a grid convergence test before the approximation is applied in practice.

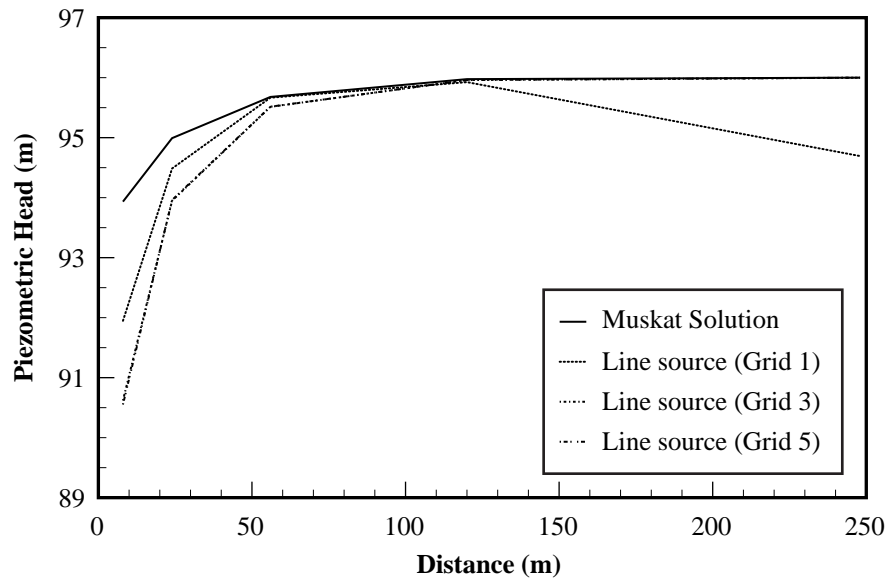


Figure 8-6 Comparison of the Muskat and line source approximation of a borehole for the different finite element grids.

Another interesting result in Figure 8-6 is the good agreement between the Muskat and line source solution at large distances, even though the Muskat solution is not strictly valid for this aquifer. The reason for this is that the boundary of the aquifer was chosen far enough for the discharge rate not to have influenced the piezometric levels near the boundary. Notice though that the line source approximation converges away from the Muskat solution at the smaller distances. However, this just illustrates the logarithmic singularity in the Muskat solution at the borehole.

8.4.4 Convergence of the Dirichlet Surface Source Approximation in Time

The first convergence test performed in time was for the Dirichlet surface source approximation. The same hypothetical aquifer and finite element grid, used in Section 8.4.2 to compare the Dirichlet surface source approximation and the Muskat solution, were used in these tests. The convergence rate of the approximation was again determined for a period of 2 h, with time steps of 1, 5, 15, 30, 60 and 120 min.

As shown in Figure 8-3, the Dirichlet surface source approximation converges away from the Muskat solution. This behaviour again illustrates the logarithmic singularity in the Muskat solution at the borehole. The approximation for the time step of 1 min was therefore used in computing the errors in Figure 8-7.

The convergence rates of the various approximations in Figure 8-7 are in excellent agreement with the linear theoretical rate, $O(\Delta t)$, for the backward finite difference used to approximate the time derivative in Program KARO. The decrease in slope with increasing radial distances, r , can be ascribed to the smaller changes in $\varphi(\mathbf{x}, t)$ at large values of r , a phenomenon also present in Figures 8-3 and 8-4.

8.4.5 Convergence of the Dirichlet Line Source Approximation in Time

The square hypothetical aquifer discussed in Section 8.4.3 was again used for this study, except that the number of elements in both the x - and y - directions was fixed at 112. The approximation of the piezometric head for the smallest time step, 1 min, was here also used for comparison purposes. As shown in Figure 8-8, the convergence is again excellent and linear.

8.4.6 Convergence of the Dirichlet Surface Source Approximation in Space

The quarter circle hypothetical aquifer of Section 8.4.2, with only one layer in the z - direction, and the finite element grid of Figure 8-9, was used to study the spatial convergence of the Dirichlet surface source approximation. The first set of tests was done by varying the angle, θ , of the angular wedges in the sequence 45° , 30° , 15° and 7.5° , while keeping the radial distances as in Table 8-1.

The approximations of the piezometric heads for the 4 grids were computed for one time step of 0.5 h. The

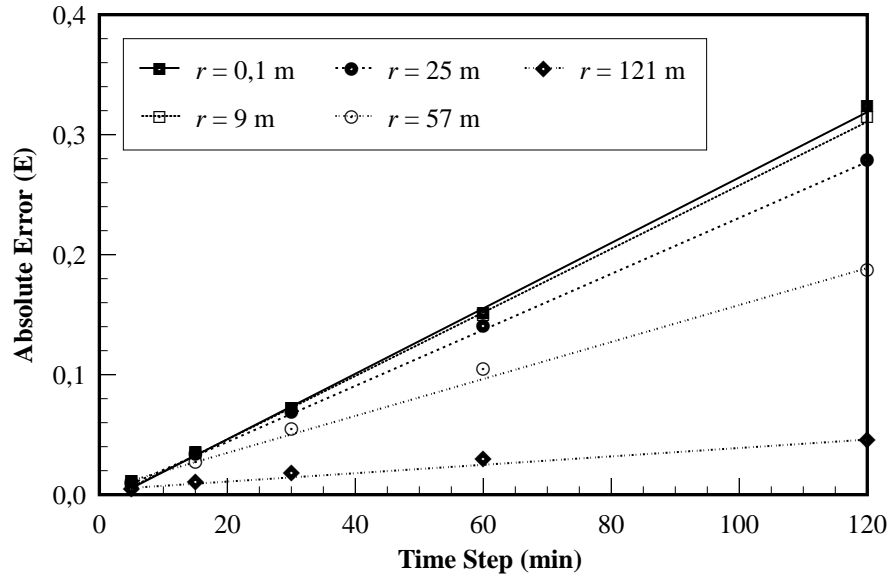


Figure 8-7 Convergence of the Dirichlet surface source approximation as a function of the time step, at different distances (r) from the borehole.

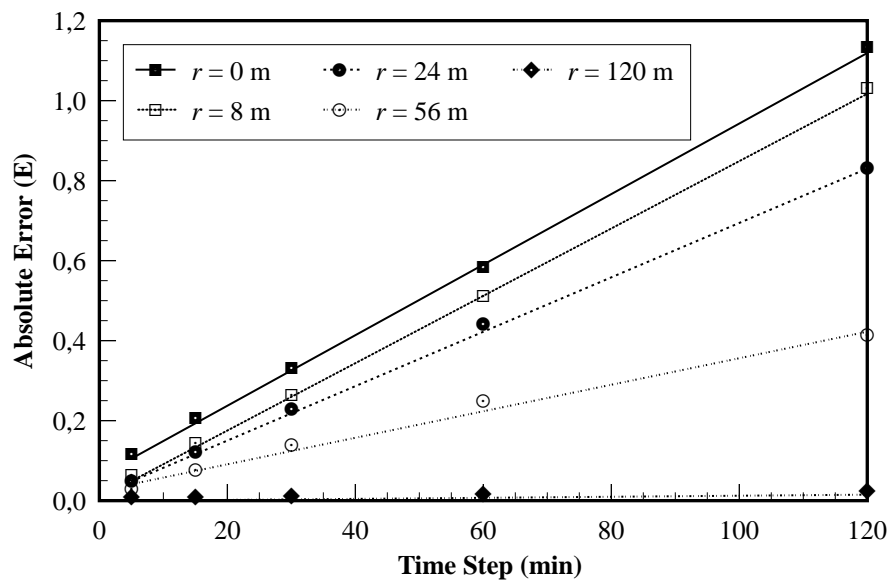


Figure 8-8 Convergence of the Dirichlet line source approximation, as a function of the time step at different distances (r) from the borehole.

errors in the approximations were computed from the approximation obtained with the grid in Figure 8-9, divided into 12 horizontal wedges ($\theta = 7.5^\circ$), and 512 curved elements. The same computations were also carried out for 0.5 h, but with a time step of 1 min. The errors in the approximations are displayed graphically in Figure 8-10 as a function of the maximum element size—defined as the length of the longest diagonal in the specific grid.

Although the numerical errors in Figure 8-10 display an $O(h^2)$ behaviour, as they should theoretically do for the tri-linear basis functions used in Program KARO, they are rather insensitive to large elements. This behaviour can probably be ascribed to the fact that the largest elements are situated on the outer boundary of the aquifer (see Figure 8-9), where the piezometric head varies slowly. One must also keep in mind that the main purpose of the Dirichlet approximation is to simulate the behaviour of the water level in the borehole. Care should therefore be exercised not to use too large elements in the finite element grid with the Dirichlet surface source approximation, particularly near the borehole.

In the second set of spatial convergence tests, the angles of the wedges were fixed at $\theta = 7.5^\circ$, and the

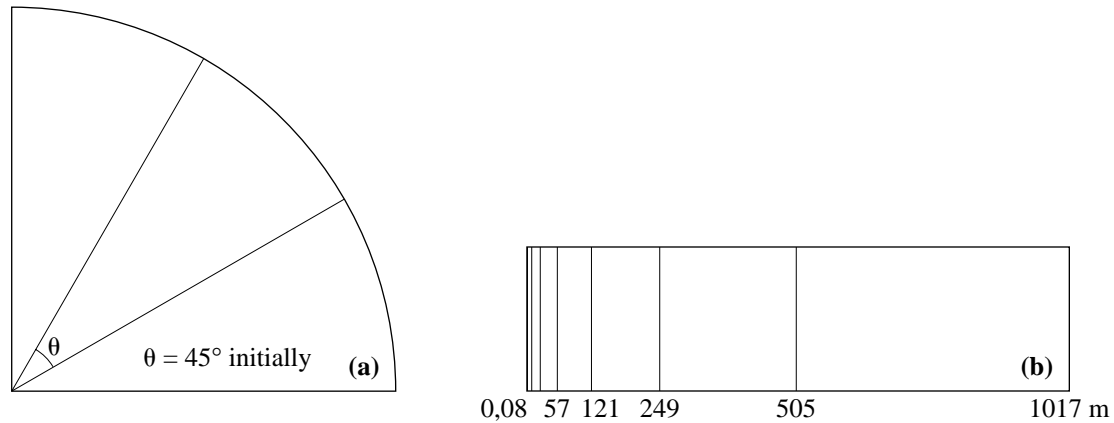


Figure 8-9 Plan (a) and side (b) views of the initial finite element grid used to study the convergence properties of the Dirichlet surface source approximation.

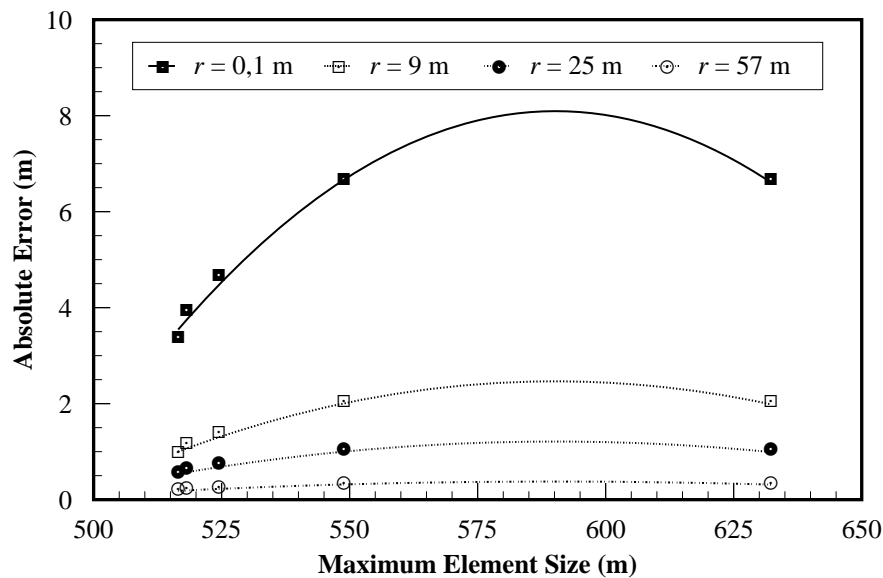


Figure 8-10 Errors in the Dirichlet surface source approximation as a function of the maximum angular element size, at different distances (r) from the borehole.

elements in the radial direction were halved for the next grid. The first six of these approximations were computed for a time of 0,5 h, with one time step. However, the seventh one, which served as reference for the errors in Figure 8-11, was computed with 30 time steps of 1 min each.

The numerical errors in Figure 8-11 again display the same $O(h^2)$ behaviour as in the angular convergence tests, except that the approximation for the first, and coarsest, grid now seems to be as accurate as the approximation of the reference grid. The first impulse was that the program contains a programming error. The true piezometric head, $\varphi(r, t)$, and its homogeneous counterpart, $\varphi'(r, t)$, defined by Equations (7.11) and (7.8) respectively, were therefore checked for possible numerical errors. However, as shown in Figure 8-12, there is nothing extraordinary in the behaviour of the approximations, except that $\varphi'(r, t)$ crosses $\varphi(r, t)$ as the time step decreased. The homogeneous Equation (7.8) is thus more sensitive for the time step than Equation (7.11).

The computations were also repeated with the Neumann surface source approximation, but its convergence was normal. The behaviour thus seems to be a further confirmation of the earlier observation that the Dirichlet surface approximation is insensitive to large finite elements.

8.4.7 Convergence of the Dirichlet Line Source Approximation in Space

The purpose of the final convergence test was to investigate the spatial convergence rate of the Dirichlet line source approximation. Five finite element grids were used for the hypothetical aquifer in Figure 8-5 in this

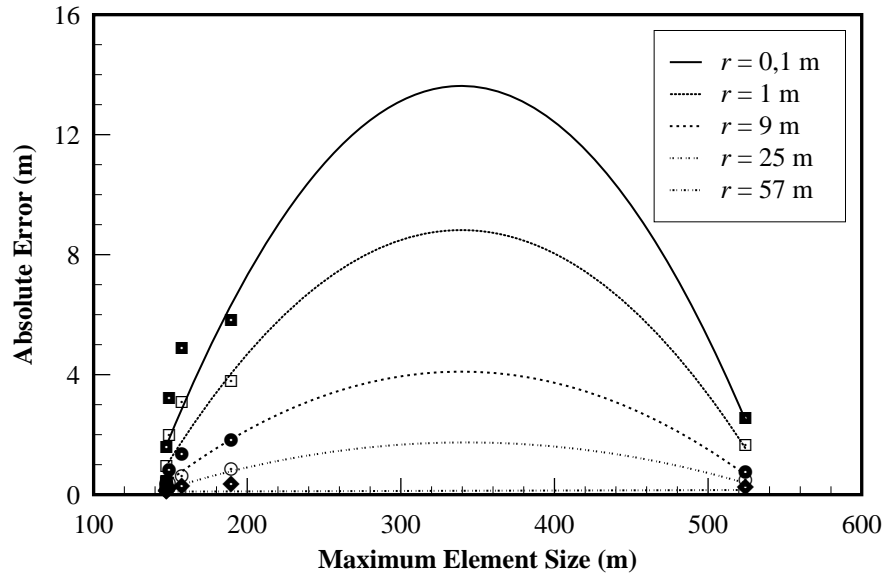


Figure 8-11 Errors in the Dirichlet line source approximation as a function of the maximum radial element size, at different distances (r) from the borehole.

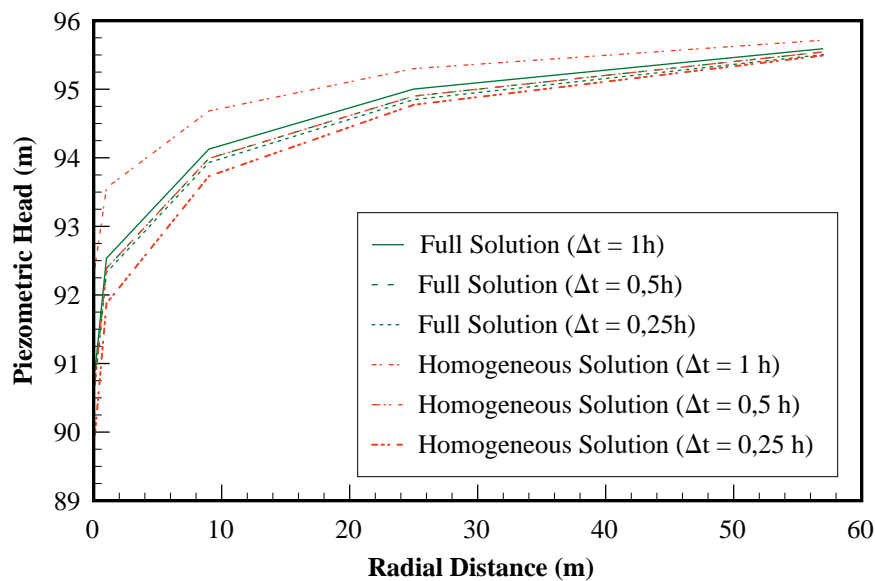


Figure 8-12 Behaviour of the true and associated homogeneous piezometric head of the Dirichlet surface source approximation as a function of the time step (Δt).

study, starting with the one described in Section 8.4.3. Every element was then halved successively for the following four grids. All approximations were computed for a time step of 0.5 h. The approximation for the final grid, computed with a time step of 1 min, was used to compute the errors in Figure 8-13.

It follows from Figure 8-13 that the errors for the Dirichlet line source approximation behave more like the theoretical $O(h^2)$ estimate than that of the Dirichlet surface source approximation. The only exception is the solution at the borehole, $r = 0$ (m), which tends to increase quite rapidly with the element size.

An interesting feature of the errors for values of $r \geq 8$ m is that they achieve their minimum values between the maximum and minimum element sizes, and not at the minimum element size as one would expect. This behaviour of the approximation error has been observed previously in three-dimensional groundwater models by Verwey and Botha (1992) and in two-dimensional models by Lynch (1982). Numerical experiments by Verwey and Botha (1992) have shown that the behaviour is caused by using a too coarse finite element grid near discontinuous initial and boundary conditions. This causes large approximation errors near the discontinuities, especially if the time step is also relatively large.

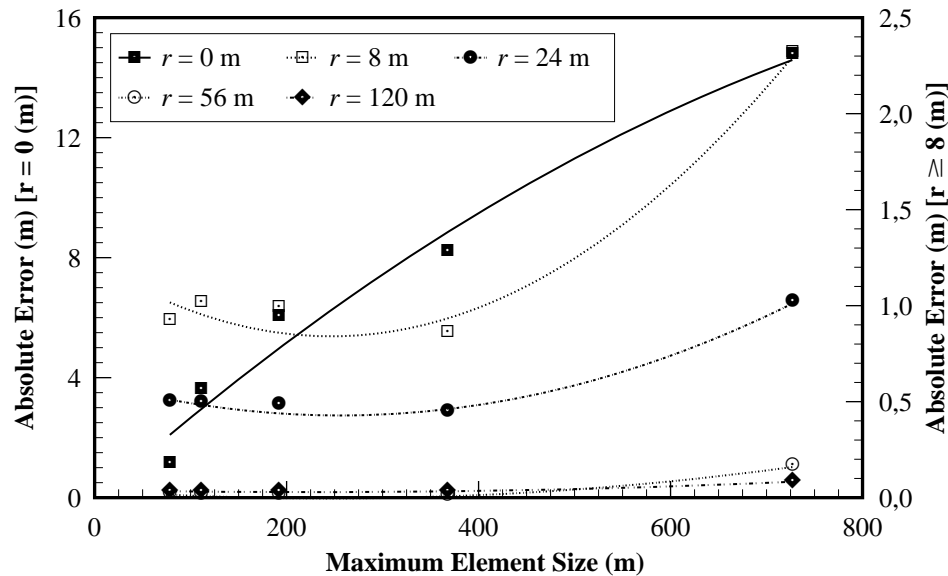


Figure 8-13 Convergence of the Dirichlet line source approximation as a function of the maximum element size, at different distances (r) from the borehole.

8.4.8 Discussion

The tests described above show that there are not any serious numerical or logical errors in Program KARO. The program can thus be used with confidence in modelling Karoo aquifers.

One rather disturbing result of the tests is the insensitivity of the Dirichlet surface source approximation to changes in the finite element sizes. There are two reasons for this concern. The first is that one cannot trust convergence studies to yield a suitable finite element grid, as is conventionally done in numerical analysis. The second is that one cannot use too large elements, even far from a borehole, with this approximation—a practice that is quite common in modelling groundwater resources. A comparison of Figure 8-11 and Figure 8-13, however, shows that the Dirichlet line source approximation does not show this insensitivity. Preference should thus be given to the Dirichlet line source approximation, when modelling three-dimensional groundwater flow. The only difficulty with the approximation is that it may be subject to the accumulation of errors. However, this behaviour can usually be detected easily in convergence studies, as shown by the results in Figure 8-13.

8.5 NUMERICAL MODEL FOR A SIMPLIFIED KAROO AQUIFER

8.5.1 Description of the Aquifer

The aim of the final numerical experiments was twofold: to see if the method of approximating discontinuous hydraulic parameters in Program KARO could handle the fractures in Karoo aquifers, and to obtain a sense for the behaviour of the program. A small hypothetical aquifer, $128 \times 128 \times 10 \text{ m}^3$, was used for this purpose. A single fracture, with dimensions $32 \times 32 \times 0,01 \text{ m}^3$, was placed at the centre of the aquifer. The reason for this was to try and keep the model simple, but as close as possible to the aquifer on the Campus Test Site. It was also assumed that the aquifer is symmetrical, so that the numerical model could be restricted to the upper right-hand quarter of the aquifer, shown in Figure 8-14.

The element sizes of the finite element grid were fixed at $4 \times 4 \text{ m}^2$ in the horizontal plane, but varied logarithmically in the vertical, as shown in Figure 8-15 and Table 8-3. The thinnest element was placed directly over the fracture. This was done so that the effects of the fracture could be identified easily, and to minimize numerical errors near the fracture, where the hydraulic parameters are discontinuous.

The field work discussed in Chapter 6 has shown that the rock matrix of Karoo aquifers can store large volumes of water, but will not release the water easily. Fractures, on the other hand, have a low storativity, but can transmit water readily. The hydraulic conductivity and specific storativity values, given in Table 8-4, were therefore used in the model.

A piezometric head of 20 m was prescribed as the initial condition, and as Dirichlet boundary conditions

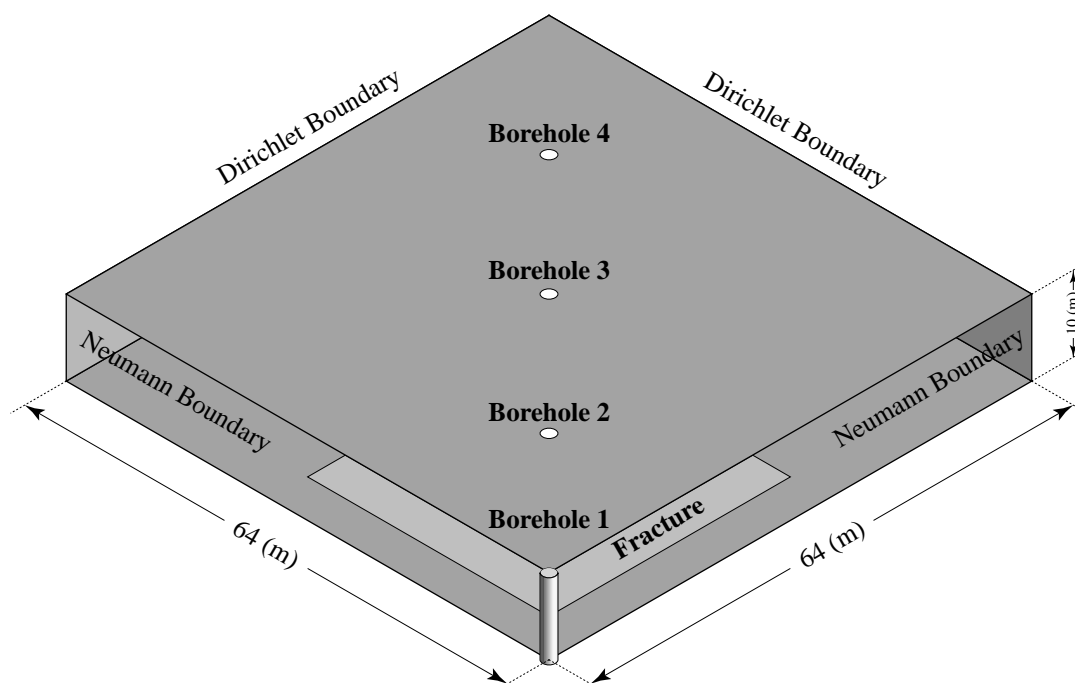


Figure 8-14 Sketch of the upper right-hand quarter of the hypothetical aquifer used to study the behaviour of a fracture in a Karoo aquifer.

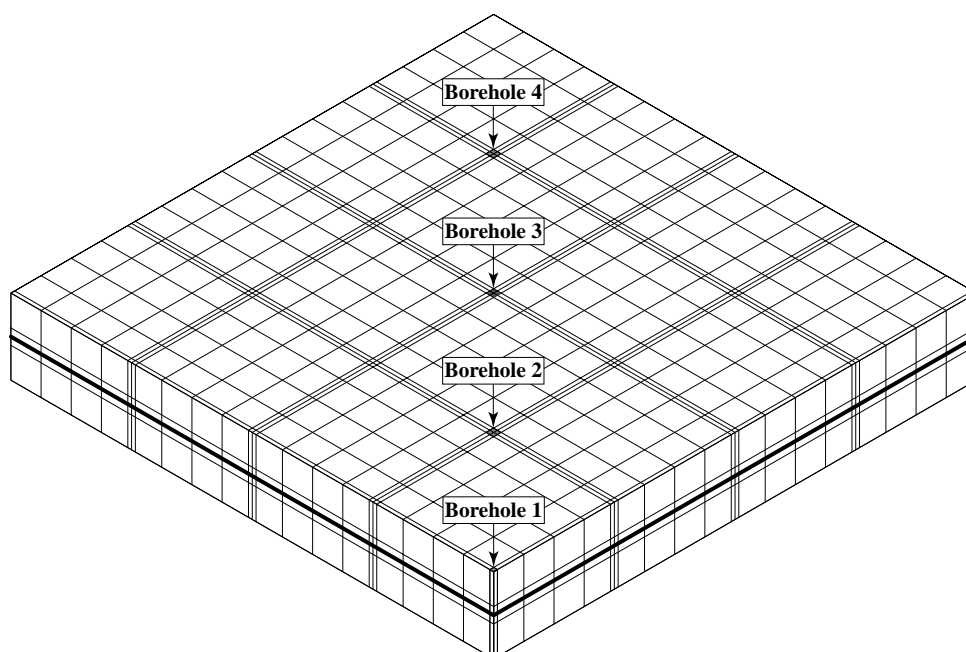


Figure 8-15 The three-dimensional finite element grid used to study the behaviour of the hypothetical aquifer, in Figure 8-14.

Table 8-3 Distances of the nodes (from the bottom up), in the vertical plane of the finite element grid in Figure 8-15.

Distance (m)	0,0	4,5	4,95	4,995	5,005	5,05	5,5	10,0
--------------	-----	-----	------	-------	-------	------	-----	------

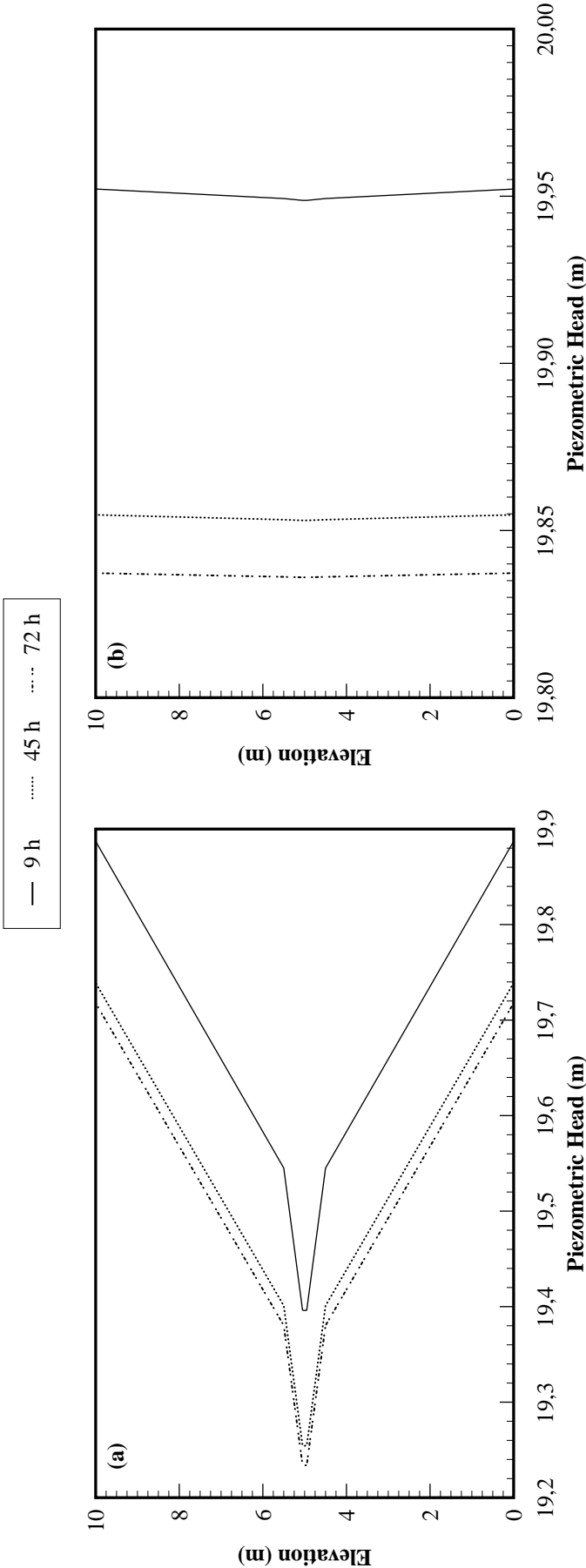


Figure 8-16 Changes in the piezometric heads of the hypothetical aquifer with elevation, at distances of (a) 0,5 m and (b) 16 m from the borehole, for different times.

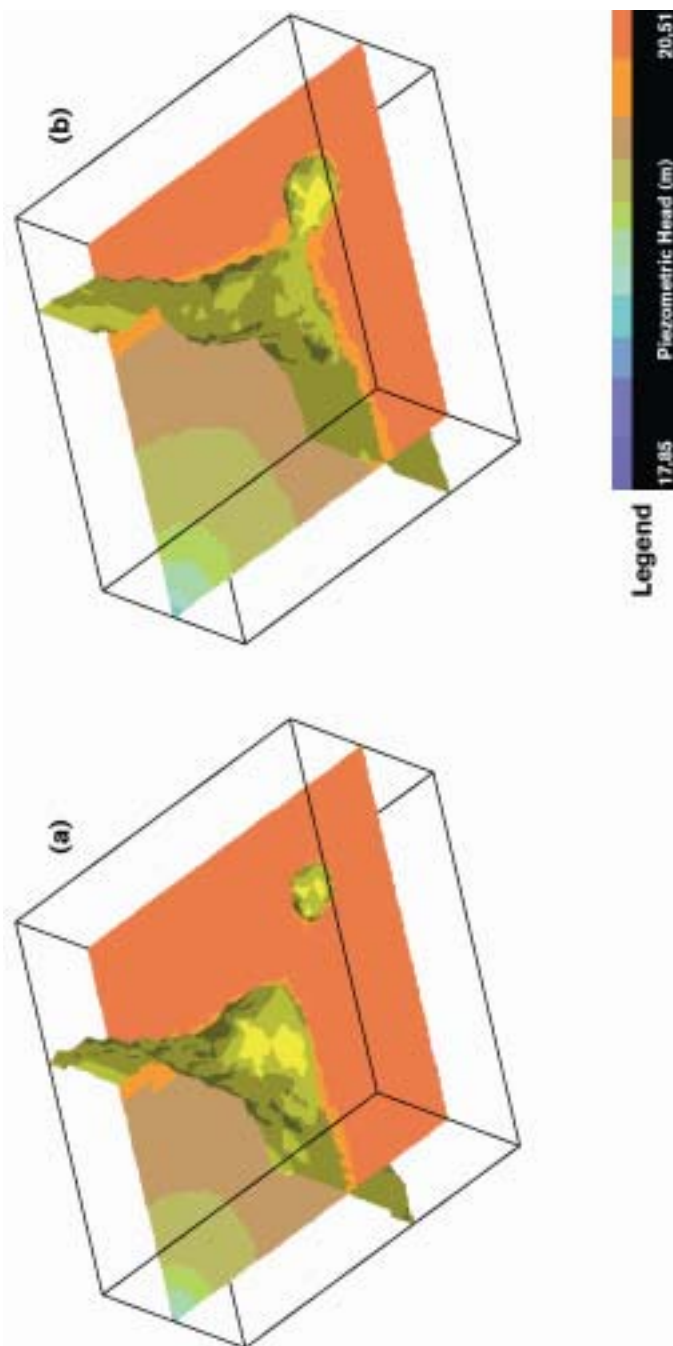


Figure 8-17 Volumetric visualization of the 19.8 m piezometric contour in the aquifer when pumping boreholes 1, 3 and 4 simultaneously, after (a) 8 h and (b) 72 h.

Table 8–4 Hydraulic conductivity and specific storativity values of the rock matrix and fracture, used in the numerical model.

	Hydraulic Conductivity (ms ⁻¹)		Storativity (m ⁻¹)
	Horizontal Direction	Vertical Direction	
Rock matrix	1,157 410·10 ⁻⁶	2,314 810·10 ⁻²	1,0·10 ⁻⁴
Fracture	1,157 410·10 ⁻⁴	2,314 810·10 ⁺⁰	1,0·10 ⁻⁵

on the two outer sides of the aquifer, while zero-flux Neumann conditions were prescribed on the inner sides, the top and the bottom of the aquifer. It was also assumed that the aquifer contains 13 symmetrically placed boreholes, four of which are shown in Figure 8–14 and Figure 8–15. The maximum discharge rate of the boreholes had to be fixed at (25%) m³ h⁻¹ to prevent unrealistic drawdowns in the aquifer. All models considered in the study were run for a period of 72 h, with a time step of 9 h.

8.5.2 Results and Discussion

The first case considered was, where only Borehole 1, at the centre of the aquifer, is pumped. The results, in Figure 8–16(a), show that there is a smooth transition in the piezometric head from the fracture to the matrix, and that the piezometric head in the fracture is considerably less than in the matrix. Moreover, the differences increase continuously and smoothly with time, in complete agreement with the observations on the Campus Test Site, in Figure 6–13. There can thus be little doubt that Program KARO is able to simulate one of the main properties of Karoo aquifers, and that the approximation used for discontinuous coefficients is excellent for practical purposes.

An interesting feature of the piezometric heads, in Figure 8–16, is that the major drawdowns occur along the fracture's plane. It is only when the fracture is sufficiently dewatered that flow from the matrix becomes important, as envisaged in Section 6.4.1. *One cannot, therefore, neglect vertical flow in aquifers that contain a horizontal fracture.*

A better view of what happens in the plane of the fracture can be obtained from Figure 8–17. This figure, drawn with Vis-5D, represents a volumetric visualization of the 19,8 m piezometric head contour, when boreholes 1, 3 and 4 are pumped simultaneously. Notice in particular that even Borehole 4, which is situated in the rock matrix itself, withdraws water from the fracture plane.

Another conclusion, supported by the results in Figure 8–17, is that flow in the fracture is essentially radial. However, the main flow occurs in the rock matrix and is vertical. This behaviour clearly supports the view that the matrix acts as the major storage unit in porous media with horizontal fractures, and that the fractures serve as conduits for water towards boreholes.



CHAPTER 9

MODELLING THE CAMPUS TEST SITE

9.1 INTRODUCTION

The success achieved with the simulation of the hypothetical aquifer with Program Karo in Chapter 8, made it easy to develop a three-dimensional numerical model for the Campus Test Site. Although the model can be used for a long-term simulation of the aquifer, the main purpose for its development was to try to simulate the results of the hydraulic tests described in Chapter 6, and to understand the behaviour of the aquifers on the Site.

The discussion below begins with a description of the methods used to calibrate and verify the model in Section 9.2. This is followed by a discussion of its application and the analyses of the hydraulic tests in Section 9.3. The major conclusions, derived from the simulations, are discussed in Section 9.4.

9.2 CALIBRATION AND VERIFICATION OF THE MODEL

9.2.1 The Finite Element Grid

The exact areal extent of the aquifers on the Campus Test Site are unknown, though it is known that the water levels in boreholes UO10 and UO21 do not respond to pumping from either boreholes UP15 and UP16. The first model of the aquifer was therefore based on the area of $144 \times 192 \text{ m}^2$, covered by the boreholes in Figure 5–15. However, the results indicated that this area is too small. The areal extent of the aquifer in the final model was therefore increased to $344 \times 392 \text{ m}^2$, by adding 100 m in each direction of the original area. The thickness of the aquifer was taken as 40 m, as discussed in Chapter 7.

The finite element grid, used for the model of the aquifer, is shown in Figure 9–1. The grid consisted of 33, 30 and 14 elements in the x -, y - and z -directions respectively. The elements in the xy -plane vary from very small near boreholes, to relatively large at the boundaries. The reason for this choice was to reduce the numerical errors in the Dirichlet line source approximation, especially near the perturbed boreholes.

The most prominent feature of the aquifer is the Mode I fracture at a depth of 21–23 m. Special care was therefore taken to represent the fracture accurately in the finite element grid. A set of two pencil elements, with vertical heights of 0,05 m, that follow the elevation of the fracture closely, was used to represent this feature. The sizes of the surrounding elements varied logarithmically in the vertical direction, as shown in Figure 9–1.

9.2.2 Calibration of the Model

The first step in the development of a numerical model for an aquifer is to calibrate the model. The main idea behind this procedure is to obtain better estimates for the hydraulic parameters, boundary and initial conditions of the specific aquifer, quantities that are usually only measured at a few points, and in many cases not at all. They must therefore be estimated by one method or another (Van Sandwyk *et al.*, 1992; Van Tonder *et al.*, 1986). These estimated values need, of course, not be representative of the aquifer. They are consequently substituted into the model and adjusted until the model reproduced a set of historic piezometric heads within an acceptable error.

Numerical solutions of the flow equation, obtained with the adjusted piezometric levels as initial conditions, usually display spikes, especially for the first few time steps. One method to avoid the spikes is to run a steady state version of the model with a set of observed piezometric heads as Dirichlet conditions, and use these new piezometric heads as the initial conditions for the model (Müller and Botha, 1986).

The correct approach in carrying out the calibration of a model is to adjust the estimated quantities across the finite element grid, until the model reproduces the given set of piezometric levels within an acceptable error. However, this can be a daunting task in a three-dimensional model for Karoo aquifers with

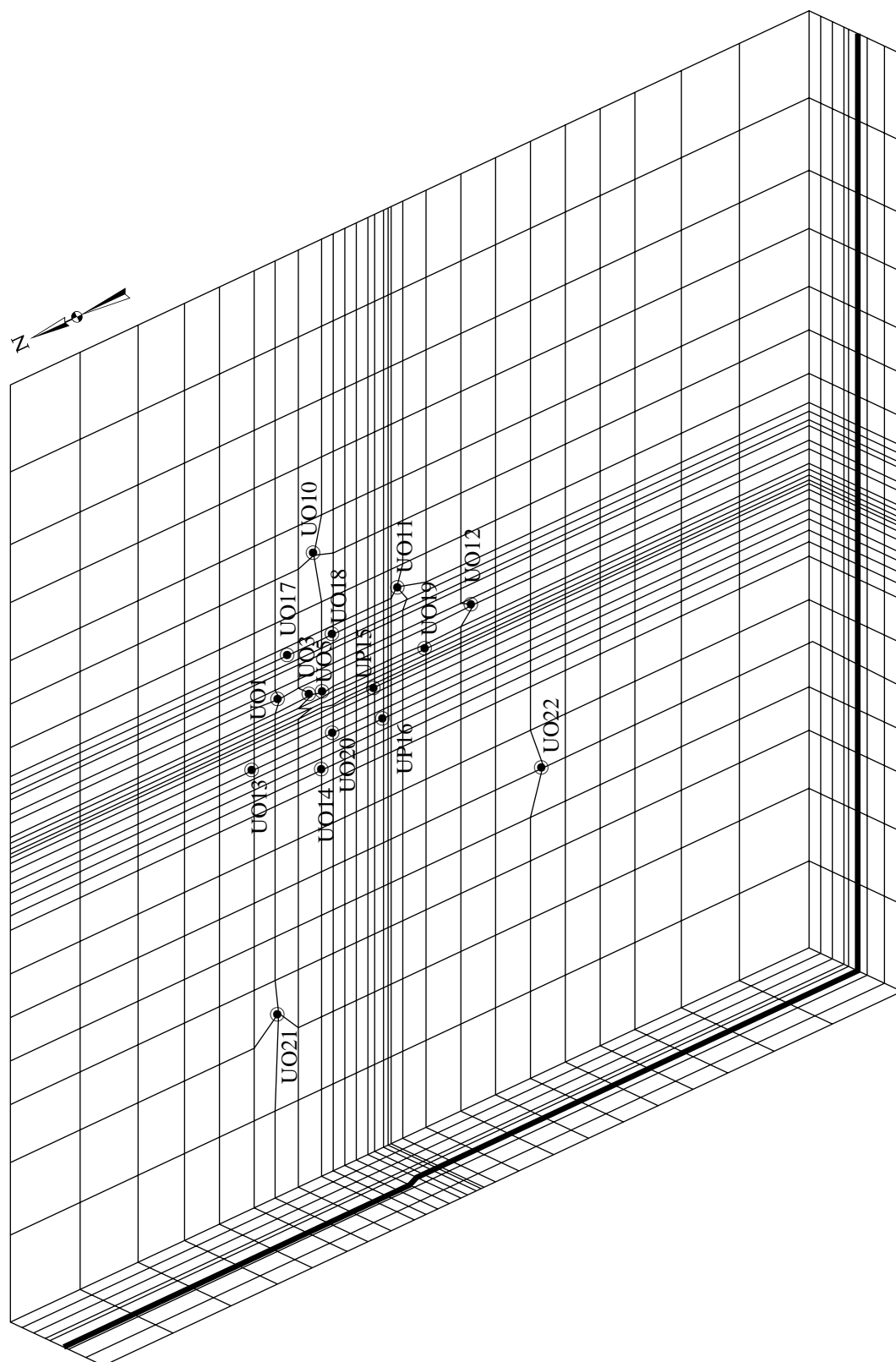


Figure 9-1 Finite element grid used in modelling the aquifer on the Campus Test Site.

their complex geometries. The following method was consequently used to calibrate the present model. Values of the hydraulic conductivity tensor and specific storativities were computed for each of the horizontal layers in Figure 9–1, as described in Section 7.3.4, and assigned to the nodes of the finite element grid. The observed piezometric heads in Table 7–2 and water levels in all the boreholes were then used to estimate piezometric levels for the layers. Zero fluxes on the top and bottom sides of the aquifer and the estimated heads on the four vertical sides of the aquifer were then prescribed as Neumann and Dirichlet boundary conditions for a steady state model of the site. The Dirichlet heads and hydraulic conductivities were then adjusted until the computed piezometric heads fitted the observed piezometric heads in Table 7–2 satisfactorily. This yielded the set of hydraulic parameters in Table 9–1, which were consequently used in the model.

Table 9–1 Principal components of the hydraulic conductivity tensor and storativities used in modelling the Campus Aquifer.

Depth Below Soil Surface (m)	Hydraulic Conductivity (m s^{-1})			Storativity (m^{-1})
	K_x	K_y	K_z	
0,00	$1,034\ 650.10^{-06}$	$1,034\ 650.10^{-06}$	$1,000\ 000.10^{-08}$	$1.0.10^{-04}$
5,00	$1,034\ 650.10^{-06}$	$1,034\ 650.10^{-06}$	$1,000\ 000.10^{-09}$	$1.0.10^{-04}$
10,00	$4,990\ 425.10^{-06}$	$1,034\ 650.10^{-06}$	$1,000\ 000.10^{-10}$	$1.0.10^{-04}$
15,00	$7,191\ 166.10^{-08}$	$5,234\ 120.10^{-08}$	$1,947\ 600.10^{-11}$	$1.0.10^{-04}$
17,00	$3,609\ 766.10^{-07}$	$1,987\ 876.10^{-07}$	$1,117\ 000.10^{-11}$	$1.0.10^{-04}$
20,00	$3,280\ 400.10^{-06}$	$1,208\ 450.10^{-06}$	$1,117\ 000.10^{-10}$	$1.0.10^{-04}$
20,75	$3,428\ 200.10^{-05}$	$1,234\ 243.10^{-05}$	$4,638\ 300.10^{-09}$	$1.0.10^{-04}$
20,95	$3,428\ 200.10^{-04}$	$1,234\ 243.10^{-04}$	$4,638\ 300.10^{-09}$	$1.0.10^{-04}$
21,00	$3,428\ 200.10^{-04}$	$1,234\ 243.10^{-04}$	$4,638\ 300.10^{-09}$	$1.0.10^{-04}$
21,05	$3,428\ 200.10^{-04}$	$1,234\ 243.10^{-04}$	$4,638\ 300.10^{-09}$	$1.0.10^{-04}$
21,25	$3,428\ 200.10^{-05}$	$1,234\ 243.10^{-05}$	$4,638\ 300.10^{-09}$	$1.0.10^{-04}$
22,00	$3,747\ 300.10^{-07}$	$1,987\ 600.10^{-07}$	$9,638\ 300.10^{-10}$	$1.0.10^{-04}$
25,00	$5,638\ 300.10^{-07}$	$2,677\ 760.10^{-07}$	$9,638\ 300.10^{-10}$	$1.0.10^{-04}$
32,50	$6,521\ 375.10^{-08}$	$3,566\ 660.10^{-08}$	$9,830\ 000.10^{-10}$	$1.0.10^{-04}$
40,00	$7,172\ 000.10^{-08}$	$5,223\ 330.10^{-08}$	$9,830\ 000.10^{-10}$	$1.0.10^{-04}$
Fracture	$9,000\ 000.10^{-03}$	$9,000\ 000.10^{-03}$	$9,000\ 000.10^{-03}$	$1.0.10^{-05}$

An attempt was made to adjust the specific storativity values with the hydraulic conductivity values during the calibration of the model. However, it turned out that the model was very sensitive to changes in the specific storativity. This behaviour of the model, and the fact that the parameters in Table 9–1 yielded an excellent fit to the observed piezometric heads in Table 7–2, suggested that the specific storativities be kept at their prescribed values.

9.2.3 Verification of the Model

The first step taken to verify the model was to try to simulate the piezometric levels observed in Piezometer UO18 by hand during the constant rate test performed on 1995–06–01 with UP 15 as the perturbed borehole, discussed in Section 6.3.5. The calibrated piezometric heads were used as initial conditions and to prescribe Dirichlet boundary conditions on the four vertical sides, while zero-flux Neumann boundary conditions were prescribed on the top and bottom of the aquifer. The results, shown in Figure 9–2, are quite satisfactory, except for Aquifer 1. However, this could have been expected, as this phreatic aquifer is represented by a confined aquifer in the model.

Since the boundaries of the aquifer are not known, it was necessary to try to determine to what extent the choice of boundary conditions can influence the piezometric heads simulated with the model. The hydraulic test performed on 1995–05–15 with UP16 as the perturbed borehole, also discussed in Section 6.3.5, was used for this purpose. The calibrated piezometric heads were again prescribed as initial and Dirichlet boundary conditions on the four vertical sides of the aquifer, with zero-flux Neumann boundary conditions on the top and bottom sides in the first test. The simulated and observed piezometric heads for piezometers UO1 and UO18 are compared graphically in Figure 9–3. The fit between the two sets of heads is quite acceptable, except for the piezometric head of Aquifer 2 in Piezometer UO18.

There are essentially two mechanisms that can cause the differences between the observed and simu-

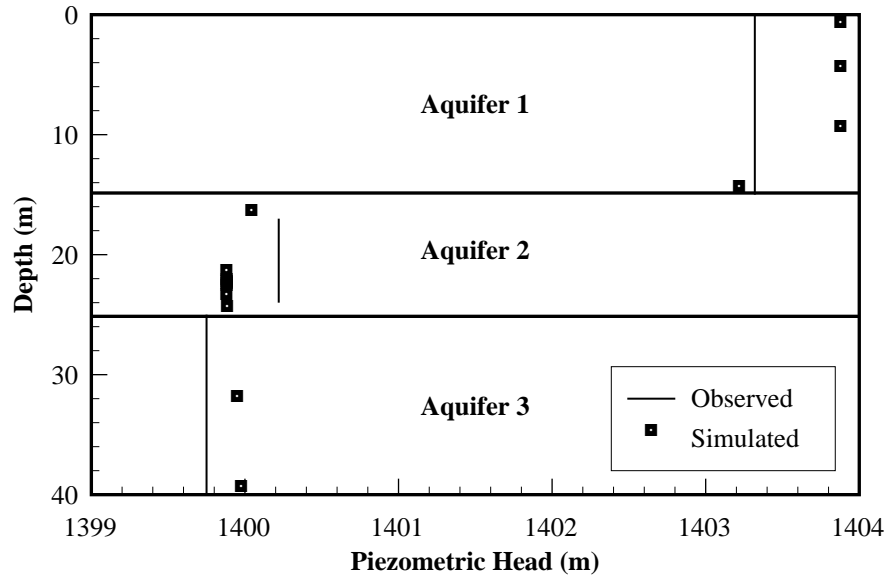


Figure 9-2 Comparison of the observed and simulated piezometric heads in Piezometer UO18, for the constant rate test performed on 1995-06-01 with UP 15 as the perturbed borehole.

lated piezometric heads in Figure 9-3.

- (a) The Dirichlet boundary conditions on the four vertical sides of the aquifer allow too much water to flow into the aquifer.
- (b) The hydraulic parameters of the model do not represent the actual hydraulic parameters accurately, especially near Piezometer UO18.

The first mechanism is ruled out by two observations. The first is the excellent fit between the observed and simulated heads for Aquifer 3 in Piezometer UO18 and the good fits for Aquifer 1, in both piezometers UO1 and UO18. The second is that the observed and simulated piezometric heads of Aquifer 2 in Piezometer UO18 do not diverge as one would expect if the model feeds too much water into the aquifer. Nevertheless, it was still thought worthwhile to repeat the simulation with zero-flux Neumann boundary conditions on the four vertical sides of the aquifer. This change in boundary conditions did improve the fit of the observed and simulated piezometric heads for Aquifer 1, while still keeping the excellent fit in Aquifer 3, as shown in Figure 9-4. This result suggests that Neumann boundary conditions would be more appropriate for the model. However, the convergence of the observed and simulated piezometric heads for Aquifer 2 shows that the model feeds too little water into Aquifer 2. Moreover, the improvement in the fit of the piezometric heads of Aquifer 1 is suspect, since one would not expect the model to represent this phreatic aquifer accurately. Inaccuracies in the hydraulic parameters, particularly the specific storativity, thus seem to be the main reason for the difference between the observed and simulated piezometric heads in Aquifer 2.

The correct procedure would have been to recalibrate the model with both Neumann and Dirichlet boundary conditions to see which type of boundary would be the best. However, the experience gained in calibrating the model indicated that this will not be a very worthwhile exercise without more detailed information on the hydraulic parameters and piezometric heads. Moreover, it would be surprising to find a perfect fit between the simulated and observed piezometric heads, since the latter represents averages over the thickness of the three aquifers, while the simulated heads are point values. The simulations of hydraulic tests discussed below were therefore all performed with the hydraulic parameters in Table 9-1 and the calibrated piezometric heads as initial and Dirichlet boundary conditions.

9.3 SIMULATION OF HYDRAULIC TESTS

9.3.1 The Constant Rate Test on Borehole UP16

The first attempt to simulate the behaviour of the Campus Test Site aquifer with Program KARO was to analyse the hydraulic test on Borehole UP16, described in Section 6.3.5. Although the observed piezometric heads in piezometers UO1 and UO18 at the start of the test differed somewhat from those used in calibrating the model, it was not thought worthwhile to recalibrate the model. The initial and boundary conditions,

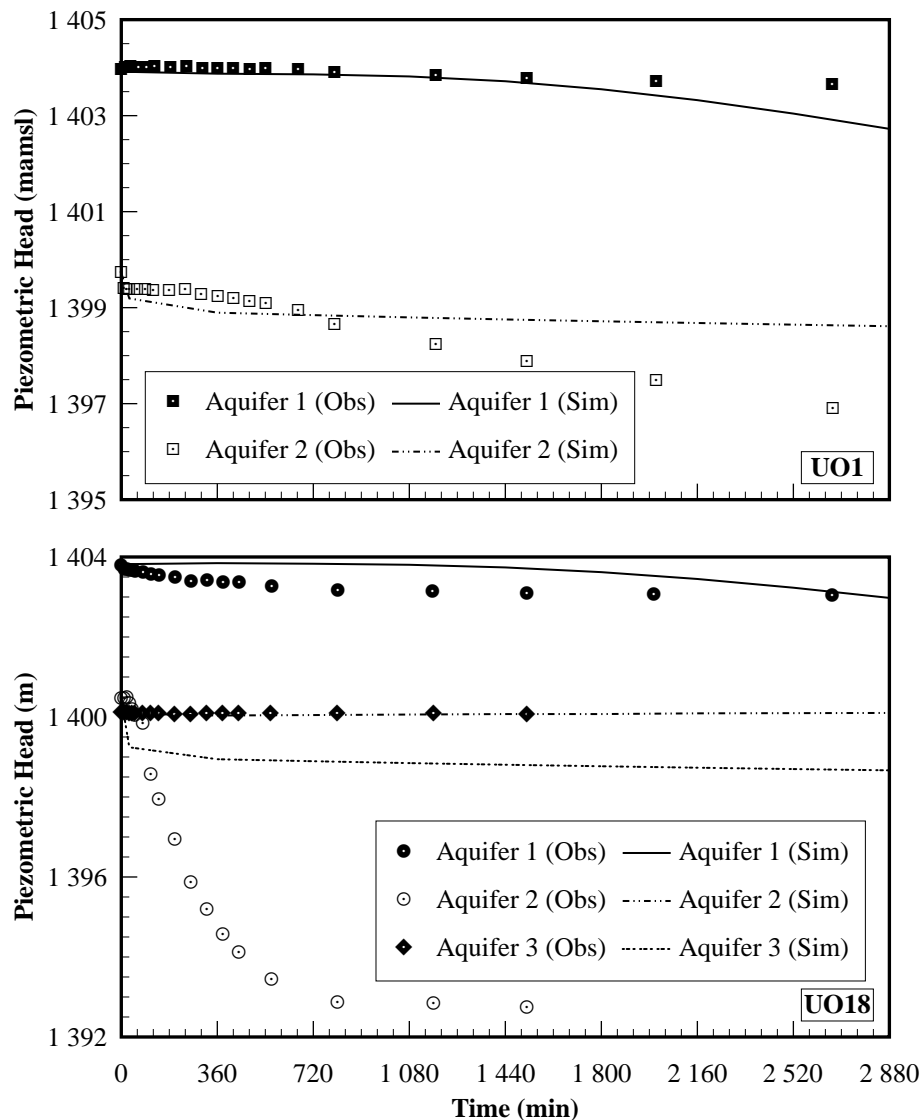


Figure 9-3 Comparison of the observed and simulated piezometric heads in piezometers UO1 and UO18, for the hydraulic test of 1995-05-15 on Borehole UP16, with Dirichlet boundary conditions on the four vertical sides of the aquifer.

derived from the steady state model of Section 9.2.2, were consequently also used in the simulation. The observed and simulated piezometric heads in piezometers UO1 and UO18 are compared graphically in Figure 9-5, at 0.5 and 1 h after the start of the test.

The 'tongue-shape' of the simulated piezometric heads near the fracture in Figure 9-5 may create the impression that there exists a considerable difference between the simulated and computed piezometric heads. However, a closer inspection of the graphs shows that the actual shifts in the observed and computed piezometric heads are practically the same. The reason for the tongue-shape is that the piezometers measure the piezometric heads over the full width of the aquifers, and not at the position of the nodes in the finite element grid. The overall fit between the observed and simulated piezometric heads, therefore, can be considered excellent, especially if one keeps in mind that the model represents Aquifer 1 as a confined aquifer.

Another conclusion that can be drawn immediately from the graphs in Figure 9-5, is that the pumping affected the piezometric heads in the fracture and Aquifer 2 more than in the other two aquifers. This behaviour confirms the field observations which indicated that fractures are the main conduits of water in Karoo aquifers.

An interesting feature in the graphs of the observed water levels and computed piezometric heads for boreholes UP16 and UO5, in Figure 9-6, is the close relation between the piezometric heads in the fracture and the observed water levels. This suggests that the water levels in open boreholes are not representative of any of the aquifers on the Campus Test Site, but represent an average of the piezometric heads in all the

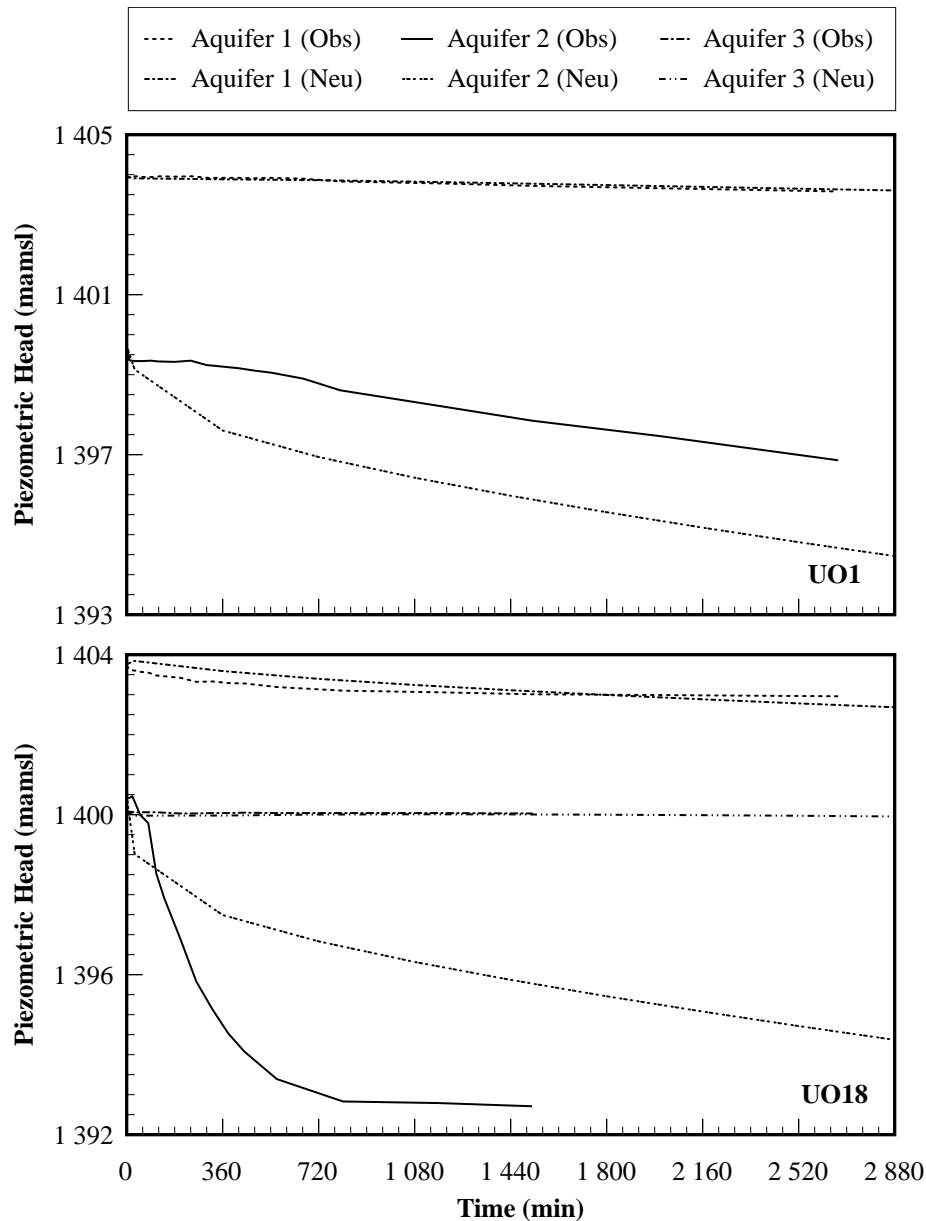


Figure 9-4 Comparison of the observed and simulated piezometric heads in piezometers UO1 and UO18, for the hydraulic test of 1995-05-15 on Borehole UP16, with zero-flux Neumann boundary conditions on the four vertical sides of the aquifer.

aquifers, weighted in favour of the piezometric head in the fracture. Hydraulic parameters derived from observations of water levels in open boreholes in Karoo aquifers, are therefore more representative of the fractures than the rock matrix, which serve as the main storage units. This dependence may have been responsible for the unrealistic storativity values observed by Kirchner *et al.* (1991).

A very interesting aspect of the results in Figure 9-6 is the behaviour of the piezometric heads near the production borehole, UP16. According to the model, water was not only withdrawn here from Aquifer 2, but also from Aquifers 1 and 3, in contrast to Borehole UO5 where water was withdrawn mainly from Aquifer 2. This again confirms that bedding-parallel fractures serve as the main conduits of water to boreholes in Karoo aquifers.

9.3.2 Simulation of a Short-term Constant Rate Test on Borehole UP15

The previous results clearly have very important consequences for the management of Karoo aquifers. It was thus thought worthwhile to repeat the analysis with data from another constant rate test to ensure that the results are repeatable. In this test, also discussed in Section 6.3.1, Borehole UP15 was pumped at a rate of

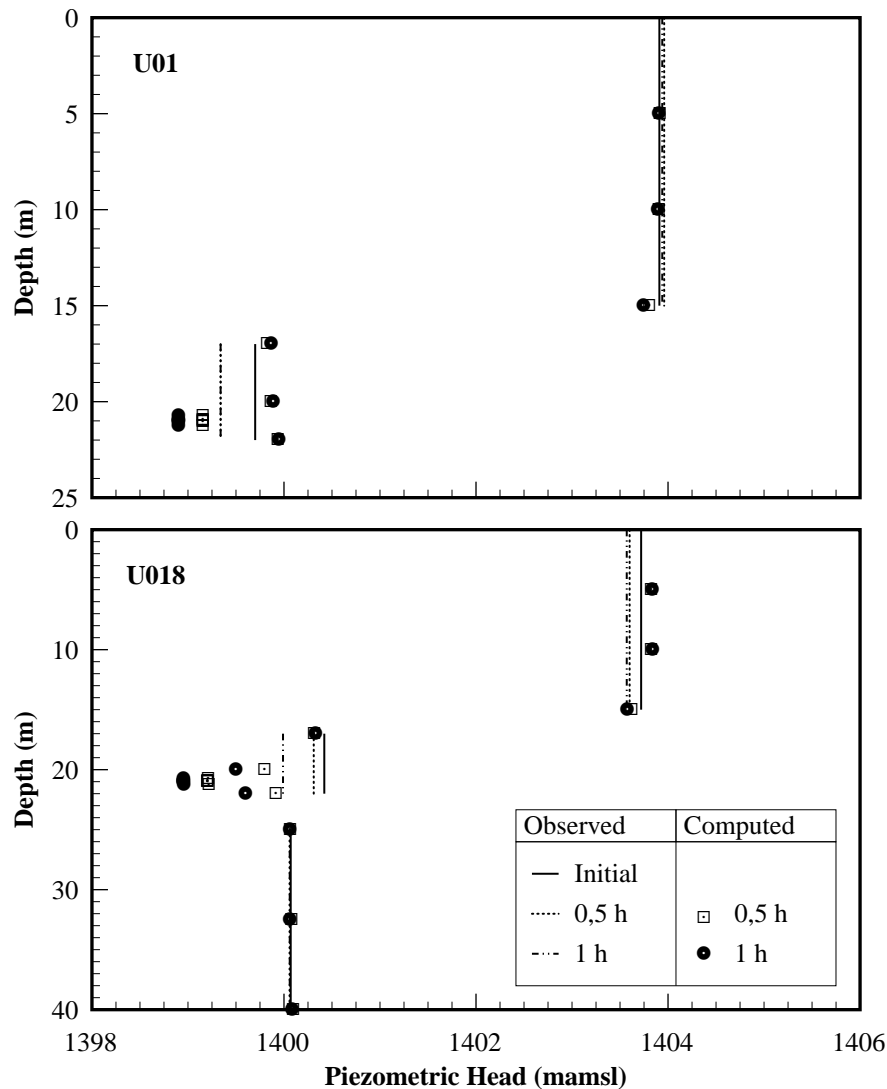


Figure 9-5 Comparison of the observed and simulated piezometric heads in piezometers UO1 and UO18, after pumping Borehole UP16 for 0,5 and 1 h.

9,72 m³ h⁻¹. The results, shown in Figure 9-7, are identical to those in Figure 9-5.

It is important to remember that the piezometer boreholes UO1 and UO18 are not connected to the fracture as shown in Figure 5-31. The considerable drop in the piezometric heads along the plane of the fracture in Figure 9-5 and Figure 9-7 thus confirms the results of Section 8.5.2, which showed that water will be preferentially withdrawn along the plane of the fracture, even in areas away from the fracture. However, water is withdrawn from all three aquifers near the discharging borehole, although the major drawdowns still occur within the fracture. The possibility thus exists that the fracture may be completely dewatered near a production borehole in a Karoo aquifer, with the result that the borehole will not be able to sustain its yield. This behaviour of the fracture may contribute to the phenomenon of *'the pump that sucks air'*, so often heard from people who depend on Karoo aquifers for their daily supply of water.

The preferential dewatering of the aquifer along the plane of the fracture implies that the vertical gradient of the piezometric head in the rock matrix must decrease with horizontal distance from the discharge point, as illustrated in Figure 9-8. The vertical flux of water towards the fracture must thus decrease with distance from the discharging borehole. There will therefore be considerably more water near the discharging borehole than farther away. A horizontal two-dimensional model can only accommodate this excess of water by adjusting its storativity for the aquifer. This explains the dependence of the storativities on the inverse distance from the perturbed borehole in Figure 6-5. Storativities derived from fitting water levels in open boreholes to the Theis curve are thus simply not representative of a Karoo aquifer.

Another interesting result in Figure 9-8 is the behaviour of the piezometric head in the sandstone,

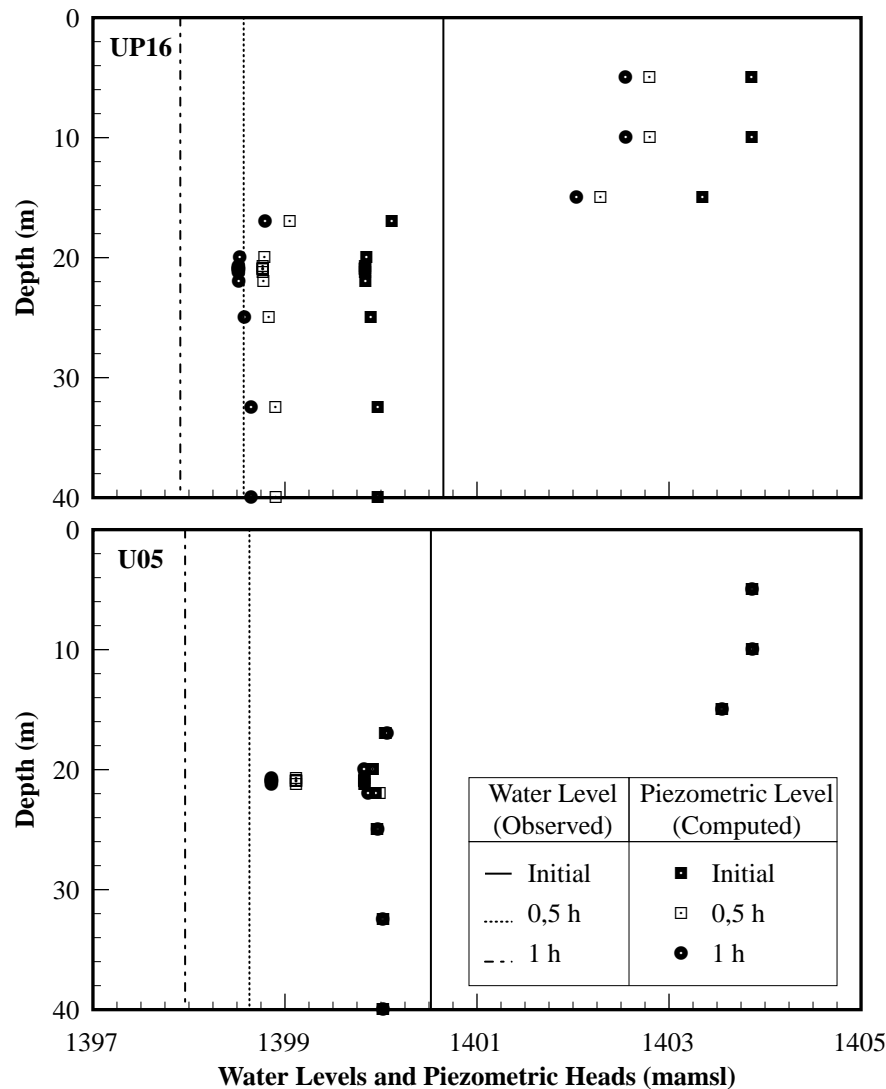


Figure 9-6 Comparison of the observed water levels and simulated piezometric heads, in boreholes UP16 and U05, after pumping Borehole UP16 for 0,5 and 1 (h).

compared to that of the fracture. The shape of the drawdown cone in the fracture remains constant with time, although the piezometric heads decrease with time. The drawdown cone in the sandstone layer, on the other hand, widens and deepens with time, and approaches the drawdown cone of the fracture. The borehole thus tends to dewater the entire aquifer near the discharging borehole, but only the plane of the fracture farther away. This behaviour was also observed in the preliminary model of the aquifer in Section 8.5.2.

It is common knowledge that the depth and width of the drawdown cone caused by a discharging borehole, increase with increasing discharge rates. The question thus arises: how will the drawdown cone in the fracture behave with increasing discharge rates? The model for the constant rate test on Borehole UP15 was therefore rerun with discharge rates of $3,6 \text{ m}^3 \text{ h}^{-1}$ and $7,2 \text{ m}^3 \text{ h}^{-1}$. The results, shown in Figure 9-9, indicate that the cone in the sandstone behaved as expected. The cone in the fracture, on the other hand, kept its shape, but its piezometric heads decreased with increasing discharge rates, just as it did in Figure 9-8.

The behaviour of the fracture's drawdown cone in Figures 9-8 and 9-9 can be explained briefly as follows. Flow in the fracture is mainly restricted to its horizontal plane, since its aperture is limited. The drawdown cone in the fracture will therefore keep its shape, provided that the surrounding rock matrix can supply it with enough water to compensate for the water lost through the pump. However, this rate will depend on the piezometric pressure of the rock matrix. A point may thus be reached where the rock matrix cannot supply enough water to the fracture, with the result that the fracture will begin to dewater. The numerical model for the Campus Test Site thus agrees with the view expressed in Section 6.4.1, that a fracture can only support a limited discharge rate determined by its piezometric pressure and that of the

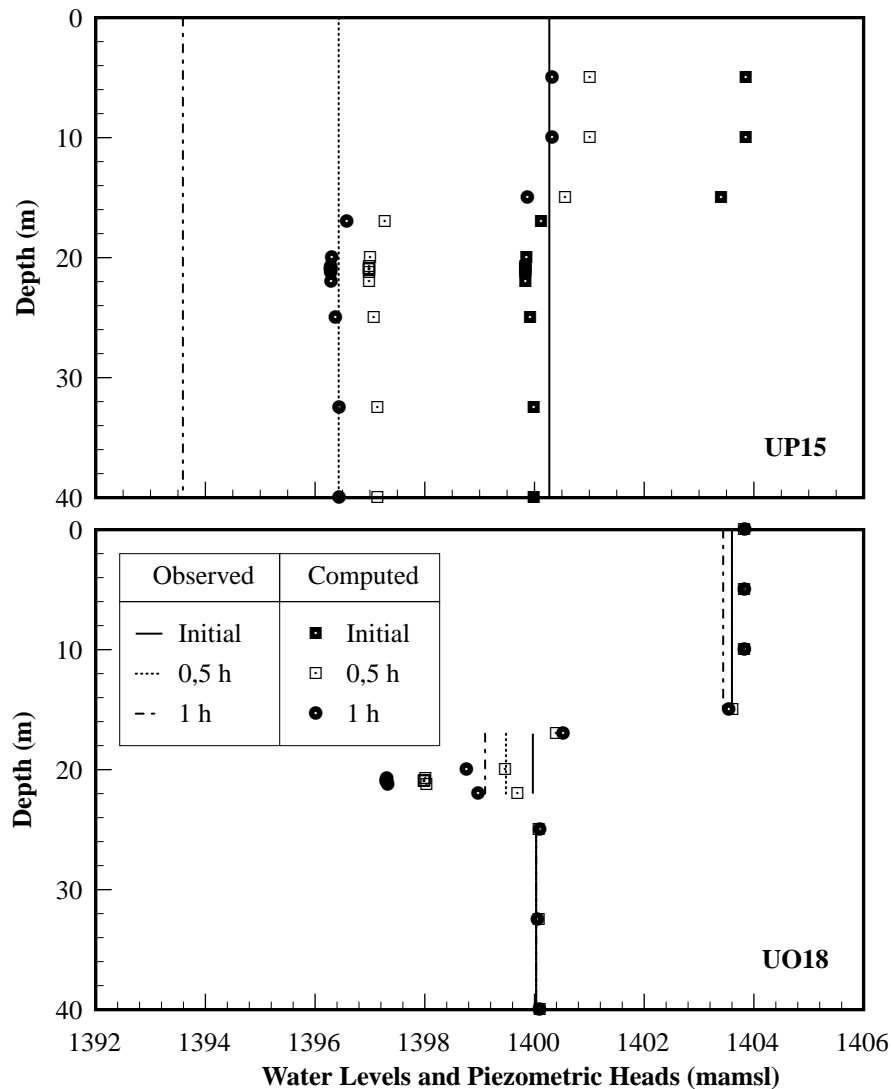


Figure 9-7 Comparison of the observed water levels and simulated piezometric heads in Borehole UP15 and Piezometer UO18, after pumping Borehole UP15 for 0,5 and 1 h at a rate of $9,72 \text{ m}^3 \text{ h}^{-1}$.

surrounding rock matrix. *There is thus a limit to the rate at which a borehole in a Karoo aquifer can be pumped*, as illustrated by the constant rate tests, discussed in Section 6.3.5.

9.3.3 Simulation of a Recovery Test on Borehole UP16

There is little doubt that Program Karo is able to simulate the major properties of the aquifers on the Campus Test Site, observed during the drawdown phases of various constant rate tests. The question that now remains to be answered is: can it also simulate the behaviour during the recovery phase of such a constant rate test? Unfortunately, no measurements were taken of the recovery phases of the constant rate tests discussed above. Simulation of the recovery phase was therefore based on the first step of a multi-rate test, in which Borehole UP16 was pumped at $11,88 \text{ m}^3 \text{ h}^{-1}$, for an hour, and then allowed to recover for an hour.

The first step in the simulation was to compute the piezometric heads in the aquifers with Program Karo for one hour. These values were then used as new initial conditions and the program was re-run with a discharge rate of $0 \text{ m}^3 \text{ h}^{-1}$. Since no measurements were taken of the piezometric levels in piezometers UO1 or UO18 during the test, the results are compared with the water levels observed in Borehole UP16, in Figure 6-10.

The first impression of the comparison in Figure 9-10 is that the fit is rather poor. However, it must be remembered that the water levels in open boreholes are always less than the simulated piezometric heads in the fracture, as shown in Figure 9-6 and Figure 9-7. Moreover, the verification of the model in Section 9.2.3,

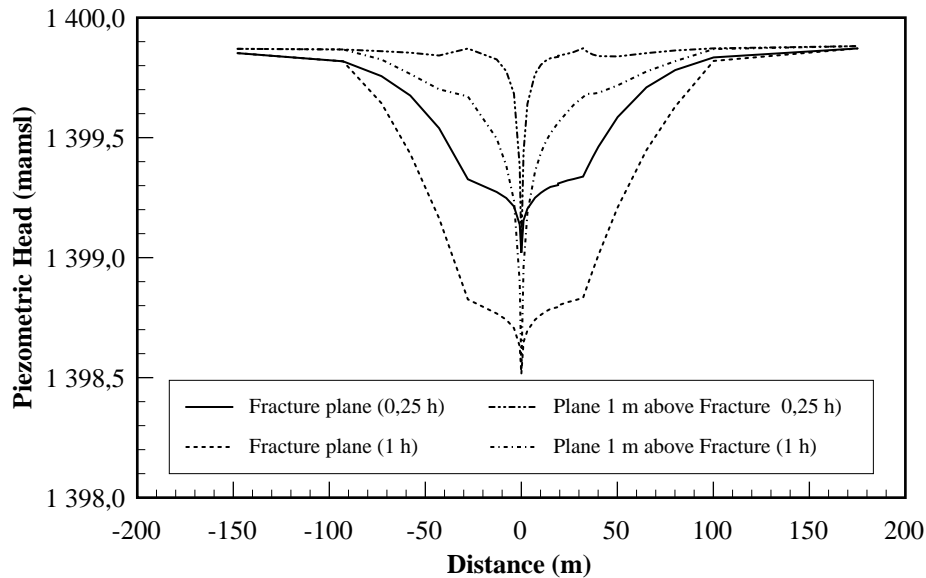


Figure 9-8 Piezometric heads in the fracture plane and a plane 1 (m) above the fracture in the sandstone layer, across a vertical cross-section through Borehole UP16, after pumping Borehole UP16 at $3,6 \text{ m}^3 \text{ h}^{-1}$ for 0,25 and 1 h.

has already shown that there may be small inaccuracies in the calibrated S_0 -values, which will enhance the differences. The fit between the simulated piezometric heads and the observed water levels in Figure 9-10, is therefore acceptable. The parallelism of the two recovery curves, incidentally, suggests that the calibrated S_0 -values are too large.

9.3.4 Linear Flow

The discussion in Section 6.7 shows that the predominant direction of flow in a stressed Karoo aquifer is vertical and that the flow is linear. The main distinction between such an aquifer and one subject to radial flow is that the drawdown in a perturbed borehole will be a function of the square root and not the logarithm of time. The ultimate test of the present model will thus be to see if it can reproduce this behaviour too. That this is indeed the case, can be seen from the graphs of the simulated piezometric heads and observed water levels in Figure 9-11. There can thus be little doubt that Program KARO is able to simulate all the major characteristics of Karoo aquifers.

From the mathematical point of view the simulated piezometric heads in Figure 9-11 are nothing more than the solution of the differential equation for groundwater flow (Equation 7.1). It is well-known that the boundary conditions determine the exact value of the solution, at any point in space and time, while the domain determines the geometrical shape of the solution. There can thus be no doubt that the geometric model of the domain in Figure 9-1, the associated hydraulic parameters and the prescribed boundary conditions, represent the three aquifers on the Campus Test Site adequately. A more important conclusion, though, is that the linearity of flow is caused by the internal geometry of the site. *It will therefore be futile to try to analyse data from Karoo aquifers with a model that does not take the aquifer's geometry into account.*

9.4 CONCLUSIONS

The most important conclusion of the numerical model for the Campus Test Site is that the physical behaviour of the aquifers is determined completely by the internal geometry of the Site. It is thus imperative that realistic models for Karoo aquifers should take this geometry into account, otherwise it will simply degenerate into a phenomenological model. Phenomenological models can, as the name implies, be quite useful in systemizing information on a given phenomenon, but cannot represent the physics of the phenomenon accurately (witness the history of particle physics). It would thus be dangerous, and wrong, to use a phenomenological model to manage or predict the future behaviour of an aquifer.

The geometry of Karoo aquifers that emerged from the discussions in Chapters 3 to 5 can, admittedly, be quite complex. However, the numerical model for the Campus Test Site indicates that it may not be neces-

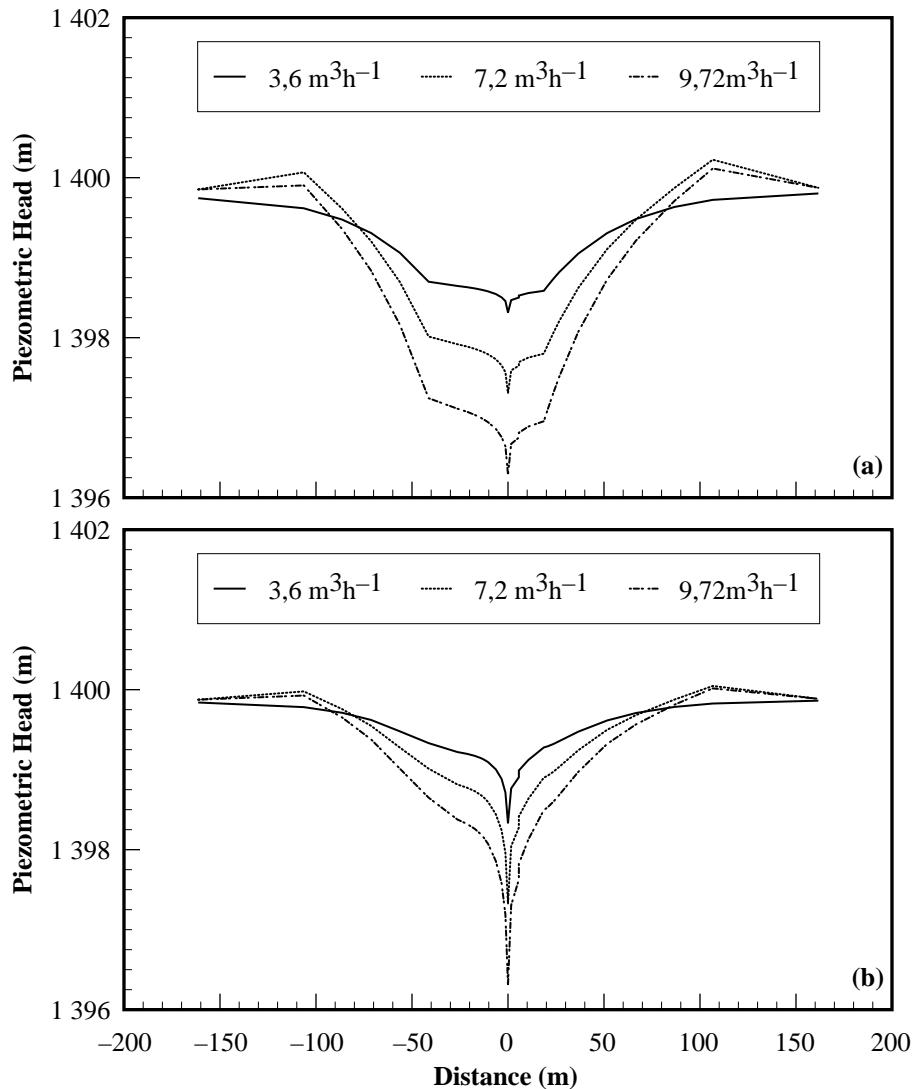


Figure 9-9 Piezometric heads in (a) the fracture, and (b) a plane 1 m above the fracture, across a vertical cross-section through Borehole UP15, after pumping Borehole UP15 at rates of 3,6, 7,2 and 9,72 m³ h⁻¹ for 1 h.

sary to know this geometry and variations in the physical properties of the constituent formations in detail. What one needs for a successful model of a Karoo aquifer, is a good knowledge of the distribution of the major geological formations within the aquifer, and the geometry of the fractures. The model, however, should be three-dimensional.

The distribution of geological formations within the aquifer can be determined directly from observations during the drilling of boreholes, and thus does not present insurmountable difficulties for the development of such a model. The determination of the fracture geometry is, unfortunately, not that easy. Indeed, it seems that there exist only two methods today that can be used for this purpose—core-boreholes and acoustic scanner surveys, both of which can be expensive. However, the present model for the Campus Test Site would not have been as successful, were it not for the information on the fracture geometry gained from the core-boreholes drilled by the Department of Water Affairs and Forestry. Attention should therefore be given to the development of more practical methods with which the geometry of the fractures can be determined.

Another important result of the present model is that the water levels in open boreholes represent an average of the piezometric heads in the fracture and surrounding rock matrix, weighted in favour of the piezometric head in the fracture. Observations of water levels in open boreholes are therefore not representative of the piezometric pressures in the multi-layered Karoo aquifers. Hydraulic parameters and other information derived from such observations, may thus be meaningless unless some provision is made for the geometry of the aquifers. The only appropriate method to study the behaviour of these aquifers is to install

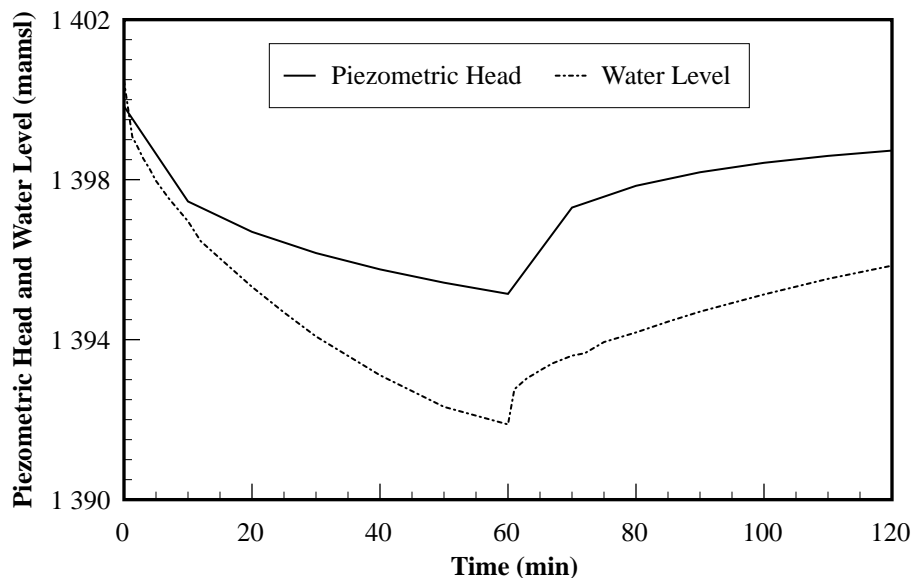


Figure 9-10 Comparison of the simulated piezometric heads, at the centre of the fracture, and the water levels in Borehole UP16, for the first step of a multi-rate test as a function of the time.

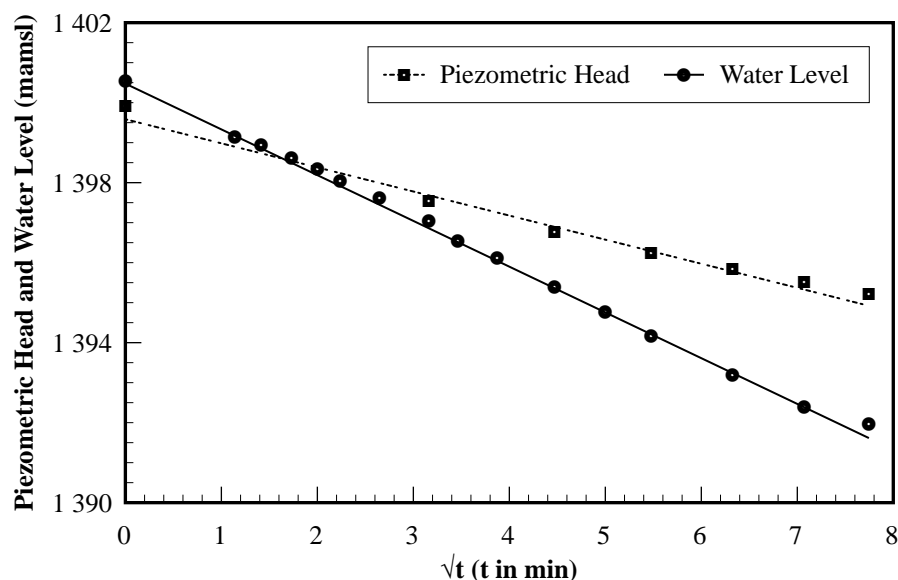


Figure 9-11 Comparison of the simulated piezometric heads, at the centre of the fracture, and the water levels in Borehole UP16, for the first step of a multi-rate test as a function of \sqrt{t} .

piezometers.

Two properties of Karoo aquifers that played a very important role in the model for the Campus Test Site, but have often been neglected in the past, are: (a) the ability of Karoo formations to store and yield water, and (b) the rates at which boreholes can be pumped. The latter property is of particular importance, since it can easily lead to the deformation of the water-yielding fractures. In fact, there are indications that the procedures commonly used in hydraulic tests may even damage the fractures. It may thus be necessary to devise new approaches for hydraulic tests in Karoo aquifers. The two properties are obviously also of the utmost importance for the management and operation of well-fields in these aquifers. Special attention should, therefore, be given to them when developing Karoo aquifers for water-supply purposes.

There are two aspects of the behaviour of Karoo aquifers not accounted for in the model for the Campus Test Site. The first is that no provision has been made for unsaturated flow in the model. The model can therefore not be used, should the aquifer be dewatered completely near the borehole; a phenomenon that may not be too rare in Karoo aquifers. The second is that the model only takes vertical compression into account,

but not horizontal deformations. The model can therefore not be used to simulate possible deformations of fractures. Both phenomena can, however, be easily included in the model, should the necessity arise. However, this will only be worthwhile if the contribution of the phenomena to the behaviour of Karoo aquifers can be quantified more precisely through field data.



CHAPTER 10

ANALYSIS OF HYDRAULIC TEST DATA FROM KAROO AQUIFERS

10.1 INTRODUCTION

Although the results from the three-dimensional, numerical model for the Campus Test Site agree excellently with the field observations, the excessive modelling time and computer resources required by the model make it difficult to use it on a routine basis. This applies in particular to situations where one only wants to analyse constant rate and perhaps step drawdown test data. What is required in such cases, is a model that describes the properties of the aquifer accurately, but not in unnecessary detail.

The simplest method to analyse vertical flow in hydraulic tests would be to use a vertical two-dimensional analytical model. However, the discussion in Chapters 5, 6 and 9 indicates that it will be difficult to incorporate all the properties of a Karoo aquifer, particularly the fracture dimensions, in a relatively simple analytical model. A new numerical, two-dimensional vertical flow model was therefore developed. The assumptions made in deriving the model and its behaviour in comparison with a fully three-dimensional model are discussed in Section 10.2.

The new two-dimensional model can be used as a preliminary model for aquifers with a significant vertical flow component. However, the main purpose in developing the present model was to have a relatively simple, yet realistic, model with which one can estimate the hydraulic parameters of Karoo aquifers. The model was therefore linked with a least squares technique to fit the observations to those predicted by the model. A computer program, RPTSOLV, developed specifically for this purpose, is discussed in Section 10.3.

There is no doubt that Program RPTSOLV has been successful in the analysis of hydraulic test data, as illustrated by the discussion of its application to case studies, in Section 10.4. However, this does not mean that the program will always fit the data perfectly. On the contrary, there are a number of aspects, particularly the representation of the perturbed borehole in the program, that needs further attention.

The original Fortran version of Program RPTSOLV is available from the Institute for Groundwater Studies. However, a more user-friendly version has recently been developed by Prof G.J. van Tonder and implemented in his Windows 95 modelling package, AQUAMOD for Windows (Van Tonder *et al.*, 1998). It is therefore recommended that prospective users, especially those with a limited background in numerical analysis, should consider the Windows version first.

10.2 THE NUMERICAL VERTICAL FLOW MODEL

10.2.1 General

The first attempt to use a numerical model for the analysis of hydraulic test data is probably that of Rushton and Booth (1976). This work was later expanded and improved by Rathod and Rushton (1984) and Rathod and Rushton (1991). However, their numerical models are rather cumbersome and do not address vertical flow, which seems to be a characteristic property of flow in Karoo aquifers.

The only way to describe a three-dimensional physical phenomenon with a two-dimensional mathematical model is to discard information in one of the dimensions. There are essentially two methods that can be used for this purpose (Botha, 1996). The first method, which Botha calls the *physical approach*, is to discard the direction one is not interested in. However, this approach should only be applied if the phenomenon is naturally, or artificially, restricted to two dimensions. The second alternative is what Botha calls the *mathematical reduction of dimensions*. What is done in this case, is to integrate the mathematical model for the phenomenon over the unwanted dimension (Bear, 1979; Bear, 1977). This approach is discussed in detail in Appendix C, where it is shown that the vertical flow in Karoo aquifers can be described by the equation

$$rS_0(r, z, t)D_t\varphi(r, z, t) = r\nabla\cdot[\mathbf{K}(r, z, t)\nabla\varphi(r, z, t)] + \frac{Q(t)}{2\pi d}\delta(r-r_0) \quad (\text{C.24})$$

where $\varphi(r, z, t)$ is the piezometric pressure, $\mathbf{K}(r, z, t)$ the hydraulic conductivity tensor and $S_0(r, z, t)$ the specific storativity of the aquifer. This equation was consequently used to develop a simplified numerical model for flow in Karoo aquifers.

Equation (C.24) differs at first sight considerably from the equation conventionally used to describe the flow of groundwater in a horizontal plane

$$S(x, y, t)D_t h(x, y, t) = \nabla \cdot [\mathbf{T}(x, y, t) \nabla h(x, y, t)] + Q(t)\delta(x - x_0)\delta(y - y_0) \quad (7.2)$$

where $h(x, y, t)$ is the observed water level, $\mathbf{T}(x, y, t)$ the transmissivity tensor and $S(x, y, t)$ the storativity of the aquifer (Botha, 1996). However, a closer examination shows that the only significant practical differences are that Equation (C.24) is based on the piezometric head, hydraulic conductivity and specific storativity and not on the water level, transmissivity or storativity, as in Equation (7.2). These differences, summarized in Table 10–1, are so small, from the mathematical point of view, that the present model could be based on the Program GCON, developed by Botha *et al.* (1990) for horizontal flow. The only adaptations that had to be made to the program, were to add the radial variable to the expressions for the storage and divergence terms, and replace the point source term with the line source term in Equation (C.24).

Table 10–1 Comparison of the hydraulic parameters and source terms required by the three-dimensional, the horizontal and vertical two-dimensional flow models.

	Three-dimensional	Horizontal Model	Vertical Model
Dimensions	(x, y, z, t)	(x, y, t)	(x, z, t)
Hydraulic	Hydraulic Conductivity	Transmissivity	Hydraulic Conductivity
Parameters	Specific storativity	Storativity	Specific storativity
Source term	Dirichlet Boundary	Point source	Line source

The revised program was debugged by comparing its output with that of Program SAT3 for the homogeneous three-dimensional aquifer, described in Section 6.2 of Verwey and Botha (1992), and the Muskat solution for the same aquifer. The same hypothetical aquifer was also used to study the convergence properties of the program extensively, with excellent results.

10.2.2 Numerical Experiments

Since the main purpose for the development of the present program was to use it in analysing hydraulic test data for Karoo aquifers, it was thus thought worthwhile to compare its output with that of the three-dimensional Program SAT3. The hypothetical aquifer used for this purpose is illustrated schematically in Figure 10–1, except that a thickness of 20 m were assigned to both layers. The aquifer was divided into 20 equally spaced vertical and 65 radial elements, spaced logarithmically along the aquifer's radius of 1 017 m. The angular direction was divided into angles of 10° each in the three-dimensional grid of Program SAT3.

The aquifer parameters for the model, given in Table 10–2, were chosen to be representative of those found in Karoo aquifers. Layer 1, supposed to correspond with the less permeable, but highly porous Aquifer 1 on the Campus Test Site, was given a low K and high S_0 value. Layer 2, on the other hand, which represented the more permeable sandstone layer and fracture in Aquifer 2 was given a higher K but lower S_0 value.

The borehole was pumped for 72 h at a rate of $7,2 \text{ m}^3 \text{ h}^{-1}$ from Layer 2. The non-homogeneous Neumann boundary values, along the length of the borehole in this layer, were computed from the discharge rate and the source term in Equation (C.24). Zero-flux boundary conditions were prescribed along all the other boundaries, except for the curved outer boundary, where a piezometric head of 60 m was prescribed.

Table 10–2 Aquifer parameters of the hypothetical aquifer used to compare the vertical flow program and the three-dimensional Program SAT3.

Campus Site				Philippolis			
Layer 1 (32 m)		Layer 2 (8 m)		Layer 1 (32 m)		Layer 2 (8 m)	
K (m d ⁻¹)	S ₀ (m ⁻¹)	K (m d ⁻¹)	S ₀ (m ⁻¹)	K (m d ⁻¹)	S ₀ (m ⁻¹)	K (m d ⁻¹)	S ₀ (m ⁻¹)
0,09	$2,4 \cdot 10^{-5}$	0,76	$3,0 \cdot 10^{-8}$	0,037	$6,9 \cdot 10^{-5}$	3,6	$1,0 \cdot 10^{-10}$

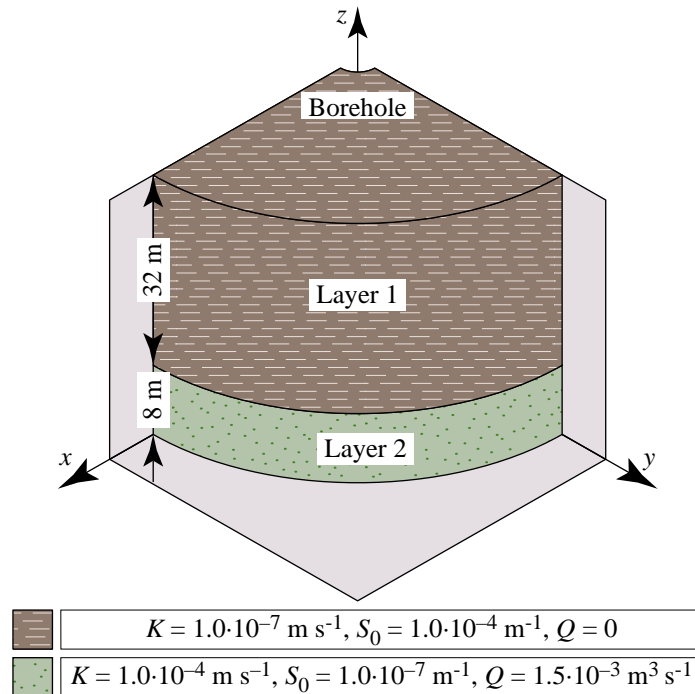


Figure 10–1 The two-layered aquifer used to represent the aquifer on the Campus Test Site in the vertical two-dimensional numerical model.

The computed drawdowns in the piezometric heads of the two layers are compared graphically in Figure 10–2 at distances of 1, 11 and 49 m from the borehole. There can thus be little doubt that the numerical vertical model is able to simulate the behaviour of a multi-layered aquifer. Notice in particular the difference in rates at which the piezometric heads in the different layers decline. This behaviour is quite characteristic of Karoo aquifers, judging from the results in Figure 6–13.

The three-dimensional model of the Campus Test Site in Chapter 9 has shown that there is a considerable difference between the drawdown cones in the fracture and the surrounding porous matrix (see Figures 9–8 and 9–9). A final numerical experiment was thus performed with the aquifer in Figure 10–1 to see how the two-dimensional vertical model represents flow in the aquifers. The initial and boundary conditions used in the previous example were also used in this case, but the discharge rate changed to $1.5 \cdot 10^{-3} \text{ m}^3 \text{ s}^{-1}$. The nodes in the radial direction were also assigned on the binary scale $\{0; 0.0625; 0.125; 0.25; 0.5; 1.0; 2.0; 4.0; 8.0; 16.0; \dots, 1\,024 \text{ m}\}$. The computed drawdowns in the piezometric heads after 48 h in Figure 10–3, agree excellently with the three-dimensional model and the previous model, in the sense that the major drawdowns also occur in the more permeable layer.

An idea of how the model interprets flow in the aquifer can be obtained from the contours of the computed drawdowns in Figure 10–4. The flow is mainly directed obliquely towards the borehole, except in the more permeable layer where it is horizontal, and at large distances, where it is more vertical. These results agree excellently, not only with those of the hypothetical Karoo aquifer in Figure 8–17, but also with the stability of the piezometric drawdown cone, in the fracture on the Campus Test Site in Figures 9–8 and 9–9.

The previous results indicate that the vertical two-dimensional vertical model is able to represent the major properties of Karoo aquifers, although not with the same accuracy as a true three-dimensional model. Nevertheless, it should be sufficient for the development of a program that it can be used to determine aquifer parameters from hydraulic tests in Karoo aquifers.

10.3 INVERSE MODELLING OF HYDRAULIC TESTS

10.3.1 General

Hydraulic test data are conventionally analysed with the help of so-called ‘type curves’ (Kruseman and De Ridder, 1991). Although this crude graphical procedure did make sense in the pre-computer era, or when one wants to get a rough indication of the parameters in the field, its practical application is limited to a small

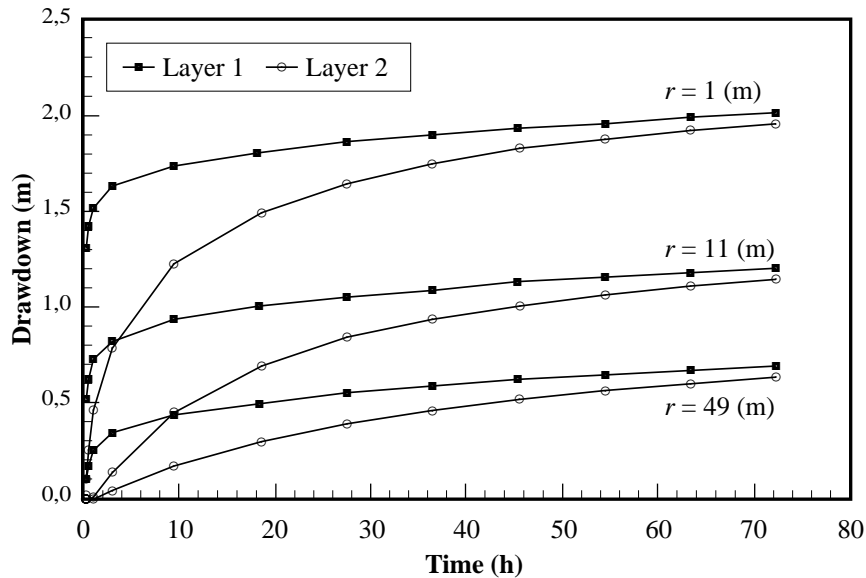


Figure 10-2 Computed drawdowns in the piezometric heads at various distances, along the centre planes of the two layers in Figure 10-1, with the new program and Program SAT3.

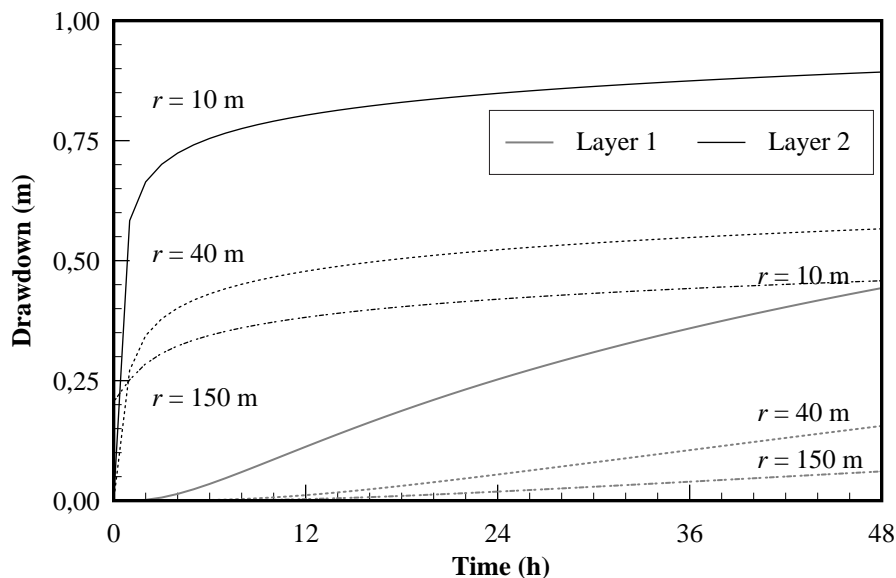


Figure 10-3 Drawdowns in the piezometric heads at various distances, along the centre horizontal planes of the two layers in Figure 10-1, computed with the vertical two-dimensional model.

number of highly simplified analytical models. It is therefore difficult to apply when the underlying mathematical model, such as Equation (C.24), does not have an analytical solution, or contain more than a couple of parameters. In such cases, one has to turn to a numerical method.

A type curve is in essence nothing more than the solution of the inverse problem, as pointed out in Section 2.3.2. One should thus still be able to determine the hydraulic parameters for mathematical models that do not have an analytical solution by solving the inverse problem of the model numerically. This is the basic philosophy behind the development of the program for the computation of hydraulic parameters discussed below.

There are a number of methods that can be used to solve the inverse and similar approximation problems numerically (Cheney, 1966). Nevertheless, there is little doubt that the method of least squares is the most appropriate when dealing with observational data. *It must be remembered, though, that the inverse problem has an infinite number of solutions. There is thus no guarantee that the computed parameters are representative of the aquifer. This can only be determined by comparing the results with field observations that have not*

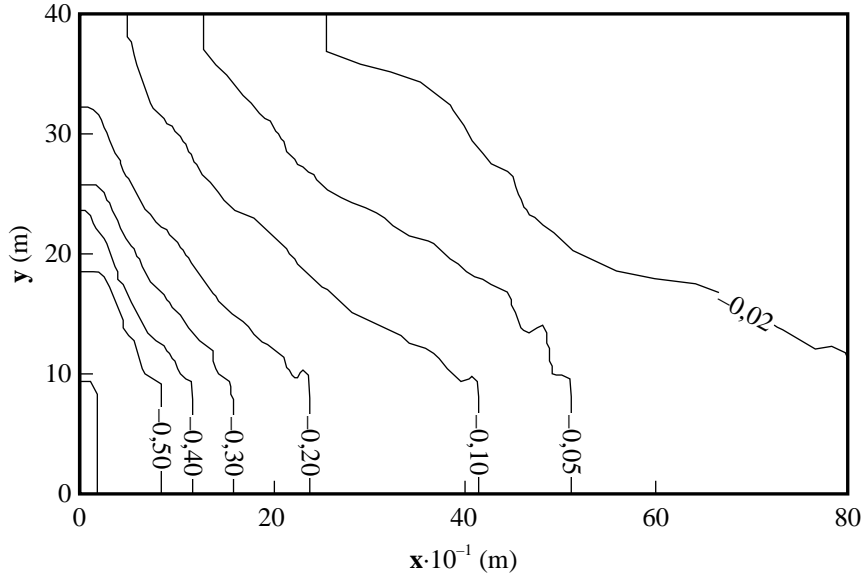


Figure 10-4 Contours of the computed drawdowns in piezometric heads after 48 h.

been included in the solution of the inverse problem, without juggling the computed parameters.

The basic objective in the method of least squares is to try to minimize the sum of squares of the residuals that exist between the observed data, say $\hat{\phi}_i(\text{obs})$, and that predicted by the assumed model, say $\phi_i(\mathbf{p})$. This is achieved by adjusting the parameters, \mathbf{p} , repeatedly, until the functional

$$E(\mathbf{p}) = \left[\sum_{i=1}^n w_i [\phi_i(\mathbf{p}) - \hat{\phi}_i(\text{obs})]^2 \right]^{1/2} \quad (10.1)$$

achieves a minimum value within prescribed limits. The factors, w_i , commonly known as *weighting factors*, are arbitrary numbers that can be used to account for the accuracy of individual observations. A common practice is to equate them with the inverse of the variances of $\hat{\phi}_i(\text{obs})$, or 1, if the variances are not known.

The equations that have to be solved in minimizing the functional in Equation (10.1) are linear in the parameters, if $\phi_i(\mathbf{p})$ is a linear function of the parameters, and can thus be solved explicitly without intervention from the user. However, this is not the case if $\phi_i(\mathbf{p})$ is a non-linear function of the parameters, or contain the parameters implicitly, which is usually the case with the analysis of hydraulic test data. The only way to proceed in such cases is that the user guesses values for the parameters and then solves the equations iteratively.

There exists a number of non-linear least squares algorithms (Sun, 1994). However, a multivariate functional, especially one constructed from experimental data, usually has a large number of local minima besides the sought-after global minimum. Unfortunately, none of the available algorithms are able to distinguish between a local and global minimum without some interaction with the user, notwithstanding contrary claims in the literature. A fully automatic implementation of a non-linear least squares algorithm can thus easily yield absurd parameters if the initial guesses are not sufficiently close to the actual parameter values. This can cause considerable difficulties for someone not acquainted with optimization theory.

The effect of the initial guesses on the minimization of Equation (10.1) can be reduced somewhat by using a robust algorithm, i.e. an algorithm that does not depend too much on the guesses. This dependence can be reduced further, by prescribing a certain range within which the parameters are expected to fall. However, this does not imply that the algorithm will yield an acceptable solution. Moreover, the possibility always exists that the user may supply an inappropriate range for the parameters. Solutions obtained with robust algorithms are usually also less accurate than those obtained with a less robust algorithm. The solution of a non-linear inverse problem should therefore never be accepted at face value.

A simple procedure to find out whether the solution of a non-linear least squares problem represents a global minimum is to repeat the calculations with different sets of guesses. However, similar solutions do not necessarily imply that a global minimum has been reached.

The Levenberg-Marquardt algorithm (Sun, 1994) is probably the best known of the robust non-linear least squares algorithms, and the one most commonly used in geohydrology (Kauffmann *et al.*, 1990). This

algorithm and the two-dimensional vertical flow model discussed above, were used to develop the Program RPTSOLV for the analysis of hydraulic test data from Karoo aquifers. *It is important to remember, though, that one is dealing with the inverse problem. The parameters computed with Program RPTSOLV, can this fit the observations perfectly, but may still not be representative of the aquifer.* However, this can only be determined by the user.

10.3.2 Computer Implementation of RPTSOLV

The present version of Program RPTSOLV tries to simulate the behaviour of a Karoo aquifer by representing it as a two-layer aquifer, illustrated in Figure 10–1 above. Layer 1, representing the Karoo formations, is assumed to be less permeable, but more porous, than Layer 2, which represents the water-yielding fractures. The perturbed borehole is represented as a Neumann boundary on the left-hand side of the vertical domain and the outer boundary as the right-hand side of the vertical domain. This representation of the aquifer and perturbed borehole is built into the program and cannot be changed by the user in the present version of the program. However, the user can choose between a constant rate and step drawdown test, and can also specify the pump position, for which there are three options: Layer 1, Layer 2, or both.

The computation of the hydraulic parameters is performed in a number of pre-set steps. The two most important steps are: the construction of the finite element mesh and the optimization step, that runs the model repeatedly until the optimized solution is found. The steps are, however, transparent to the user. The only action the user has to take, is to supply the program with two sets of parameters—the geometric parameters and the simulation parameters. The geometric parameters include:

- (a) thickness of Layer 2,
- (b) total thickness of the aquifer
- (c) distance to the aquifer boundary and
- (d) radial distance of the observation borehole.

Default values are built into the program for the parameters, but it is always preferable that the user supplies the appropriate values for the test at hand. Note that the thickness of Layer 2 has to be specified as a fraction of the total aquifer thickness, and not as a length.

The simulation parameters, *which must be supplied by the user*, include:

- (a) the type of test,
- (b) duration of the test,
- (c) position of the pump,
- (d) observed water levels,
- (e) position of the observation borehole,
- (f) the discharge rate, or rates, in the case of a step drawdown test and
- (g) type of boundary condition to consider on the outside boundary.

The latter can be specified as either a zero-flux Neumann boundary or a constant head Dirichlet boundary. The positions of the pump and the observation borehole can be specified as situated in Layer 1, Layer 2 or both. However, the last option only makes sense if one is working with a single-layer aquifer.

Other options available to the user include: the units in which the in- and output parameters are specified, whether the water levels are supplied as drawdowns or hydraulic heads and whether the full or a subset of the water levels be used in the simulation.

The finite element mesh, constructed by the program, consists of 20 equally spaced vertical elements, allocated proportionately to the two layers, and 16 to 20 elements in the radial direction, depending on the number of observation boreholes. These nodes are located at binary distances of

$$r = 2^k \quad (k = -4, -3, \dots, 0, 1, \dots, 10)$$

with the positions of observation borehole inserted at its specified position.

The program assigns all drawdown data to the centre lines of the layer, if the data are specified as piezometric heads, and use both values in the least squares fit. However, water levels and drawdowns are considered to represent the piezometric head at the centre line of the layer in which the perturbed borehole is situated. The same applies to the observation borehole.

The first three geometric parameters, the thicknesses of Layer 1 and aquifer and distance to the aquifer boundary are usually not known and have to be estimated. Since these parameters have a considerable influence on the fitted hydraulic parameters, the user must always try to represent them as accurately as possible in the model. A few approaches that can be used for this purpose are discussed below.

It is important to remember that Program RPTSOLV computes the *three-dimensional* hydraulic conductivity and specific storativity [K and S_0 in Equation (C.24)], and not the horizontal *two-dimensional* transmissivity and storativity (T and S in Equation (7.2)). It is only after the fit has been completed successfully that the parameters are multiplied by the thicknesses of the two layers to obtain the more common parameters

$$S_i = S_{0i}d_i, \quad T_i = K_id_i \quad (i = 1, 2) \quad (10.2)$$

where d_i is the thickness of the i -th layer. Since there are advantages in working with K and S_0 , instead of T and S , the program supplies both sets of parameters to the user. However, the user can specify the initial guesses as T and S values, which is then converted internally by the program to K and S_0 values.

The program includes a facility to represent the observed and simulated drawdowns graphically. This not only enables the user to obtain a better idea of the fit, but also to see what effect changes in the parameters have on the fit. A help facility to assist users that are unfamiliar with text editors is also built into the program.

10.3.3 Thickness of the Aquifer

The thickness of the aquifer, provided by the user, is used to determine the height of the finite element mesh. An unknown thickness can be approximated as the difference between the water level and depth of the main water strike, or with the default value of 40 m. The exact thickness of the aquifer does not have a critical influence on the fitted hydraulic parameters, but that of Layer 2 has, as shown in Figure 10-5. However, this is not unexpected, since an increase in fracture thickness will increase the volume of water available to the pump. The user should therefore experiment with the thickness of Layer 2, before accepting the fitted hydraulic parameters.

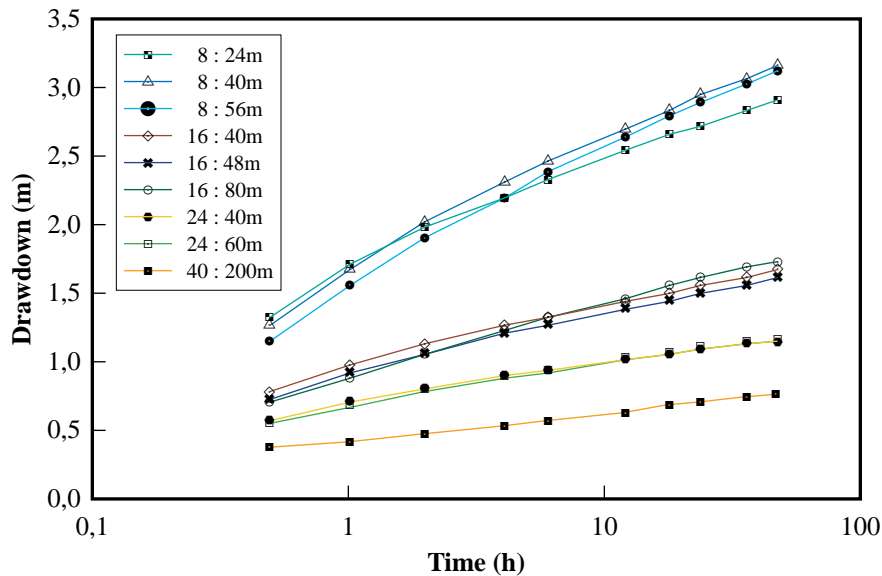


Figure 10-5 Influence of the thickness of Layer 2 and the aquifer, expressed as the ratio ($x : y$), on the drawdowns of a hypothetical aquifer.

The present default values for the thickness of the aquifer (40 m) and the ratio for the thickness of Layer 2 (0,2), in Program RPTSOLV, were determined from the analysis of a large number of case studies. All indications are that these values are sufficient for the analysis of most hydraulic tests in Karoo aquifers.

Numerical experiments have shown that a change in the thickness of the aquifer, Layer 2, or both, does not influence the fitted values of K and S_0 significantly, provided that the changes are within reasonable limits. However, the same is not true for the values of T and S . These parameters are functions of the thickness, as shown by Equation (10.2) and must therefore change with the thickness. Users who are comfortable with the three-dimensional hydraulic parameters may therefore prefer to work with them instead of the two-dimensional parameters T and S .

10.3.4 Aquifer Boundary

A particular advantage of Program RPTSOLV above the more common analytical methods, is that it allows the user to change the aquifer boundary. Unfortunately, this freedom has a negative side, in that it forces the user to supply a value for the boundary; something that is rarely known in practice. The user therefore has to experiment with the boundary radius, especially when there are indications that the observed water levels may be influenced by an impermeable boundary. However, this may be easier said than done. The reason for this is that the least squares algorithm will always try to fit the data as closely as possible with the given set of geometric parameters. It may thus be difficult to distinguish graphically between the influence of different boundaries. Consider, for example, the hydraulic test at Kokstad in Figure 6–14. This test was first analysed with the default thicknesses and aquifer radius ($= 1\,024\text{ m}$), and a zero-flux Neumann boundary condition on the outside boundary. The analysis was then repeated with aquifer radii of 528 and 2 048 m. As shown in Figure 10–6, it is impossible to decide which one of the three fits is the best.

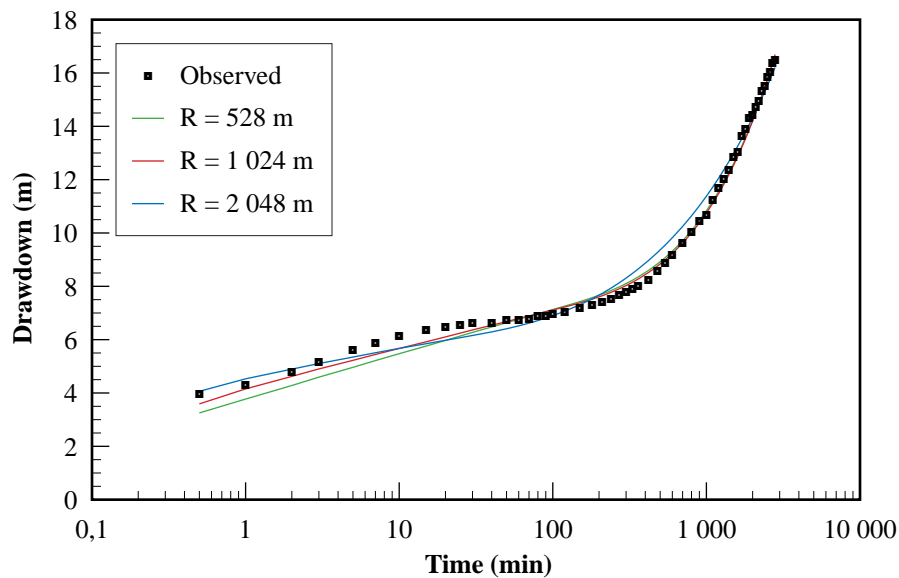


Figure 10–6 Comparison of the observed and fitted drawdowns for the Kokstad hydraulic test, with aquifer radii of 528, 1 024 and 2 048 m.

One approach to avoid this difficulty is to use an option in RPTSOLV to just compute the solution of Equation (C.24) with prescribed parameters, and force-fits the parameters to a prescribed aquifer radius. For example, one may choose the radius $R = 1\,024$ and compute the solution of Equation (C.24), first with the hydraulic parameters, obtained from fitting the data to the radius $R = 528\text{ m}$, and then with the parameters from $R = 2\,048$. As shown in Figure 10–7, there is now little doubt about which radius is the correct one to use.

There are two difficulties associated with the previous approach. The first is that it demands of the user to draw graphs of the various solutions, and the second is that it does not provide a guide-line as to which radius should be used in the force-fits. Fortunately, these difficulties can be avoided by looking at the least squares error of the various fits, and select the one with the smallest error. This quantity, denoted by the symbol χ^2 in Table 10–3 below, can be obtained from the ‘Result File’ created by RPTSOLV, where it is denoted as the ‘Root Mean Square Error’.

Table 10–3 Hydraulic parameters and least squares error (χ^2) for the three fits of the Kokstad data in Figure 10–6 and Figure 10–7.

	R = 528 m	R = 1 024 m	R = 2 048 m
K_1	$8,362 \cdot 10^{-5}$	$1,726 \cdot 10^{-5}$	$6,252 \cdot 10^{-5}$
K_2	$1,275 \cdot 10^{+1}$	$1,471 \cdot 10^{+1}$	$1,914 \cdot 10^{+1}$
S_{01}	$1,278 \cdot 10^{-4}$	$3,279 \cdot 10^{-5}$	$1,902 \cdot 10^{-6}$
S_{02}	$1,000 \cdot 10^{-9}$	$1,000 \cdot 10^{-9}$	$1,000 \cdot 10^{-7}$
χ^2	5,505	2,961	8,103

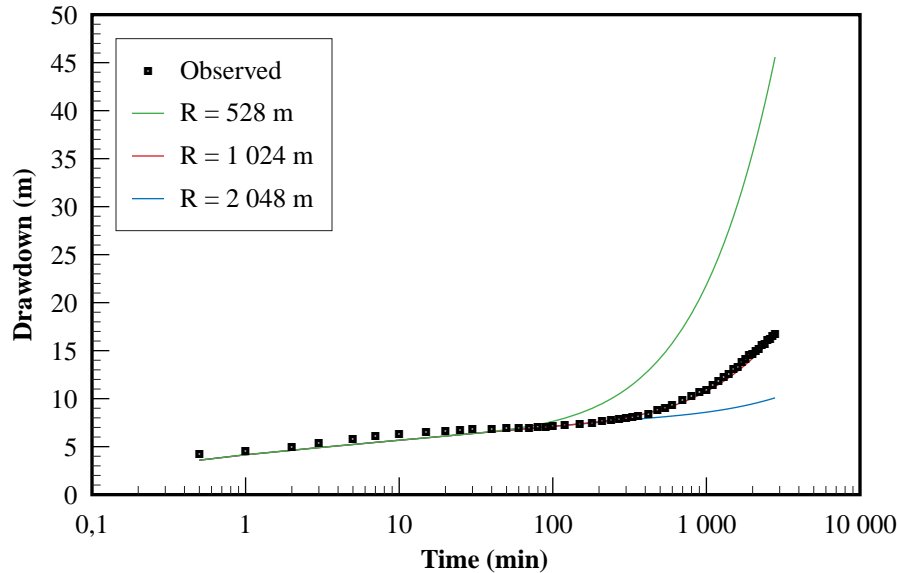


Figure 10-7 Comparison of the observed and fitted drawdowns for the Kokstad hydraulic test, with the default aquifer radius of 1 024 m, and the force fitted drawdowns of the 528 and 2 048 m radii data.

The mathematically correct approach in comparing the least squares errors is to ensure that all fits satisfy the same minimum value, prescribed by the user. However, it is sometimes possible to obtain an idea which radius is the more appropriate by simply looking at the rate at which the least squares error decreases during the fitting.

10.3.5 Boundary Conditions on the Outside Boundary

The program allows the user to specify one of two types of boundary conditions on the outside boundary of the aquifer—a zero-flux Neumann condition, and a constant head Dirichlet boundary condition. The water level will decrease sharply at the boundary in the case of a zero-flux boundary condition, but will remain constant at the prescribed head, if a constant head condition is prescribed. The result is that the water level in an observation borehole generally drops faster in an aquifer subject to a zero-flux Neumann boundary condition than one subject to a constant head Dirichlet boundary condition, as illustrated in Figure 10-8. This behaviour is especially noticeable in a small aquifer.

Figure 10-8 leaves no doubt that a Dirichlet boundary condition is completely inappropriate for the specific aquifer at Kokstad. This conclusion is further confirmed if one compares the hydraulic parameters for the two types of boundary conditions in Table 10-4. The Dirichlet hydraulic parameters, especially the specific storativities, is unacceptable from the physical point of view.

An interesting interpretation of the results in Table 10-4 is that a similar aquifer, subject to a Dirichlet boundary condition, would not need large hydraulic parameters to satisfy the discharge rate. The fact that the results are best represented by the zero-flux Neumann boundary condition with large hydraulic parameters, may therefore be an indication that there is an unknown internal boundary present in the aquifer.

The dependence of the fitted water levels on the outer boundary condition can sometimes be used to determine whether a prescribed radius of the aquifer is sufficient or not. All the user has to do, is to run the

Table 10-4 Comparison of the hydraulic conductivities and specific storativities obtained from Program RPTSOLV for the Kokstad data with Dirichlet and Neumann boundary conditions.

	R = 512 m		R = 1 024 m		R = 2 048 m	
	Dirichlet	Neumann	Dirichlet	Neumann	Dirichlet	Neumann
K_1	$1,090 \cdot 10^{-8}$	$8,362 \cdot 10^{-5}$	$1,726 \cdot 10^{-9}$	$1,726 \cdot 10^{-5}$	$1,090 \cdot 10^{-12}$	$6,252 \cdot 10^{-5}$
K_2	$6,533 \cdot 10^{+0}$	$1,275 \cdot 10^{+1}$	$7,357 \cdot 10^{+0}$	$1,471 \cdot 10^{+1}$	$5,869 \cdot 10^{+0}$	$1,914 \cdot 10^{+1}$
S_{01}	$3,913 \cdot 10^{-3}$	$1,278 \cdot 10^{-4}$	$3,185 \cdot 10^{-3}$	$3,279 \cdot 10^{-5}$	$7,881 \cdot 10^{-3}$	$1,902 \cdot 10^{-6}$
S_{02}	$1,000 \cdot 10^{-7}$	$1,000 \cdot 10^{-9}$	$1,000 \cdot 10^{-9}$	$1,000 \cdot 10^{-9}$	$1,000 \cdot 10^{-6}$	$1,000 \cdot 10^{-7}$

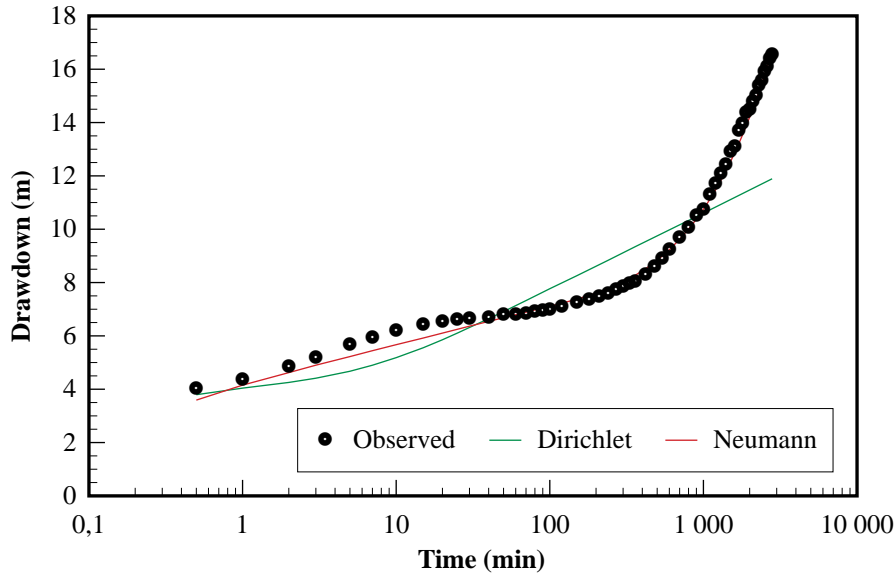


Figure 10-8 The effect of zero-flux and constant head boundary conditions on the fitted drawdowns for the hydraulic test at Kokstad ($R = 1\,024$ m).

program first with one type of boundary condition, and then with the other. The two sets of fitted water levels, hydraulic parameters and least squares errors should be similar if the aquifer radius is appropriate for the specific test. The method, however, may not work, if there are unknown internal boundaries in the aquifer, as seems to be the case with the Kokstad data in Figure 10-8. In such cases, the user may have to turn to the force-fitting procedure, described above, or rely on the least squares errors to obtain an indication of which radius is appropriate for the problem at hand.

10.4 EXAMPLES OF HYDRAULIC TESTS ANALYSED WITH PROGRAM RPTSOLV

10.4.1 Constant Rate Tests at the Campus Test Site and Philippolis

Two actual field tests will now be discussed to illustrate the practical application of the method. In the first test, the high-yielding Borehole UO5 on the Campus Test Site was pumped at a rate of $5,4\text{ m}^3\text{ h}^{-1}$ for 6 h and the water levels were observed in Borehole UP15, 22,191 m from Borehole UO5. The other test was performed as part of the investigations to extend the water supply of the Municipality of Philippolis (Botha *et al.*, 1996). In this test, described in Section 6.3.5, Borehole D20 was pumped at a rate of $6,84\text{ m}^3\text{ h}^{-1}$ for 72 h, and its water levels, as well as those in Borehole D19, 54 m from Borehole D20, were monitored for 120 h. Since the geology at the two sites is very similar, the analyses were performed with the same two-dimensional model described above, except for the hydraulic parameters of course, which were determined from the model.

As shown in Figure 10-9, the observed and fitted drawdowns agree excellently. This applies in particular to the steady behaviour of the drawdowns in Borehole D20, which lasted approximately 54 h. It is only during the recovery phase of boreholes D20 and D19 that the observed and fitted drawdowns differ somewhat. However, this difference is never more than 0,5 m.

The fitted values of K and S_0 for each layer are given in Table 10-5. The values of the specific storativities in Layer 2 agree very well with the values Kirchner *et al.* (1991) derived from their water-balance studies of Karoo aquifers.

Table 10-5 Aquifer parameters for the two field tests, determined with the two-dimensional vertical flow model.

Campus Site				Philippolis			
Layer 1 (32 m)		Layer 2 (8 m)		Layer 1 (32 m)		Layer 2 (8 m)	
K (m d ⁻¹)	S ₀ (m ⁻¹)	K (m d ⁻¹)	S ₀ (m ⁻¹)	K (m d ⁻¹)	S ₀ (m ⁻¹)	K (m d ⁻¹)	S ₀ (m ⁻¹)
0,09	$2,4 \cdot 10^{-5}$	0,76	$3,0 \cdot 10^{-8}$	0,037	$6,9 \cdot 10^{-5}$	3,6	$1,0 \cdot 10^{-10}$

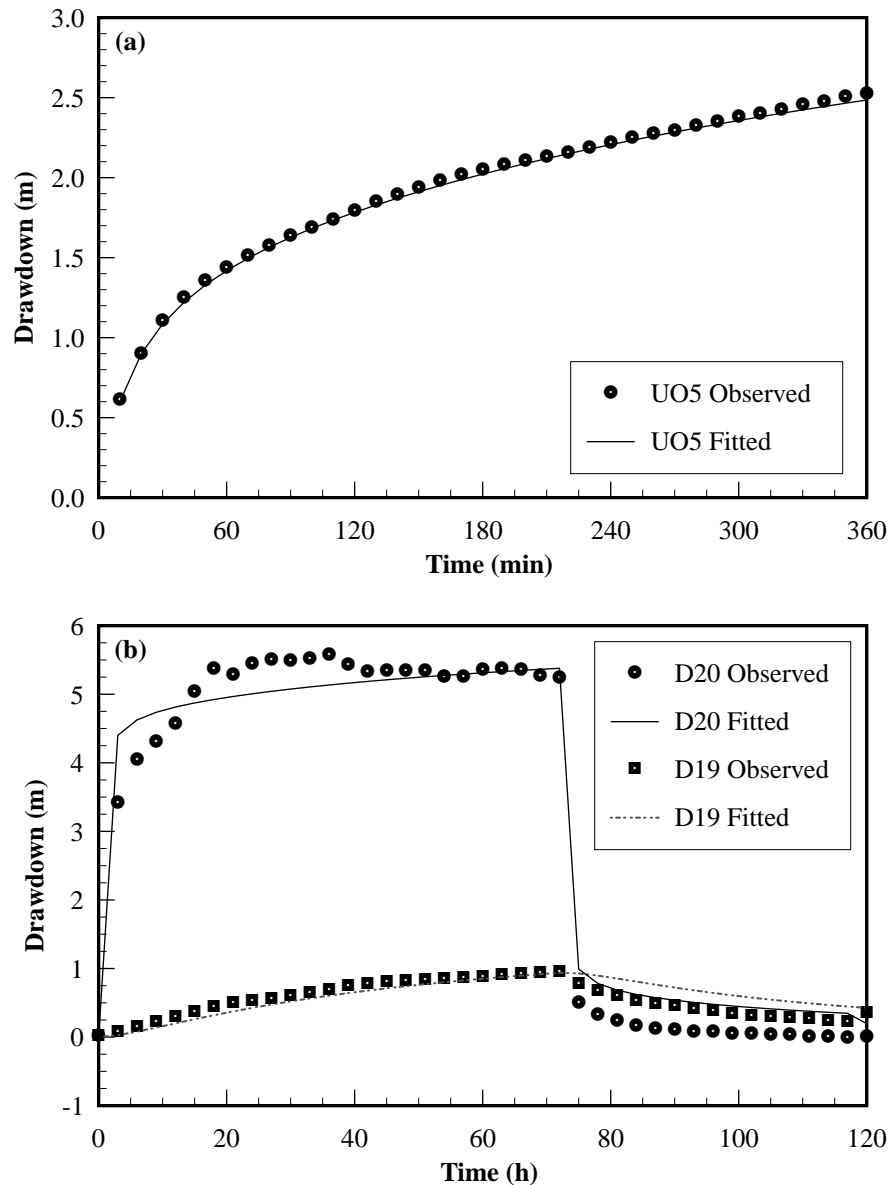


Figure 10-9 Comparison of the observed and fitted drawdowns for: (a) Borehole UP15 on the Campus Test Site, and (b) boreholes D19 and D20 at Philippolis.

10.4.2 Step Drawdown Test at Philippolis

A step drawdown test was also performed on Borehole A14 at Philippolis as part of the investigations to extend the water supply of the Municipality of Philippolis. A summary of the test is given in Table 10-6.

Borehole A14 was drilled through the tip of a negatively weathered ring dyke on the western side of the dyke. The dyke itself is highly weathered for the first 13 m, but impermeable at depth (Botha *et al.*, 1996).

Table 10-6 Summary of the step drawdown test performed on Borehole A14 at Philippolis.

Step No.	Duration (min)	Pumping rate ($\text{m}^3 \text{h}^{-1}$)
1	70	2,0
2	70	4,0
3	70	6,0
4	70	8,5
Recovery	70	

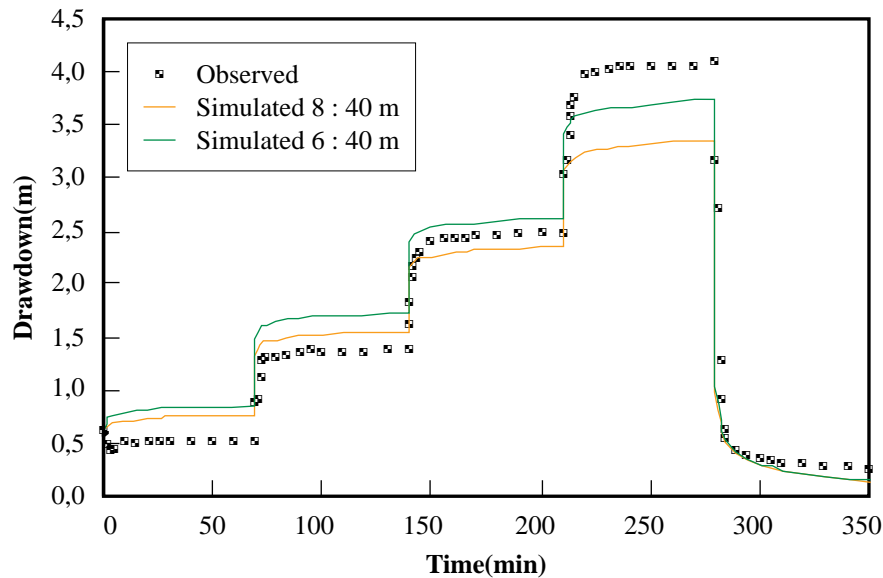


Figure 10–10 Observed and fitted drawdown curves for the step test on A14 at Philippolis district, with an aquifer thickness of 40 m and Layer 2 thicknesses of 6 and 8 m.

Table 10–7 Fitted hydraulic parameters for Borehole A14 at Philippolis.

T_1 (m^2d^{-1})	S_1	T_2 (m^2d^{-1})	S_2
0,3	$2,2 \cdot 10^{-3}$	85,3	$1,0 \cdot 10^{-5}$

The major water strikes occurred at the contact zones of a dark green shale and light grey siltstone, 10 m below the dyke, and the same light grey siltstone and grey-green sandstone, 2 m deeper. The site thus does not correspond fully with the two-layer model, which has been used thus far in the discussion. The observed and fitted drawdowns in Figure 10–10, nevertheless, show that the model is able to fit the observed drawdowns reasonably. The averaged T and S values in Table 10–7 are also of the same order as that of the boreholes described above. However, the results leave little doubt that a multi-layered aquifer model would have been more suitable for this test.

10.4.3 Dependence of Storativity on Distance

The major critique in Section 6.3.2 against the use of Theis' equation to analyse constant rate tests from Karoo aquifers, is that the fitted storativities depend on the distance from the perturbed borehole. It was thus thought worthwhile to see if the parameters fitted with RPTSolv, are free from this behaviour. The data from the constant rate test performed on Borehole UP16, also described in Section 6.3.2, were therefore analysed with the Theis equation and RPTSolv, assuming that Layer 1 is 32 m thick and Layer 2 8 m thick. The results in Table 10–8 again confirm the earlier observation that there is very little difference between the two sets of transmissivities, but the storativities differ considerably, although

Table 10–8 Comparison of the hydraulic parameters derived from fitting drawdowns, observed during a constant rate test on Borehole UP16, with RPTSOLV and the Theis equation.

Borehole		RPTSolv		Theis	
		T ($\text{m}^2 \text{s}^{-1}$)	S	T ($\text{m}^2 \text{s}^{-1}$)	S
UO7	26,117	$2,662 \cdot 10^{-4}$	$3,6 \cdot 10^{-3}$	$2,108 \cdot 10^{-4}$	$1,508 \cdot 10^{-4}$
UO9	35,720	$2,315 \cdot 10^{-4}$	$1,9 \cdot 10^{-3}$	$2,023 \cdot 10^{-4}$	$7,826 \cdot 10^{-5}$
UO11	43,910	$1,968 \cdot 10^{-4}$	$3,0 \cdot 10^{-3}$	$1,738 \cdot 10^{-4}$	$1,185 \cdot 10^{-4}$
UO13	52,979	$2,315 \cdot 10^{-4}$	$1,1 \cdot 10^{-3}$	$1,859 \cdot 10^{-4}$	$6,543 \cdot 10^{-5}$
UO15	14,234	$3,125 \cdot 10^{-4}$	$4,6 \cdot 10^{-3}$	$2,033 \cdot 10^{-4}$	$4,220 \cdot 10^{-4}$

the Theis-fitted values are not unacceptable.

The graphs of the storativities as functions of the inverse distance from the perturbed borehole in Figure 10–11 are disappointing, however. They not only show that both sets of storativities depend on the inverse distance, but even suggest that the rate at which the RPTSOLV storativities decrease with distance increases with distance, while their Theis-fitted counterparts approach a limit. It is difficult at the moment to decide what causes this behaviour. However, the fact that the storativities in Figure 10–11 fit two different curves, suggests that the dependence is caused by representing the perturbed borehole as a line source in Equation (C.24). Moreover, as pointed out in Section 7.4.2, one can expect the line source to cause a discontinuity that will tend to propagate through the solution with time. Although the discussion in Section 2.3.2 shows that such a discontinuity will die out in time, its influence on a short-term solution of Equation (C.24) cannot be neglected. It is therefore interesting that the differences between the observed drawdowns for Borehole UO7, and those fitted with RPTSOLV, at first increase with time, before they decrease and tend to a steady value, as shown in Figure 10–12.

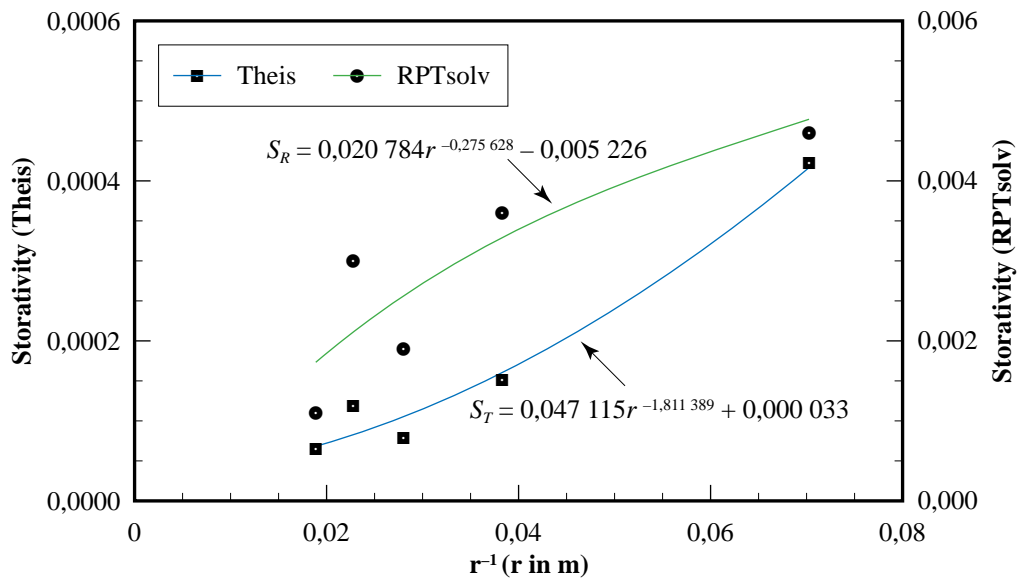


Figure 10–11 Graphs of the storativities in Table 10–8 as a function of the inverse distance from the perturbed borehole.

The most satisfactory approach to solve the distance dependent problem would have been to implement the method of Huang, used in Program Karoo, to approximate the perturbed borehole in RPTSOLV. However, the program was only developed at the very end of the project, with the result that there was not sufficient time left to study the behaviour further. The two researchers responsible for the development of RPTSOLV also left the Institute for Groundwater Studies before the behaviour was observed.

10.5 DISCUSSION

Modern computers, even some desktop computers, are able to handle large three-dimensional groundwater models. However, the field data required by these models often do not exist. The use of simpler mathematical models will, therefore, always be in demand, either to analyse field data rapidly, or to ease the burden of obtaining the field data required by the three-dimensional models. The development of such simpler models, however, must always be based on valid approximations. These considerations led to the development of a new vertical two-dimensional model for Karoo aquifers.

The previous approach is, of course, not invulnerable. One danger that always exists is that the model may be applied to situations that do not satisfy the assumptions of the model. This situation, for example, arises if the Theis equation, which is based on a porous medium, is applied to the multi-porous Karoo aquifers. The user of such simplified models must, therefore, always ensure that the model he or she proposes to use, is appropriate for the aquifer.

Although the current version of the model usually gives excellent results when applied to observation boreholes, difficulties are experienced when trying to fit data from the perturbed borehole itself. There is

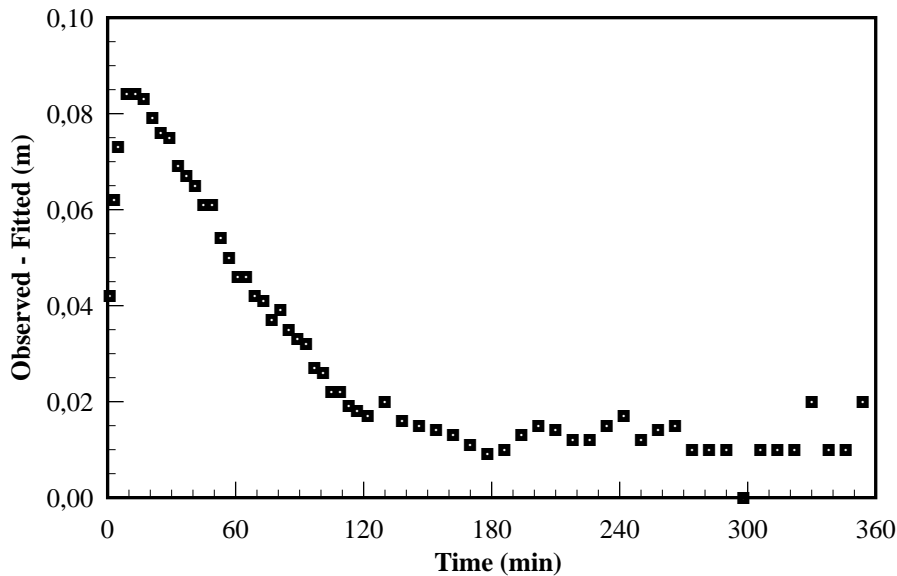


Figure 10-12 Differences between the drawdowns observed in Borehole UO7 and those fitted with RPTSOLV .

little doubt that this behaviour and the distance dependence of S in Figure 10-11, are caused by approximating the perturbed borehole as a line source in Equation (C.24). It is therefore recommended that this approximation should be replaced with the Dirichlet approximation of Huang (1973) in future versions of the program, as described for the three-dimensional Program KARO in Chapter 7. The effect of the approximation can, however, sometimes be reduced by specifying its distance as the order of 1–2 m, instead of its radius, as is frequently done in the analysis of hydraulic test data.

The initial guesses for the hydraulic parameters and the default geometric parameters, built into program RPTSOLV , are based on numerous case studies of data from Karoo aquifers. They should thus be sufficient for hydraulic tests from boreholes in these aquifers. However, difficulties were sometimes experienced in cases where the Karoo rocks have an extremely low K -, but high S_0 value, while the fracture has a relatively high K -, but very limited S_0 value. In these cases, it may be necessary to either change the distance of the outside boundary, or the S value of Layer 1.

A clear indication that the distance of the outside boundary is incorrect is when the fitted drawdowns tend to be lower than the observed drawdown, especially near the boundary, or if the program yields T values that differ considerably for observation boreholes in the same aquifer. Too large drawdowns are, on the other hand, an indication that the initial guess for the S_0 value of Layer 1 is too small. However, an unrealistic S_0 value may again be an indication that the outside boundary was situated too close to the perturbed borehole.

Although Program RPTSOLV has been applied successfully to a large number of constant rate and step drawdown tests, a number of case studies have shown that it will be worthwhile to increase the number of the layers in a future version of the program. It may also be necessary to implement the water-yielding fractures more efficiently than the crude Layer 2 in the present version.

One difficulty, commonly experienced with existing methods for the analysis of hydraulic tests, is the presence of unknown boundaries in an aquifer (Milne-Home, 1988). Although Program RPTSOLV does not solve this difficulty completely, it at least allows the user to change the position of such a boundary, if and when the need arises, and can also assist in detecting the existence of such boundaries. However, this can only be determined by the user.

There are two difficulties that some users experienced with the program. The first is that the program uses the three-dimensional hydraulic conductivity and specific storativity, and not the horizontal two-dimensional transmissivity and storativity, as the more conventional models. The reason for this is that the latter parameters arise only in the equation for horizontal flow, when one multiplies the hydraulic conductivity and specific storativity with the thickness of the aquifer (Bear, 1977; Botha, 1996). They are thus not true physical parameters for groundwater flow, but rather mathematical artefacts. It is thus impossible to try to account for natural vertical variations in the flow parameters, with a model based on flow parameters derived for horizontal flow. However, the user who wants to use transmissivity and storativity can easily recover them from the hydraulic conductivity and specific storativity, since the thickness of the aquifers must be known *a priori*, to use Program RPTSOLV .

The second difficulty is the inability of the program to handle arbitrarily spaced observation boreholes and multiple perturbed boreholes. However, this limitation is typical of all dimensionally reduced equations. For example, it is equally impossible to apply a horizontal flow model to a multi-layered aquifer, as the discussion in Chapter 9 shows. In such cases, one has to turn to a full three-dimensional model. This does not mean to say that one cannot use more than one borehole with Program RPTSOLV , but then they must lie in a straight horizontal line, or their positions must be projected onto a straight line.



CHAPTER 11

SUMMARY AND RECOMMENDATIONS

11.1 GENERAL

Groundwater is a very important source, sometimes the only source, of potable water for rural communities, farms and towns in South Africa. The Karoo aquifers, which underlie approximately 50% of South Africa, can therefore be an important source of water for these communities. Unfortunately, this source is usually considered unreliable. The present study has shown that this view can be ascribed to the complex geometry of these aquifers. This geometry was the result of two factors: the sedimentary processes responsible for the deposition of the formations, and the intrusion of dolerites at the fragmentation of Gondwanaland during the Jurassic age.

All indications are that the intrusion of the dolerites was caused by the widespread volcanism, at the beginning of the Jurassic Age, that ended the Karoo sedimentation. This magmatic activity was caused by the tectonic movement of Gondwanaland, during the late Triassic to early Cretaceous ages, which seems to have occurred in pulses. This interpretation is supported by the fact that one can clearly distinguish three types of dolerite intrusions in the Karoo landscape—sills, ring dykes and linear dykes. The ring dykes are conventionally regarded as undulating dolerite sills. However, a review of the historical evolution of the Karoo Supergroup of geological formations, suggested that it may be more natural to interpret the ring dykes as the peripheral dykes, often associated with laccolithic intrusions. This suggests that both the sills and ring dykes intruded as laccoliths, while the linear dykes intruded through matrix melting. This interpretation may be controversial, but has the advantage over conventional interpretations in that it provides a natural explanation for the existence of the structures, without invoking some rather esoteric mechanisms.

The contact zones of the ring dykes are often metamorphosized, which suggests that the temperature of the intruding magma was very high. It is thus virtually impossible to drill successful boreholes near ring dykes, especially positively weathered ring dykes, if the experience at Philippolis can be taken as a norm. The contact zones of linear dykes, on the other hand, are usually highly fractured. Most boreholes in Karoo aquifers are consequently sited along the linear dykes, because they are easy to detect, and there is a higher probability to strike a fracture near a dyke. However, the dykes are often impermeable and could thus act as a restrictive boundary for groundwater flow.

Karoo formations are best described as a heterogeneous, anisotropic and slightly fractured porous medium, according to the discussion of their formation and physical properties in Chapters 3–5. The presence of horizontal fractures, moreover, implies that Karoo aquifers must *always* be viewed as multi-layered aquifers. This type of multi-layered medium has not attracted very much attention in the literature on groundwater phenomena. There thus does not exist a suitable mathematical model for the physical behaviour of these aquifers, nor are there suitable instruments with which the behaviour of a fracture can be measured. The attempt to evaluate the applicability and reliability of existing conceptual models for the description and analysis of hydraulic tests in Karoo aquifers therefore failed. This presented somewhat of a problem for the research team as it meant that one of the major original objectives of the project could not be fulfilled. The only alternative was thus to develop a numerical three-dimensional model that could be used to study the interaction between the fractures and rock matrix. The application of this model to the aquifer on the Campus Test Site, combined with information gained from the core-boreholes, provided valuable insight into the physical behaviour of Karoo aquifers.

11.2 SUMMARY OF THE RESULTS

The most important conclusion derived from the present study is that *the behaviour of a stressed Karoo aquifer is determined by its very complex geometry*, that results from the presence of bedding-parallel fractures and the multi-porosity of the rock matrix. Any neglect of this property in the management and operation of these aquifers can ruin an aquifer completely. Indeed, all indications are that the inability of previous

investigators to take the internal geometry of Karoo aquifers into account, must be regarded as the main reason for the difficulties experienced with these aquifers, and why people distrust them.

Although the concept that the behaviour of an aquifer is largely determined by its geometry is well-known, this dependence is usually neglected in groundwater investigations. One reason for this is that the methods commonly applied in these investigations are all based on porous formations, whose geometry is so simple that it is often neglected (Black, 1993). However, as Black points out, this geometry is of vital importance in the analysis and interpretation of hydraulic tests in any secondary aquifer—a view shared by Prof. Ghislain de Marsily (Personal Communication).

The apertures of the bedding-parallel fractures in Karoo aquifers are not very large (see Figure 5-26), although a fracture can have a considerable areal extent. The fracture can, therefore, only store a limited volume of water. *The major storage units of water in Karoo aquifers must thus be the formations themselves, while bedding-parallel fractures provide the main conduits of water to boreholes.*

The first indication of the important role that bedding-parallel fractures play in the ability of Karoo boreholes to yield water came from an analysis of the cores from the core-boreholes drilled on the Campus Test Site and Dewetsdorp. These cores showed that the water-yielding fractures in the boreholes on these sites are parallel to the bedding planes of the Karoo formations, and therefore mainly horizontally orientated. This conclusion was further confirmed by observations during the drilling of boreholes at Philippolis and Rouxville. The study of the regional fracture development in the sediments in and around Bloemfontein also supports this conclusion and, moreover, showed that subvertical fractures only provide conduits for surface water. The best place to site boreholes in Karoo aquifers is thus in those areas where bedding-parallel fractures are present.

The bedding-parallel fractures in the Karoo formations have a very low frequency and weak connectivity. However, a borehole that does not intersect such a water-yielding fracture does not have a high yield. Although this fact is well-known to groundwater practitioners, they usually pay very little attention to the nature of fracture, or how it influences the movement of water in these aquifers. One reason for this lack of interest is the assumption that the water-yielding fractures in Karoo aquifers are vertically or subvertically orientated, and do not influence the flow pattern. This assumption seems to have been quite common amongst geologists, judging from their reaction when the first cores showed the fractures to be horizontally orientated. It thus seems natural to ask: why do bedding-parallel fractures exist in the Karoo formations?

The circular dolerite dykes in the Karoo landscape of the southern Free State and adjacent areas have been associated above with the intrusion of magma in the form of laccoliths. The theory behind the intrusions shows that bedding-parallel fractures will form naturally in the area surrounded by the peripheral dyke of a laccolith. Bedding-parallel fractures should therefore be present in areas away from the ring dykes, if their previous association with high-yielding boreholes is correct. This view is supported by the hydrocensus of Burger *et al.* (1981), which showed that 63% of the 1 245 boreholes, surveyed in the districts of Bethulie, Springfontein and Trompsburg, are not situated near dolerite dykes. It is, therefore, interesting to observe that the new geological model of Bloemfontein and its immediate surroundings revealed that the city is situated on a dome-shaped structure, typical of laccolithic intrusions. This laccolithic intrusion may thus have been responsible for the existence of the water-yielding, bedding-parallel fracture on the Campus Test Site, which is certainly not associated with any dolerite dyke.

There are a number of very important consequences, particularly for the management of Karoo aquifers, that can be derived from the three-dimensional model of the Campus Test Site. The first, and perhaps most important one, is that the movement of water in these aquifers is from the matrix towards the fractures, which implies that flow takes place *mainly in the vertical direction*. The behaviour of Karoo aquifers should, therefore, differ from aquifers in which the flow is horizontal. This conclusion has been confirmed by a number of constant rate tests, performed at the Campus Test Site, Philippolis and Rouxville. What typically happened in these tests is that the water level in the perturbed borehole at first drops continuously until it reaches a depth of approximately 2 m above a water-yielding fracture. Here the water level stabilizes, for as long as the fracture can sustain the yield. This phenomenon repeats itself for every water-yielding fracture that the borehole intersects, only to drop to the pump intake, if the test is performed long enough. The water level, nevertheless, recovers almost instantaneously to the depth of the fracture, and then gradually when the pump is switched off, or the discharge rate is decreased. However, at no stage did the water levels in nearby observation boreholes, *even those that intersect the water-yielding fracture*, drop below the fracture in any of the tests.

It was very difficult to explain the ‘fracture-controlled’ behaviour of boreholes in Karoo aquifers from the field observations alone. One possibility that did emerge, though, is that the behaviour is caused by the fact that water first has to flow from the Karoo formations to the bedding-parallel fractures before it reaches the borehole. The major flow direction in a stressed Karoo aquifer thus seems to be vertical and not horizon-

tal, as is commonly assumed in groundwater flow models. This meant that it will be difficult, if not impossible, to study the behaviour of these aquifers without the use of a three-dimensional flow model.

Three-dimensional mathematical models of groundwater flow are not very popular in geohydrological circles, mainly for two reasons. The first is that such models require considerably more field data and sophisticated computer resources than an equivalent two-dimensional model. The second is that very little attention is usually paid in field investigations to the geometry and structure of an aquifer; factors that are of prime importance in the development of three-dimensional flow models. Fortunately, there were sufficient observational data available to develop such a model for the Campus Test Site. The three-dimensional computer program, SAT3, developed in a previous contract with the Water Research Commission (Verwey and Botha, 1992), was therefore adapted and used to develop a numerical model for the Campus Test Site. This model showed that the piezometric head declines constantly throughout the fracture during the time that a borehole is pumped. The piezometric cone in the fracture thus does not widen with time, as is conventionally assumed, but always keeps the same shape as the piezometric heads decrease. The piezometric gradient, and thus the discharge rate, from the fracture to the borehole must therefore remain constant during the time a borehole is pumped. *There thus exists a limit to the rate at which a borehole in a Karoo aquifer can be pumped*—a conclusion supported by the observation that the phenomenon is only observed if the discharge rate of a borehole is above a certain value. This limiting rate does not depend on the conventional hydraulic parameters, transmissivity and storativity, but on the hydraulic conductivities and specific storativities of both the fracture and rock matrix, and on the areal extent of the fracture. *It is thus imperative that the geometry of a Karoo aquifer must be known before the aquifer is developed for the supply of water to the larger communities.*

The geometry of Karoo aquifers, outlined above, differs completely from that of the media usually considered in the literature on aquifer mechanics, particularly in horizontal flow models. The hydraulic parameters, transmissivity and storativity, derived from conventional two-dimensional horizontal flow models, are therefore meaningless for Karoo aquifers. No wonder that Bredenkamp *et al.* (1995) and Kirchner *et al.* (1991) experienced difficulties in interpreting their hydraulic test data. The only way to study the behaviour of a Karoo aquifer is to use a three-dimensional model. *The common practice to analyse hydraulic test data from these aquifers with horizontal flow models should thus be discouraged.*

There is, unfortunately, not sufficient information or appropriate computer equipment available in South Africa to run a three-dimensional groundwater model on a routine basis. Although steps should be taken to correct the situation if Karoo aquifers are to play a significant role in the future water budget of the country, it is unrealistic to expect that this will be achieved in the short term. A new two-dimensional vertical flow model for the analysis of hydraulic test data was therefore developed towards the end of the project, when it became clear that the flow in Karoo aquifers is mainly vertical. The model is therefore still not fully developed, but case studies have shown that it at least yields more realistic hydraulic parameters than horizontal two-dimensional flow models. *However, this two-dimensional representation will not be suitable for a management model of these aquifers.*

One alternative approach that may solve the problem of inconsistent hydraulic parameters is the horizontal fracture model of Gringarten and Ramey (1974). This rather complex analytical model was only discovered after the completion of the project. No attempt was therefore made to evaluate the applicability of the method to Karoo aquifers.

Another interesting result that followed from the three-dimensional model of the Campus Test Site is that the water level in an open borehole represents an average of the piezometric levels in the fracture and the aquifer, weighted in favour of the piezometric level in the fracture. It is thus difficult to decide precisely how to interpret the water levels. Future observations of Karoo aquifers should therefore preferably be conducted with piezometers. This may add to the cost in developing these aquifers, but then one will be able to interpret the results meaningfully, and at the same time to collect the data required by a three-dimensional model.

The limited capacity of a water-yielding fracture implies that it can be dewatered easily, with a number of undesired consequences of which the first and most obvious, one is a reduction in the borehole's yield. However, there are other and more serious consequences that may take a long time to become noticeable. For example, the three-dimensional model of the Campus Test Site has shown that the flow velocities in the fracture are very high. The borehole and pump may thus become clogged with mud particles set loose by the high flow velocities.

A fully or even partially dewatered fracture may also deform and even collapse. Deformation in an aquifer or borehole is usually neglected in the management and operation of Karoo boreholes. However, there are strong indications that the deformation of water-yielding fractures is more common than usually thought. The complaint: *'my borehole has dried up'*, often heard from people who depend on Karoo aquifers for their water

supply, may indeed be the result of a collapsed fracture. This interpretation is supported by the observation that it is often possible to drill a new, successful borehole within a short distance from the one that ‘dried up’. Another, less spectacular, but probably related, phenomenon is a borehole whose yield decreases with time. The phenomenon has never been discussed in the literature, to the knowledge of the authors, but discussions with farmers indicated that it is quite common in Karoo boreholes older than 10 years. Hydraulic tests, performed during the project, also indicated that the deformation of a borehole in a Karoo aquifer may affect its yield adversely. However, none of these observations could provide an estimate of the magnitude of such a deformation. This only became apparent when one of the high-yielding boreholes on the Campus Test Site was imaged with an acoustic televiewer, in June 1996. This borehole was surveyed geophysically on two previous occasions; the first one carried out by the Department of Water Affairs and Forestry on 1992-06-04 and the second one by the consulting firm BPB Instruments Ltd on 1993-12-01. As shown in Figure 4–35, the fracture zone that contains the water-yielding fracture is clearly visible at a depth of 23,0 m on both surveys. However, neither the subvertical fracture, between 22,5 and 23,0 m, nor the highly warped zone at 23,8 m, appears on the scans of these surveys. These features must therefore have developed after December 1993, possibly through the reactivation of existing planes of weakness, caused by the extensive hydraulic tests performed on this borehole. This suggests that the observed decrease in the transmissivity of the borehole over the past five years, may have been caused by the deformation of the borehole. Deformations, be it only of the boreholes themselves, may be thus be more common in Karoo aquifers than previously thought.

In conclusion, it can be said that there is little doubt that the behaviour of boreholes in Karoo aquifers is completely determined by the presence of bedding-parallel fractures, which are mainly horizontally orientated. This does not mean that there are no vertical or subvertical fractures in these aquifers, or that they play an insignificant role, but only that they do not influence the behaviour of boreholes significantly. Indeed, there are indications that vertical and subvertical fractures play a significant role in recharging the aquifers. For, as shown by the contour map in Figure 4.39 of Kirchner *et al.* (1991), Karoo aquifers are not recharged locally, but only in the surrounding hill tops, which usually contain large numbers of vertical fractures.

11.3 RECOMMENDATIONS

The most important conclusion of the present study is that Karoo aquifers do not necessarily contain insufficient quantities of water, but that their complex geometry makes it difficult to withdraw the water reliably. There is thus no reason, in principle, why Karoo aquifers cannot make a significant contribution to the water budget of the country. The only prerequisite is that *they are managed properly*, and in accordance with their basic physical properties, although this is probably more easily said than done. Admittedly, this interpretation differs, considerably from the conventional interpretation of the aquifers. However, it is the only interpretation the project team is aware of, that allows one to interpret the observed behaviour of the aquifers concisely and consistently.

The present interpretation of Karoo aquifers emerged from a study of the history of the aquifers, and the interpretation of a limited number of hydraulic tests with a three-dimensional numerical model. Nevertheless, it did show that one will have to take the three-dimensional nature of the aquifers into account, in managing the aquifers. However, this should not be so much of a problem, provided that the following prerequisites are met.

It is well-known that any management model is useless, unless supported by sound and accurate measurements. Unfortunately, previous studies of Karoo aquifers were usually based on the assumption that flow in these aquifers is horizontal. Little attention was therefore paid to the three-dimensionality of these aquifers. Future studies should therefore try to correct this imbalance in the observational data.

The success in implementing such an approach will ultimately depend on the solution of two related problems—what observational techniques to use, and how to gather, store and manipulate the observational data. The observational equipment available today, such as packers, is quite expensive and their applicability often limited. Special attention should therefore be given to the development of less expensive, and perhaps more appropriate observational equipment. The present attempt to develop more suitable and less expensive packers at the Institute for Groundwater Studies should thus be encouraged. Attention should also be given to incorporate more innovative techniques, such as *in situ* flow measurements, into the observations. Nevertheless, there are some steps that can be taken immediately, without increasing the cost of the study exorbitantly. These include:

- (a) Detailed geological logs must be kept of *all* new boreholes drilled in Karoo aquifers, with special emphasis on the depths of water strikes.

- (b) At least one observation borehole should be drilled for every production borehole and equipped with piezometers.
- (c) Every production borehole should be equipped with a flow meter.
- (d) The discharge rates of production boreholes and piezometric levels in the observation boreholes should be measured routinely and stored in a suitable database.

Experience at Philippolis has shown that the local population is quite prepared to gather the necessary information, accurately and reliably, if they are trained sufficiently and given the reason for collecting the data. No severe difficulties are thus foreseen with the gathering of the data, which incidentally may also create more jobs. The storage and manipulation of the observational data are another matter, however. As anyone with experience in three-dimensional modelling knows, such models are quite complex, cannot be duplicated at will, and require special computer resources and highly trained personnel. It may thus be worthwhile for the Department of Water Affairs and Forestry to establish a special unit that controls Karoo aquifers and directs their management, operation and future investigations.

The single most important prerequisite to satisfy the program outlined above, is also perhaps the most difficult to achieve. That is, to change the attitude of groundwater practitioners. Considerable progress has been made in the physics and chemistry of groundwater flow, yet these new principles are often shrugged off with the remark: '*... it cannot easily be used by practitioners*', or the present methods are quite successful, so why bother with new methods? As Sir Winston Churchill once said: '*Men occasionally stumble over the truth, but most pick themselves up and hurry off as if nothing ever happened.*' It is therefore important to remember that *Nature behaves in its own subtle ways, and not as prescribed by man*. The possibility thus always exists that factors discarded today in managing Karoo aquifers may have devastating effects on the future behaviour of the aquifer, as the Love Canal disaster (Princeton University Water Resources Program, 1984) has shown. Since the Karoo aquifers have not been used extensively until recently, and groundwater moves very slowly, there may still be a chance to avoid such a disaster, but only if appropriate observational and managerial techniques are implemented now. This will not only ensure that future generations will still be able to withdraw water from the aquifers, but can also lead to a considerable reduction in development costs, if recent experiences in the oil industry (Clementz, 1997) can be used as a measure.

All known physical properties of Karoo aquifers were included in the computer program used to establish the three-dimensional model for the Campus Test Site. However, as pointed out in Chapter 2, it is almost impossible to achieve this objective in an initial study. The present version of the computer program is no exception to this rule. For example, the model does not take the deformation of the fracture, or the aquifer, into account. The simulated flow velocities near the fracture in a perturbed borehole are also very high. A future version of the model, therefore, may have to be based on the more general Navier-Stokes equation, rather than the conventional groundwater flow equation in Equation (7.1), as in the present version of the program. However, there does not exist sufficient observational data to justify such a drastic revision of the model at the moment. It is therefore recommended that particular attention be given to: (a) the behaviour of the *in situ* flow field, and (b) the deformation of the water-yielding fractures and aquifers in future investigations of Karoo aquifers.

The most controversial aspects in using Karoo aquifers for water-supply purposes are probably to site suitable production boreholes and to determine the depth where the water will be struck. These problems were not addressed specifically in this study, but were especially noticeable in the investigations at Rouxville. Here, water was struck only at depths greater than 90 m, in contrast to the depths of 20–30 m, at Campus Test Site, Dewetsdorp and Philippolis. None of the available geophysical techniques is able to detect at which depths water will be struck, or delineate the bedding-parallel fractures in Karoo aquifers. It is therefore recommended that attention be given to more innovative geophysical techniques that may solve these problems.

A particularly interesting method that promises to solve both problems at once, is the nuclear magnetic resonance method, developed by Russian scientists (Schirov *et al.*, 1991). This method is based on properties of the hydrogen nucleus itself. It should thus not be influenced by clay, or other electrically conductive layers that frequently appear in Karoo formations and influence electromagnetic techniques adversely.

Another technique that seems equally promising is the seismic method of Rector and Marion (1991). This method, which uses the drill bit as the seismic source, is able to provide real time data on the structure of the aquifer and the horizons below the drill bit. However, it may be necessary to use more sophisticated analytical techniques than is commonly used in seismic work, even those used in the original paper, if the method is to be applied successfully.

Irrigation farmers are perhaps the people that benefit most from Karoo aquifers at the moment. However, the water canon and sprinkler systems they use are inefficient and a waste of water and money. An attempt should therefore be made to encourage them to use more efficient irrigation methods, such as drip-

and micro-irrigation systems. Experience in Israel has shown that these systems conserve considerable quantities of water and increase crop production at the same time. Moreover, the systems do not require high-yielding boreholes, and are therefore ideal for Karoo aquifers. An irrigation farmer who installs one of these systems, therefore, will not only increase the productivity of his farm, but will also contribute to the conservation of perhaps the most precious natural resource in South Africa: water.

Boreholes are undoubtedly the most cost-effective method to withdraw water from an aquifer. However, the dependence of a borehole's yield on the presence and properties of a fracture raises the question if boreholes are the best method with which to withdraw water from Karoo aquifers. Although some of the adverse effects can be limited by pumping and spacing the boreholes judiciously, it may still be advantageous to introduce other production methods, such as the ganats of the ancient Persians, in future studies of these aquifers.

APPENDIX A

THE INTRUSION OF LACCOLITHS

A.1 INTRODUCTION

The intrusion of magma into relatively undeformed sedimentary rocks, at high levels in the earth's crust, received considerable attention in the late nineteenth and early twentieth centuries. One of the first of these attempts was that of Gilbert, who studied many intrusions exposed on the flanks of the Henry Mountains in south-eastern Utah (Johnson and Pollard, 1973).

Magma must obviously have a pathway before it can intrude into the earth's surface. The available literature indicates that there are mainly two processes that may form such pathways. The first, and perhaps the best known example, is the fracturing of the earth's crust by tectonic events (Rubin, 1995), and the second, matrix melting (Maaløe, 1985). The main effect of matrix melting is the production of elongated narrow dykes (Maaløe, 1985). This type of intrusion, therefore, could have been responsible for the numerous linear dykes that is a characteristic of the Karoo landscape. However, judging from the discussion in Maaløe (1985), it is difficult to see how matrix melting could have caused the formation of the large laccolithic structures and the ring-shaped dykes, so typical of the Karoo landscape. A physical, more attractive explanation of these structures is Gilbert's theory for the intrusion of laccoliths, as discussed by Johnson and Pollard (1973). Since these structures seem to play a very important role in the geohydrology of Karoo aquifers, this theory will now be described in more detail.

A.2 GILBERT'S THEORY FOR THE INTRUSION OF A LACCOLITH

To discuss Gilbert's theory, consider the schematic representation of a cylinder of overburden, lifted by a normal force, acting in the vertical plane, as in Figure A-1. Suppose that the pressure of the magma (per unit area), p , is equal across the base of the cylinder. The magnitude of the force \mathbf{N} , normal to the base of the cylinder with radius a , can then be expressed as:

$$N = \pi a^2 p$$

Similarly, if the shearing force, σ , is constant over the contact area, the total shearing force, S , acting on the contact area of the overburden, with thickness d , is,

$$S = (2\pi ad)\sigma$$

If ρ_r denotes the density of the rock, the weight of the overlying rock mass is given by,

$$W = \pi a^2 \rho_r g d = \pi a^2 p_r$$

An intrusion therefore cannot lift the overburden, unless the difference between the magma force, \mathbf{N} , and the weight of the overburden, \mathbf{W} , exceeds the shearing force, \mathbf{S} , that is

$$a(p - p_r) \geq 2\sigma d \quad (\text{A.1})$$

The magma must thus have a minimum area, which Gilbert calls the limital area, or spread out laterally as a sill, before it can lift the overburden.

It is important to note that Gilbert's theory does not require an external force to drive the magma. To see this, one only has to look at the expression for the driving pressure, p_d , which, in the case of a Newtonian magma, assumes the form

$$p_d = p - p_r = (p_0 - \rho_m g h) - p_r$$

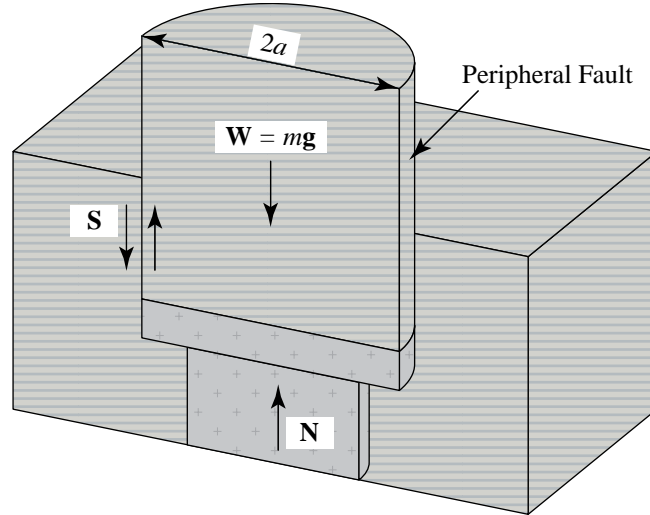


Figure A-1 Gilbert's model for the intrusion of magma.

where ρ_m is the density of the magma, p_0 the lithostatic pressure at the source and h the height of the fracture above the source. Figure A-2 shows a graph of the driving pressure in an overburden 40 m thick, with the given density distribution, and a magma density of 2600 kg m^{-3} . Notice also that the driving pressure increases from the source up to the zone where the density of the host rock and magma is equal, and then decreases. The driving pressure of the magma is thus highly dependent on the difference in density of the magma and the host rocks.

Magma can, of course, also be squeezed upwards by tectonic events. Pore fluids in the host rock that volatilize, or fluids dissolved in the magma, can also contribute to the total driving pressure. However, these forces are not necessary to drive the intrusion of the magma. As pointed out in Section 4.2.1, the major dolerite intrusions in the Karoo Supergroup occurred during the second pulse of the fragmentation of Gondwanaland, which means that the continent was largely under the influence of stresses. The tectonics of the event may thus have created the fractures for the intrusion, but did not necessarily partake in the intrusion.

The limit area of a laccolith essentially depends on two parameters: the thickness of the overburden and the shearing force, according to Equation (A.1). Smaller laccoliths may therefore occur inside larger ones, but higher up in the succession, as Burger *et al.* (1981) have observed at Philippolis.

A.3 BENDING OF THE OVERBURDEN

A.3.1 Uniform Driving Pressure

In the previous discussion, attention was mainly paid to the intrusion of magma. Nothing was consequently said about the behaviour of the overburden. Pollard and Johnson (1973) based their study of the overburden's behaviour on the theory of plates; an approach that will also be followed here.

The basic assumption of Pollard and Johnson (1973) is that the strata in the overburden can be represented by a series of thin plates, as shown in Figure A-3. They further assume that each layer is homogeneous and isotropic, but that different layers may have different elastic properties. With these assumptions, the vertical displacement, $w(x, y)$, in a single layer above the laccolith must satisfy the well-known differential equation of Sophie Germain for plates

$$D_x^4 w(x, y) + 2D_x^2 D_y^2 w(x, y) + D_y^4 w(x, y) = p_d(x, y)/D \quad (\text{A.2})$$

where $p_d(x, y)$ is the driving pressure. The parameter

$$D = Et^3/[12(1 - \sigma^2)] = Bt^3/12 \quad (\text{A.3})$$

with t the thickness of the plate, E Young's modulus, σ Poisson's ratio, and B the elastic modulus, is commonly known as the *flexural rigidity* of the plate.

A further assumption of Pollard and Johnson is that the magma spreads out laterally over the elliptical area

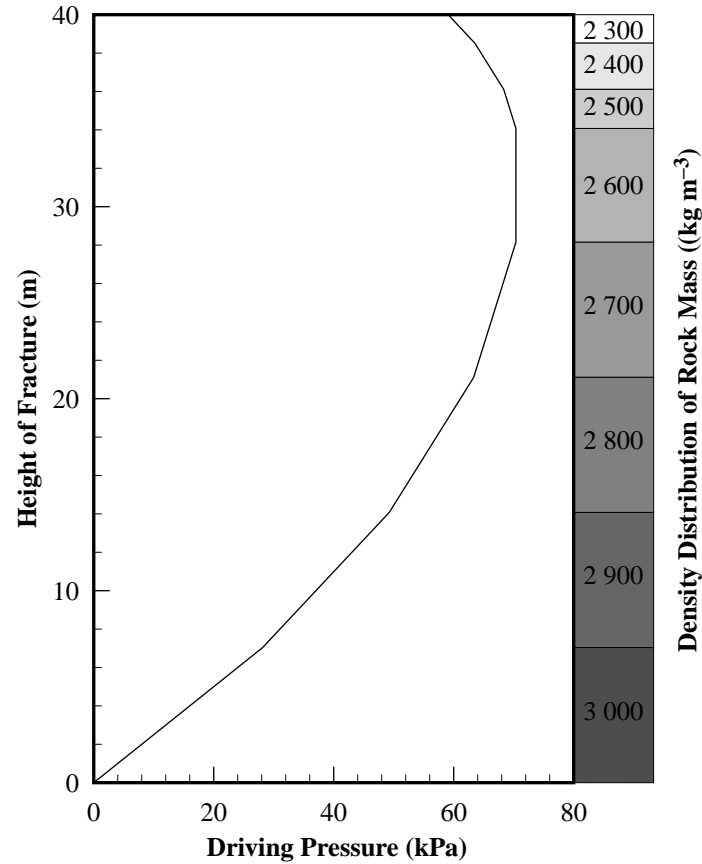


Figure A–2 Relation between the driving pressure of the magma and height of a fracture, in an overburden 40 m thick, for a given density.

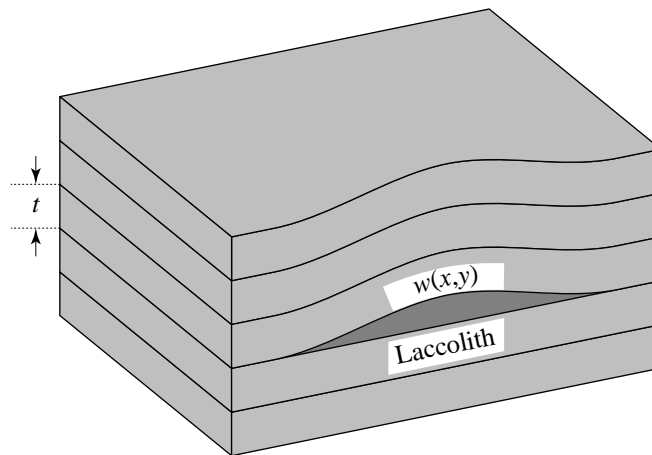


Figure A–3 Schematic representation of the intrusion of magma into an overburden consisting of different strata.

$$(x^2/a^2) + (y^2/c^2) = 1 \quad (\text{A.4})$$

This assumption may seem to be very restrictive, at first sight. However, as shown in Figure A–4, the most probable geometrical shapes the magma can assume can all be regained from this equation by varying the coefficients a and c .

Pollard and Johnson (1973) made two further assumptions to obtain the necessary boundary conditions for Equation (A.2).

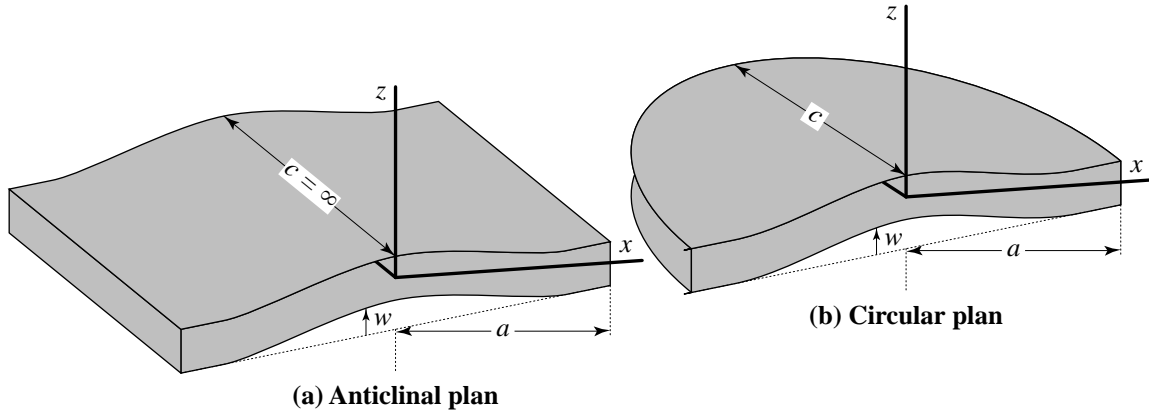


Figure A-4 Two common plan shapes described by Equation (A.4).

- (a) The driving pressure is constant over the entire area of the intrusion.
- (b) The displacement and slope on the centre plane of the layer are zero at the boundary of the elliptical area, defined by Equation (A.4).

This yields the boundary conditions

$$\begin{aligned} p_d &= \text{constant} & [(x^2/a^2 + y^2/c^2) \leq 1] \\ w(x, y) = D_x w(x, y) = D_y w(x, y) &= 0 & [(x^2/a^2 + y^2/c^2) = 1] \end{aligned} \quad (\text{A.5})$$

The solution of Equation (A.2), subject to the boundary conditions in Equation (A.5), is given by (Filonenko-Borodich, 1965; Pollard and Johnson, 1973)

$$w(x, y) = (p_d / 8D)[1 - (x/a)^2 - (y/c)^2] / [(3/a^4) + (4/c^4) + (2/a^2c^2)] \quad (\text{A.6})$$

The displacement of any layer can thus be calculated if the driving pressure, elastic constants, geometric constants and thickness of the layer are known. Figure A-5 shows cross-sections of the displacement in the xz -plane ($y = 0$) for an anticlinal intrusion

$$w(x, 0)|_{c=\infty} = p_d(a^4 - 2a^2x^2 + x^4) / 24D \quad (\text{A.7})$$

and a circular intrusion

$$w(x, 0)|_{a=c} = p_d(a^4 - 2a^2x^2 + x^4) / 64D \quad (\text{A.8})$$

All other elliptically shaped intrusions have displacement magnitudes and shapes between these two extremes.

An interesting result that follows immediately from Figure A-5 and Equation (A.6), is that the plan shape of the intrusion determines the displacement in the z -direction. For example, the maximum displacement for a circular intrusion is only 37.5% of that of an anticlinal intrusion, while the vertical displacement increases with the fourth power of the distance that the magma spreads out laterally. The doubling of a circular laccolith's diameter will therefore increase its maximum displacement 16 times.

It is obvious that the magma has to crystallize before the overlying layer reaches its elastic limit, if the laccolithic intrusion has to preserve its form. Otherwise the layer will be significantly fractured, with a corresponding deformation of the laccolith. The possibility to observe laccolithic structures in the field cannot therefore be too high. Nevertheless, as shown in Figure 4-7, such structures do occur in the Karoo landscape.

A.3.2 Linear Driving Pressure

The discussion thus far was limited to a uniform distribution of the driving pressure, over the entire area of the intrusion. However, it is well-known that the velocity and pressure in a fluid generally increase towards the centre of a conduit. It is thus rather unlikely that a uniform distribution of the driving pressure will ever occur, even in the case of magma.

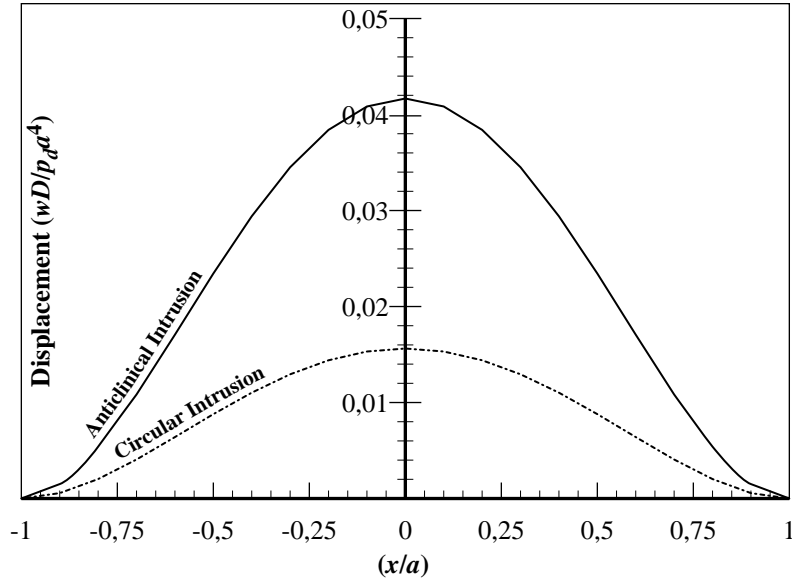


Figure A-5 Cross-sections of the displacements caused by (a) an anticlinal and (b) a circular laccolithic intrusion.

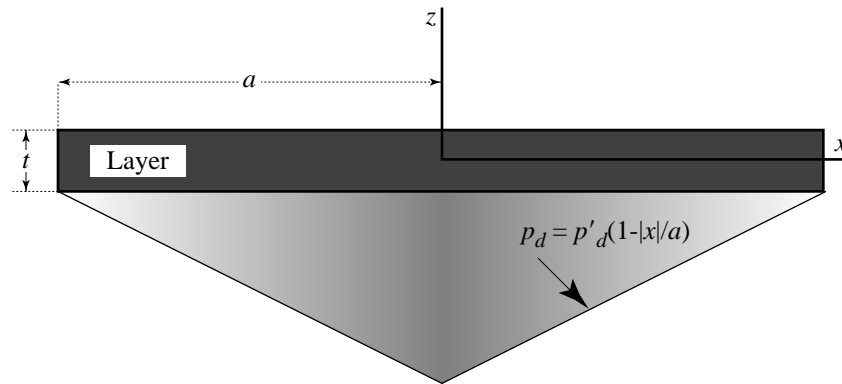


Figure A-6 Linear pressure distribution over an anticlinal laccolithic intrusion.

The introduction of a non-uniform driving pressure can complicate the discussion of laccoliths considerably (Filonenko-Borodich, 1965). The following discussion will therefore be limited to the case of an anticlinal laccolith experiencing a linear driving pressure with the feeder conduit at the laccolith's centre, as shown in Figure A-6.

It follows from Equation (A.4) that the displacements caused by the laccolithic intrusion in Figure A-6, will only be a function of the co-ordinate in the x -direction, in which case Equation (A.6) reduces to the one-dimensional equation,

$$D_{xxx} w(x) = p_d / D \quad (\text{A.9})$$

The displacement of the linear driving pressure can thus be calculated easily by integrating Equation (A.9) four times. The solution for the linear driving pressure in Figure A-6, subject to the boundary conditions,

$$\begin{aligned} w(x) = D_x w(x) &= 0 \quad (x = \pm a) \\ D_{xxx} w(x) &= 0 \quad (x = 0) \end{aligned}$$

is given by

$$w(x) = (p'_d / 240D) [10x^4 - (2|x|^5/a) - 15a^2x^2 + 7a^4]$$

with $|x|$ the absolute value of x . This displacement profile is compared graphically with the one for a uniform driving pressure in Figure A-7.

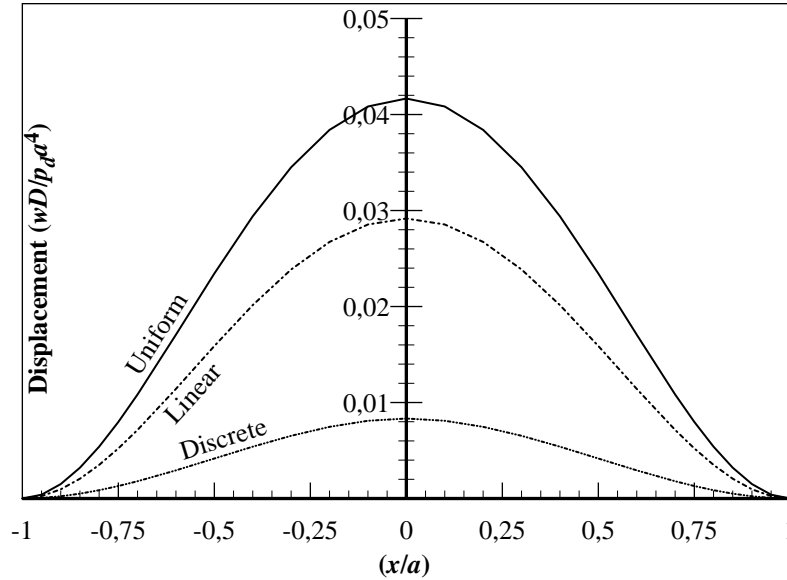


Figure A-7 Displacement profiles of the layers over an anticlinal laccolith subject to: (a) a uniform, (b) a linear and (c) a discrete driving pressure.

The displacements in Figure A-7, are very similar, except that the maximum displacement for the linear driving pressure is only 70% of that of the uniform pressure distribution. Nevertheless, this exercise shows that the thickness of a laccolith and the consequent deformation of the overburden depend on both the magnitude and distribution of the driving pressure.

A.3.3 Distribution of Shearing Stresses in the Overburden

Pollard and Johnson (1973) evaluated the model of Equation (A.6) further by correlating the distribution of the shearing stresses with the isochromatic patterns in photo-elastic gelatin layers. In the case of an anticlinal laccolith, these stresses can be expressed as (Filonenko-Borodich, 1965)

$$\begin{aligned}\sigma_{xx} &= -EzD_{xx}w(x)/(1-\sigma^2) = p_d z(6x^2 - 2a^2)/t^3 \\ \sigma_{zz} &= 0 \\ \sigma_{xz} = \sigma_{zx} &= E(z^2 - t^2/4)D_{xxx}w(x)/[2(1-\sigma^2)] = 6p_d x(t^2/4 - z^2)\end{aligned}\quad (\text{A.10})$$

Contours of the maximum shear stresses are compared with the isochromatics of two gelatin layers, numbered from lower to higher order, in Figure A-8.

Although the match between the theoretical and experimental shear stresses in Figure A-8 is not perfect, most probably because of differences between the theoretical and experimental boundary conditions, there are some striking similarities. High shear stresses are concentrated at the top and bottom of the layer, over both the centre and the periphery, with the extreme values at the contact of the plate and the tip of the laccolith.

The shearing stresses in Equation (A.10) are linear in the driving pressure, p_d , but cubic in the thickness, t , of the layer. A layer with a thickness, $2t$, will thus deform eight times less than one with a thickness, t , for the same driving pressure. The deformation of a layer thus depends more on its thickness than on the driving pressure.

A.4 DEFORMATION OF THE DISPLACED OVERBURDEN

A.4.1 Viscosity of the Magma

The previous expressions for the displacement of the overburden have all been derived with the implicit assumption that the magma remains in a state of fluidity. Any crystallization of the magma must obviously have some effect on the distribution of the driving pressure, and thus on the shape of the laccolith. Indeed Paige (Pollard and Johnson, 1973) has argued that the crystallization of the magma, from the ends of the intrusion to ward the feeder, will cause a central bulging of the laccolith. To investigate this possibility,

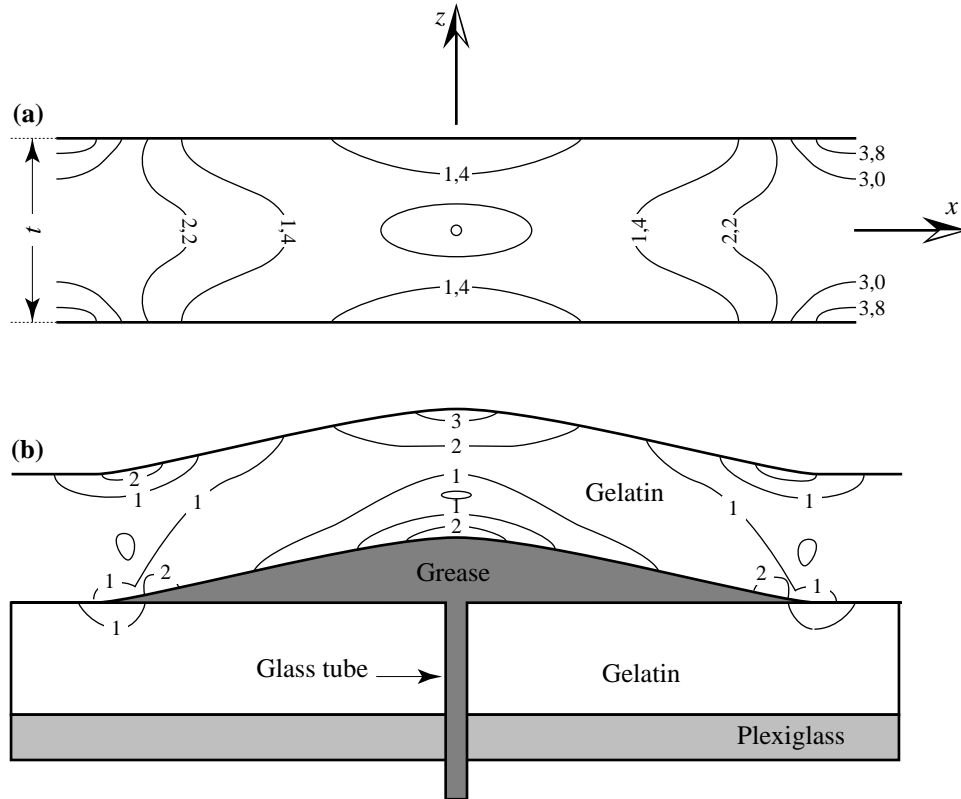


Figure A-8 Distribution of the maximum shear stresses in a layer overlying a laccolithic intrusion. (a) Theoretical distribution for a layer, with a length to thickness ratio of 4. (b) Contours of the isochromatics determined from a photo-elastic gelatin model. [Redrawn from Pollard and Johnson (1973).]

consider the case where the magma is only restricted to a small part, l , of the laccolith shown in Figure A-9. In this case the shearing forces must satisfy the equation

$$S_x = D \cdot D_{xxx} w(x) = p_d' l / 2$$

if equilibrium is to be maintained in the z -direction. The resulting displacement in the z -direction, subject to the boundary conditions,

$$w(x)|_{x=\pm a} = 0 \quad \text{and} \quad D_x w(x)|_{x=0, \pm a} = 0$$

is then of the form

$$w(x) = p_d' l (2|x|^3 - 3ax^2 + a^3) / 24D$$

This displacement, which is also shown in Figure A-7 for the case where $l = a/5$, is smaller than those caused by the uniform and linear distributed driving pressures. However, its shape does not differ drastically from that of the uniform and linear distributed driving pressures. The shape of a laccolithic intrusion thus does not seem to correlate with the magma viscosity. This conclusion is further strengthened by the analysis of the shearing stresses and bending moments of the laccolith (Pollard and Johnson, 1973).

A.4.2 Stretching of the Overburden

The conventional theory of plates assumes that the centre plane will not stretch during the deformation of the plate. This will only be true if the centre plane is detached from its boundary and is able to slide horizontally towards the centre of the deformation. Since such a sliding is not very likely in geological strata, the centre planes in laccolithic intrusions are probably stretched.

To derive an expression for the stretching of the layer, consider the situation shown in Figure A-10, where the layer has been stretched from its original length, a , to its final length, a' . The longitudinal strain of

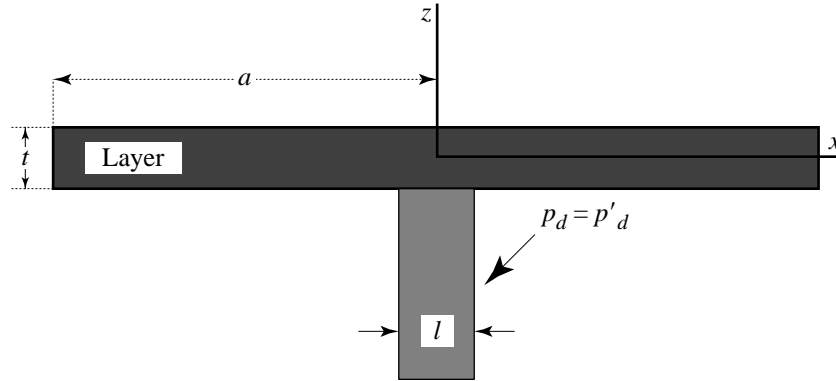


Figure A-9 Schematic representation of a non-uniform pressure distribution over a laccolithic intrusion. The driving pressure with a constant magnitude, p'_d , acts out only over the distance l in the x -direction.

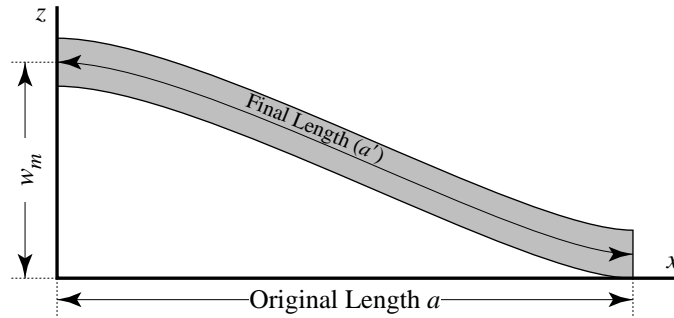


Figure A-10 Schematic representation of the stretching in the centre plane of a layer displaced to its maximum, w_m , by an intruding laccolith.

a layer, due to stretching, can then be defined as

$$e_{xx}^s = (a - a')/a \quad (\text{A.11})$$

The final length of the layer's centre plane can be computed from the expression for the length of a line segment

$$a' = \int_0^a [1 + \{D_x w(x)\}^2]^{1/2} dx$$

and the expressions for the displacement in Equations (A.7) and (A.8), to obtain

$$a' = \int_0^a [1 + 16w_m^2 (x^6 - 2a^2 x^4 + a^4 x^2) / a^8]^{1/2} dx \quad (\text{A.12})$$

where w_m is the maximum displacement, which equals $p_d a^4 / 64D$ for a circular laccolith and $p_d a^4 / 24D$ for an anticlinal laccolith.

The integral in Equation (A.12) can be evaluated by expanding the square root term with the binomial theorem, to obtain

$$e_{xx}^s \approx -0.61(w_m/a)^2 + 0.27(w_m/a)^4 \quad (\text{A.13})$$

The expression for strain in the plane due to bending can be computed from its expression in Equation (A.10), and is given by

$$e_{xx}^b = 4w_m z(3x^2 - a^2) / a^4 \quad (\text{A.14})$$

The bending strain is thus a function of x and z . The strain, which is zero on the centre plane ($z = 0$), also known as the neutral plane, varies linearly across the layer and achieves its maximum at the top and bottom

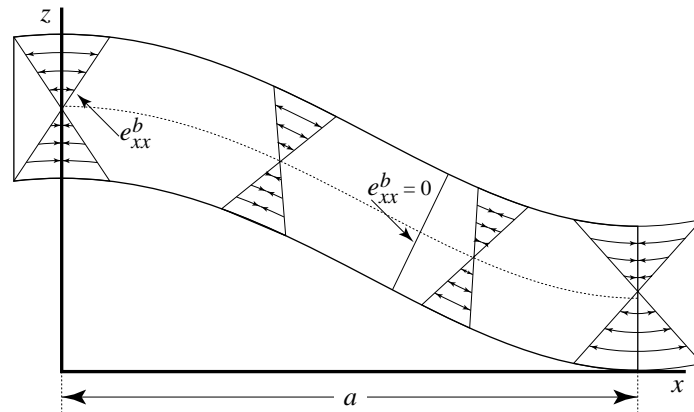


Figure A-11 Schematic representation of the longitudinal bending strains across a layer deformed by a laccolith.

surfaces of the layer, as indicated in Figure A-11.

An important result that follows immediately from Equation (A.14) and Figure A-11 is that the bending strains are contractions over the bottom surface of the layer at the laccolith's centre, and extensions over its periphery. Bending thus encourages magma to penetrate the overlying layer on the periphery, but discourages it at the centre of the intrusion. Moreover, the largest longitudinal extension in the plane of the layer acts perpendicular to the periphery. The first extension fractures to form an over-stretched layer should, therefore, appear on the periphery of the layer and open downward. The easiest way for the magma to intrude, is thus into the fractures on the periphery of the layer, thereby forming a peripheral dyke. Figure A-12 shows the development of such a peripheral dyke, as observed by Pollard and Johnson (1973) in their experimental studies with gelatin models.

The total strain obtained by adding the longitudinal strain in Equation (A.13) to the bending strain in Equation (A.14), will tend to move the neutral surface upwards over the intrusion's periphery and down over its centre. Extensions due to bending will thus be enhanced and contractions diminished during the intrusion of a laccolith. Large longitudinal strains will therefore improve the conditions for the formation of peripheral dykes.

It is important to note that the longitudinal bending strain is a function of z . A thick layer of overburden will therefore develop a proportionally larger strain than a thin layer, for the same values of a and w_m , and will thus be more susceptible to the formation of peripheral dykes than a thin layer of overburden.

A.5 A MULTI-LAYERED OVERBURDEN

The discussion has thus far concentrated exclusively on the effect that an intrusion will have on a single layer directly above it. This situation will rarely occur, if ever, in the Karoo Supergroup with its various layers of mudstones, siltstones, shales and sandstones. One approach to this problem is to represent each lithological

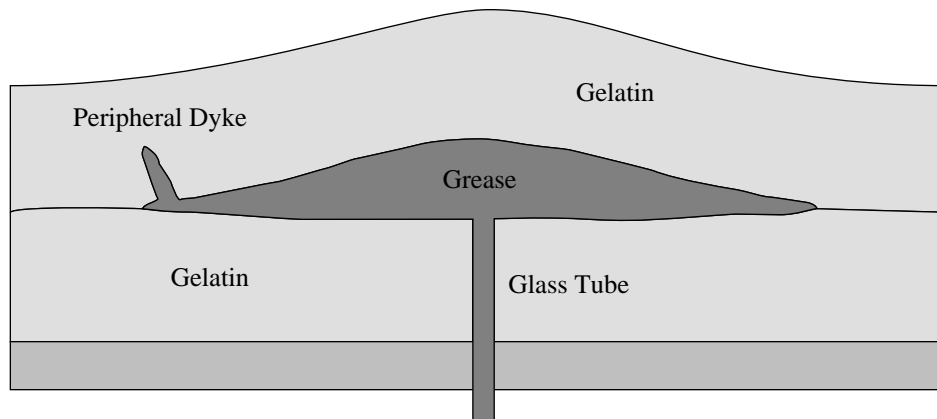


Figure A-12 Formation of a peripheral dyke in experimental gelatin models. [Redrawn from Pollard and Johnson (1973).]

unit as a distinct layer, free to slide over the adjacent layers. Real lithological units will undoubtedly experience some bonding and friction. However, the large-scale fracturing at the contact planes of the units in the cores, from the Campus and Dewetsdorp test sites, suggests that this approximation is not too unrealistic for the Karoo Supergroup, particularly its Beaufort and Eccma members. In any case, it is possible to extend the model to more complicated situations, ranging from the free-sliding to perfectly bonded layers, should the need arise. The discussion to follow, however, will be restricted to an overburden composed of n free-sliding layers with individual thicknesses, t_i , and elastic moduli, B_i .

The effective flexural rigidity, D_e , of a set of n free-sliding layers is just the sum of the individual rigidities, as defined in Equation (A.3), that is

$$D_e = \sum_{i=1}^n (B_i t_i^3 / 12) \quad (\text{A.15})$$

Equation (A.15) can also be expressed in the form

$$D_e = B T_e^3 / 12$$

where B is the effective thickness of the n layers—the thickness of a single layer that has the same flexural rigidity as the stack of n layers—and

$$T_e^3 = \sum_{i=1}^n (t_i^3)$$

if all the layers have approximately the same elastic moduli. It is not difficult to show that the cube root of a sum is always less than the sum, that is

$$\sqrt[3]{\sum_i (t_i^3)} < \sum_i (t_i)$$

The effective thickness of a free-sliding n -layer overburden is thus always less than the thickness of the n layers. A thick-layered overburden, therefore, will not present as large a resistance to elastic deformation as one might have thought.

The layers of Karoo sedimentary rocks certainly have different elastic moduli, while their original contact planes were rough. It will therefore be difficult for such layers to slide across one another when displaced by a laccolith, without weakening or fracturing their contact planes. The intrusion of laccoliths may thus have been responsible, or at least have contributed, to the existence of a major feature of Karoo formations—bedding-parallel fractures. The frequency with which bedding-parallel fractures occur in Karoo formations and their sizes can be judged from the photograph of the core from Borehole CH6 on the Campus Test Site in Figure 4–9. The intrusion of laccoliths therefore presents an ideal mechanism for the formation of the numerous ring-shaped structures in the Karoo landscape and the bedding-parallel fractures that play such an important role in the physical behaviour of Karoo aquifers.



APPENDIX B

DESCRIPTION OF EQUIPMENT USED IN THE HYDRAULIC TESTS

B.1 GENERAL

The hydraulic parameters of an aquifer can only be determined by evaluating the reaction of the aquifer under stress. Special attention was therefore given to the development of accurate and versatile equipment to: (a) induce stress in the aquifer, (b) measure the reaction of the aquifer under stressed conditions and (c) develop the necessary software for data capturing, in the project. Since this equipment differs substantially from that commonly used in hydraulic tests, their development and application are briefly discussed in this appendix.

B.2 THE PUMPING SYSTEM

The main aim of the project was to investigate a number of aquifers in the Karoo formations. This necessitated the development of a pumping system that could be transported easily. A pumping system, consisting of

- (a) a 5 kW electricity generator,
- (b) a submersible pump with a maximum capacity of $2,2 \cdot 10^{-3} \text{ m}^3 \text{ s}^{-1}$,
- (c) a flow meter with a range of $2,7 \cdot 10^{-4}$ to $2,7 \cdot 10^{-5} \text{ m}^3 \text{ s}^{-1}$,
- (d) a winch to install and withdraw the pump to a depth of 60 m,

with the necessary valves, pipes and cables was therefore mounted on a trailer, as illustrated in Figure B-1. The system has been used very successfully during the project.

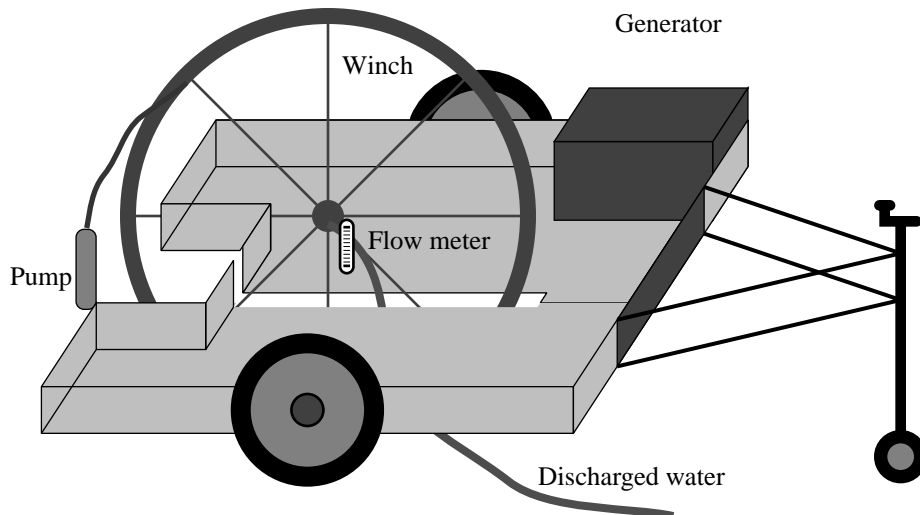


Figure B-1 Graphical illustration of the pumping system used in most of the hydraulic tests described in the report.

B.3 PRESSURE TRANSDUCERS

Changes in water levels and piezometric levels are the most important observables in hydraulic tests. It is therefore of the utmost importance that these quantities are recorded reliably and accurately. The measurements were therefore taken with commercial SensorTechnics model PT2015G4 pressure transducers, each housed in a water tight brass container. This meant that their calibration curves

$$I = ah + b \quad (\text{B.1})$$

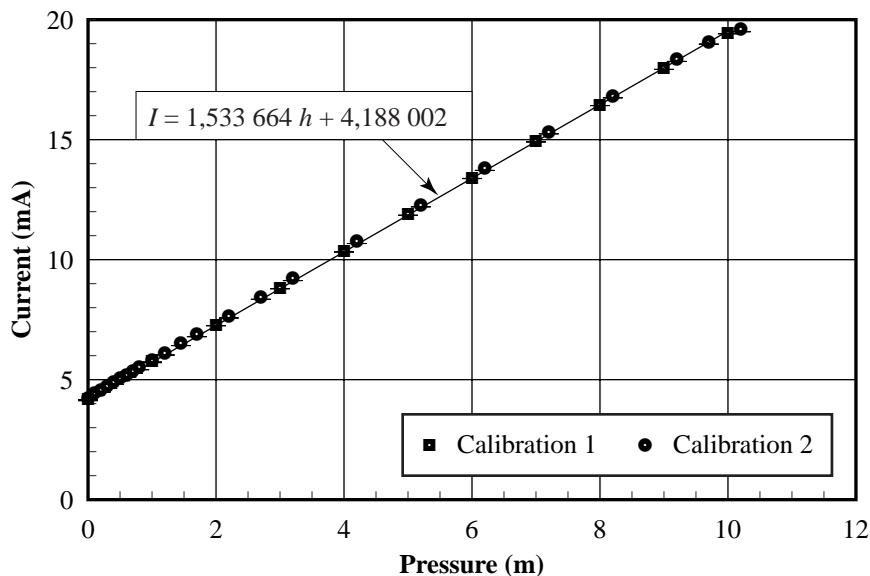


Figure B-2 Calibration curve for one of the transducers used in the project.

had to be determined individually. Two methods were used for this purpose. In the first method, the transducers were placed at fixed depths in a drum. Their currents, I , and the water pressures, h , were then measured at every depth. The process was repeated three times for each transducer, and the averaged values fitted to Equation (B.1) with a linear least squares algorithm. The procedure was also repeated in a borehole. The full calibration was repeated six months later to ensure that the calibration curves were not subject to experimental drift. The results for transducer No. 12 are shown in Figure B-2.

Measurements with the transducers were all recorded electronically on an IBM-compatible personal computer that also served as the storage device for the data. A new program, which also allows the user to display the progress of a test and quality of the data, was written in C for this purpose.

APPENDIX C

MATHEMATICAL REDUCTION OF DIMENSIONS

C.1 INTRODUCTION

The fundamental concept in the mathematical reduction of dimensions of a given physical phenomenon is to integrate the governing equation(s) over the dimension to be omitted. This is a relatively straightforward procedure in Cartesian co-ordinates (Botha, 1996), but can become somewhat involved if one also wants to transform the co-ordinates themselves, as envisaged in Chapter 10. The various mathematical procedures are therefore briefly discussed in this appendix, be it merely for the benefit of readers who are not acquainted with the fundamental procedures of transformations.

C.2 MATHEMATICAL PRELIMINARIES

C.2.1 Transformation of the Elementary Volume Element

The elementary volume element is the most basic concept in the transformation of one co-ordinate system into another. Although the concept can be applied to any type of co-ordinate system, the present discussion will be limited to the two orthogonal co-ordinate systems

$$\mathbf{x} = (x, y, z) \quad \text{and} \quad \mathbf{u} = (u, v, w)$$

Let

$$d\Omega = dx dy dz \quad \text{and} \quad d\Gamma = du dv dw$$

denote the elementary volume elements in the two co-ordinate systems respectively, and let $(\mathbf{i}, \mathbf{j}, \mathbf{k})$ and $(\mathbf{e}_u, \mathbf{e}_v, \mathbf{e}_w)$ be two sets of orthogonal unit vectors, associated with the co-ordinate systems, as illustrated in Figure C-1.

Application of the chain rule for differentiation (Hildebrand, 1976) shows that the elementary distance vectors in the two co-ordinate systems, $d\mathbf{x}$ and $d\mathbf{u}$, must be related by an equation of the form

$$d\mathbf{x} = \begin{pmatrix} dx \\ dy \\ dz \end{pmatrix} = \mathbf{J} \begin{pmatrix} du \\ dv \\ dw \end{pmatrix} = \mathbf{J} d\mathbf{u}$$

where

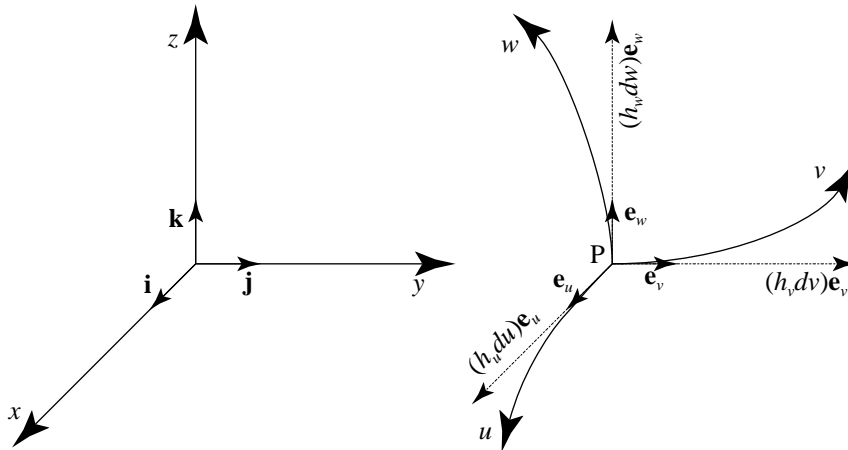


Figure C-1 Schematic representation of the unit vectors associated with two orthogonal co-ordinate systems.

$$\mathbf{J} = \begin{pmatrix} D_u x & D_v x & D_w x \\ D_u y & D_v y & D_w y \\ D_u z & D_v z & D_w z \end{pmatrix}$$

is known as the *Jacobi matrix*, and its determinant

$$J = \det(\mathbf{J}) = \begin{vmatrix} D_u x & D_v x & D_w x \\ D_u y & D_v y & D_w y \\ D_u z & D_v z & D_w z \end{vmatrix} \quad (\text{C.1})$$

as the *Jacobian* of the transformation.

Consider now the triple product $(\mathbf{a} \times \mathbf{b}) \cdot \mathbf{c}$ of the three vectors $(\mathbf{a}, \mathbf{b}, \mathbf{c})$ directed along the three axes of the \mathbf{x} -co-ordinate system. Since the co-ordinate system is orthogonal

$$(\mathbf{a} \times \mathbf{b}) \cdot \mathbf{c} = (\mathbf{i}a \times \mathbf{j}b) \cdot \mathbf{k}c = abc \quad (\text{C.2})$$

The elementary volume element, $d\Omega = dx dy dz$, spanned by the elementary vector

$$d\mathbf{r} = d\mathbf{r}(x, y, z) = \mathbf{i}dx + \mathbf{j}dy + \mathbf{k}dz \quad (\text{C.3})$$

in the \mathbf{x} -coordinate system, can thus also be expressed as

$$d\Omega = (\mathbf{i}dx \times \mathbf{j}dy) \cdot \mathbf{k}dz$$

Let \mathbf{r} be the position vector from the origin of the \mathbf{x} co-ordinate system to the origin of the \mathbf{u} co-ordinate system, denoted by P in Figure C-1, and let $D_v(x)$ and $D_x v(x, t)$ denote the ordinary and partial derivative of v with \mathbf{r} respect to x respectively. It is well-known that the derivative of a function $f(x)$, $Df(x)$, is always tangent to the function at the point x . This means that the vector

$$D_u \mathbf{r} = \mathbf{i}D_u x + \mathbf{j}D_u y + \mathbf{k}D_u z \quad (\text{C.4})$$

must be tangent to the u -axis at the point P . The vector

$$\mathbf{e}_u = D_u \mathbf{r} / h_u \quad (\text{C.5})$$

is thus a unit vector tangent to the u -axis, where

$$h_u = (D_u \mathbf{r} \cdot D_u \mathbf{r})^{1/2}$$

denotes the Euclidean norm, also known as the *scaling factor*, of $D_u \mathbf{r}$, with similar factors for the other two unit vectors, \mathbf{e}_v and \mathbf{e}_w . The elementary radius vector, $d\mathbf{r}$, in Equation (C.3) therefore assumes the form

$$d\mathbf{r} = D_u \mathbf{r} du + D_v \mathbf{r} dv + D_w \mathbf{r} dw = (h_u du)\mathbf{e}_u + (h_v dv)\mathbf{e}_v + (h_w dw)\mathbf{e}_w$$

in the \mathbf{u} co-ordinate system, after another application of the chain rule for differentiation.

The size of the volume element, $d\Omega$, must clearly only depend on the magnitude of $d\mathbf{r}$ and not the co-ordinate system used for its definition. This means that $d\Omega$ must satisfy the equation

$$d\Omega = (h_u du \mathbf{e}_u \times h_v dv \mathbf{e}_v) \cdot h_w dw \mathbf{e}_w = h_u h_v h_w du dv dw = h_u h_v h_w d\Gamma$$

in the \mathbf{u} co-ordinate system, according to Equation (C.5), or

$$\begin{aligned} d\Omega &= (D_u \mathbf{r} \times D_v \mathbf{r}) \cdot D_w \mathbf{r} d\Gamma \\ &= [(\mathbf{i}D_u x + \mathbf{j}D_u y + \mathbf{k}D_u z) \times (\mathbf{i}D_v x + \mathbf{j}D_v y + \mathbf{k}D_v z)] \cdot (\mathbf{i}D_w x + \mathbf{j}D_w y + \mathbf{k}D_w z) d\Gamma \\ &= [D_u x D_v y D_w z + D_u y D_v z D_w x + D_u z D_v x D_w y - D_w x D_v y D_u z - D_w y D_v z D_u x - D_w z D_v x D_u y] d\Gamma \\ &\equiv J d\Gamma \end{aligned} \quad (\text{C.6})$$

where J is the Jacobian of the transformation, as defined in Equation (C.1), if one uses the expressions for $d\mathbf{r}$ and \mathbf{e}_i in Equations (C.4) and (C.5), respectively.

The previous results are particularly useful in deriving expressions for the vector differentiation and integration of scalar and vector functions (Spiegel, 1974). Two expressions that will be particularly useful in the following discussion are the gradient of the scalar function $\Phi(u, v, w)$

$$\nabla\Phi(u, v, w) = D_u\Phi(u, v, w)\frac{\mathbf{e}_u}{h_u} + D_v\Phi(u, v, w)\frac{\mathbf{e}_v}{h_v} + D_w\Phi(u, v, w)\frac{\mathbf{e}_w}{h_w} \quad (\text{C.7})$$

and the divergence of the vector-valued function $\mathbf{A}(u, v, w)$

$$\nabla \cdot \mathbf{A}(u, v, w) = [D_u(h_v h_w A_u) + D_v(h_w h_u A_v) + D_w(h_u h_v A_w)]/J \quad (\text{C.8})$$

C.2.2 Cylindrical Co-ordinates

Although there are other orthogonal co-ordinate systems that are very important in the theory of groundwater flow, the present discussion will be limited to the cylindrical co-ordinates that are particularly important for the discussion in Chapter 10. These co-ordinates, conventionally denoted by the symbols (r, ϕ, z) , are closely related to the Cartesian co-ordinates (x, y, z) , through the equations

$$x = r \cos \phi, \quad y = r \sin \phi, \quad z = z \quad (r \geq 0, \quad 0 \leq \phi \leq 2\pi, \quad z = z)$$

as shown in Figure C-2. The scaling factors and Jacobian of cylindrical co-ordinates are thus given by

$$h_r = 1, \quad h_\phi = r, \quad h_z = 1, \quad J = r \quad (\text{C.9})$$

and the Cartesian volume element by

$$d\Omega = dx dy dz = r dr d\phi dz = J d\Gamma \quad (\text{C.10})$$

where

$$d\Gamma = dr d\phi dz$$

is the volume element in cylindrical co-ordinates.

C.2.3 Leibnitz' Rule for a Vector-valued Function

The main tool for the mathematical reduction of dimensions is Leibnitz' rule for the differentiation of an integral of a vector-valued function. This rule is usually quoted in textbooks [see e.g. Hildebrand (1976)] in

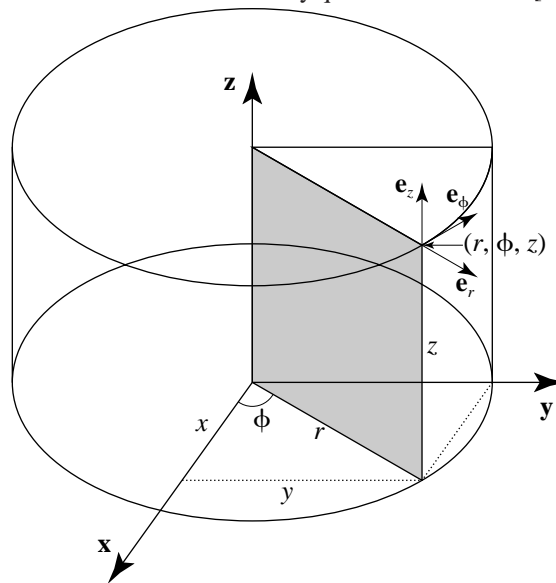


Figure C-2 Diagrammatic illustration of the relation between the Cartesian co-ordinates, (x, y, z) , and cylindrical co-ordinates (r, ϕ, z) .

the form

$$D_x \int_{a(x)}^{b(x)} f(x, \tau) d\tau = \int_{a(x)}^{b(x)} D_x f(x, \tau) d\tau - f(x, a) Da(x) + f(x, b) Db(x) \quad (C.11)$$

In this form the rule applies only to functions of one variable. However, it can easily be expanded to vector-valued functions.

To achieve this, let σ represent one of the three orthogonal coordinates $\xi = (\xi, \eta, \zeta)$ and t the time, and consider the vector-valued functions $\mathbf{F}(\xi, t)$ and $\mathbf{f}(\xi, t, \tau)$ defined by the integral

$$\mathbf{F}(\xi, t) = \int_{a(\xi, t)}^{b(\xi, t)} \mathbf{f}(\xi, t, \tau) d\tau$$

The function $\mathbf{F}(\xi, t)$ may thus also be considered as a function of the parameters $a(\xi, t)$ and $b(\xi, t)$, that is $\mathbf{F}(\xi, t) \equiv \mathbf{F}(\xi, t, a, b)$. Therefore, if $u(\xi, t, \tau)$ denotes the x -component of the function $\mathbf{f}(\xi, t, \tau)$, the x -component of $\mathbf{F}(\xi, t)$ can be expressed as

$$U(\xi, t, a, b) = \int_{a(\xi, t)}^{b(\xi, t)} u(\xi, t, \tau) d\tau$$

Since the spatial dimensions, ξ , are independent of the time, the partial derivative of $U(\xi, t, a, b)$, with respect to one of the spatial dimensions, $\sigma (= \xi, \eta \text{ or } \zeta)$, can, if it exists, be expressed through the chain rule of differentiation (Hildebrand, 1976) as

$$D_\sigma U(\xi, t, a, b) = D_\sigma U(\xi, t, a, b) \Big|_{a, b} + D_a U(\xi, t, a, b) D_\sigma a(\xi, t) + D_b U(\xi, t, a, b) D_\sigma b(\xi, t) \quad (C.12)$$

where $D_\sigma U(\xi, t, a, b) \Big|_{a, b}$ is used to denote the partial derivative of U when $a(\xi, t)$ and $b(\xi, t)$ are both kept fixed. To evaluate the other partial derivatives appearing in Equation (C.12), let $G(\xi, t, \tau)$ be a function such that

$$u(\xi, t, \tau) = D_\tau G(\xi, t, \tau)$$

The integral of $U(\xi, t, a, b)$ can thus also be expressed as

$$U(\xi, t, a, b) = \int_{a(\xi, t)}^{b(\xi, t)} D_\tau G(\xi, t, \tau) d\tau \equiv G(\xi, t, b) - G(\xi, t, a)$$

The partial derivatives of $U(\xi, t, a, b)$ with respect to a and b are thus of the form

$$\begin{aligned} D_a U(\xi, t, a, b) &= -D_a G(\xi, t, a) = -u(\xi, t, a) \\ D_b U(\xi, t, a, b) &= D_b G(\xi, t, b) = u(\xi, t, b) \end{aligned}$$

Substituting these values into Equation (C.12) and keeping in mind that a and b are fixed in the first term on the right-hand side, Equation (C.11) can be used to rewrite Equation (C.12) as

$$D_\sigma \int_{a(\xi, t)}^{b(\xi, t)} u(\xi, t, \tau) d\tau = \int_{a(\xi, t)}^{b(\xi, t)} D_\sigma u(\xi, t, \tau) d\tau - u(\xi, t, a) D_\sigma a(\xi, t) + u(\xi, t, b) D_\sigma b(\xi, t) \quad (C.13)$$

Although Equation (C.13) has been derived with special reference to the σ -component of the vector-valued function $\mathbf{f}(\xi, t)$, it is clearly also valid for the other components. Equation (C.13) can thus be expressed in vector notation as

$$\nabla \cdot \int_{a(\xi, t)}^{b(\xi, t)} \mathbf{f}(\xi, t, \tau) d\tau = \int_{a(\xi, t)}^{b(\xi, t)} \nabla \cdot \mathbf{f}(\xi, t, \tau) d\tau - \mathbf{f}(\xi, t, a) \cdot \nabla a(\xi, t) + \mathbf{f}(\xi, t, b) \cdot \nabla b(\xi, t) \quad (C.14)$$

while

$$\nabla \int_{a(\xi, t)}^{b(\xi, t)} u(\xi, t, \tau) d\tau = \int_{a(\xi, t)}^{b(\xi, t)} \nabla u(\xi, t, \tau) d\tau - u(\xi, t, a) \nabla a(\xi, t) + u(\xi, t, b) \nabla b(\xi, t) \quad (C.15)$$

A particular important application of Equations (C.14) and (C.15) arises when τ is taken as one of the spatial dimensions and the integration performed in this dimension. To be more specific, let σ again denote one of the spatial dimensions ξ , η , or ζ , and σ' the remaining two. Consider now the first term on the right-hand side of Equation (C.14)

$$\int_{\sigma_1}^{\sigma_2} \nabla \cdot \mathbf{f}(\xi, t, \sigma) d\sigma = \int_{\sigma_1}^{\sigma_2} \nabla' \cdot \mathbf{f}(\xi', t, \sigma) d\sigma + \int_{\sigma_1}^{\sigma_2} D_{\sigma} f_{\sigma}(\xi', t, \sigma) d\sigma$$

where, ∇' denotes the gradient operator associated with ξ' , $f_{\sigma}(\xi', t)$ the σ -th component of $\mathbf{f}(\xi, t, \sigma)$ and (σ_1, σ_2) the integration limits corresponding to $a(\xi, t)$ and $b(\xi, t)$, respectively. This equation can further be transformed by applying Equation (C.13) to the first term on its right-hand side, to obtain

$$\begin{aligned} \int_{\sigma_1}^{\sigma_2} \nabla \cdot \mathbf{f}(\xi', t, \sigma) d\sigma &= \nabla' \cdot \int_{\sigma_1}^{\sigma_2} \mathbf{f}(\xi', t, \sigma) d\sigma + \mathbf{f}(\xi', \sigma_1, t) \cdot \nabla' \sigma_1(\xi', t) - \mathbf{f}(\xi', \sigma_2, t) \cdot \nabla' \sigma_2(\xi', t) \\ &\quad - f_{\sigma}(\xi', \sigma_1, t) + f_{\sigma}(\xi', \sigma_2, t) \end{aligned} \quad (\text{C.16})$$

and similarly for $\nabla u(\mathbf{x}, t)$

$$\begin{aligned} \int_{\sigma_1}^{\sigma_2} \nabla u(\mathbf{x}', \sigma, t) d\sigma &= \int_{\sigma_1}^{\sigma_2} \nabla' u(\xi', \sigma, t) d\sigma + \kappa \int_{\sigma_1}^{\sigma_2} D_{\sigma} u(\xi', \sigma, t) d\sigma \\ &= \nabla' \cdot \int_{\sigma_1}^{\sigma_2} u(\xi, \sigma, t) d\sigma + u(\xi', \sigma_1, t) \nabla' \sigma_1(\xi', t) - u(\xi', \sigma_2, t) \nabla' \sigma_2(\xi', t) \\ &\quad + \kappa u(\xi', \sigma_1, t) - \kappa u(\xi', \sigma_2, t) \end{aligned} \quad (\text{C.17})$$

where κ is the unit Cartesian vector in the direction of σ .

C.3 REDUCING THE DIMENSIONS OF THE GROUNDWATER FLOW EQUATION

The groundwater flow equation

$$S_0 D_t \varphi(\mathbf{x}, t) = \nabla \cdot \mathbf{K}(\mathbf{x}, t) \nabla \varphi(\mathbf{x}, t) + f(\mathbf{x}, t) \quad (7.1)$$

is nothing more than the mathematical expression for the conservation of fluid mass in the elementary volume element $d\Omega$ of Equation (C.10), also known as the *local* conservation of mass. The *global* form of the equation, which is more suitable for the development of the two-dimensional flow equation, is obtained by integrating Equation (7.1) over the whole domain, Ω , of the aquifer to which it applies. This yields the equation

$$\int_{\Omega} S_0 D_t \varphi(\mathbf{x}, t) d\Omega - \int_{\Omega} \nabla \cdot \mathbf{G}(\mathbf{x}, t) d\Omega - \int_{\Omega} f(\mathbf{x}, t) d\Omega = 0 \quad (\text{C.18})$$

where

$$\mathbf{G}(\mathbf{x}, t) = \mathbf{K}(\mathbf{x}, t) \nabla \varphi(\mathbf{x}, t)$$

The easiest way to reduce Equation (C.18) to a two-dimensional vertical form is to rewrite the equation in terms of the cylindrical co-ordinates, defined in Section C.2.2, and then integrate over the angular co-ordinate. Consider for this purpose first the term on the left-hand side of Equation (C.18), which can be expressed in cylindrical co-ordinates through Equation (C.6) as

$$\int_{\Omega} S_0 D_t \varphi(\mathbf{x}, t) d\Omega = \int_{\Gamma} r S_0 D_t \varphi(r, \phi, z, t) d\Gamma = \int_{\Gamma} r S_0 D_t \varphi(r, \phi, z, t) dr dz d\phi$$

The discussions in Sections 6.7 and 9.3.4 have shown that the predominant direction of flow in stressed Karoo aquifers is vertical. This implies that the Darcy velocity varies only in the vertical direction, that is

$$\mathbf{q}(\mathbf{x}, t) = -\mathbf{K} \nabla \varphi(\mathbf{x}, t) = -\mathbf{K} D_z \varphi(z, t)$$

and thus that the piezometric head, $\varphi(r, \phi, z, t)$, and the source term, $f(r, \phi, z, t)$, must be independent of ϕ . The term on the right-hand side of the equation can therefore be integrated directly to obtain

$$\int_{\Gamma} r S_0 D_t \varphi(r, \phi, z, t) dr dz d\phi = \int_{r,z} r \left[\int_0^{2\pi} S_0 D_t \varphi(r, z, t) d\phi \right] dr dz = 2\pi \int_{r,z} r S_0 D_t \varphi(r, z, t) dr dz \quad (C.19)$$

if it is assumed that S_0 is independent of ϕ .

The first term on the right-hand side of Equation (C.18) can likewise be expressed as

$$\int_{\Omega} \nabla \cdot \mathbf{G}(\mathbf{x}, t) d\Omega = \int_{\Gamma} \nabla \cdot \mathbf{G}(r, \phi, z, t) r d\phi dr dz = \int_{r,z} \left[r \int_0^{2\pi} \nabla \cdot \mathbf{G}(r, \phi, z, t) d\phi \right] dr dz \quad (C.20)$$

The integral in square brackets on the right-hand side can also be expressed through Equation (C.16) as

$$\int_0^{2\pi} \nabla \cdot \mathbf{G}(r, \phi, z, t) d\phi = \nabla' \cdot \int_0^{2\pi} \mathbf{G}(r, \phi, z, t) d\phi + G_{\phi}(r, \phi_2, z, t) - G_{\phi}(r, \phi_1, z, t)$$

since the integration boundaries are both constants. The assumption of vertical flow implies that $\mathbf{G}(r, \phi, z, t)$ is also independent of ϕ . The last two terms in the previous equation are thus identical and vanish. Equation (C.20) can thus finally be expressed as

$$\int_{\Omega} \nabla \cdot \mathbf{G}(\mathbf{x}, t) d\Omega = \int_{r,z} r \left[\nabla' \cdot \int_0^{2\pi} \mathbf{G}(r, z, t) d\phi \right] dr dz = 2\pi \int_{r,z} r \nabla \cdot \mathbf{G}(r, z, t) dr dz \quad (C.21)$$

The last term of Equation (7.1) to consider, is the source term. This term represents the volume of water discharged from (or recharged to) the aquifer. It is therefore related to the rate at which water is discharged from (or recharged to) an aquifer. For example, the rate at which a single borehole is pumped in a constant rate, step drawdown or multi-rate test, $Q(t)$, must satisfy the equation

$$Q(t) = \int_{\Omega} f(\mathbf{x}, t) d\Omega = \int_{\Gamma} f(r, \phi, z, t) r dr d\phi dz$$

The term on the right-hand side of this equation can be integrated at once with respect to ϕ , since $f(r, \phi, z, t)$ does not depend on ϕ , to obtain

$$\int_{r,z} \left[r \int_0^{2\pi} f(r, z, t) d\phi \right] dr dz = 2\pi \int_{r,z} r f(r, z, t) dr dz \quad (C.22)$$

Unfortunately, there does not exist an explicit expression for $f(\mathbf{x}, t)$. This difficulty is usually surmounted in two-dimensional flow models by assuming that the source can be represented as a point source, defined as

$$f(\mathbf{x}, t) = Q(t) \delta(\mathbf{x} - \mathbf{x}_0)$$

where \mathbf{x}_0 is the position of the source and $\delta(\mathbf{x} - \mathbf{x}_0)$ the three-dimensional Dirac delta function, defined by the equation

$$\iiint_{\Omega} g(\mathbf{x} - \mathbf{x}_0) \delta(\mathbf{x} - \mathbf{x}_0) d\Omega = \int_{-\infty}^{+\infty} \int_{-\infty}^{+\infty} \int_{-\infty}^{+\infty} g(\mathbf{x} - \mathbf{x}_0) \delta(x - x_0) \delta(y - y_0) \delta(z - z_0) dx dy dz = g(\mathbf{x}_0)$$

with $g(\mathbf{x})$ an arbitrary function of \mathbf{x} . The same approach can also be applied here, except that the point source must be replaced by the line source

$$f(r, z, t) = \frac{Q(t) \delta(r - r_0)}{2\pi r d}$$

where d is the thickness of the aquifer and r_0 the position of the borehole. Substitution of this expression for $f(r, z, t)$ into Equation (C.22) yields

$$\int_{r,z} \left[r \int_0^{2\pi} f(r, z, t) d\phi \right] dr dz = \frac{Q(t)}{d} \int_{r,z} \delta(r - r_0) dr dz \quad (C.23)$$

The global, vertical, two-dimensional flow equation can now be obtained by substituting Equations (C.19), (C.21) and (C.22) into Equation (C.18), to obtain

$$2\pi \int_{r,z} r S_0 D_t \varphi(r, z, t) dr dz - 2\pi \int_{r,z} r \nabla \cdot \mathbf{G}(r, z, t) dr dz - \frac{Q(t)}{d} \int_{r,z} \delta(r - r_0) dr dz = 0$$

or

$$2\pi \left[\int_{r,z} r \left\{ S_0 D_t \varphi(r, z, t) - \nabla \cdot \mathbf{G}(r, z, t) - \frac{Q(t)}{2\pi r d} \delta(r - r_0) \right\} dr dz \right] = 0$$

Since there are no constraints on the domain of the integral, this equation can only be valid if the integrand vanishes, that is

$$r S_0(r, z, t) D_t \varphi(r, z, t) = r \nabla \cdot [\mathbf{K}(r, z, t) \nabla \varphi(r, z, t)] + \frac{Q(t)}{2\pi d} \delta(r - r_0) \quad (\text{C.24})$$

This is the equation that governs groundwater flow in a vertical two-dimensional plane.

=====

REFERENCES

- Bakk es, G. N. (1977) *Die Beweging van Grondwater. 'n Studie van 'n Model gebaseer op Eindige Elemente*. Unpublished M.Sc. Thesis. Department of Applied Mathematics, University of the Orange Free State, Bloemfontein.
- Bar enblatt, G. E., Zhelto v, I. P. and K ochina, I. N. (1960) Basic concepts in the theory of seepage of homogeneous liquids in fissured rocks (strata). *Journal of Applied Mathematical Mechanics (USSR)*. **24**, 1286–1303.
- Bear, J. (1972) *Dynamics of Fluids in Porous Media*. American Elsevier Environmental Science Series. American Elsevier Publishing Company, Inc., New York.
- Bear, J. (1977) On the aquifer's integrated balance equations. *Advances in Water Resources*. **1** (1), 15–23.
- Bear, J. (1979) *Hydraulics of Groundwater*. Water Resources and Environmental Engineering. McGraw-Hill, Book Co., New York.
- Bear, J. and Pinder, G. F. (1979) Porous medium deformation in multiphase flow. *J. Eng. Mech. Div. Am. Soc. Civ. Eng.* **104** (Em4), 881–894.
- Beukes, N. J. (1969) *Die Sedimentologie van die Etage Holkranssandsteen, Sisteem Karoo*. Unpublished M.Sc. Thesis. Department of Geology, University of the Orange Free State, P.O. Box 339, Bloemfontein.
- Black, J. H. (1993) Hydrogeology of fractured rocks—a question of uncertainty about geometry. In: Proceedings of the *Hydrogeology of Hard Rocks. Memoires of the XXIVth Congress of the IAHR*. S. Banks and D. Banks (eds.) Ås (Oslo), Norway. Vol 2, 783–796. International Association of Hydrogeologists.
- Blatt, H., G., M. and Murray, R. (1980) *Origin of Sedimentary Rocks*. Prentice-Hall Inc., Englewood Cliffs, New Jersey.
- Boehmer, W. K. and Boonstra, J. (1986) *Flow to Wells in Intrusive Dykes*. Akademisch Proefschrift. Vrije Universiteit, Amsterdam.
- Botha, J. F. (1994) *Models and The Theory of Groundwater Motion*. Unpublished Report. Institute for Groundwater Studies, University of the Orange Free State, P.O. Box 339, Bloemfontein.
- Botha, J. F. (1996) *Principles of Groundwater Motion*. Unpublished Lecture Notes. Institute for Groundwater Studies, University of the Orange Free State, P.O. Box 339, Bloemfontein 9300.
- Botha, J. F. and Bakk es, G. N. (1982) Galerkin finite element method and the groundwater flow equation: 1. Convergence of the method. *Advances in Water Resources*. **5**, 121–126.
- Botha, J. F. and Magda, L. (1993) *Geometry and the Behaviour of Hard-rock Aquifers*. Progress Report to the Water Research Commission. Institute for Groundwater Studies, University of the Orange Free State, P.O. Box 339, Bloemfontein 9300.
- Botha, J. F. and Pinder, G. F. (1983) *Fundamental Concepts in the Numerical Solution of Differential Equations*. John Wiley & Sons, New York, N.Y.
- Botha, J. F. and Verwey, J. P. (1992) Aquifer test data and numerical models. In: Proceedings of the *IX International Conference on Computational Methods in Water Resources*. T. F. Russel, R. E. Ewing, C. A. Brebbia, W. G. Gray and G. F. Pinder (eds.) Denver, Colorado. Vol 1, 459–466. Elsevier Applied Science, New York.
- Botha, J. F., Buys, J., Verwey, J. P., Tredoux, G., Moodie, J. W. and Hodgkiss, M. (1990) *Modelling Groundwater Contamination in the Atlantis Aquifer*. WRC Report No 175/1/90. Water Research Commission, P.O. Box 824, Pretoria 0001.
- Botha, J. F., Van Tonder, G. J., Verwey, J. P. and Kinzelbach, W. (1996) Analysis of hydraulic test data from Karoo aquifers. In: Proceedings of the *ModelCare '96 Conference on the Calibration and Reliability in Groundwater Modelling*. K. Kovar (eds.) Golden, Colorado. IAHS.
- Botha, J. F., Vivier, J. J. P. and Verwey, J. P. (1996) *Grondwaterondersoek te Philippolis*. Verslag opgestel vir die Firma Cahi De Vries. Instituut vir Grondwater studies, Universiteit van die Oranje-Vrystaat, Posbus 339, Bloemfontein 9300.
- Bredenkamp, D. B., Botha, L. J., Van Tonder, G. J. and Janse van Rensburg, H. J. (1995) *Manual on Quantitative Estimation of Groundwater Recharge and Aquifer Storativity*. WRC Report No TT 73/95. Water

- Research Commission, P.O. Box 824, Pretoria 0001.
- Burger, C. A. J., Hodgson, F. D. I. and Van der Linde, P. J. (1981) *Hidrouliese Eienskappe van Akwifere in die Suid-Vrystaat*. Bulletin 7. Instituut vir Grondwater studies, Universiteit van die Oranje-Vrystaat, Posbus 339, Bloemfontein.
- Buys, J. (1992) *Triangular Irregular Meshes and Their Application in the Graphical Representation of Geohydrological Data*. Unpublished Ph.D. Thesis. Department of Computer Science, University of the Orange Free State, P.O. Box 339, Bloemfontein.
- Caçás, M. C., Ledoux, E., De Marsily, G., Tillie, B., Barbrau, A., Durand, E., Feuga, B. and Peaudecerf, P. (1990) Modelling fracture flow with a Stochastic discrete fracture network: calibration and validation. 1. The flow model. *Water Resources Research*. **26** (3), 478–489.
- Cheney, E. W. (1966) *Introduction to Approximation Theory*. International Series in Pure and Applied Mathematics. McGraw-Hill Book Company, New York, N.Y.
- Chorley, R. J. (1969) *Water, Earth and Man*. Methuen & Co. Ltd., London.
- Clementz, D. M. (1997) Company R&D: Does it add value to the bottom line? *Journal of Petroleum Technology*. **49** (2), 144–148.
- Cole, D. I., Labuschagne and Söhng, A. P. G. (1991) Aeroradiometric survey for uranium and ground follow-up in the main Karoo Basin. *Geological Survey Memoirs*. **76**, 171.
- Davis, R. A. (1983) *Depositional Systems. A Generic Approach to Sedimentary Geology*. Prentice-Hall Inc., Englewood Cliffs, New Jersey.
- De Marsily, G. (1986) *Quantitative Hydrogeology*. Academic Press, Inc., New York.
- Department of Water Affairs (1986) *Water Resources of the Republic of South Africa*. Department of Water Affairs and Forestry, Pretoria.
- Driscoll, F. G. (1986) *Groundwater and Wells*. Johnson Division, St. Paul, Minnesota.
- Du Toit, A. L. (1954) *The Geology of South Africa*. (3rd ed.) Oliver and Boyd, London.
- Duffield, G. M. and Rumbaugh, J. O. (1991) *AQTESOLV Aquifer Test Solver*. Version 1.1. Geraghty & Miller Modelling Group, 1895 Preston White Drive, Suite 301, Reston VA 22091.
- Dverstorp, B., Andersson, J. and Nordqvist, W. (1992) Discrete fracture network interpretation of field tracer migration in sparsely fractured rock. *Water Resources Research*. **28** (9), 2327–2343.
- Eriksson, P. G. (1981) A palaeoenvironmental analysis of the Clarens Formation in the Natal Drakensberg. *Transactions of the Geological Society of South Africa*. **84**, 7–17.
- Filonenko-Borodich, M. (1965) *Theory of Elasticity*. Dover Publications, New York, N.Y.
- Fitch, F. J. and Miller, J. A. (1984) Dating Karoo igneous rocks by the conventional K-Ar and ⁴⁰Ar/³⁹Ar age spectrum methods. *Special Publication of the Geological Society of South Africa*. **13**, 247–266.
- Freeze, A. L. and Cherry, J. A. (1979) *Groundwater*. Prentice-Hall Inc., Englewood Cliffs, New Jersey.
- Geological Survey (1966) *Sheet 2926 Bloemfontein, 1066. Scale 1:250 000*. Geological Survey, Pretoria.
- Gilbrech, D. A. (1966) *Fluid Mechanics*. Iliffe Books Ltd., London.
- Gringarten, A. C. (1982) Flow-test evaluation of fractured reservoirs. In: *Recent Trends in Hydrogeology*. T. A. Narasimhan (Ed.) Geological Society of America. Special Paper 189. 237–263.
- Gringarten, A. C. and Ramey, H. J. (1974) Unsteady-state pressure distributions created by a well with a single horizontal fracture, partial penetration or restricted entry. *Society of Petroleum Engineers Journal*. **14** (5), 413–426.
- Hargraves, R. B. (1980) *Physics of Magmatic Processes*. Princeton University Press, Princeton, New Jersey.
- Hess, K. M., Wolf, S. H. and Celia, M. A. (1991) Estimation of macrodispersivities from the spatial variability of hydraulic conductivity in a sand and gravel aquifer, Cape Cod, Massachusetts. In: *Proceedings of the US Geological Survey Toxic Substances Hydrology Program. Proceedings of the Technical Meeting, Monterey, California, March 11-15, 1991. Water-Resources Investigations Report 91-4034*. 15–22.
- Hibbard, B. and Saintek, D. (1994) *VIS-5D*. Wisconsin Space Science and Engineering Centre, University of Wisconsin, Wisconsin.
- Hildebrand, F. B. (1976) *Advanced Calculus for Applications*. (2nd ed.) Prentice-Hall, Inc., Englewood Cliffs, New Jersey.
- Hsieh, P. A., Neuman, S. P. and Simpson, E. S. (1983) *Pressure Testing of Fractured Rocks – A Methodology Employing Three-dimensional Cross-hole Tests*. Topical Report. Report No. NUREG/CR-3213R W. Department of Hydrology and Water Resources, Univ. of Arizona, Tucson, AZ 85721.
- Huang, Y. H. (1973) Unsteady Flow toward an Artesian Well. *Water Resources Research*. **9** (2), 426–433.
- Huyakorn, P. S. and Pinder, G. F. (1983) *Computational Methods in Subsurface Flow*. Academic Press, Inc., New York, N.Y.
- Issar, A. (1985) Fossil water under the Sinai-Negev Peninsula. *Scientific American*. **253**, 82–90.

- Johnson, A. M. and Pollard, D. D. (1973) Mechanics of growth of some laccolithic intrusions in the Henry Mountains Utah I. *Tectonophysics*. **18**, 261–309.
- Kaiser, J. (1996) Scientists angle for answers. *Science*. **274** (5294), 1837–1838.
- Kaufmann, C., Kinzelbach, W. and Fried, J. J. (1990) Simultaneous calibration of flow and transport models and optimization of remediation measures. In: *Proceedings of the ModelCare 90: Calibration and Reliability in Groundwater Modelling*. K. Kovar (eds.) The Hague. IAHS Press, Wallingford, Oxfordshire.
- Kingsley, C. S. and Theron, J. C. (1964) Palaeocurrent directions in arkose of the Beaufort Series in the Orange Free State. *Annals of the Geological Survey*. **3**, 71–74.
- Kirchner, J. O. G., Van Tonder, G. J. and Lukas, E. (1991) *Exploitation Potential of Karoo Aquifers. Appendix*. WRC Report No 170/2/91. Water Research Commission, P.O. Box 824, Pretoria 0001.
- Kitching, J. W. (1977) *The Distribution of the Karoo Vertebrate Fauna*. Bernard Price Institute for Palaeontological Research, University of the Witwatersrand, Johannesburg.
- Konikow, L. F. and Bredehoeft, J. D. (1992) Ground-water models cannot be validated. *Advances in Water Resources*. **15**, 75–83.
- Kruseman, G. P. and De Ridder, N. A. (1991) *Analysis and Evaluation of Pumping Test Data*. (2nd ed.) Publication 47. International Institute for Land Reclamation and Improvement, P.O. Box 45, 6700 Wageningen, The Netherlands.
- Lynch, S. D. (1982) *Grondwatermodellering en Parameteridentifikasie van die Sishen Akwifer*. Unpublished M.Sc. Thesis. Department of Geology, University of the Orange Free State, P.O. Box 339, Bloemfontein.
- Maaløe, S. (1985) *Principles of Igneous Petrology*. Springer-Verlag, Heidelberg.
- Meyboom, A. F. and Wallace, R. C. (1978) Occurrence and origin of ring-shaped dolerite outcrops in the Eastern Cape and Western Transkei. *Transactions of the Geological Society of South Africa*. **81**, 95–99.
- Milne-Home, W. A. (1988) Interpretation of aquifer tests in fractured aquifers: from theory to routine field analysis. In: *Proceedings of the IV Canadian/American Conference on Hydrology: Fluid Flow, Heat Transfer and Mass transport in Fractured Rocks*. Banff, Alberta, Canada. 177–184.
- Moench, A. F. (1984) Double-porosity models for a fissured groundwater reservoir with fracture skin. *Water Resources Research*. **20**, 831–846.
- Müller, J. L. and Botha, J. F. (1986) *A Preliminary Investigation of Modelling the Atlantis Aquifer*. Bulletin 14. Institute for Groundwater Studies, University of the Orange Free State, P.O. Box 339, Bloemfontein.
- Muskat, M. (1937) *The Flow of Homogeneous Fluids Through Porous Media*. McGraw-Hill Book Company, New York.
- Odling, N. E. (1993) An investigation into the permeability of a 2D Natural Fracture Pattern. In: *Proceedings of the Hydrogeology of Hard Rocks. Memoires of the XXIVth Congress of the IAH*. S. Banks and D. Banks (eds.) Ås (Oslo), Norway. Vol 1, International Association of Hydrogeologists.
- Park, R. G. (1989) *Foundations of Structural Geology*. (2nd ed.) Chapman and Hall, New York, N.Y.
- Partridge, T. C. and Hubert, G. L. (1993) Integrated use of Geological and Geophysical Techniques for Groundwater Development: A case Study in an area north of Kuruman, Northern Cape. In: *Proceedings of the International Conference: Africa Needs Groundwater*. University of the Witwatersrand, South Africa. Vol 1, Groundwater Division of the Geological Society of South Africa and the Borehole Water Association of Southern Africa.
- Pinder, G. F. and Gray, W. G. (1977) *Finite Element Simulation in Surface and Subsurface Hydrology*. Academic Press, Inc., New York, N.Y.
- Pissanetzky, S. (1984) Automatic three-dimensional finite element mesh generation using the program KUBIK. *Computer Physics Communications*. **32**, 245–265.
- Pollard, D. D. and Johnson, A. M. (1973) Mechanics of growth of some laccolithic intrusions in the Henry Mountains Utah II. *Tectonophysics*. **18**, 261–309.
- Price, N. J. (1966) *Fault and Joint Development in Brittle and Semi-brittle Rock*. Pergamon Press Ltd, Oxford.
- Princeton University Water Resources Program (1984) *Groundwater Contamination from Hazardous Wastes*. Prentice-Hall Inc., Englewood Cliffs, New Jersey.
- Rathod, K. S. and Rushton, K. R. (1984) Numerical method of pumping test analysis using microcomputers. *Ground Water*. **22**, 602–608.
- Rathod, K. S. and Rushton, K. R. (1991) Interpretation of pumping from two-zone layered aquifers using a numerical model. *Ground Water*. **29**, 499–509.
- Rector, J. W. and Marion, B. P. (1991) The use of drill-bit energy as a downhole seismic source. *Geophysics*. **56** (5), 328–634.

- Reid, D. L. and Rex, D. C. (1994) Cr etaceous d ykes associated with the opening of the South Atlantic: The Mehlberg Dyke, northern Richtersveld. *South African Journal of Geology*. **97** (2)
- Reineck, H. E. and Singh, I. B. (1973) *Depositional Sedimentary Environments*. Springer-Verlag, Heidelberg.
- Rowell, D. M. and Desvarats, A. M. J. (1976) Diagenesis in Cape and Karoo sediments, South Africa, and its bearing on their hydrocarbon potential. *Transactions of the Geological Society of South Africa*. **79** (1), 181–145.
- Rubin, A. M. (1995) Propagation of magma-filled cracks. *Annual Review of the Earth Planetary Sciences*. **23**, 287–336.
- Rushton, K. R. and Booth, S. J. (1976) Pumping test analysis using a discrete time, discrete space numerical model. *Journal of Hydrology*. **28**, 13–27.
- Ryan, M. P. (1990) *Magma Transport and Storage*. John Wiley & Sons, New York, N.Y.
- Ryan, P. J. (1967) *Stratigraphic and palaeocurrent analysis of the Ecca Series and lowermost Beaufort beds in the Karoo Basin of South Africa*. Unpublished Ph.D. Thesis. Department of Geology, University of the Witwatersrand, Johannesburg.
- Sahimi, M. (1995) *Flow and Transport in Porous Media and Fractured Rock*. VCH Verlagsgesellschaft mbH, Weinheim.
- Scholle, P. A. and Spearling, D. (1982) *Sandstone Depositional Environments*. The American Association of Petroleum Geologists, Tulsa, Oklahoma.
- Selley, R. C. (1976) *An Introduction to Sedimentology*. Academic Press, London.
- Schirov, M., Legchenko, A. and Creer, G. (1991) A new direct non-invasive ground water detection technology for Australia. *Exploration Geophysics*. **22**, 333–338.
- Spiegel, M. R. (1974) *Theory and Problems of Vector Analysis*. Schaum Outline Series. McGraw-Hill Book Company, New York.
- Stroud, A. H. and Secrest, D. (1966) *Gaussian Quadrature Formulas*. Prentice Hall Series in Automatic Computation. Prentice Hall, Inc., Englewood Cliffs, N.J.
- Sun, N.-Z. (1994) *Inverse problems in Groundwater Modelling*. Theory and Applications of Transport in Porous Media. Kluwer Academic Publishers, Dordrecht.
- Tankard, A. J., Jackson, M. P. A., Eriksson, K. A., Hobday, D. K., Hunter, D. R. and Minter, W. E. L. (1982) *Crustal Evolution of Southern Africa*. Springer-Verlag, New York.
- Theis, C. V. (1935) The relation between the lowering of the piezometric surface and the rate and duration of discharge of a well using ground water storage. *Transactions of the American Geophysical Union*. **16**, 519–524.
- Theron, J. C. (1970) *Some Geological Aspects of the Beaufort Series in the Orange Free State*. Unpublished D.Sc. Thesis. Department of Geology, University of the Orange Free State, P.O. Box 339, Bloemfontein.
- Theron, J. C. (1975) Sedimentological evidence for the extension of the African Continent southwards during the Late Permian - Early Triassic Times. In: *Proceedings of the Third Gondwana Symposium, Gondwana Geology*. K. S. W. Campbell (eds.) Canberra. 61–71. Australian National University Press, Canberra, Australia.
- Truswell, J. F. (1970) *Historical Geology of South Africa*. Purcell, Cape Town.
- Van Sandwyk, L., Van Tonder, G. J., De Waal, D. J. and Botha, J. F. (1992) *A Comparison of Spatial Bayesian Estimation and Classical Kriging Procedure*. WRC Report No 271/3/92. Water Research Commission, P.O. Box 824, Pretoria 0001.
- Van Tonder, G. J., Buys, J., Lukas, E. and Staats, S. (1998) *Extension and Refinement of the AQUAMOD Computer Software*. WRC Report No 640/1/98. Water Research Commission, P.O. Box 824, Pretoria 0001.
- Van Tonder, G. J., Janse van Rensburg, H., Botha, J. F. and Br edenkamp, D. B. (1986) Die modellering van grondwater vlakke in die Grootfonteinkompartement in Wes-Transvaal. *Water SA*. **12**, 151–160.
- Verwey, J. P. and Botha, J. F. (1992) *A Comparative Study of Two- and Three-dimensional Groundwater Models*. WRC Report No 271/1/92. Water Research Commission, P.O. Box 824, Pretoria 0001.
- Visser, J. N. J. (1984) A review of the Stormberg Group and Drakensberg volcanics in Southern Africa. *Palaeont. Afr.* **25**, 5–27.
- Visser, J. N. J. (1989) *Course Notes on Geology 216: Sedimentology*. Lecture delivered at University of the Orange Free State, P.O. Box 339, Bloemfontein 9300, Republic of South Africa.
- Visser, J. N. J. and Kingsley, C. S. (1982) Upper Carboniferous glacial valley sedimentation in the Karoo basin, Orange Free State. *Transactions of the Geological Society of South Africa*. **85**, 71–79.
- Walker, F. and Polder vaart, A. (1949) Karroo dolerites of the Union of South Africa. *Bulletin of the Geological Society of America*. **60**, 591–706.

-
- Weaver, J., Conrad, J. and Eskes, S. (1993) Valley calcretes: Another Karoo groundwater exploration target. In: Proceedings of the *Groundwater '93 Conference: Africa Needs Groundwater*. University of the Witwatersrand, Johannesburg. Groundwater Division of the Geological Society of South Africa and Borehole Water Association of Southern Africa.
- Wedepohl, E., Meyer, R. and Mitchell, G. (1995) *The Application of Seismic Tomography and Ground Penetrating Radar for the Determination of Fractures and Hydraulic Properties of Fractured Rock Aquifers*. Interim report to the Water Research Commission. Emmausk, CSIR, P.O. Box 395, Pretoria 0001.
- Weideman, J. A. C. (1980) *The groundwater Flow Equation and the Optimal u-method*. Unpublished M.Sc. Thesis. Department of Geohydrology, University of the Orange Free State, P.O. Box 339, Bloemfontein.
- Zumberge, J. H. and Nelson, C. A. (1984) *Elements of Physical Geology*. John Wiley & Sons Inc., New York.
-
-

Index

A

Abrahamskraal Formation 18
Acceleration of gravity 97
Adelaide Subgroup 18, 37, 38, 67. *See also*
 Beaufort Group: subdivisions
 composition of 18
 subdivision of 18
Alluvial beds 22
Alluvium 22
Analytical model 9, 22, 37. *See also* Karoo
 aquifers: analytical models for
 and an aquifer's physical behaviour 10
 and the behaviour of Karoo aquifers 75
 constraints on 10
 representation an aquifer's geometry 10
 vertical two-dimensional 133
Anisotropic rocks 18
 defined 18
 hydraulic conductivity of 18
AQUAmod for Windows 133
Aquifer 7, 8, 9
 analytical model for 10
 behaviour of 7, 8, 11
 best approach to study 11
 dependence on void geometry 7
 influence of its geometry 7, 150
 structural geology and 15
 classes of 10
 conceptual model for 10, 11
 flow in natural 9
 geometrical properties 10
 geometry of 6, 7, 8, 9, 11, 37
 influence on behaviour of boreholes 77
 preconceived notions 11
 represented by contours of water levels 77
 hydraulic parameters 11
 mathematical model for 10
 numerical models for an 95
 difficulties with 98
 origin and evolution 8
 physical behaviour of 5, 7–11
 physical properties 10
 specific storativity 97
 storage capacity of 1
 structure of 6
 three-dimensional representation of 6

 void geometry 7
 determination of 7–8
 methods to determine 7
Aquifer 1 88, 95, 96, 121, 122, 123, 134
Aquifer 2
 88, 95, 96, 98, 99, 121, 122, 123, 124, 134
Aquifer 3 88, 96, 98, 122

B

Backward finite difference 109
Balfour Formation 18, 67
 properties of 69
Basaltic magma 30
 temperature of 30
Basis function 99, 100
Beaufort Group 13, 18–19, 27, 37, 38, 67
 behaviour of aquifers in 19
 composition of 18
 deposition of 18
 hydrological properties of 18
 properties of aquifers in 19–20
 stratigraphic column 39
 subdivisions 18
Bedding planes 5, 27
 development of fractures along 22
Bedding-parallel fractures 5, 22, 32, 60
 and complex behaviour of Karoo aquifers 75, 92
 as sites for boreholes 71, 150
 association with laccolithic intrusions 32, 71–
 73, 150
 conduits of water in Karoo aquifers
 32, 71, 75, 92, 124, 150
 created by other processes 32
 creation of 32, 164
 development on Campus Test Site 60
 difficulties in detecting 71
 frequency of 32
 relation to high-yielding boreholes 32
 relation to vertical flow 92
 significance for yields of boreholes 64
 sizes of apertures 5, 60, 150
Bending 30
 caused by a laccolith 31
 caused by a linear dyke 31
Bessel functions 105

- Bethulie 32, 150
- Bloemfontein 4, 5, 37, 38, 39
- basal contacts of Adelaide Subgroup 37
 - Beaufort strata 38
 - geological columns for 38, 39
 - Beaufort stratigraphy 39
 - Ecce-Beaufort contact 38, 39
 - inconsistency in mapping 39, 71
 - features of landscape 38
 - foreland basin 38
 - platform facies of 38
 - geology of 37–38, 150
 - previous studies 37–38
 - regional survey 38
 - Karoo Supergroup
 - sediments of 38
 - oval shaped domal structure 46, 150
 - palaeofluvial environment 71
 - regional structural geology 45–48
 - rock mass structure 46–48
 - development of fractures 46, 150
 - stratigraphic correlation 45
 - difficulties with 45
 - structural-stratigraphic mapping 5, 45–46
- Borehole 1, 5, 6, 8
- blow-yield of 30
 - decreasing yield 152
 - ‘dried up’ complaint 89, 151
 - caused by a dewatered fracture 89, 151
 - efficiency to produce water 93
 - fractured-controlled behaviour of 95, 150
 - geological profile of 8
 - determination of 8
 - geometrical dimensions
 - of Dirichlet boundary 101
 - numerical representation of 95, 99–101
 - as a Dirichlet boundary 95, 100, 100–101, 103, 105
 - as a Neumann boundary 100
 - as a point source 99, 107
 - logarithmic singularity in point source 95, 99, 145
 - observation 10
 - perturbed 10
 - definition of 10
 - fracture-controlled behaviour of 87
 - sitting of 73
 - yield of
 - influence of a dyke’s grain size 34
- Borehole CH1 50, 55, 66
- acoustic scanner image of 60
- Borehole CH2 55, 58
- Borehole CH3 56, 58, 63, 65
- Borehole CH4 50, 56, 58
- Borehole CH5 50
- Borehole CH6 32, 50, 164
- Borehole CH7 50, 96
- Borehole UO1 77, 98, 123, 125, 127
- Borehole UO10 84, 98, 119
- Borehole UO11 77, 84, 85, 86, 90
- Borehole UO12 79
- Borehole UO13 84
- Borehole UO14 60, 78, 84, 96
 - behaviour of 78–79
- Borehole UO18 96, 98, 123, 125, 127
- Borehole UO2 84
- Borehole UO20 84, 85, 86, 88
- Borehole UO21 98, 119
- Borehole UO22 84, 98
- Borehole UO3 63, 77, 82, 84
 - blow-yield of 63
- Borehole UO4 79, 82, 97
- Borehole UO5
 - 60, 63, 77, 80, 84, 86, 123, 126, 142
 - acoustic scanner image of 60, 66
 - alteration zones in 63
 - interpretation of 63
 - blow-yield of 63
 - elastic deformation of 60–63, 89, 152
- Borehole UO6 84
- Borehole UO7 145, 146
- Borehole UO8 79
- Borehole UO9 82, 84
- Borehole UP15
 - 50, 60, 84, 86, 90, 119, 121, 124, 127, 129, 142
- Borehole UP16
 - 50, 60, 77, 80, 84, 86, 97, 119, 121, 125, 130, 144
 - presumed behaviour of 85
- Boundary conditions 95, 98, 119
- Dirichlet 100, 103, 106, 107, 113, 121, 122
 - definition of 98
- internal 96
- mixed, definition of 98
- Neumann
 - 100, 103, 105, 106, 117, 121, 122, 134, 140
 - definition of 98
- Braided river 19, 44
- Breccias 29
- Burgersdorp Formation 18. *See also* Tarkastad Subgroup
- ## C
- Calcite precipitation 91
 - dependence on pressure in rock matrix 91
- Calcrete 22
 - formation of 22
- Calcrete aquifers 22
 - recharge rate of 22
- Caledon River 22
- Calvinia 77, 92
 - Borehole G39973 91, 92
- Campus Sandstone 44–45, 50, 60, 71
 - deposition of 45
 - fractures in 60

-
- mudstone layers underlying 45
 - deposition of 45
 - properties of 45
 - rock mass structure 57–63
 - Campus Test Site 38, 48–65, 69, 71, 113
 - aquifers on 63
 - boundaries of 121
 - difference in water levels 63
 - Campus Sandstone body
 - isopach contour map of 57
 - shape of 57–60
 - Carbonaceous shale layer on 63, 96
 - influence on aquifers 95
 - classes of boreholes on 77
 - association with Mode I fracture 77
 - constant rate tests 77–81
 - purpose of 77–81
 - cross-borehole packer tests 81–82
 - double packer tests 82
 - geological column 50
 - deposition of 52
 - interpretation of 50–52
 - variation in competency 52–57
 - geology of 50
 - geometry of dolerite intrusions 46
 - geometry of the aquifer 63–67, 84, 95–96, 128
 - hydraulic tests 77–87
 - interaction between aquifers 95
 - mathematical model for 95, 96–99, 97
 - Mode I fracture on 60–63, 96, 119
 - areal extent 65
 - areal extent of 60
 - boundary of 77
 - considered as a porous medium 96
 - geometry of 60
 - influence on constant rate tests 84, 86
 - role in geohydrology of the site 82
 - necessity for three-dimensional model 95
 - numerical model for 6, 95–
 - 101, 133, 135, 150, 151
 - application of 6, 119–131, 149
 - areal extent 119
 - boundaries of 96
 - boundary conditions for 98
 - calibration and verification of 6, 119–122
 - calibration of the model 119–121
 - convergence properties of 103
 - discretization of flow equation 99, 103
 - finite element grid 119
 - fit of the 121–122
 - hydraulic parameters for 98–99, 121
 - implementation of the 103–117
 - improving the fit 122
 - initial condition for 98
 - method used in calibrating 121
 - objective of 96
 - pre- and post-processors 103
 - purpose of 119
 - recalibration of 122
 - representation of aquifers 96
 - results from 6, 149, 150, 151
 - steady state version of 119
 - steps taken to verify 121
 - verification of 121–122
 - presence of subvertical fractures 65
 - prominent features of 96
 - simulation of hydraulic tests 122–128
 - constant rate test on UP15 124–127
 - constant rate test on UP16 122–124
 - recovery test on UP16 127–128
 - results 123–124
 - spatial geometry 45, 95–96
 - stratigraphy and sedimentology 50–57
 - structure of vertical lithofacies 60
 - topography of 50
 - use of a unsaturated-saturated flow model 96
 - difficulties with 96
 - void geometry 96
 - difficulties to represent the fracture 96
 - Cape Fold Belt 13, 15, 16, 18, 20
 - formation of 15
 - Cape-Vaal Craton 38
 - Carbonaceous shale layer 84
 - Carboniferous 5, 13, 38
 - Cave Sandstone. *See* Clarens Formation
 - Cementation 21–22
 - Central Free State 17, 22
 - geology of 37
 - geomorphology of 38–45
 - Chain rule for differentiation 167
 - Chilled edge 31
 - Clarens Formation 20, 22. *See also* Stormberg Group
 - hydrological properties of 21
 - Classical yield test 84–88
 - Colluvium 22
 - Compaction 21–22
 - Computer package 3
 - Computer program 6, 103, 105
 - checking for errors 105
 - effort in writing a new 103
 - three-dimensional 6
 - tool to study behaviour of Karoo aquifers 6
 - Computer resources
 - 6, 96, 98, 101, 107, 133, 151, 153
 - Conceptual model 3, 4, 9, 11, 22
 - derivation of 11
 - description of 4
 - limitations for Karoo aquifers 75
 - prerequisite to derive a 10, 128
 - representation of aquifer's geometry 11
 - Confined aquifer 96, 106
 - Conglomerates 15
 - Constant rate test. *See* Hydraulic test

- Constitutive parameters 9, 10
 relation to hydraulic parameters 9
- Cooper-Jacob method 91
 association with radial flow 91
 basic assumption 91
- Core-borehole 5, 8, 11, 149
 stratigraphic classification of 39
- Creep fracture 29
- Cretaceous 5, 25, 149
- Cretaceous period 27
- Cylindrical co-ordinates 169
- D**
- Daptocephalus zone 38
- Darcy's law 9
- Deep-water sedimentation 18
- Density of water 97
- Department of Geohydrology 5, 50, 78, 84
- Department of Geology 4
- Department of Water Affairs and Forestry
 5, 8, 67, 69, 77, 91, 129, 152, 153
- Dewetsdorp 4, 8, 64, 67
 Borehole B1 69
 Borehole B10 69
 Borehole B11 69
 Borehole B2 69
 Borehole B3 69
 Borehole B4 69
 Borehole B5 70
 Borehole B6 70
 Borehole B7 70
 Borehole B8 70
 Borehole B9 69
 Borehole C5 69
 Borehole G36430 69
 Borehole G36464 69
- Dewetsdorp test sites 67–70
 difference in water levels 69
 geohydrology of 69–73
 effects of dolerite intrusions on 69
 geology of 67–69
 presence of faults 70
 properties of geological units 70
- Dicynodon Assemblage Zone 38, 39, 44
- Dicynodon fossils 38
- Dilation 30
 properties of 30
- Dirac delta function 172
- Dirichlet line source approximation
 103, 105, 107–109
 convergence of 109
 dependence on element size 107
 in space 111–112
 in time 109
 influence of finite element grid 112
 numerical errors in 119
- Dirichlet surface source approximation 105, 105–
 107
 behaviour of 106, 107
 changes in finite element sizes 113
 insensitivity to 113
 convergence of
 dependence on element size 108, 110
 in space 109–111
 in time 109
- Discharge rate 100
- Discontinuous hydraulic parameters
 103, 104, 113
 as internal boundaries 103
 avoiding 104
 smearing of 103, 104, 117
- Discontinuous parameters
 correct handling of 104
- Dolerite dykes 30, 32, 75, 90
 as sites for boreholes 90–91, 149
 difficulties with 71, 90–91, 149
 at Dewetsdorp 69
 properties of 69
 weathering of 32–34
 dependence on grain size 32–34
 influence on success rate of boreholes 32, 35
 weathering pattern 35
- Dolerite intrusions 27, 149. *See also* Magmatic
 intrusions
 effects on Karoo sediments 30
 geohydrology of 30
 types of 149
- Dolerite sill 25, 27
 definition of 27
 emplacement of 27
 form of 27
 interpreted as a laccolith 27
 properties of 27
 time of emplacement 27
 undulating 26, 149
 weathered 35
- Drakensberg lavas 21, 25, 30
 associated intrusions 25
 association with ring dykes 26
 support for 26
 effect on nearby regions 25
 extent of cover 25
 outpour of 25
 incongruous 25
 intrusion into fractures 25
 less-extensive phases 25
 thickness of 25
- Drill chips 8
- Dwyka diamictite 15
 clasts in 15
- Dwyka Formation 13, 15
 composition of 15
 deposition of 15
 interpretation of 15

-
- hydrological properties of 15
 - ordering in cycles 15
 - Dwyka shales 15
 - Dwyka tillites 15
 - Dyke
 - Gap 29
 - linear. *See* Linear dolerite dykes
 - ring. *See* Ring dyke
 - ring-shaped. *See* Ring dyke
 - E**
 - Eastern Cape Province 25, 26
 - Eccla Group 16–18, 27, 38, 39
 - composition of 17
 - delta systems 16
 - deposition of 16–17
 - fluvial systems 16
 - hydrological properties of 17
 - prodelta sandstones 18
 - volcanic activity 17
 - Eccla sediments
 - reworking of 17
 - Eccla shales
 - as sources of groundwater 17
 - densities of 17
 - porosities of 17
 - Electronic recording of drawdowns 77
 - advantages of 77
 - Element 104, 112, 113
 - Element boundaries 104
 - Element sizes 104, 107, 108, 110, 112, 113
 - Elementary distance vectors 167
 - Elementary radius vector 168
 - Elementary volume element 167
 - definition of 168
 - transformation of 167–169
 - Elliot Formation 20. *See also* Stormberg Group
 - hydrological properties of 21
 - sedimentation of. *See* Sedimentation: Elliot
 - Excess pressure 27
 - Experimental sites 4–5, 37. *See also* Test sites
 - at Dewetsdorp 5
 - purpose of 4, 37
 - F**
 - Factors
 - controlling flow in aquifers 9
 - Fauresmith 29
 - Ficksburg 22
 - Field observations 6
 - Finite element grid 99, 105, 110, 111, 112
 - generation of 104
 - Flexural rigidity of a plate 156
 - Flow velocities 98
 - in situ measurement of 98
 - Fluvio-glacial environment 15
 - Force
 - adhesive 7
 - Fracture 27, 29
 - contraction of 90
 - dewatering of 126
 - expansion of 90
 - flux of a fluid through 76
 - dependence on aperture 76
 - Fracture aperture
 - effects of dewatering 90, 125
 - effects of rewatering 90
 - influence on borehole yields 90
 - Fracture drawdown cone 126
 - behaviour of 126
 - Fracture flow 76
 - properties of 76
 - Fracture hydraulics 87–88
 - influence of multiple fractures 88
 - influence of piezometric pressures 88
 - role of fracture recharge 87
 - role of rock matrix 87
 - Fracture mechanics 89–90
 - Fracture plane 6
 - preferential dewatering of 117, 125, 126
 - Fracture propagation
 - velocity of 29
 - Fracture skin 91
 - Fracture velocity 29
 - Fracture zones 8
 - Fractures 4, 5, 22, 25, 30, 32
 - as sources of water 30, 65
 - bedding-plane. *See* Bedding-parallel fractures
 - density of 30
 - formation of 35
 - subvertical 71
 - conduits for surface water 71, 150, 152
 - Free State 20, 26, 29, 38
 - G**
 - Galerkin finite element method 99, 104
 - Gaussian quadrature rule 104
 - Geological boundary 95
 - Geological formations 1, 4, 9
 - heterogeneity of 10
 - Geophysical techniques 30
 - Gilbert's theory
 - for the intrusion of a laccolith 155–156
 - Glaciomarine conditions 15
 - Gondwanaland 13, 15
 - fragmentation of 25, 27, 149, 156
 - tectonic movement of 5, 25, 149
 - Grid generator Qbik 104
 - Gringarten-Ramey model 92, 151
 - dependence on fracture size 92–93
 - Groundwater 1
 - in South Africa 1, 149
 - occurrence of 4
 - scientific study of 4

- Groundwater flow equation 97, 171
 conservation of fluid mass 171
- Groundwater model 8, 9
 three-dimensional 6, 95, 112
 difficulties with 151
 two-dimensional 112, 125, 133
 two-dimensional vertical flow 133, 135, 151
 limitations of 151
- H**
- Harmonic tremors 29
- Hexahedral elements 104
- Horizontal flow model
 analytical 91
 inapplicability to Karoo aquifers 91
- Hydraulic conductivity 15, 113, 139
 horizontal 82, 95
- Hydraulic conductivity tensor 97, 121, 134
- Hydraulic parameters 6, 9, 119, 122. *See also* Storativity; Transmissivity
 dependence on depth of pump 80
 derivation of 10
 difficulties with 10–11
 from numerical solution of inverse problem 136
 determination of 1
 determined by aquifer's void geometry 11
 estimation of unknown 119
 inverse problem 11
 representative of an aquifer 10
- Hydraulic test 1, 7, 9, 10, 37. *See also* Packer tests
 analysis of 1–3, 3, 22
 analysis of vertical flow 133
 analytical models
 inadequacy of existing 37
 and behaviour of an aquifer 7
 conceptual models
 inadequacy of existing 149
 constant rate test 133, 172
 behaviour of water levels 84, 85, 86, 150
 decline and stabilizing of water levels 84, 150
 disadvantage of 81
 length of stability phase 86
 performed at De Aar 87
 performed at Dewetsdorp 87
 performed at Philippolis 84–88
 performed on the Campus Test Site 85
 stabilization of water levels 85
 difficulties with 10, 11, 150
 equipment used in 165–166
 pressure transducers 165–166
 pumping system 165–166
 inverse modelling of 135–142
 multi-rate test 127, 130, 172
 step drawdown test 86, 88, 133, 138, 143, 172
 time-dependence of 10
 invalid interpretation of 10
- Hydrocensus 32, 150
- Hydrochemical actions 75, 90–91
 relation to groundwater chemistry 91
- Hypothetical aquifer 107, 109, 113, 119
- I**
- Initial condition 98, 105, 106, 107, 119
- Institute for Groundwater Studies
 4, 103, 133, 145, 152
- Interactions 8
- Inverse model 11
- Inverse problem 11
 difficulty with 11
 methods to solve 136
 non-uniqueness of solution 11, 136
- Island arc 15
 definition of 15
 development of 15
 relation to Cape Fold Belt 15
- J**
- Jacobi matrix 168
- Jacobian 168, 169
- Jagersfontein 29
 diamond mine at 29
- Jurassic 5, 13, 25, 38
- Jurassic age 27
- K**
- Karoo 1
- Karoo aquifers 1, 8, 104, 113, 117, 135
 ability to transmit water 76, 150
 influence of bedding-parallel fractures 76
 analytical models for 91–92
 difference between radial and linear 91–92
 difficulties in establishing 91
 importance of vertical flow 91
 as dual porosity aquifers 75
 availability of water 1, 152
 factors influencing the 130, 150
 behaviour of 3, 6, 8, 75–
 93, 92, 95, 117, 125–126, 149, 150. *See also* Bedding-parallel fractures: conduits of water in Karoo aquifers
 controlled by bedding-parallel fractures 64, 76, 87, 92, 149, 152
 controlled by complex geometry 75, 92, 128, 152
 controlled by dolerite dykes 90
 factors influencing the 90, 117
 global 75
 local 75
 constant rate tests 77
 repeatability of 77, 79
 deformation of 6, 89, 92–93, 151
 evidence for 89–90, 90

- mass transport and 93
- fracture geometry 45, 150
 - determination of 129
 - methods to determine 129
- geohydrology of 32
 - influence of linear dolerite dykes 35
 - related to laccolithic intrusions 32
- geometrical representation of 65
- geometry of 5, 37, 75
 - complexity of 73, 149
 - description of the 73
 - deviation from other media 5
 - explanation of 35, 37, 149
 - influence of bedding-parallel fractures 73
 - influence on hydraulic behaviour 75, 149
 - influence on management 75, 128
 - significance for nature of flow 128
 - significance for solving problems associated with 73, 150
- Gringarten-Ramey model for 92, 151
- hydraulic conductivity of 65
 - influence of microfractures 65
- hydraulic parameters 6, 133
 - constraints on determining 129
 - interpretation of 124
- influence of linear dykes 35
- linear and radial flow
 - distinction between 128
- linear flow in 75, 91, 128
- management of 23, 124
 - factors influencing the 130, 149, 152
 - influence of pump depth 81
- nature of flow in 75–76, 92, 117, 128
 - control by bedding-parallel fractures 75, 92
- numerical model for 95
 - advantages of 95
 - dependence on physical properties of the medium 95
- pollution of 73
- properties of 22–23, 75, 113, 133, 149
 - related to palæo-environment 5
- radial flow in 91
- recharge areas 32
- recharge potential of 1
- requirements of a successful model 129
- role of fractures 5
- sedimentary rocks as main storage units for water 65, 75–76, 86
- significance of linear dolerite dykes 35
 - reasons for 35
- storativity of 65
 - influence of microfractures 65
- sustainability of discharge rates 88
- types of flow in 75
- unreliability of 1
- vertical flow in 91, 128, 133
 - significance of 73, 76, 117, 150
- water balance studies of 1
- yields of boreholes 22, 87
 - controlled by bedding-parallel fractures 76, 87
 - sustainability of 76
- Karoo Basin 13, 15, 18
 - location of 13
 - subsidiary basins 13
- Karoo boreholes
 - fractured-controlled behaviour of 6, 87–90
 - absence of in single-layered aquifer 88
 - explanation for 88
 - related to fracture deformation 90
 - relation to boundary effects 88
 - relation to dolerite dykes 88
 - limit to efficient pumping rate 87, 88, 127
- Karoo formations 5, 8
 - conceptualization of 95
 - deformations of 6
 - mechanical 30
 - interpretation of 37
 - microfractures in 75
 - presence of fractures 5
 - susceptibility to matrix diffusion 63
 - yields of boreholes 1
- Karoo landscape 5, 25
 - characteristic feature of 34
 - ring-shaped dyke structures 26
- Karoo rocks 22
 - hydraulic conductivity of 76
 - mechanical deformation of 30–32
 - bending 30, 31–32
 - dilation 30–31
 - porosity of 22
- Karoo sedimentation 15
 - end of 21, 25, 149
- Karoo strata 50
- Karoo Supergroup
 - 1, 4, 8, 18, 20, 30, 37, 39, 48, 164
 - aquifers in 1
 - properties of 22
 - composition of 1
 - depositional environment 13, 38
 - development of 13–23
 - dolerite intrusions 156
 - dolerite sills 27
 - as dominant form of emplaced 27
 - evolution of 149
 - formation of 13
 - isostatic uplift
 - development of fractures 22
 - transformations of original sediments 21
- Katberg Formation 18, 67. *See also* Tarkastad Subgroup
 - properties of 67
- Kimberlites 29
 - contribution to groundwater 29
 - high-yielding boreholes associated with 29

- method of intrusion 29
Kokstad 88, 141, 142
- L**
- Laccolith 26–27
classical gelatin models 26
limital area of 156
parameters influencing 156
position of stem 27
reasons for not observing 26
- Laccolithic intrusions 6, 27, 32
displacement profiles 159
displacements caused by 159
distribution of shearing stresses 160
properties of 160
fractures associated with 32
fracturing of contact planes 32
sliding of layers in overburden 32
theory of 31
- Laccolithic structures 26
matrix melting and 155
possibility to observe 158
- Language of physics 4
- Laplace's equation 7
- Law of mass conservation 10
- Laws of physics and chemistry 4
- Leeuberg 39
- Leibnitz' rule 169
for a vector-valued function 169
for differentiation of an integral 169
- Lesotho 25
- Levenberg-Marquardt algorithm 137
- Linear dolerite dykes 27, 27–29, 69
age of 27
as sources of water 30
association with fractures 30, 149
form of during intrusion 29
methods of intrusion 27–29, 155
occurrence of 27
- Linear equations 99
- Linear flow 91, 128
- Lithification 21–22, 22
- Lithostatic pressure 156
- Lystrosaurus zone 38, 39
- M**
- Magma
baking of the Karoo sediments 30
metamorphosing of the Karoo sediments 30
pressure of 155
- Magma chamber 27
- Magma density 156
- Magma force 155
- Magma intrusion 5, 155
as laccoliths 5, 150
displacement in z-direction 158
driving pressure in overburden 156
contributions to 156
properties of 156
geometrical shapes 157
limital area 155
pathway for 155
plan shape of 158
types of pathways for 155
- Magmatic activity 5, 25
extrusive phase 25
pulses in 25
related to the tectonic movement of Gondwana-land 5
shifting of centre 25
- Magmatic intrusions 25–35
dislocation of host rock 29
in jerks 29
method of 25
options for 26
theory of 25
- Marker beds 38
- Mass transport 6
- Mathematical model 6, 9, 10, 149
necessity for a simple 145
reduction of dimensions 133–134, 167–173
fundamental concept in 167
groundwater flow equation 171–173
the mathematical approach 133–134
the physical approach 133–134
three-dimensional 6, 151
difficulties with 6, 151
- Matrix diffusion 63, 73
susceptibility of Karoo formations 73
- Matrix flow 75–76
- Matrix geometry 9
- Matrix melting 25, 27, 30, 149, 155
effect of 155
mechanism of 27
- Megascopic domal structure 6, 46, 71
consequences of 71
extent of 46. *See also* Bloemfontein Area
influence on regional groundwater 71
- Mesozoic history of Africa 25
- Method of least squares 136
and analysis of hydraulic test data 137
non-linear algorithms for 137
initial guesses 137
limitation of available 137
principle of the 137
- Microfractures 65, 73
- Modder River 38
- Model 7
analytical. *See* Analytical model
conceptual. *See* Conceptual model
definition of 8
kinds of 9
mathematical. *See* Mathematical model
numerical. *See* Numerical model

- porous flow 9
 relation to theory 9
 Molteno Formation 20. *See also* Stormberg Group
 hydrological properties of 21
 sedimentation of. *See* Sedimentation: Molteno
 Multi-layered overburden. *See* Overburden multi-layered
 Multi-rate test. *See* Hydraulic test: multi-rate test
 Musgrave Sandstone 38, 39–45, 71
 as a major groundwater resource 46
 examples of cross-bedding 43
 interpretation of depositional environment 43
 major feature of 44
 Muskat solution 105, 106, 107, 109, 134
- N**
- National Museum 38
 Nature of Groundwater Motion 4
 Neumann surface source approximation
 105, 106, 111
 behaviour of 106, 107
 convergence of 111
 dependence on number of elements 107
 Northern Beaufort Formation 38
 Northern Cape Province 13, 22, 26, 27
 Northern Free State 17
 Numerical model 9
 calibration of
 idea behind 119
 for vertical flow 133–135, 135
 ability to represent Karoo aquifers 135
 numerical experiments 134–135
 representation of flow in the aquifers 135
 three-dimensional 6, 149, 152
 two-dimensional vertical 133
 purpose in developing 133
- O**
- Observable 9
 Oudenodon baini 44
 Overburden 21, 22
 bending of
 and theory of plates 156
 conditions for lifting 155
 contact area of 155
 weight of 155
 Overburden bending of 156–160
 and the theory of plates
 assumptions 156, 157
 equation of Sophie Germain 156
 distribution of shear stresses 160
 linear driving pressure 158–160
 uniform driving pressure 156–158
 likelihood to occur 158
 Overburden deformation of 160–163
 and viscosity of the magma 160–161
 bending strains 162
 properties of 163
 correlation with the magma viscosity 161–163
 effect of magma crystallization on 160
 stretching 161–163
 and formation of peripheral dyke 163
 Overburden multi-layered 163–164
 representation of 163
 Overpressure 27
- P**
- Packer tests 82
 cross-borehole 5, 81–82, 98
 advantages of 82
 failure in Karoo aquifers 82
 reasons for failure in Karoo aquifers 82
 usefulness in Karoo aquifers 82
 double 82
 and hydraulic conductivity 82
 and specific storativity 82
 principle of 82
 spacing of boreholes 82
 Palæo-coastline 15
 Palæo-environment 5
 Parabolic partial differential equation 10, 98
 describing flow of groundwater 11
 properties of solution 10–11
 Percussion borehole 5
 Peripheral dyke 26
 association with a laccolith 26, 149
 formation of 163
 influence of layer thickness 163
 Permian 5, 13
 Petrusburg 22
 Phenomenological model 101
 description of 101
 limitation of 101, 128
 Philippolis 4, 5, 64, 77, 149
 Borehole A14 143
 Borehole D19 84–88, 142, 143
 Borehole D20 86, 88, 142, 143
 fracture properties 88
 Photo-elastic gelatin layers 160
 isochromatic patterns in 160
 Phreatic aquifer 96
 Piezometer 5, 84, 130
 advantages of 151
 Piezometer UO1 84, 96, 98, 121, 123, 125
 Piezometer UO18
 84, 85, 88, 96, 98, 121, 123, 125, 127
 Piezometric head
 97, 106, 109, 113, 117, 134, 135
 historic 119
 Playa lakes 21
 Poisson's ratio 156
 Position vector 168
 Pre-existing fault 31
 Precambrian granitic rocks 15

-
- Preconceived ideas 101
 - Pressure transducers 165
 - calibration of 165
 - recording of measurements 166
 - Primary porosity 15
 - Prodelta 16, 17
 - creation of 16
 - Program Gcon 134
 - Program Karo 103–
 - 105, 109, 110, 113, 117, 119, 122, 145
 - ability to simulate aquifers on Campus Test Site 127, 128
 - checking for errors 105
 - compared with analytical models 105–113
 - Pre- and Post-Processors 104–105
 - Program Kubik 104
 - Program Meshpro 104
 - properties of 105
 - Program RPTsolv 133, 138, 146, 147
 - advantage of 140
 - aspects that needs attention 133
 - availability of 133
 - computation of hydraulic parameters 138
 - computer implementation of 138–139
 - influence of aquifer boundary 140–141
 - influence of aquifer thickness 139
 - influence of boundary conditions 141–142
 - default parameters 138
 - applicability of 139
 - difficulties experienced by users 146–147
 - difficulties experienced with 146
 - distance dependence of storativity 144–145
 - comparison with Theis values 144–145
 - possible prevention of 145
 - representation of perturbed borehole 145
 - examples of analysed hydraulic tests 142–145
 - Campus Test Site 142
 - Philippolis 142
 - step drawdown test at Philippolis 143–144
 - finite element mesh for 138
 - fitted hydraulic parameters 139
 - influence of exact aquifer thickness 139
 - future amendments 145–146
 - graphical presentation of results 139
 - handling of hydraulic data 138–139
 - handling of hydraulic parameters 139
 - limitations of parameters computed with 138
 - prescribed boundary conditions 141
 - dependence of aquifer radius on 141–142
 - effects of available options 141–142
 - example of inappropriate 141
 - indication of an internal boundary 141
 - options available 141
 - prescribing aquifer boundary 140
 - approaches to 140–141
 - difficulties with 140
 - user responsibility 140
 - using the least squares error in 140–141
 - representation of a Karoo aquifer 138
 - user supplied parameters 138
 - geometric 138
 - other options available to user 138
 - simulation parameters 138
 - Program Sat3 6, 99, 103, 104, 105, 134, 151
 - Pumping test. *See* Hydraulic test
- Q**
- Qanats 21
 - Quadrature points 104
 - Quadrilateral elements 104
 - Quantum mechanics 26
 - Quartz grains 60
 - fracturing of 60
- R**
- Radial direction 6
 - Radial flow 91
 - Radial symmetric aquifer 105
 - Radiometric anomalies 38
 - Rayton Ridge Sill 46
 - Recent Formations 13, 22, 23
 - as sources of groundwater 22
 - Receptacles for groundwater 32
 - Ring dyke 5
 - horn of 26. *See also* Peripheral dyke. *See also* Dyke: peripheral: associated with a laccolith
 - controlled by elastic properties 26
 - interpretation of
 - as a dolerite sill 34, 149
 - as a laccolith 26, 155, 164
 - Ring dykes 26–27, 30, 32
 - age of 27
 - in relation to linear dykes 27
 - as sources of water 30
 - as undulating dolerite sills 26
 - difference between 30
 - properties of 26
 - Ring-shaped dyke structures 25, 34
 - Rock matrix 7
 - represented by porous matrix 7
 - Rouxville 4, 5, 64, 77
- S**
- Saturated flow equation 95, 96–98
 - Scaling factor 168
 - Secondary aquifers 3
 - Secondary porosity 15
 - Sedimentation 13, 15, 18, 22
 - Elliot 20
 - Molteno 20
 - Seismic observations 29
 - Shearing force 155
 - Sheet
 - mathematical deformation of 26

- Simplified Karoo aquifer
 numerical model for 113–117
 properties of 117
- Slickensided calcite 69
- Slickensided quartz 30, 69
- Slickensides 30
- Sources and sinks
 strength of 97
- Specific storativity 22, 113, 134, 139
- Spitskop Sandstone 44, 45, 50, 71
 deposition of 44
 ferruginized and leached nature of 44
 lithology of 44
- Springfontein 32
- Step drawdown test. *See* Hydraulic test: step drawdown test
- Storativity 79, 97, 134, 139
 dependence on discharge rate 80
 dependence on distance 79, 144
 explanation of 125
 dependence on position of perturbed borehole 79
 specific 121
 reduced by cementation 22
 reduced by compaction 22
 reduced by lithification 22
- Stormberg Basin 20
 formations in 20
 properties of the strata 20
- Stormberg Group 13, 20–21
 hydrological properties of 21
- Stratigraphic assemblages 38
- Stratigraphic column 38
- Stratigraphic control 38
 biostratigraphic markers for 38
- Streams
 braided 18, 20
 meandering 18, 20, 45
- Structural geology 15
- Strydenburg 22
- Surface tension 7
 of water 7
- Surface water 1
- T**
- Tafelkop 44
- Tarkastad Subgroup 18, 37, 38, 67. *See also* Beaufort Group: subdivisions
 composition of 18
 subdivision of 18
- Tectonic events 25
 fracturing of earth's crust 155
 upwards squeezing of magma 156
- Teekloof Formation 18
- Test sites 5
- Theis model 79. *See also* Theis model
 applicability of 79
 assumptions of 79
 inapplicability to Karoo aquifers 79, 80, 81
- Theory 4
 advantages of 9
 description of 4
 for groundwater motion 9
 in geohydrology 8
 in the exact sciences 7, 8
 of flow
 through a porous medium 9
- Theory of elasticity 26
- Three-dimensional flow 6
- Three-dimensional flow equation 6
- Three-dimensional groundwater flow model 95, 101
 difficulties with 95, 101
 justification for 101
- Time derivative 109
- Tracer tests 98
- Transmissivity 79, 139
 dependence on depth of pump 81
 explanation of 81
 dependence on discharge rate 80
 dependence on distance
 explanation of 80
 relation to vertical flow 80
- Transmissivity tensor 97, 134
- Tri-linear basis functions 110
- Triassic 5, 13, 25, 149
- Trompsburg 32
- Tuffs 29
- Two-dimensional flow models 101, 172
 advantages of 101
 disadvantages of 101
 inapplicability of 101
 popularity of 101
- Type curve 1
 application in hydraulic tests 1–3, 135
 limitation of 135
 relation to inverse problem 136
- U**
- Uniform aquifer 105
- Unit normal vector 99
- Unit vector 168
- University of the Free State 4, 48
- Unsaturated flow 91
- Unsaturated-saturated flow model 96, 130
- Uplift isostatic 22
 consequences for underlying strata 22
 formation of fractures 22
- Uraniferous rocks 38
- V**
- Varved shales 15
- Vertical flow 172
- Vertical flow model
 two-dimensional 6, 95, 173

- derivation of 6
- Void 5, 22
- Void geometry 5, 7, 11
 - methods to determine 5
 - geological 7
 - geophysical 8
 - neglect of 7
 - in aquifer studies 7
 - relation to geological formation 7
 - types of media used to represent 96
- Void primary 15

W

- Wadi 21
- Water fresh 1
 - occurrence on earth 1
- Water levels in open boreholes 129
 - interpretation of 123, 151
 - limitations of 129
- Water pressure 97

- Water Research Commission 3, 4, 5, 6, 151
- Water surface 7
 - radii of curvature 7
 - determined by void's geometry 7
- Water-yielding fracture 6
 - collapse of
 - consequences of 89
 - deformation of 6, 89, 130, 151
 - consequences of 151–152
 - reasons for 89–90
 - dewatering of 6
 - relation to bedding-parallel fractures 89, 150
- Weighting factors 137

Y

- Yields of Karoo boreholes 70
 - and bedding-parallel fractures 71
 - variations in 70
- Young's modulus 156